Evaluation of Factors that Affect Contrast-Detail in Digital X-Ray and Computed Tomography

A thesis submitted in fulfilment of the requirements for the degree of PhD of Medical Radiations Science

Haney A. Alsleem

Medical Imaging Technologist

DR087 - Doctor of Philosophy

School of Medical Sciences

College of Science, Engineering & Health

RMIT University

March 2014

Declaration

I certify that, except where due acknowledgement has been made, the work is of the author alone; the work has not been submitted previously, in whole or in part, to qualify for any other academic award; the content of the thesis is the result of work which has been carried out since the official commencement date of the approved research program; any editorial work, paid or unpaid, carried out by a third party is acknowledged; and, ethics procedures and guidelines have been followed.

I declare the cooperation and support of Artinis Medical Systems in designing and manufacturing our invention and developing the dedicated software.

Haney A. Alsleem

19/03/2014

Dedication

This thesis is dedicated to the soul of my mother. I also dedicate this work to my family and my many friends who have supported me throughout the process. I also dedicate the thesis to my wife and kids for being there for me throughout the entire doctorate program. I will always appreciate all they have done. Words of encouragement and push for tenacity ring in my ears.

Acknowledgement

complete my study. I would like to give my special thanks to my kids for being there for me throughout the entire doctorate program.

Table of the contents

List of Figures

xviii

xix

List of Tables

List of Equations

Publications from this work

- Alsleem, H & Davidson, R 2012, 'Quality parameters and assessment methods of digital radiography images', *The Radiographer*, vol. 59, no. 2, pp. 46-55 (Appendix 1a).

- Alsleem, H & Davidson, R 2013, 'Factors affecting contrast-detail performance in computed tomography: a review', *JMIRS*, vol. 44, no. 2, pp. 62-70 (Appendix 1b).

- Alsleem, H & Davidson, R 2013, Effects of radiographic techniques (kVp and mAs) on the low contrast-detail detectability performance of different digital radiography systems. *Radiologic Technology* (accepted for publication, 2013) (Appendix 1c).

Glossary

ACR: American College of Radiology.

AEC: Automatic exposure control.

ALARA: As Low As Reasonably Achievable

ALARP: As Low As Reasonably Practicable

Artefacts: Features that occur on an image and mask or mimic clinical features are called artefacts.

ASIR: Adaptive statistical iterative reconstruction. It is a technique of iterative reconstruction algorithms. It was developed and established by GE Healthcare in 2008.

ASTM: American Society for Testing and Materials.

CDCT phantom: Low contrast-detail computed tomography phantom.

CNR: Contrast-to-noise ratio.

Contrast: The difference in brightness between light and dark areas of an image.

Contrast resolution: Refers to an imaging system's ability to distinguish between small objects with small differences in density. Also called low contrast resolution.

CR: Computed radiography.

Cross-plane resolution: Explains the spatial resolution in z direction.

CT: Computed tomography.

CTIQF$_{inv}$: CT inverse image quality figure—a measure of low contrast-detail detectability performance of CT.

DDR: Direct-conversion direct digital radiography.

DFOV: Display field of view. It determines how much of the scan field of view (SFOV) is reconstructed into an image. DFOV can be less than or equal to the SFOV and cannot be more than the SFOV. DFOV is also called reconstruction field of view (RFOV).

DICOM: Digital Imaging and Communications in Medicine.

Digital radiology images: Medical soft-copy images which are a numeric representation of the transmitted x-ray intensities through the patient, displayed on a computer monitor. Digital images consist of quantisation symbolised in pixels, the smallest individual component in an image. The quantities of pixels represent the brightness of specific point.

Distortion: The misrepresentation of object size or shape as projected onto radiographic recording media.

DQE: Detective quantum efficiency is commonly used as a tool for image quality assessment and medical imaging system performance in general.

DR: Direct digital radiography.

DSCT: Dual source CT—two radiation sources in multiple detector computed tomography (MDCT) scanners.

eDQE: Effective detective quantum efficiency. It is a modified and improved approach of DQE to another approach of image quality evaluation.

EI: Exposure index. A numeric value represents the exposure that the image receptor received. It may also be called the sensitivity number. It is important to check the exposure index by verifying that the digital images were obtained with the least possible dose to the patient.

FBP: Filtered back-projection.

FDD: Focal to detector distance.

FPCT: Flat-panel CT. CT scanners utilise flat-panel detectors instead of the multiple detector rows in MDCT.

FPD: Flat-panel detector. A solid-state detector utilised in direct digital radiography and some imaging systems.

High contrast-detail: Small objects close to each other with large differences in density.

HU: Hounsfield Unit.

iDose: A technique of iterative reconstruction algorithms established by Philips in 2009.

IDR: Indirect-conversion direct digital radiography.

Image data: Pixel values calculated from the scan data that are used to display and analyse images. Also called reconstructed data.

Image interpreters: The ones who make a decision regarding the interpreted image, as to whether or not it represents an abnormality of that patient.

Image quality: Good image quality is the image that allows physicians to interpret the image most accurately and effectively.

In-plane resolution: The spatial resolution in x/y direction.

IQF$_{inv}$: Inverse image quality figure—a measure of low contrast-detail detectability performance of radiography.

IRIS: Image reconstruction in image space. It is a technique of iterative reconstruction algorithms implemented by Siemens in 2009.

Iso-centre: Is the point in space where x-ray beams intersect when the CT gantry is rotated during exposure time. Iso-centre is also defined as the three-dimensional centre point of the gantry that the x-ray tube and detector rotate around.

Iterative reconstruction techniques: Statistical reconstruction algorithms. This technique requires higher computational capabilities compared to analytical methods such as FBP.

kVp: Kilo voltage peak—a unit for measuring the potential difference across the x-ray tube.

LCD detectability analysis: Low contrast-detail analysis provides quantitative evaluations of low contrast and small detail measurement of medical images.

LCD detectability performance: Low contrast-detail detectability performance. It is an evaluation method of image quality based on the ability of medical images or imaging systems to detect low contrast and small detail of low contrast-detail phantom.

LCD phantom: Low contrast-detail phantom. It consists of a range of objects with different contrasts and diameter sizes. LCD phantom is used to measure image quality in terms of low contrast-detail detectability performance.

Linearity: It defines the relationship of the CT number values assigned to objects representing different types of tissue to be imaged, compared to the linear attenuation coefficients measured at the average energy of the scanner.

Low contrast-details: Small objects with similar densities.

LSF: Line spread function.

mA: Milliamperes—a unit for measuring x-ray tube current or the number of electrons flowing from the cathode to anode.

mAs: Milliampere seconds—the product of tube current and exposure time.

Matrix: Two-dimensional grid of pixels, used to compose images on a display monitor. The matrix determines the number of rows and columns.

MDCT: Multiple detector computed tomography.

MTF: The modular transfer function describes system ability to reproduce and preserve the information of spatial frequency contained in the incident x-ray signal.

NEMA: National Electrical Manufacturers Association.

Noise: A random disturbance that obscures or reduces clarity; translates into a grainy or mottled appearance of the image.

NPS: Noise power spectrum. It describes the frequency content of the noise in the spatial frequencies of the system image.

PACS: The picture archiving and communications systems technology.

Partial volume effect: When different tissues/objects are represented by the same voxel. Each tissue/object only partially fills the voxel and is therefore a partial volume. Also call partial volume averaging.

Pitch: The ratio of the table feed per x-ray tube rotation to the width of x-ray beam for single spiral CT. For MDCT, the pitch is the table movement per single rotation of x-ray tube.

Pixel: Two-dimensional picture element that makes up the matrix, which is a collection of pixels.

Pixel size: The pixel size can be calculated by dividing the DFOV in mm by 512 (the matrix). The depth of the pixel represents is determined by the slice thickness.

Prospective data: An image automatically reconstructed from the scan data.

PSF: Point spread function.

Reconstruction type: Mathematical formula used to convert scan data into image data. Different types of algorithms enhance different aspects of the data.

Reformatted image: An image created from axial image data. When the axial data is re-arranged to represent other planes such as coronal and sagittal.

Reliability: The consistency degree of the results, i.e. when an experiment is repeated, it yields the same results.

Resolution: The recorded sharpness or detail of structures on the image.

Retrospective image: An image reconstructed at the operator's request from scan/raw data.

RFOV: Reconstruction field of view determines how much of the scan field of view is reconstructed into an image. RFOV is also called display field of view (DFOV).

ROC: Receiver-operating characteristics analysis. It is a task-based evaluation method used to measure the sensitivity and specificity to assess the accuracy of diagnostic imaging systems.

SAFIRE: Sinogram affirmed iterative reconstruction. It is a technique of iterative reconstruction algorithms which currently implemented by Siemens.

Scan plane: Position in degrees that describes the location of the x-ray tube for a scout scan. When the tube is at the top centre of the gantry it is at 0° azimuth.

Scan/raw data: Binary numbers that represent the digitised x-ray signal collected by the detector.

Screen saved data: A copy of a displayed image, which is sometimes described as an electronic photograph.

Sensitivity: A measure of the probability that a patient who actually has the disease is determined as having a disease by image interpreters.

SFOV: Scan field of view. The parameter that determines how much anatomy is scanned. The SFOV should exceed the dimensions of the anatomy.

SNR: Signal-to-noise ratio. It is calculated to measure image quality based on linking the mathematically calculated SNR to the results of detection examinations. SNR describes noise and resolution characteristics of image and human visual system.

Spatial resolution: An imaging system's ability to differentiate and/or distinguish small objects of sharp edges that are adjacent to one another and differ greatly in density.

Specificity: A measure of the probability that a patient who truly does not have a certain disease is determined as not having that disease by image interpreters.

Temporal resolution: Temporal resolution refers to the measurement accuracy and precision with respect to time.

Consistency of the CT number: A measure of stability which implies that the CT numbers of the reconstructed phantom image should not vary when that phantom is scanned at different times, with different slice thicknesses, and/or in the presence of other objects.

Uniformity of CT number: A measure of the homogeneity or heterogeneity of the CT image of a uniform phantom. Implies that the CT number measurement of phantom images should not change when changing location of the selected ROI or by shifting the phantom position relative to the iso-centre of the scanner.

Validity: The used construct or tool really and correctly measures the aims.

VEO: A technique of iterative reconstruction algorithms. It is a more complex model-based iterative reconstruction method which implemented by GE Healthcare.

VGC: Visual grading characteristics, also known as visual grading analysis (VGA). It is an evaluation method used to assess image quality based on quality criteria and anatomical landmarks stated by professional experts.

Voxel: Three-dimensional element of anatomy represented by the two dimensional pixel.

Window level: The centre CT number value displayed by the gray-scale range.

Window width: The range of CT numbers displayed by the gravy scale, the CT numbers above the range are demonstrated as white and CT numbers below the range are demonstrated as black.

Summary

The central aim of this project was to develop a new methodology of evaluation and optimisation of image quality based on low contrast-detail (LCD) detectability performance of computed tomography (CT). This method is well established in digital radiography however similar tool of image evaluation and quality optimisation for CT images are not available. The method of LCD detectability performance for CT image evaluation and optimisation requires a certain specification and specific properties of an LCD phantom that are not commercially available. In comparison with other image evaluation methods, the evaluation tool of LCD detectability performance—particularly the automated approach—is a good choice for image quality optimisation. This method helps to determine appropriate exposure factors to provide optimum image quality while maintaining a lower radiation dose to patients. This method is a straightforward and direct way to assess image quality as it provides quantitative evaluations of low contrast and small detail measurements of medical images. The subjectivity of image evaluation methods based on human observers is avoided via automated scoring software that is utilises in automated approach of LCD detectability performance. The trade-offs between perceived image quality, diagnosis efficacy and exposure dose can be determined by LCD detectability measurements. To achieve the aim of the project, the current methods of LCD detectability performance in digital radiography and CT were evaluated.

The first phase of the project evaluated the effects of exposure factors, mAs and kVp, on the LCD detectability performance of three digital radiography systems: one computed radiography (CR) system and two direct digital radiography (DR) systems. The DR systems included indirect conversion DR (IDR) and direct conversion DR (DDR). An LCD phantom (CDRAD) and dedicated software (Artinis Medical Systems, Netherlands) were

used to evaluate the influences of radiography exposure factors on LCD detectability methods. The LCD detectability performance, as measured by the inverse image quality figure (IQF$_{inv}$) for different exposure factors from different radiography systems, was evaluated using software scoring and radiographers' assessment results. The results of the first phase showed that the LCD detectability performance of dedicated software is higher and more reliable than using radiographers with respect to the optimisation and evaluation of image quality for digital radiographs.

The second phase of the study aimed to evaluate the feasibility of the current objective methods of CNR measurements on LCD CT phantom images as an assessment tool of LCD detectability performance. The Catphan® 600 (Phantom Laboratory, Cambridge, NY) was used to investigate the influences of protocol parameters on image quality based on CNR measurements of the objects in the phantom. The CNR measurements were obtained using scripts developed for use in MATLAB (MathWorks, Massachusetts). The results of the second phase showed that the evaluation method of CT image quality based on CNR measurements was sensitive to changing reconstruction algorithms, kVp, mAs and slice thickness. However, this method is not an appropriate tool to measure the CT LCD detectability performance as it cannot evaluate and assess the effects of object size on LCD detectability. In addition, this method was limited by currently available CT LCD phantoms, the sizes of which do not consider large body organs such as the chest and abdomen. Hence, a new method should be developed to evaluate the LCD detectability performance of CT images.

The third phase of the project aimed to develop a new evaluation method of LCD detectability performance based on a newly designed LCD CT (CDCT) phantom and dedicated software. The specifications of the phantom design were optimised based on the

2

standard recommendations of phantom manufacturing and the requirements of the proposed new evaluation methodology. The new CDCT phantom was manufactured and dedicated software was developed with the cooperation of Artinis Medical Systems (Zetten, The Netherlands). The CT inverse image quality figure (CTIQF$_{inv}$) was determined as a measure of LCD detectability performance of CT images. An equation was developed and implemented in the software to calculate and objectively measure CTIQF$_{inv}$ values.

The fourth phase aimed to validate the new proposed method of LCD detectability performance based on the newly designed and manufactured CDCT phantom and dedicated software. This method was validated by evaluating the influences of exposure factors kVp and mAs, slice thicknesses and object location on image quality in terms of CTIQF$_{inv}$ values based on software and radiographers' scoring results. The results of the fourth phase showed that the new evaluation methodology-based CDCT phantom, along with the automated measurement of CTIQF$_{inv}$ value, had generally shown to be consistent with a prior knowledge of image quality in relation to change of mAs, kVp and slice thickness settings. This work showed that the CDCT phantom and the measurement of CTIQF$_{inv}$ values can provide a measure of CT image quality in terms of LCD detectability performance. This method has a promising role for CT image evaluation and optimisation, and has the potential to effectively evaluate the effects of protocol parameters on image quality of different CT scanners and systems. Future changes to the phantom design and/or software is required to overcome some of the current limitations.

Chapter 1 Introduction

1.1 Introduction

Digital radiation imaging technologies—including planar digital radiography and computed tomography (CT)—have an essential role in pathologic diagnosis and therapeutic procedures. Planar digital radiography imaging systems currently used in clinical settings are either computed radiography (CR) or direct digital radiography (DR). DR is of two main types: indirect conversion DR (IDR) and direct conversion DR (DDR). These systems have replaced conventional film/screen radiography due to their superior performance capabilities (Weatherburn et al. 2003). Indeed, recent advancements have extended the number of imaging applications and improved the efficacy of examinations. With the introduction of new improvements in radiography and CT, for example, image quality can be improved and the radiation dose to patients can be minimised. While higher image quality is required for more relevant diagnosis information and to confidently detect pathologic lesions and abnormalities (Hendee & Ritenour 2002), there are trade-offs between image quality and radiation dose. That is, image quality should be optimised to maintain a lower radiation dose without sacrificing the appropriate image quality (Yu et al. 2009).

The main objective of image quality optimisation is to determine the appropriate image quality required for certain imaging purposes and specific diagnostic tasks (Uffmann & Schaefer-Prokop 2009). The imaging performance of radiography systems should be routinely evaluated and the quality of images should be regularly optimised to obtain appropriate image quality with a lower radiation dose (The International Society of Radiographers and Radiological Technologists 2004; Uffmann & Schaefer-Prokop 2009).

There are several image evaluation methods, both *objective* and *subjective*. Objective methods, which include statistical measurements, have lower validity. Subjective methods, which involve human observers, have lower reliability (Bath 2010). Low contrast-detail (LCD) detectability performance—particularly the automatic approach—can overcome the limitations of subjective and objective methods (Pascoal et al. 2005). This is because the automated LCD detectability performance method is based on an LCD phantom and software that works as a mathematical model of human eyes (De Crop et al. 2012; Shet, Chen & Siegel 2011; Tapiovaara 2008). LCD detectability performance is considered a direct evaluation approach and includes all imaging procedures from image detection to image interpretation. It is considered as a clinical relative approach because the phantom image is a representative of diagnostic information for the interpreters (Bath 2010; De Crop et al. 2012).

1.2   Theoretical framework

The automated approach of the LCD detectability performance method is well established in radiography systems. Based on the study results of Pascoal et al. (2005) and Lin et al. (2012), LCD detectability performance has the potential to examine and gain deep understanding with respect to the influence of exposure factors on image quality. As such, this method can be used to optimise image quality and minimise the radiation dose delivered to the patient.

1.3   Statement of the problem or 'gap' in the research

The introduction of digital imaging systems has enabled planar radiographic image quality to improve and patient radiation dose to reduce (Korner et al. 2007; Williams et al. 2007). Required exposure factors and optimisation techniques for a digital radiography image are different to those of radiography film. Similarly, the data acquisition and image processing principles of CR and DR differ from that of conventional radiography. Despite this, many radiographers still operate in a 'film like' world (Reiner et al. 2006), using similar exposure factors for both film/screen and digital radiography. The problem is that CR and DR have the potential to increase patient radiation dose due to their wide dynamic range (Gibson & Davidson 2012), so patients may be overexposed with more radiation than is required for a diagnostically sufficient image (Schaefer-Prokop et al. 2008; Williams et al. 2007).

The most concerning issue in CT scan imaging is the radiation dose, as CT examinations are responsible for the highest radiation dose of all modes of medical imaging (Hayton et al. 2010; Smith-Bindman et al. 2012). As such, radiation dose reduction is a key goal in CT applications (Mahesh 2009), although using low radiation dose techniques also reduces the quality of CT scan images (Van Uitert et al. 2008).

More detector rows and incomplete slices may also lead to artefacts that negatively influences the quality of CT images (Barrett & Keat 2004; Romans 2011).

Digital radiography and CT images should be regularly evaluated and optimised to ensure adequate diagnostic image quality while maintaining lower doses delivered to patients (Uffmann & Schaefer-Prokop 2009). Importantly, image quality is largely determined by the imaging system type, model and unit specification, which cannot be controlled by radiographers. That said, radiographers can play an essential role in improving system

performance and image quality by effectively controlling and adjusting exposure factors (Davidson & Sim 2008). Indeed, the essential principle of image optimisation and dose reduction is to understand the effects of exposure factors on image quality (The International Society of Radiographers and Radiological Technologists 2004). Hence, it is important to have a deep understanding of these effects in different imaging systems. Several evaluation tools of image quality and imaging performance are used to evaluate and optimise images according to specific diagnosis tasks and imaging purposes (Bath 2010).

The evaluation method of LCD detectability performance—particularly the automated approach—is a good choice for image quality optimisation (Bath 2010). Automated LCD detectability performance is based on an LCD phantom and dedicated software, and therefore does not require volunteers, patients or image interpreters. This method provides quantitative evaluations of low contrast and small detail measurements of medical images, and is therefore considered a straightforward and direct way to assess image quality (Bath 2010; Uffmann et al. 2004). The subjectivity of LCD based on human observers is avoided via automated scoring software that utilises a mathematical model of the human visual system based on measurements of signal-to-noise ratio (SNR) (Shet, Chen & Siegel 2011; Tapiovaara 2008). LCD detectability measurements can determine the trade-offs between perceived image quality, diagnosis efficacy and exposure dose. This method also helps to determine appropriate exposure factors and provides optimum image quality while maintaining a lower radiation dose to patients (Shet, Chen & Siegel 2011). While this method is well established in digital radiography, similar tools of image evaluation and quality optimisation for CT images are not available, at least according to the knowledge of the researcher. In addition, the method of LCD detectability performance for CT image

evaluation and optimisation requires a certain specification and specific properties of an LCD phantom that are not commercially available.

1.4 Aims of the project

This research project aimed to:

a. design and manufacture a new LCD CT phantom

b. develop and evaluate the proposed automated LCD CT measurement tool to assess CT equipment performance and image quality.

The outcome of this project will be to:

a. produce a new CT phantom to evaluate equipment performance and to assess CT image quality based on LCD measurement

b. develop and assess a new methodology of LCD assessment in CT.

1.5 Methodology

The project comprised four phases. Phase 1 aimed to evaluate the effects of exposure factors on the LCD detectability performance of different digital radiography systems, and included the experiments of CR, IDR and DDR systems. This phase of the study used an LCD for radiography (CDRAD) phantom and dedicated images analyser software. Polymethyl methacrylates (PMMA) plates were used to attain soft tissue attenuation thickness. The inverse value of image quality figure (IQF_{inv}) was calculated for each image, to be used as a measure of LCD detectability performance.

Phase 2 included the experiments of CT with a commercially available LCD phantom. This phase aimed to evaluate the influences of protocol parameters—including mAs, kVp, slice thickness and reconstruction algorithm—on image quality. The study also aimed to examine this method as a tool to evaluate LCD detectability performance of CT images. An objective method—based on contrast-to-noise ratio (CNR) and LCD phantom, Catphan® 600 (Phantom Laboratory, Cambridge, NY)—was used for this study. Software based on MATLAB (MathWorks, Massachusetts) was developed to objectively calculate CNR values for the phantom image objects.

Phase 3 included the design and manufacture of the proposed LCD phantom for CT, in addition to the development of dedicated software. The functionality of this phantom was examined by testing its consistency across CT platforms. This phase also aimed to develop a method to calculate the inverse value of image quality figure for CT ($CTIQF_{inv}$) values of CT images.

Phase 4 included the experiments of CT with the newly developed phantom. This phase aimed to examine and validate the developed evaluation methodology based on the new LCD phantom and dedicated software.

Each phase required certain materials and equipment, and included several procedures.

1.5.1   Phase 1

The study of Phase 1 required:

a. a CDRAD phantom

b. images analyser software

c. PMMA plates

d. compact discs (CDs) to save the digital images

e. a display monitor (3MP medical colour LCD).

Phase 1 included the following procedures:

a. obtaining digital images for the phantom from CR, IDR and DDR

b. scoring the images by the dedicated software. The software was used to calculate the IQF_{inv} value for each image

c. scoring the images by radiographers. They were asked to indicate the faintest centre spot seen and determine the location of the corner spot seen in each square for each fixed object diameter. Each image was scored six times by six different radiographers. Completed scoring forms were then corrected. The IQF_{inv} value was manually calculated for each image

d. comparing images of each system based on their IQF_{inv} values, including images of

    i. same mAs at different kVp in each system

    ii. same kVp and different mAs in each system

e. comparing images of different systems based on their IQF_{inv} values

f. comparing the scoring results of radiographers and software.

1.5.2 Phase 2

The study of Phase 2 required:

a. a CT Catphan® 600 phantom, LCD module (from Austen and Alfred Hospitals)

b. software based on MATLAB (developed)

c. CDs to save the digital images.

Phase 2 included the following procedures:

a. obtaining CT images of the phantom from multiple detector (MDCT) scanners (16-MDCT, 64-MDCT and 80-MDCT)

b. scoring the images based on quantitative measurements of CNR. Software based on MATLAB (MathWorks, Massachusetts) was developed to calculate CNR values for the phantom image objects (details) of outer location with 5, 6, 7, 8, 9 and 15 mm.

c. comparing CNR values between

    i. different object sizes of the image

    ii. images of different reconstruction algorithms (soft, standard, lung) for each scanner

    iii. images of same mAs and slice thickness at different kVp for each scanner

    iv. images of same kVp and slice thickness at different mAs for each scanner

    v. images of same kVp and mAs at different slice thicknesses

    vi. images from different CT scanners.

1.5.3 Phase 3

Phase 3 included the following procedures:

a. designing a new low contrast-detail CT (CDCT) phantom based on

    i. recommended material and specification of the American Society for Testing and Materials (ASTM)

    ii. optimising the limitations of available phantoms

iii. satisfying the requirement of the phantom purpose (to be used to measure the detectability performance)

b. cooperating with a company to manufacture the phantom and write dedicated software program.

1.5.4 Phase 4

The study of phase 4 required:

a. a low contrast-detail CT phantom (developed)

b. software (developed)

c. a display monitor (3MP or 5MP medical colour LCD)

d. CDs to save the digital images.

Phase 4 included the following procedures:

a. obtaining CT images for the newly developed phantom from 64-MDCT

b. scoring the images by developed software. The software was used to calculate $CTIQF_{inv}$ values, with three values covering the outer, centre and total areas for each image

c. scoring the images by radiographers. This required the radiographers to indicate the objects that they could observe. The $CTIQF_{inv}$ values were manually calculated, with three values covering the outer, centre and total areas for each image

d. comparing images based on their $CTIQF_{inv}$ values, including images of

i. same mAs and slice thickness at different kVp

ii.   same kVp and slice thickness at different mAs in each system

iii.   same kVp and mAs at different slice thicknesses

e. comparing different location levels at each image

f. comparing the scoring results of radiographers and software.

1.6   Thesis outline

This thesis consists of eight chapters. Chapter 1 is an introduction, which includes a brief background and rationale for the study. This chapter also summarises the aims and methodology of the project. Chapter 2 is a literature review of Phase 1, with respect to the radiography experiment phase. It explains the physics of digital radiography systems, determines image quality parameters and discusses the evaluation tools available to the radiography. This chapter also discusses the factors that affect LCD detectability performance. Chapter 3 includes the radiography experiments of Phase 1. This chapter introduces the aims of the study's experiments, explains the methodology and discusses the results and conclusions. Chapter 4 includes the literature review of Phase 2, with respect to CT experiments. It briefly explains the physics of CT and discusses image quality parameters and the evaluation tools of CT image quality. This chapter also determines the factors that affect the LCD detectability performance of different CT scanners. Chapter 5 includes the studies of Phase 2: CT experiments based on the commercially available LCD phantom and CNR measurements. The chapter examines the influences of parameter factors—including object size, reconstruction algorithms, kVp, mAs, slice thickness and system types—on image quality in terms of CNR values. Chapter 6 includes the procedures of Phase 3, and discusses the process of the new phantom and dedicated software

development. The chapter also includes the procedure of phantom consistency testing across CT platforms, and explains the calculation process for $CTIQF_{inv}$ values. Chapter 7 includes the studies of Phase 4: the experiments of validating the new methodology of LCD detectability performance in CT. The chapter explains the evaluation process of the new methodology based firstly on the reading of radiographers and then on the scoring of the software. Chapter 7 then provides a comparison study of the radiographers' assessments and software scoring. The final chapter, Chapter 8, concludes by articulating the findings of this thesis, including limitations and recommendations.

Chapter 2 Low contrast-detail in digital radiography

2.1 Introduction

Digital radiographic images have significant advantages in health services, including improved image quality and a reduction in patient radiation dose. Digital radiographic systems include computed radiography (CR) and direct digital radiography (DR), each of which requires a different type of detector: storage phosphor plate detectors in CR, and flat-panel detectors (FPDs) in DR (Korner et al. 2007; Williams et al. 2007).

No clinical detector can perfectly absorb all the incident x-ray photons. Some photons pass straight through the x-ray detector, while others may be absorbed but then re-emitted and exit the detector. In both cases there is a loss in primary information. The quality of the image may also be degraded by noise from the amorphous array or readout electronics of the detector (Cowen, Kengyelics & Davies 2008). Reliable diagnosis requires regular maintenance of technology alongside regular clinical evaluation of image quality (Pascoal et al. 2005). The essential principle of radiation protection—As Low As Reasonably Achievable (ALARA) or As Low as Reasonably Practicable (ALARP)—should be applied to minimise the radiation exposure to workers and patients (Engel-Hills 2006). Images should therefore be regularly evaluated to ensure the lowest level of patient exposure in order to achieve image quality that enables accurate interpretation. That is, the criteria of optimum image quality should be determined and recognised (Uffmann & Schaefer-Prokop 2009).

This chapter reviews the parameters of image quality and the factors that influence these parameters. It also considers the different image quality evaluation methods that are used to measure CR and DR image quality, and discusses the advantages and limitations of each

method. Accordingly, it also discusses the main topic of this project: the factors that control the LCD detectability evaluation method. Therefore, this chapter includes four main sections. Firstly, it will include a brief background of digital radiography physics. Secondly, it will discuss image quality parameters and, thirdly, will describe the evaluation methods of image quality. The chapter will then conclude with a discussion of the factors affecting LCD detectability performance. The first three parts of this chapter have been published (Appendix 1a) (Alsleem & Davidson 2012).

2.2   Digital radiography systems

Digital radiography comprises two main types: CR and DR. DR may also be further divided between indirect conversion DR (IDR) and direct conversion DR (DDR). The following paragraphs provide a brief description of the physics, properties and advantages of each detector type, followed by results from previous studies that compare and contrast these detectors based on LCD detectability performance.

2.2.1   Computed radiography (CR)

CR systems consist of storage phosphor plates enclosed in a cassette, which are used to detect and store attenuated x-ray photons that pass through patients being imaged (Figure 2.1). The storage phosphor plates are based on material such as barium fluorohalide activated with divalent europium ions or powder-based materials (BaFBr:Eu) (Figure 2.2a). A laser digitiser reads the exposed plates to produce the image (Lanca & Silva 2009b; Samei et al. 2004). CR systems are relatively inexpensive and can be adapted in film/screen

based x-ray units, making them ideal for portable and bedside imaging (Schaefer-Prokop et al. 2008). A recent development of CR employs needle-crystalline CR detectors and utilises dual reading CR. The structure of needle-crystalline detectors—a thicker layer and light pipe shape—increases quantum efficiency and enhances detail resolution (sensitivity and sharpness) of CR systems (Figure 2.2b). These detectors are found to have better low-contrast resolution and potential for dose reduction (Cowen, Davies & Kengyelics 2007; Schaefer-Prokop et al. 2008). Dual reading CR systems are based on transparent detector material: double-sided storage phosphor. These systems utilise light collection optics in the sides, front and back of detectors. Consequently, these new technologies improve quantum efficiency of CR and hence reduce patient doses (Cowen, Davies & Kengyelics 2007; Schaefer-Prokop et al. 2008).
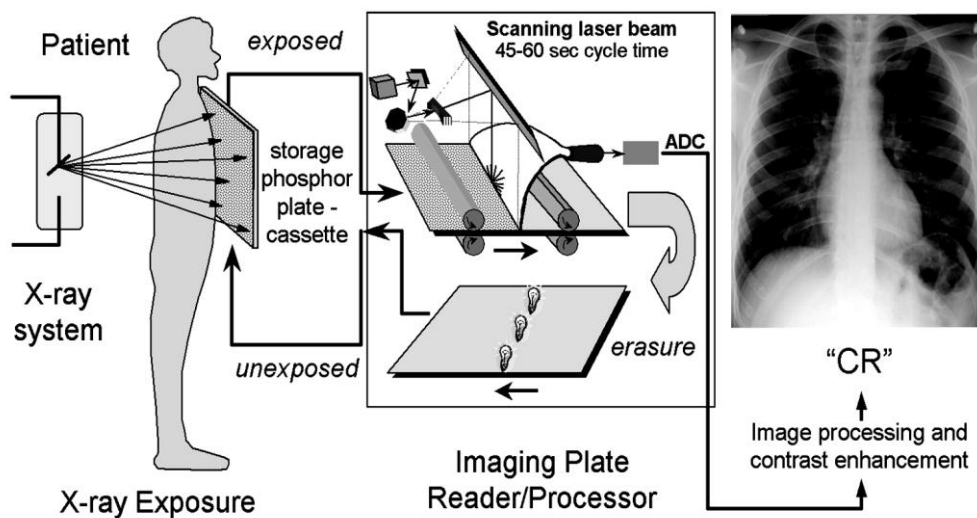
Figure 2.1   Schematic of a CR imaging system including storage phosphor plate and laser scanner (Samei et al. 2004).
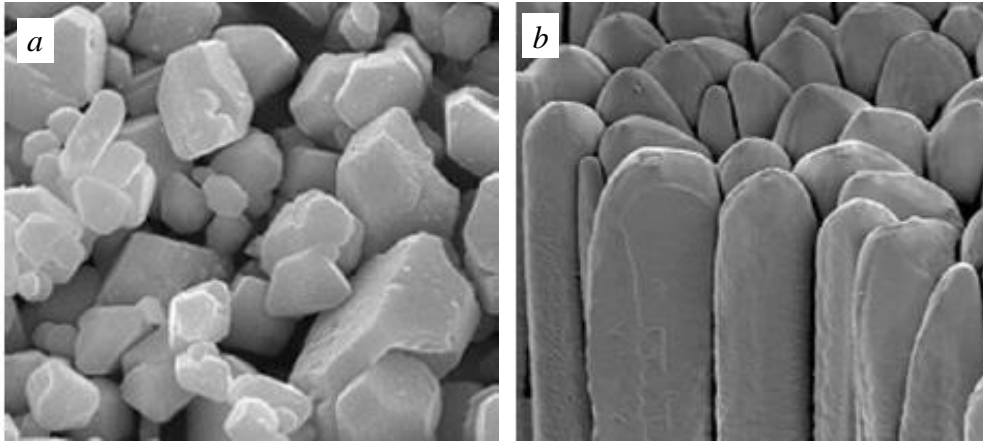
Figure 2.2   Electron microscopic images from powder (a) and needle-structured (b) storage phosphor plates (courtesy of Dr Schaetzing, Agfa, Mortsel, Belgium)(Schaefer-Prokop et al. 2008).

2.2.2   Direct digital radiography (DR)

While storage phosphor plates are utilised in CR, DR employs solid-state FPDs (Figure 2.3). In CR, an image processor (digitiser) scans the exposed storage phosphor to produce the final image, whereas DR utilises flat-panel technology to detect and process attenuated photons from the patient. As mentioned, there are two principal designs of FPDs systems, IDR and DDR. IDR is based on x-ray scintillators and DDR is based on x-ray photoconductors (Figure 2.4).
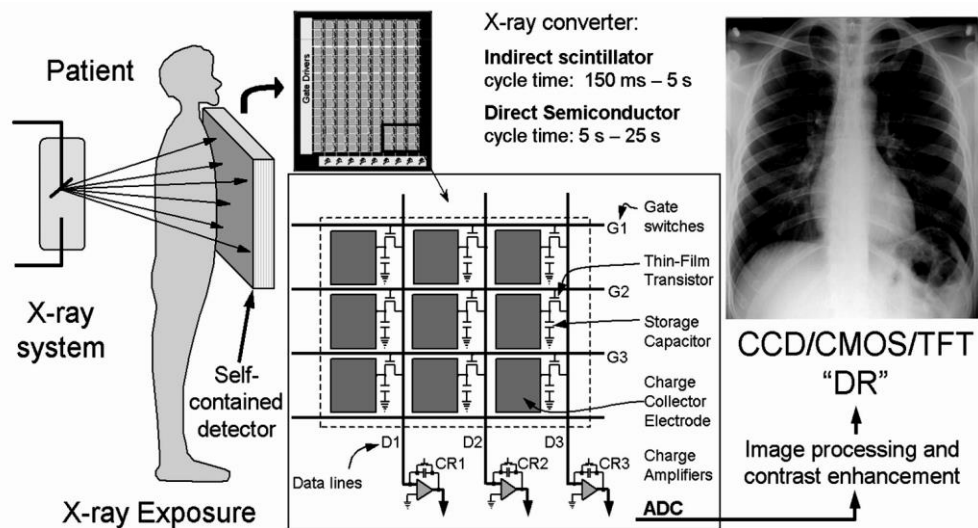
Figure 2.3   Schematic of a direct DR imaging system based on a flat-panel detector, including a thin-film-transistor (TFT) (Samei et al. 2004).
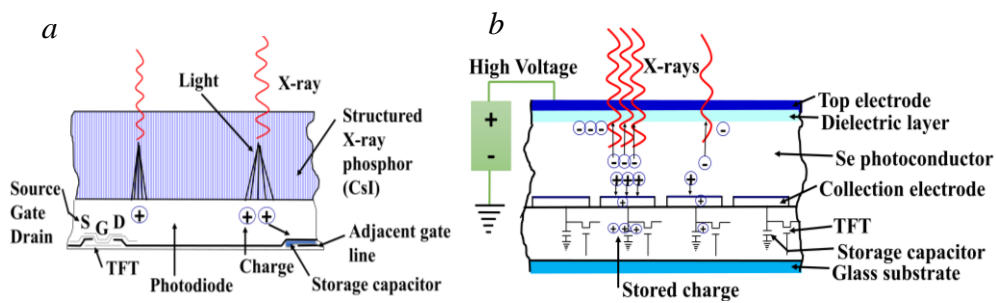
Figure 2.4   Working principle comparison between direct DR (a) and indirect DR (b) (Seibert 2009).

2.2.2.1   Indirect-conversion DR (IDR)

IDR is based on x-ray scintillator materials such as cesium iodide doped with thallium (CsI:Tl). In IDR, the attenuated x-ray photons transmitted through the patient are captured and converted to light photons by fluorescent material. Fluorescent light is then converted to an electronic signal by a two-dimensional readout array of amorphous silicon with added hydrogen impurity (a-Si: H) photo-diodes (Figure 2.4a). The material used for this (CsI:Tl) is an excellent x-ray photons absorber due to its high atomic number, 53 (Cowen, Kengyelics & Davies 2008). The high atomic number and high density of CsI allow for

19

good capture of attenuated x-ray photons and ensure superior IDR performance at low spatial frequencies. In addition, using the needle-like structure of CsI reduces light spreading in the scintillators, as can happen with regular CR systems. A thicker layer can also be utilised to maximise detection efficiency (Veldkamp, Kroft & Geleijns 2009).

2.2.2.2 Direct-conversion DR (DDR)

DDR is based on x-ray photoconductor materials such as amorphous selenium (a-Se) alloyed with re-crystallised arsenic (Seibert 2009). In a DDR detector, there is no intermediate stage of image acquisition, as attenuated x-ray photons from patients are directly captured and converted to electrical signals. An array of photo-conductor material—a-Se alloyed with re-crystallisation arsenic—is used in DDR detectors (Figure 2.4b). The a-Se induces free electrical charge carriers when exposed to x-ray photons (Schaefer-Prokop et al. 2009). Because DDR detectors require no light-to-charge conversion, they are potentially less susceptible to conversion noise than IDR detectors (Samei 2003b).

2.2.3 Comparing between systems

In comparison with film/screen radiography, CR and DR have some limitations. These limitations may include a higher initial cost—particularly for DDR—and the requirement for consistent feedback to obtain optimal acquisition, which may not be available for technologists. Another potential drawback is that, due to the wide dynamic range of digital systems, patients may be exposed to more radiation than is required for a diagnostically

sufficient image. It is also possible that diagnostic information may be suppressed as a result of suboptimum image processing (Schaefer-Prokop et al. 2008; Williams et al. 2007).

In comparison with IDR and DDR, CR is more affordable and more applicable in some aspects. That said, the price of DR is decreasing and the viability of portable DR is becoming available. One significant drawback of CR is the delay in image reporting due to the time-consuming process of cassette handling and phosphor plate scanning (Cowen, Davies & Kengyelics 2007). In contrast, DR images can be obtained with lower radiation dose and can be displayed on-line as digital data (Cowen, Kengyelics & Davies 2008). DDR has performed better than IDR at the higher spatial frequencies, as DDR systems show less blurring of the image signal (Veldkamp, Kroft & Geleijns 2009).

2.3   Image quality parameters

Resolution, noise and artefacts are the main parameters that characterise the quality of digital images. (Goldman 2007). Image quality parameters and their influence factors are demonstrated in Figure 2.5.

Figure 2.5   The parameters of image quality and the influence factors of each parameter.

Resolution relates to the ability of imaging systems to produce medical images that can discriminate between tiny adjacent structures of tissue. Resolution implies that the signals from detected photons during imaging process should be sufficiently recorded—in space, intensity, and possibly time—to acquire an appropriate diagnostic image. Therefore, resolution can be classified into three main categories: spatial resolution (detail visualised in the image), contrast resolution (range of intensities visualised in the image) and temporal resolution (time relationship between images). Appropriate image quality requires higher resolution to enable successful interpretation of tissue structures and organ functions (Bourne 2010). Temporal resolution is not discussed in this chapter, as it is more closely

related to digital fluoroscopy and advance-imaging modalities such as computed tomography (CT).

2.3.1 Spatial resolution and/or blur

Spatial resolution refers to the ability of an imaging system to detect and discriminate small high contrast objects that are close together (Williams et al. 2007). Spatial resolution is influenced by the size of pixels and the spacing between them, with smaller pixel sizes improving spatial resolution. When pixels are smaller than the size of a single element of the detector, however, the image structures may be smeared out. This can cause contrast to be reduced, unless the structures have inherently high contrast (Williams et al. 2007). Spatial resolution is also influenced by other factors, such as blur elements caused by image processing and zooming (Bourne 2010; Chotas, Dobbins & Ravin 1999; Williams et al. 2007). Blur factors that relate to resolution are sometime included as quality parameters (Hendee & Ritenour 2002; Tsai, Lee & Matsuyama 2008). Image blur refers to a sharpness of object boundaries in the image, with 'sharp' images depicting well-defined organ structures (Samei 2003b). The blur is caused by four main factors: subject blur, geometric blur, motion blur and receptor blur (Samei 2003b).

Subject blur—or object blur—is caused by the shape and anatomical structure of the object (Samei 2003b). Geometric blur is formed by the geometry of imaging systems and image production procedures, with the main factors being the focal spot size of the x-ray tube, the distance between the x-ray source and the patient, and the distance between the patient and the image receptor. Larger focal spot sizes, and greater distance between the patient and the image receptor, can increase border blur (Samei 2003b). Unequal magnification of

organ constructions can also cause image distortion (that is, blur or distortion in the image details). For example, the closer the tissue is to the image receptor, the lesser the magnification and hence the lower the image blur (Hendee & Ritenour 2002).

Motion blur is the most problematic blur factor, occurring when organs move during the imaging process. In such cases, the boundaries of patient structures are blurred as they move from their original position. The motion that originates from the anatomic region being imaged can be either a voluntary action of the patient or an involuntary physiologic process. Voluntary motion can mostly be controlled by applying short-time examinations, providing appropriate instructions to the patient, and utilising physical restraints and anaesthetics. Involuntary motion—including heartbeats and bowel peristalsis—cannot be stopped; their motion influences may only be minimised by medication or through very short examinations (Samei 2003b).

Receptor blur originates from the image receptor, where the data is produced and gathered during the imaging process. Physical detector characteristics determine the spatial resolution. The intrinsic spatial resolution of structured caesium iodide utilised in CR and IDR is higher than that of unstructured scintillators. The detectors of the intrinsic spatial resolution of amorphous selenium utilised in DDR system is higher than that of structured caesium iodide (Chotas, Dobbins & Ravin 1999). Receptor blur features are also influenced by the thickness of the detector; thicker detectors increase receptor blur and detector sensitivity reduces with thicker detectors (Hendee & Ritenour 2002).

Receptor blur is also formed by scatter radiation and photoelectric interactions in the detector when the photon energy dissipates. This blur is caused when the photon energy—or at least part if it—deposits somewhere in the detector other than the original point of entry. The movement and scattering of the laser beam—which is used to stimulate the

storage plate in CR system—are also sources of blur (Samei 2003b). This blur is the primary source of special resolution loss in CR during storage plate readout by laser light (Williams et al. 2007). The blur increases with thicker phosphor as the scattering depth increases, although thinner detectors are possible with the introduction of structured phosphor which provides better detection efficiency without much loss of spatial resolution (Williams et al. 2007).

Receptor blur and/or special resolution loss is also caused when the light photons spread during the x-ray-to-light conversion process in IDR. Utilising structured phosphor—which increases detection efficiency and minimises scattering light—can improve spatial resolution. DDR does not suffer from this effect as the electrons within the photoconductor material are directed towards the TFT array so that the spread of electrons is limited (Williams et al. 2007).

Image processing and post-processing applications may also alter image spatial resolution, however the noise that deteriorates the image quality may increase with excessive use of image processing (Bourne 2010).

Spatial resolution can be evaluated by different methods, including the point spread function (PSF), line spread function (LSF) and the modular transfer function (MTF) (Samei et al. 2006).

2.3.2 Contrast resolution

Contrast resolution refers to the ability of imaging systems to discriminate objects of low contrast or of small attenuation variety on the image (Williams et al. 2007). Contrast

resolution explains how well the image discriminates subtle structures in organs being examined (Hendee & Ritenour 2002). While high frequency or high contrast regions refer to spatial resolution, low contrast regions refer to *contrast* resolution. High frequency is the area between two small objects with large differences in density, whereas the low-contrast region is the area between two small objects with small density difference (Goldman 2007).

Contrast resolution can be attained by recording the information of examined tissues with sufficient intensity resolution to discriminate the contrast-details (Bourne 2010). In comparison to spatial resolution—which is affected by the digitisation phase or sampling in space—contrast resolution is affected by quantisation of the signal intensity phase and the gravy-scale bit depth (Krupinski et al. 2007).

Contrast resolution is influenced by tube collimation, beam filtration, number of photons, noise, scatter radiation, detector properties and image algorithmic reconstruction (Goldman 2007). It depends on four factors: subject contrast, imaging methods and techniques, detector contrast, and displayed contrast (Hendee & Ritenour 2002).

Subject contrast refers to the intrinsic factors of the objects being imaged, including their anatomical and physiological characteristics. This is also called 'intrinsic', 'object' or 'patient' contrast. Tissues that have very subtle differences in composition—such as the breast—are called low intrinsic contrast tissues. Subject contrast is influenced by the physical density differences between tissues and thickness differences between organs (Hendee & Ritenour 2002).

Imaging technique is the second major factor that can influence image contrast resolution. Adjusting exposure techniques appropriately for specific tissues—and for certain purposes—greatly enhances image contrast. Low kVp and small amounts of beam

filtration, for example, are preferable in mammography to discriminate the small differences between tissue structures. On the other hand, high kVp and large amounts of beam filtration are used in chest radiography to demonstrate a wide range of tissue densities (such as lung and bone tissues). These techniques are essential to detect lesions and diagnostic details of the examined tissues (Hendee & Ritenour 2002).

Introducing contrast enhancement materials into the body can change subject contrast and hence improve image contrast. Contrast media changes photon attenuation properties from those of the surrounding tissues and therefore provides signal differences (Hendee & Ritenour 2002).

Contrast resolution of the image is also greatly influenced by detector contrast, which is determined by the characteristics of the detector. Detector contrast is explained principally by how the detector detects and converts energy into signal output. The contrast resolution of the image is influenced by the detector's dynamic range (Hendee & Ritenour 2002), which is the ratio of the maximum to minimum input x-ray intensities on the detector surface. The dynamic range of CR and DR varies from 1,000:1 to 10,000:1, while the dynamic range of film/screen radiography varies from 10:1 to 100:1 (Williams et al. 2007).

Contrast resolution of digital images is influenced by the attributes of image display that are utilised to produce and demonstrate the final image. For example, image contrast can be altered and adjusted when the images are displayed on a screen. The data of images can be demonstrated in a wider range of a gray-scale when viewed digitally. While digital imaging systems can enhance contrast resolution of images (Hendee & Ritenour 2002), the process and equipment—particularly for primary display or diagnostic interpretation—should be compliant with the current standard of Digital Imaging and Communications in Medicine (DICOM). DICOM standards are regulated by, for example, the American

College of Radiology (ACR) and the National Electrical Manufacturers Association (NEMA), particularly on gray-scale displays.

There are two categories of image display size: small matrix and large matrix. The small matrix is used in CT, digital fluorography and digital angiography. The large matrix is used in CR, DR and digital mammography. A monitor of 5 megapixels (MP)—typically 2048 x 2560 pixels—is sufficient for viewing digital images, particularly CR and DR images. It is important to utilise zooming and roaming display functions to achieve a correspondence between the display pixel matrix and the detector element matrix; this avoids resolution limitations of the monitor for partially displayed images. Appropriate display luminance should be uniform over the entire display and at a level of at least 200 cd/m^2. Bit depth resolution controls luminance quantification of the soft copy display, therefore larger bit depth resolution is recommended to prevent the loss of contrast-details or the appearance of contour artefacts. Viewing environment and conditions—such as room lighting and the light reflection of other display monitors—can also affect image display quality (Krupinski et al. 2007).

2.3.3 Noise

Noise is distracting information caused by the statistical fluctuation of value from pixel to pixel (Goldman 2007; Sprawls 1995). It is typically recognised by a grainy appearance and characterised by a salt and pepper pattern on the image (Goldman 2007). Noise relates to the number of x-ray photons that are logged in each pixel (for DDR) or in each small area of the image (for CR and IDR) (Samei 2003b; Tapiovaara 2008). Goldman (2007) classifies

noise sources as three types: quantum noise, electronic/detector noise and computational/quantisation noise.

Quantum noise appears when too few photons are received from the body by detectors. The lower the number of attenuated photons at the detector, the higher the image noise (Samei 2003b). The quantum noise increases with a larger body and smaller pixel size. The anatomical noise is the disturbing anatomic background variability (Tapiovaara 2008).

Detector or receptor noise—the effects of which are sometimes called electronic noise (Williams et al. 2007)— is produced as a result of a non-uniform response to a uniform x-ray beam (Sprawls 1995). It originates from different causes—mainly internal to the image receptors—and creates unwanted signals or unrelated structures on the image. Manufacturing defects in the receptor's elements, for example, can form such unrelated structures (Williams et al. 2007). The main causes of structure noise, particularly in DR, are variations in pixel-to-pixel sensitivity and linearity, dead pixels, and detector-response non-uniformities (Samei 2003b). The noise that has fixed correlation to a location on the receptor can be largely eliminated through post-processing stages (Williams et al. 2007).

Conversion noise is also called instrumentation noise, and results from fluctuations in generated energy per detected photons. It can be reduced by utilising a higher-intensity scanning laser in CR detectors and brighter phosphor screens in IDR. This enables more secondary energy carriers to be generated, which reduces image noise. In addition, conversion noise can be reduced by lowering the number of conversion stages in the process (Samei 2003b).

Quantisation noise occurs during the digitisation process, which involves translating the analogue output voltage of the detector to discrete pixel values (gray-scale values). The

range of pixel values is determined by bits, binary on-off channels; the recommended range to minimise quantisation noise is 10 to 14 bits, which have range of digital values from 1,024 to 16,384 (Williams et al. 2007).

Scatter radiation is also a factor of noise formation on an image. Subject contrast and signal-to-noise ratio (SNR) can be negatively affected by scatter radiation that causes image noise. Noise from scatter radiation effects can be reduced by using the grid, although the signals of incomplete transmission of the primary radiation by the grid are also reduced (Williams et al. 2007).

2.3.4   Artefacts

Image artefacts are features that occur on the image and mask or mimic clinical features (Willis, Thompson & Shepard 2004). Hardware (mainly the detector) and software processes are the main causes of digital image artefacts (Bushong 2013; Honey & Mackenzie 2009; Shetty et al. 2011), although image 'acquisition' artefacts are caused due to errors by the operator or radiographer. These errors include inappropriate exposure factors, improper grid usage, exposed image receptors and handling carelessness (Shetty et al. 2011). Object artefacts are also caused by incorrect patient position, improper x-ray beam collimation, patient motion and double exposure (Drose, Reese & Hornof 2008). Moreover, improper collimation of the exposure field can lead to very noisy images, either very dark or very white. Inappropriate histogram selection and histogram analyses errors can also cause object artefacts (Bushong 2013), as can metal objects (Drose, Reese & Hornof 2008).

Receptor artefacts of digital images occur with rough handling, dust, malfunction of pixels, faulty construction or detector scratches and cracks (Shetty et al. 2011). In addition, malfunction of rollers in the digitiser of CR image plates can cause defective scanning that can result in artefacts. Receptor artefacts are also caused by partial erasure of a previous image, which creates ghost artefacts particularly in the image storage plate of CR. Similarly, ghost artefacts can be caused by environmental radiation (Bushong 2013). Receptor artefacts that result from dead or faulty pixels cannot be treated and therefore the detector may need to be replaced (Shetty et al. 2011).

Software artefacts occur with inappropriate use of software filters of grid suppression, low pass spatial frequency filter and blur masking (Honey & Mackenzie 2009). Software artefacts can be caused by image transmission (communication) errors or failures (Shetty et al. 2011), and may occur with incorrect flat field corrections and a failing amplifier (Honey & Mackenzie 2009). They are also caused by dead pixels of detectors during the image processing stage. Even though a few dead pixels may not interfere with diagnosis, many of these faults must still be corrected. Image compression is employed to facilitate transmitting and archiving of images, but software artefacts may be created by lossy compression techniques that cause redundancy of data.

2.3.5   Image quality and radiation dose

The central goal of medical imaging is to achieve optimal image quality at the lowest possible radiation dose to patients, without losing the diagnostic value of the image (Seibert 2004). This objective is explained by the principle of radiation protection—ALARA or ALARP—that should be implemented to control radiation exposure to workers and patients

(Engel-Hills 2006). The minimum required level of image quality and the amount of dose reduction should be determined based on diagnostic requirements (Schaefer-Prokop et al. 2008). The opportunity for image quality optimisation has been increased with the introduction of CR and DR (Seibert 2004), although radiation dose factors should still be recognised. The main factors that control radiation dose include mAs, kVp, detector properties and patient size (Seibert 2004).

There is a linear relationship between mAs and radiation dose: radiation dose to patient reduces with reducing mAs. However, noise is associated with lower radiation dose and hence SNR reduces with lower mAs levels. Lower radiation dose deteriorates contrast resolution of the image and increases the risk of losing diagnostic details due to the higher noise (Aichinger et al. 2012).

Selecting lower kVp techniques is more likely to improve SNR in CR and DR, and hence improve the contrast resolution of the image (Schaefer-Prokop et al. 2008). Lower kVp increases x-ray attenuation and consequently can improve the contrast of structures. Lower voltage also increases the detection efficiency of the detectors and therefore improves image quality (Launders et al. 2001). Despite this, low kVp techniques may increase the radiation dose when other exposure factors adjusted, which also may increase image blur with longer exposure time selection (Schaefer-Prokop et al. 2008). Uffmann et al. (2005) found that 90 kVp demonstrates the anatomic structure more clearly than 120 and 150 kVp, without increasing the radiation dose to patients. Changing kVp from 102 to 133 did not significantly improve contrast resolution of CR and DR (De Hauwere et al. 2005), although thicker body organs require higher kVp to optimise the contrast resolution of the image (Olaf & Wolfgang 2009).

Higher kVp techniques may cause blooming or pixel saturation. Blooming occurs when the saturation of the detectors is exceeded by illumination. When pixels are overfilled, they lose their ability to accommodate additional charge and hence the excess charge leaks to other pixels, causing the image quality to deteriorate (Rahn et al. 1999).

Different detector systems have different detection efficiency and hence different ability for radiation dose reduction (De Hauwere et al. 2005). Thicker detectors have better detection efficiency and hence higher ability for dose reduction (Uffmann et al. 2004), whereas smaller detector elements require a higher radiation dose but provide better spatial resolution of the image (Seibert 2004).

The parameters discussed above are not independent, as there are trade-offs between them when they are manipulated individually. Therefore, these parameters should be manipulated to acquire appropriate image quality for specific purposes and specific regions. Figure 2.6 demonstrates the dependent relationship between image quality parameters: when spatial resolution is increased to get better image quality for bone tissue, the noise of the image visually increases (Goldman 2007). Eliminating or limiting the effects of image degradation factors is essential in image quality optimisation (Kalender & Khadivi 2011; Seeram 2009), and radiation dose—which is a fundamental principle of image quality—should therefore be considered beside these parameters. Optimal image quality is the balance between image quality parameters and maintaining a low dose to patients, based on the region   being studied and the case being examined (Kalender & Khadivi 2011; Seeram 2009).

Figure 2.6   Optimum image quality has adequate spatial resolution and contrast, and a low noise level, as demonstrated in the image (A). Image B has high spatial resolution and low noise, but it has almost low image contrast and high brightness. Image C has low noise and high contrast, but very reduced spatial detail. Image D has high spatial resolution but has high noise level, which has also reduce the image contrast.

As above, a good understanding of radiation dose factors—and their influences on image quality—is essential to maintaining lower radiation dose without losing the image quality required for the specific purpose.

Spatial resolution, contrast resolution, noise/dose and artefacts are judged objectively and/or subjectively to measure image quality level. Objective assessments are based on static measurements and subjective judgments are based on human observation (Tapiovaara 2008).

2.4 Image quality evaluation methods

The usefulness of radiologic images and the accuracy of image interpretation depend on two main factors: the quality of images and the ability of the interpreter. Good image quality allows physicians to interpret the image more accurately and quickly (Krupinski & Berbaum 2009). Therefore, images should be optimised to maintain lower radiation dose to patient without losing the required level of quality (Seibert 2004). To ensure this, image quality—and the performance of imaging systems—should be regularly evaluated.

Certain attributes are required for evaluation tools of image quality to be used as quality control. These tools should directly describe diagnostic performance, sensitively detect changes in the imaging system, are not be too expensive or labour-intensive (Tapiovaara 2008). Several methods are used to assess image quality parameters and imaging performance of DR systems, including physical (quantity measurements), clinical (observers/diagnostic) performance or psychological (Figure 2.7). Physical methods include detection quantum efficiency (DQE) and information entropy (IE). Clinical performance measurement methods include receiver-operating characteristics (ROC) and visual grading characteristic (VGC). Psychophysical evaluation methods include the Rose model (RM) and low contrast-detail (LCD) detectability performance. Figure 2.8 summarises the different evaluation methods of image quality and imaging system performance.
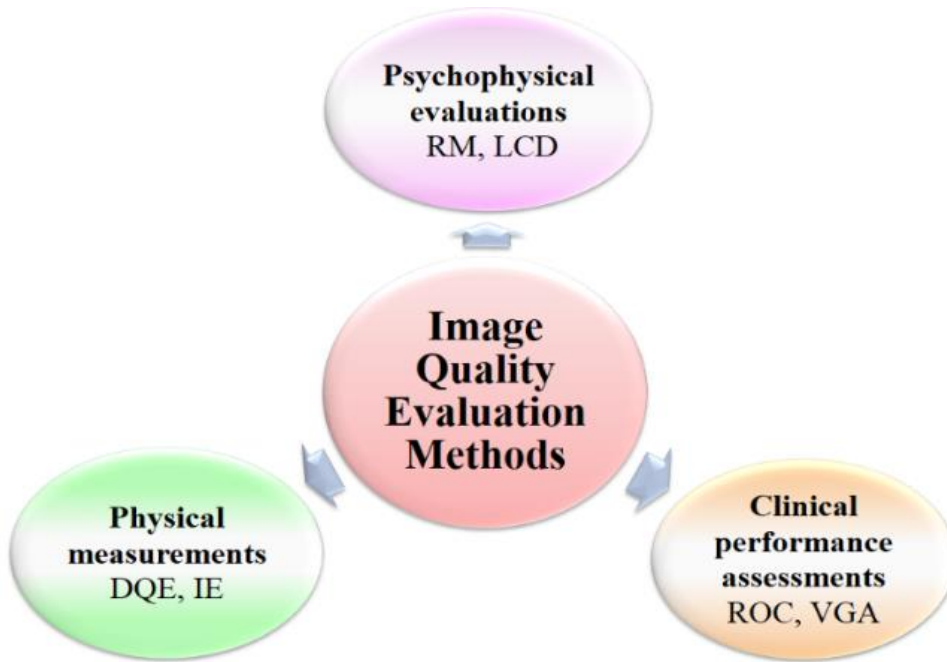
Figure 2.7   The types of evaluation methods of image quality.

Detective quantum efficiency (DQE)	• Measurement parameters are MTF and NPS • Focus on image receptor performance
Information Entropy (IE)	• Measuring (quantitatively) how much information (randomness/uncertainty) is transmitted by signal/image
Receiver operating characteristics (ROC)	• Measuring sensitivity & specificity of imaging system by comparing images to true disease status of patient
Visual Grading Characteristic (VGC)	• Using one or more reference images or quality criteria to assess visibility of specific features on image.
Rose Model (RM)	• Using images to estimate the maximum of information can be translated into visible image by photons numbers
Low Contrast Detail (LCD) Detectability	• Using phantom of a range of different densities & sizes of samples (quantitative measurements)

Figure 2.8   Evaluation tools used to assess image quality and imaging system

performance

2.4.1 Detective quantum efficiency (DQE)

The evaluation method of DQE is commonly used to assess the image receptor performance of imaging systems. DQE is based on a purely quantitative analyses of objective parameters related to detector performance, and is therefore considered an indirect method of image quality evaluation (Pascoal et al. 2005). DQE characterises image quality by quantifying SNR for the number of incident x-ray photons (Ranger et al. 2007). It is based on linear systems analysis (LSA), which is used to assess the ability of the detector to transfer a signal and to characterise the noise associated with the detector. The main measurement parameters of DQE methods are the modulation transfer function (MTF) of the system and the noise power spectrum (NPS). The MTF describes the system's ability to reproduce and preserve the information of spatial frequency contained in the incident x-ray signal, while the NPS describes the frequency content of the noise in the spatial frequencies of the image (Bath 2010; Tsai, Lee & Matsuyama 2008). MTF is calculated in different ways, which will alter the approach and quantities of DQE. MTF has also been used separately as a tool of image quality assessment (Bath 2010). DQE ranges from 0 to 1; a perfect detector performance that produces information content exactly corresponding to that of photons beam has a DQE of 1 (Miracle & Mukherji 2009).

In general, the DQE method and its different approaches have several drawbacks. For example, these approaches do not provide a description of all components in the imaging process, and therefore provide limited information about the final characteristics of the image. Dose level and display factors that influence final image appearance are not considered in DQE; nor are factors such as scatter radiation and image processing. DQE and its approaches also fail to consider the observer, which is the second key element in reliable radiology diagnosis. Similarly, they do not consider anatomical background, which

may hinder observer performance in detecting pathology (Bath 2010). Anatomical background refers to the ability of observers to detect the influence of anatomical details, although the mechanism of this effect is not clearly understood (Tapiovaara 2008). Recent DQE approaches have exhibited higher reliability with respect to providing accurate measurement of information transfer, however their validity in assessing the entire imaging process is relatively low (Bath 2010). In addition, the approaches of DQE are difficult to implement as regular evaluation procedures of image quality assessment. They are time consuming, complex (Pascoal et al. 2005) and do not describe the sharpness of the final image (Bath 2010).

Effective DQE (eDQE)—the modified and improved approach of DQE—addresses some limitations of DQE (Samei et al. 2009). For example, eDQE considers scatter radiation and image processing that influence the quality of the final image (Samei et al. 2008, 2009).

2.4.2   Information entropy (IE)

The evaluation method of IE is a quantitative measure of the information transmitted by the image (Tsai, Lee & Matsuyama 2008). IE evaluates the physical measurements of image quality (Uchida & Tsai 1978) and measures how much information (randomness/uncertainty) is provided by the signal or image. IE is a simple and straightforward method as it is based on a single parameter: transmitted information (Uchida & Tsai 1978). In this method, step wedge phantoms of varying thicknesses are used to measure the image quality. The images of the phantom show a gradual scale of grey level with diverse values, and are obtained with a variety of exposure times to assess the

image quality of the radiography system. The more information conveyed and included in the image, the better image quality acquired (Uchida & Tsai 1978).

The main advantage of IE is that the final image is considered in the evaluation procedure. IE also has simple computation and a combined assessment of image noise and spatial resolution. Despite these strengths, the validity of this method is limited because human observers are not involved in the evaluation process. In addition, reliability is limited by the simplicity of the phantom used. The step wedge phantom contains several different thicknesses but does not consider the sizes of objects/details (Tsai, Lee & Matsuyama 2008). IE measures also do not provide frequency information compared with MTF and NPS, and do not demonstrate the effects of different noise sources such as the electronic noise and structural noise.

2.4.3   Receiver-operating characteristics analysis (ROC)

ROC is a task-based method used to evaluate image quality and performance of imaging systems. It involves human observers to measure sensitivity, specificity and accuracy of diagnostic imaging systems. The sensitivity measurement describes the ability of the imaging system to assist interpreters to correctly diagnose the disease when the patient actually *has* the disease. The specificity measurement describes the ability of the system to assist observers to correctly *exclude* the disease when the patient does *not* have the disease (Bath 2010; Obuchowski 2003).

ROC measures the accuracy of the imaging system by comparing the results of the system with the true disease status of the patient (Obuchowski 2003). There are several variations of ROC analysis, including the ROC curve, multiple-reader multiple-case, and free-

response ROC analysis. ROC and ROC-related approaches are considered the gold standard to measure the accuracy of imaging systems and to compare different imaging modalities in terms of detectability of specific pathology (Bath 2010).

However, ROC evaluation methods depend solely on the existence of pathology or a certain disease—or signals of the disease—in the evaluated images. This dependency is considered a serious drawback of ROC. The clarity percentage of disease or signals in the image differs from case to case, as some patients suffer from that disease only at 1% and other patients suffer at 99%. Hence, an appropriate evaluation tool should be independent of the prevalence of disease or signals. The ROC evaluation method and related approaches also require a large number of cases, making it cumbersome and time consuming. Additionally, reliability of the ROC method and related approaches is relatively low. Interpreters, even experienced radiologists, may behave differently in an experimental environment compared with a clinical environment (Bath 2010).

2.4.4 Visual grading characteristics (VGC)

The method of VGC, which is also known as VG analysis (VGA), is a common clinical-based evaluation tool of image quality. It is based on the ability to detect and perceive pathology and correlates well with precise anatomical demonstration (Bath 2010; Ludewig, Richter & Frame 2010). VGC comprises relative grading and absolute grading approaches. In the relative grading approach, observers use one or several reference images to evaluate the quality of each images with the matching landmark. The decisions of observers are categorised on a scale of 3, 5 or 7 points. For example, a 5 points scale includes +2 = much

better, +1 = slightly better, 0 = equal, −1 = slightly worse, and −2 much worse (Ludewig, Richter & Frame 2010).

In the absolute grading approach there is no reference image, but instead a standard list of features is used to evaluate image quality. These features are called 'quality criteria' (Bath & Mansson 2007), which have been developed by professional radiologists, technologists and physicists, and describe physical and anatomical characteristics of image appearance and dose level. For example, chest examination criteria are used to evaluate chest images by letting experienced radiologists and technologists determine to what extent the image fulfils the criteria (Bath 2010).

Observers are asked to state their decisions based on the visibility of specific features in the image being assessed, with their decisions typically categorised by a grading scale ranging from 4 to 7 points. A five point grading scale, for example, includes excellent image quality, good image quality, sufficient image quality, restricted image quality and poor image quality. Excellent image quality implies no limitations for clinical use. Good image quality means that there are minimal limitations for clinical use. Sufficient image quality implies moderate limitations but no considerable loss of information. Restricted image quality indicates relevant limitations and clear loss of information. Poor image quality implies that the image must be repeated due to information loss (Ludewig, Richter & Frame 2010). The absolute grading method has several advantages which make it preferable, but still has some important limitations (Ludewig, Richter & Frame 2010).

VGC evaluation methods have high validity as they consider almost all imaging factors that control image quality, including image processing, recording, post-processing and interpreting. These methods are also based on the visualisation of clinically relevant standards and daily situations. In addition, VGC methods have easier procedures and

require less work than ROC. That is, the required time for interpreters to read images is reasonable, resulting in no real barriers to participation (Ludewig, Richter & Frame 2010). VGC can also be used to compare the imaging performance of different imaging modalities (Bath 2010).

The main limitations of VGC include false positive features and/or irrelevant clinical situations (Bath & Mansson 2007). Another limitation relates to the difficulties in analysing uncertain data from VGC, as it is difficult to establish if the underlying reasons for the uncertainty relate to poor image quality, observer influence or other factors (Ludewig, Richter & Frame 2010). Furthermore, the reliability of this method is limited by the subjectivity of observers (Bath 2010).

2.4.5   The Rose model (RM)

The method of RM is based on SNR, and evaluates the quality of digital radiographic images. Radiographic images of a phantom model are used to estimate the maximum amount of information carried by transmitted photons that can be translated into a visible image. RM is a simple model utilised to assess the detectability of signals by human observation, providing a description of an object's visibility in an image (Burgess 1999). Later, a phantom of a number of disc-like objects of different size (0.3–8.0 mm diameters) and diverse contrast, represented by sample depth (0.3–8.0 mm), is used to measure image quality based on SNR measurements. SNR describes image noise and resolution features and human visual system (Giovanni et al. 2006).

However, RM has some drawbacks that influence its reliability and validity. SNR, which is an essential measurement of RM, does not consider the effect of object size on

detectability. Moreover, the noise description that is used in SNR is overly simplistic for observers who are sensitive to noise features. In addition, observers are mostly not interested in single pixel values and are not affected by the pixel-to-pixel variations. Observers are also seldom affected by pure noise from the anatomical background. As such, the validity of using SNR methods to measure image quality is very low, and RM is therefore not recommended to compare different imaging systems or processing procedures (Bath 2010).

2.4.6   Low contrast-detail (LCD) detectability performance

The method of LCD detectability performance is a widely used tool to evaluate image quality, providing quantitative evaluations of low contrast objects and small detail measurements of medical images (Bath 2010; Uffmann et al. 2004). LCD detectability performance originated from the theory of signal detection, which implies that the detectability performance of LCD is related to the internal SNR of the observer (Swets et al. 1978; Uffmann et al. 2004). The main assumption of the theory is that noise from different sources interferes with the sensory stimuli of the human observer (Green & Swets 1988). The LCD detectability performance of a system is determined by its ability to visualise small objects of low contrast (Chao et al. 2000). The detectability of detail increases with increasing object size and/or contrast between object and background. For example, the detectability of objects with the same contrast will increase in line with an increase in object size. Similarly, when object size is maintained, detectability will increase with increasing contrast. Hence, small objects can have higher contrast than larger objects for the same detectability (Davidson 2007; Faulkner & Moores 1984).

LCD detectability performance is measured by utilising a LCD phantom containing details (drilled holes of varying diameter) of different contrast levels (varying depth) (Lu et al. 2003) (Figure 2.9). The ability of observers to detect the smallest objects of different contrast with the background is measured to assess the image quality in terms of LCD detectability performance. Therefore, LCD detectability performance is considered a subjective evaluation method (Pascoal et al. 2005). LCD detectability performance is measured by asking observers to indicate what they can detect on the phantom image on the first three rows, and to indicate and locate the objects that they can detect on the remaining rows. The objects are located in different corners to avoid a false positive score. The LCD curve can be obtained by plotting the smallest visible diameter (D_i) against the smallest visible depth (C_i) for each row (i). Equation 2.1 is used to calculate the inverse values of image quality figure (IQF_{inv}) (De Hauwere et al. 2005). The greater the value of the IQF_{inv}, the better LCD detectability performance (De Hauwere et al. 2005).

$$IQF_{inv} = \frac{100}{\sum_{i=1}^{15} Ci,th * Di,th} \qquad \qquad Equation\ 2.1$$

Where $C_{i,th}$ is threshold contrast, and $D_{i,th}$ is threshold detail (De Hauwere et al. 2005).
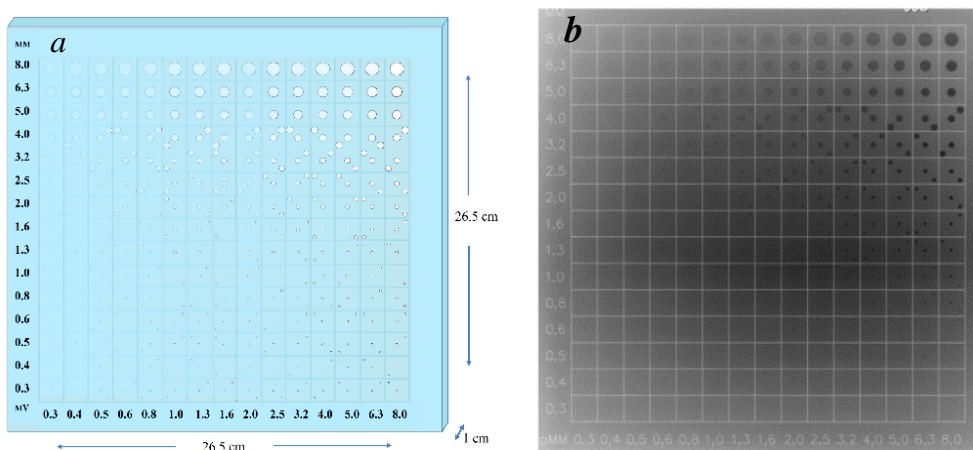
Figure 2.9   Schematic diagram of CDRAD phantom (a). A radiograph of CDRAD phantom (b).

The evaluation method of LCD detectability performance provides quantitative measurements of low contrast and small detail detectability of medical images. It is a direct and straightforward method of image quality evaluation (Bath 2010; Uffmann et al. 2004). As it considers imaging factors such as detector design, x-ray parameters, image acquisition, processing, manipulation and image display, this method provides insightful understanding of digital imaging systems (Aufrichtig & Xue 2000). It is also based on the use of phantoms, and therefore does not require volunteer patients, and can effectively determine the trade-offs among perceived image quality, diagnosis efficacy and exposure dose (Shet, Chen & Siegel 2011). This method can also be used to compare and contrast the image quality of different systems (Uffmann et al. 2004), and is therefore useful for quality control and standardisation purposes, and for indicating typical or acceptable performance in medical imaging systems (Tapiovaara 2008). A recent study by De Crop et al. (2012) investigated the correlation between the results of LCD detectability performance measurements and clinical image quality assessments in chest radiography. The researchers found that a correlation exists between the two methods, and concluded that LCD detectability performance is the appropriate method for image quality optimisation (De Crop et al. 2012).

There are two main approaches with the LCD evaluation method: the subjective approach based on human observation or the objective approach based on automated software (Pascoal et al. 2005). It is essential to first discuss the process of human observation in order to then justify the importance of the automated software approach.

2.4.6.1 LCD analysis - human observation

Human observers—or interpreters—are ultimately responsible for making decisions regarding whether or not an image represents an abnormality for the patient (Bath 2010). Therefore, the role of image interpreters—radiologists—is essential and they should be equipped with appropriate interpretation expertise. Given that radiologists must read LCD phantom images in order to measure image quality and detectability performance of image systems, it is essential to now recognise and discuss the process of human observation.

The perception of visual information comprises three chronological processes: detection, recognition and perception. Detection of visual signals by the observer is the first process. Detected visual information is integrated into the perceptual procedure, which means that observers may be unable to detect important information of radiologic images because visual signals are not well understood. Hendee and Ritenour (2002) found that observers miss 20% to 30% of the information contained in medical images. There are also inter-observer variations for the same images (occurring in 10% to 20% of images) and *intra*-observer variations (5% to 10% of images), which refer to disagreement with a previous reading by the same observer (Hendee & Ritenour 2002).

Recognition is the next process of visual perception, where the detected information is distinguished as normal or abnormal, important or unimportant, and expected or unexpected. Observers may ignore important visual signals because they are considered inconsequential and are not fully understood or appreciated. Giger, Chan and Boone (2008) found that characterisations of abnormalities on images by observers are not always accurate. Recognised visual information is then incorporated into the interpretive process.

The interpretation process is the third phase of visual perception, where the detected important information is gathered and processed to correctly diagnose the medical condition depicted in the images (Hendee & Ritenour 2002). Berlin and Berlin (1995) found that diagnoses are missed because approximately 60% of readily detectable abnormalities are simply not seen due to perceptual errors. Berlin (1996) has shown that the error rate for this type of oversight could be as high as 75%. Indeed, perception errors and classification errors can occur during the interpretation of diagnostic images (Orzel & Berlin 2003), to the extent that Abe et al. (2003) have stated that the problem of 'not seeing' lesions seems to be the greatest issue in the diagnosis of cancer.

The causes of these errors are the limitations in the human eye-brain visual system, distraction, overlapping structures that cover-up disease represented in images, and the massive number of normal cases seen in imaging systems (Giger, Chan & Boone 2008). Another important cause of misdiagnoses is the fatigue suffered by radiologists while reading electronically displayed images. The introduction of new and advanced technologies, including ultra-fast image acquisitions and isotropic images, has altered the approaches to image interpretation and may be another factor relating to interpretation errors. Isotropic images (or resolution) are obtained when the depth of the voxel, Z dimension is the same length as the pixel's dimensions, X and Y (Krupinski & Berbaum 2009).

According to the above discussion, even though the LCD method based on human observation has high validity with respect to assessing detectability performance, its reliability is affected by the variation of human perceptions and decisions. Furthermore, the visual assessment of image quality by the human observer is time-consuming and arduous, and may lead to incorrect results in many situations (Pascoal et al. 2005). Therefore,

automated software, instead of human observation, was suggested to solve the limitation of the subjective approach of the LCD detectability performance method.

2.4.6.2   Automated LCD

Pascoal et al. (2005) have suggested an objective LCD method to assess image quality by utilising automated scoring via a software package (CDRAD analyser). This software uses a mathematical model of the human visual system based on measurements of SNR (Shet, Chen & Siegel 2011; Tapiovaara 2008), and can therefore avoid the subjectivity related to assessing LCD detectability performance.

It is suggested that this automated approach avoids the subjectivity of the LCD evaluation method because it is based on measurements of image data such as SNR (Tapiovaara 2008). Even though the CDRAD analyser proves more sensitive to smaller low contrast variations, human observation is still able to detect smaller details (Pascoal et al. 2005). LCD methods are useful for quality control, for standardisation purposes and for indicating typical or acceptable performance of medical imaging systems (Tapiovaara 2008).

However, using LCD evaluation methods is still criticised because they are based on homogeneous patient-simulating phantoms and do not represent the real situation. Noise from anatomical background—which effects detecting ability—is simply not considered in such evaluation methods. The ability to detect objects is often much more limited by anatomical background structure than by noise from the imaging system (Tapiovaara 2008).

According to the above discussion, DQE—which is based on pure statistical measurement—is the most effective evaluation method to objectively assess detector performance of imaging systems (Cowen, Kengyelics & Davies 2008). DQE has a high degree of reliability in providing accurate measurement of the ability for information transfer. However, this validity is low with respect to assessing the entire imaging system and to measuring the clinical performance of imaging systems (Bath 2010). DQE does not consider image processing, display or the response of the observer (Bath 2010). On the other hand, ROC and VGC—which involve human observers—are valid methods to evaluate entire imaging systems, but their reliability is limited as they suffer from the subjectivity of the observers (Figure 2.10) (Bath 2010). The relationship between the results of different evaluation methods of image quality—including physical quantities measurement, phantom based evaluations and clinical performance assessment—is not clear nor fully understood (Tapiovaara 2008). Despite ongoing study and effort, there is no image quality evaluation approach that resolves the gap between these evaluation methods (Bath 2010).
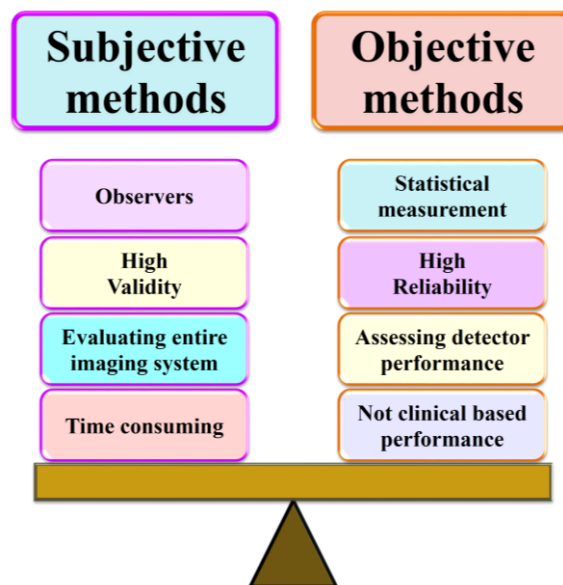
Figure 2.10   Subjective vs objective evaluation methods of imaging systems.

The automated method of LCD detectability performance does not suffer from the subjectivity of human eyes, and can be used for image quality optimisation in routine quality control and the clinical environment. The factors that influence the LCD detectability performance should be recognised to maximise its benefits.

2.5 Factors affecting LCD detectability performance

Recognising the factors that influence LCD detectability performance is fundamental to the effectiveness—and potential benefits—of the LCD evaluation method. The main factors include the detector system type and properties, tube current and dose, tube voltage, image processing techniques and display procedures.

2.5.1 Detector properties

The image quality of CR is affected by blur that occurs in the capture elements caused by the laser beam scattering used to stimulate the phosphor material. The movement of the laser beam causes an additional source of blur during the scanning process in CR detectors. That is, the emission of photostimulable light occurs with a finite decay, approximately microseconds. The capture element blur, however, is negligible for DDR detectors because charge dissipation is practically eliminated by the application of an electric field (Samei 2003a).

This blur can be moderated by reducing the thickness of the sensitive layer, however this also reduces the detector efficiency (DQE) and hence can increase image noise (Samei 2003b).

In terms of image quality and radiation dose reduction, many studies have been conducted to assess digital radiography systems (CR, DDR and IDR) and compare their performance (Schaefer-Prokop et al. 2009; Veldkamp, Kroft & Geleijns 2009). Dual-readout CR was better than single-readout CR for both low- and high-attenuation areas and for overall performance and all lesion subtypes (BacherSmeetsVereecken, et al. 2006). McEntee, Frawley and Brennan (2007) found that the IDR system proved to have considerably better LCD detectability performance. The image quality of IDR, in terms of LCD detectability performance, was comparable to that of CR (McEntee, Frawley & Brennan 2007), although the study by Niimi et al. (2007) showed that IDR had better detectability than CR. IDR also provided higher SNR values, which improve LCD detectability performance, than DDR (Giovanni et al. 2006). Cowen, Kengyelics and Davies (2008) concluded that IDR detectors were better than DDR in two aspects: reducing required radiation dose and their capability of balancing between image quality and radiation dose (Giovanni et al. 2006). DDR detectors are less suitable for the chest because they suffer from a lower dose efficiency, particularly for vascular and interstitial structures and infiltrates in the lung (Schaefer-Prokop et al. 2008). That said, DDR detectors showed great performance in full-field digital mammography detectors, as they are excellent for the high spatial frequencies Cowen, Kengyelics and Davies (2008).

The study of BacherSmeetsVereecken, et al. (2006) showed that IDR allowed significant reduction in the effective dose while maintaining acceptable image quality compared with

DDR. Moreover, IDR performed significantly better in an LCD phantom study with lower exposure doses to patients compared with DDR (BacherSmeetsVereecken, et al. 2006).

Veldkamp, Kroft and Geleijns (2009) concluded that the varieties found between different systems are ambiguous, and there are differences between manufacturers of detectors, research methodology and evaluation methods of image quality. Each method has its own set of properties and, therefore, limitations.

2.5.2   Tube current and dose

CR and DR systems offer high flexibility and radiographers can play a significant role in optimising image quality and lowering radiation dose (Schaefer-Prokop et al. 2008). In CR and DR, noise is associated with lower radiation dose. Lowering radiation dose decreases the SNR and thus deteriorates image quality, whereas high noise level images increase the risk of diagnostic detail loss. On the other hand, overexposed images cannot be simply recognised as a 'too-black' image. As overexposed images increase the detail visualised in the image, these images are less likely to be rejected by radiologists. As a result, the use of CR and DR can lead to a continuous increase in acquisition dose without notification, particularly if exposure factors are set manually (Uffmann & Schaefer-Prokop 2009). This phenomenon is called exposure creep, the gradual increase over time in the exposure that radiographers use for a given radiographic anatomical projection (Gibson & Davidson 2012; Warren-Forward et al. 2007). The main cause of exposure creep is that the radiographers prefer overexposed images rather than the grainy or noisy appearance of underexposed images (Warren-Forward et al. 2007). Manufacturers utilise an exposure indicator or exposure index (EI) to give the radiographers feedback about the actual

detector dose level of the digital radiography image. EI makes the radiographers aware of the dose delivered to the patient (Gibson & Davidson 2012; Schaefer-Prokop et al. 2008) by measuring the dose at the detector surface. However, it is difficult to compare exposure values among systems because the manufactures vary in the definition of EI (Schaefer-Prokop et al. 2008). The question to be answered is what minimum dose is required for different digital radiography systems in order to acquire appropriate or optimum image quality.

According to the previous discussion, increasing mAs generally increases the performance of LCD detectability; however, the dose to the patient will increase as well. It is essential to investigate the effects of mAs on the LCD detectability performance of different digital radiography systems to optimise image quality while maintaining lower dose to patients.

2.5.3 Tube voltage (kVp)

Lowering kVp—which is a measure of tube voltage—increases x-ray attenuation and consequently improves the subject contrast. Lower kVp also increases the DQE of the detectors and improves SNR of digital systems when other exposure factors are adjusted (Geijer, Norrman & Persliden 2009; Launders et al. 2001; Spahn 2005). However, low kVp techniques increase exposure doses and image blurring, due to increasing mA and exposure time (Schaefer-Prokop et al. 2008).

Uffmann et al. (2005) found that 90 kVp—without increasing the radiation dose to the patient—provided a superior demonstration of the anatomic structure compared to 120 and 150 kVp. De Hauwere et al. (2005) also found that changing the tube voltage (102–133 kV) did not significantly improve the low contrast visibility of CR and DR. The study

results of Olaf and Wolfgang (2009) suggested that kVp can be adjusted depending on body part thickness. For example, 70 kVp can be selected for a body part of 8 cm thickness or less, 80 kVp can be selected for 7 to 13 cm thickness, and 100 kVp can be used for more than 13 cm thickness. Body parts of above 18 cm thicknesses can be exposed with 121 kVp.

From the above, it can be concluded that lowering kVp (if other exposure factors are adjusted) improves subject contrast and hence the LCD detectability performance is enhanced. Meanwhile, kVp should be adjusted for the size of the body part, in order to optimise subject contrast. However, lowering kVp increases the dose to the patient (when mA and/or time are adjusted to maintain the same dose on the image plate). On the other hand, if the window width and level of the image are carefully adjusted, choosing a higher kVp is still possible in order to minimise radiation dose without significantly affecting the overall image contrast. Altering kVp to match the detector specification of each system will improve LCD performance. None of these options can be undertaken in isolation; they all need to be considered when selecting a kVp for an anatomical projection.

2.5.4   Image processing technology

Image appearance is greatly influenced by image processing stages, and image quality can be improved by utilising different image processing software and techniques (Korner et al. 2007). Frequency processing techniques—such as unsharp mask filtering and multi-frequency processing algorithms—enhance image contrast, extend dynamic range and/or enhance visualisation of selected structures of a certain size or contrast (Schaefer-Prokop et al. 2009). Smoothing processing techniques are used to suppress image noise. A

subtraction processing technique is utilised to remove superimposed structures to make the anatomic area of interest clearer. Edge enhancement and contrast enhancement are used to reduce noise, remove technical artefacts and optimise contrast by altering pixel values (Korner et al. 2007).

Employing image-processing applications is not a simple task, because improving one image feature may suppress others. Strong enhancement of edges used to enhance visualisation of certain structures can lead to misrepresentation of normal structures (Schaefer-Prokop et al. 2009). The smoothing technique may also degrade spatial detail (Fauber 2013; Korner et al. 2007). Image processing should be optimised according to the system's specification, adapted for targeted anatomic structures, and adjusted for intended diagnostic purpose (Korner et al. 2007).

2.5.5   Softcopy image displays

High display contrast is required to visualise LCD features. That can be achieved by increasing the contrast of the monitor and by reducing window width as far as possible without loss of diagnostic image information (Warren 1984). LCD detectability performance can be improved by using high-resolution liquid-crystal displays monitors (LCDMs) and by utilising the interactive adjustment of brightness and contrast of digital images (BacherSmeetsDe Hauwere, et al. 2006).

2.6   Conclusion

The relationship between the quality parameters of digital radiographic images—including spatial resolution, contrast resolution, noise and artefacts—is complicated. There are trade-offs between these parameters, as improving one parameter may deteriorate another. Optimising these parameters is thus not a simple task; optimising image quality while reducing the radiation dose makes the task even more complicated. Additionally, the quality of the images from different digital radiography systems is not influenced at exactly the same level by the image quality parameters. The only way to optimise image quality parameters while maintaining low radiation dose is to understand deeply the effects of these parameters on each other, including the influence factors and their impact on the radiation dose for each different digital radiographic system.

Several methods are used to evaluate the quality of digital radiographic images and the performance of imaging systems. Some methods relate to pure statistical measurement—such as DQE—which are called objective methods (Bath 2010). Other methods involve human observers—such as ROC, VGC and LCD detectability performance—which are called subjective methods (Bath 2010; Ludewig, Richter & Frame 2010; Obuchowski 2003). Objective methods have low validity as the entirety of the imaging system is not considered; subjective methods have limited reliability because they suffer from the subjectivity of observers (Bath 2010; Ludewig, Richter & Frame 2010; Obuchowski 2003). Each of the available evaluation methods has a unique set of advantages and limitations. Therefore, each evaluation method should be utilised and employed according to its aptitudes to improve image quality and imaging process. Automated LCD detectability analysis is suggested to be the appropriate choice to avoid the limitations of the subjective and objective methods and to optimise image quality. Exposure factors—including kVp

and mAs, and other controllable factors that influence LCD detectability—are the ultimate key to optimising image quality while maintaining a low radiation dose to patient. Therefore, radiographers can play an essential role in improving system performance and image quality if they understand deeply the influences of these factors.

The effects of exposure factors on image quality will be evaluated in Chapter 3 in terms of LCD detectability performance based on human observation and automated approaches. The next chapter will also examine the effectiveness and efficiency of LCD detectability performance as an image quality evaluation method and optimisation tool of image quality.

Chapter 3   Evaluation of contrast-detail in digital radiography

3.1   Introduction

Digital radiographic imaging systems that are currently used in clinical settings are either computed radiography (CR) or direct digital radiography (DR). There are two principal designs of DR: indirect-conversion DR (IDR) and direct-conversion DR (DDR) (Lanca & Silva 2009a; Schaefer-Prokop et al. 2009; Seibert 2009; Veldkamp, Kroft & Geleijns 2009). The physical and working principles of these systems have been described in Chapter 2. The advantages and drawbacks of digital radiographic systems have also been discussed. These systems have replaced conventional film/screen radiography due to their performance capabilities (Weatherburn et al. 2003), as they have improved radiographic image quality and reduced the radiation dose to patients (Korner et al. 2007; Williams et al. 2007). Despite this, there are still drawbacks, as CR, IDR and DDR have the potential to increase patient radiation dose due to their wide dynamic range (Gibson & Davidson 2012). Patients may therefore be exposed to more radiation than is required for a diagnostically sufficient image (Schaefer-Prokop et al. 2008; Williams et al. 2007). Hence, radiographic images should be regularly evaluated to ensure adequate diagnostic image quality and the delivery of low doses to patients (Uffmann & Schaefer-Prokop 2009).

Radiographers have the responsibility for image optimisation and radiation reduction, and should select an appropriate combination of exposure factors to produce optimum quality radiographs that support diagnostic issues while maintaining lower radiation doses (The International Society of Radiographers and Radiological Technologists 2004). The x-ray potential voltage (kVp), tube current (mA), time (S), focal to detector distance (FDD), focal spot size, and other parameters should be carefully and appropriately selected (Australian Institute of Radiography 2007). Radiographers also have the responsibility for monitoring

equipment performance regularly and evaluating image quality (The International Society of Radiographers and Radiological Technologists 2004). While radiographers can play an essential role in improving system performance and image quality by effectively controlling and adjusting exposure factors, image quality is also inherent to the system type and unit specification, and can therefore not be entirely controlled by radiographers (Davidson & Sim 2008). Radiographers can still also operate in a 'film like' world (Reiner et al. 2006). There are different evaluation methods of image quality, which have been outlined Chapter 2.

As discussed in Chapter 2, the evaluation method of low contrast-detail (LCD) detectability performance is suggested to be the choice for image optimisation of radiography images (Alsleem & Davidson 2012). This method is based on the use of LCD phantoms and it does not require volunteer patients. The method is also helpful to predict the influence of lower exposure factors on image quality and diagnostic efficacy. Hence, the method of LCD detectability performance assists to determine the exposure factors that provide optimum image quality while maintaining lower radiation doses. LCD detectability measurements can also determine the trade-offs between perceived image quality, diagnosis efficacy and radiation dose (Shet, Chen & Siegel 2011). The main limitation of the LCD detectability method is the subjectivity of the human observers who score the phantom images. This subjectivity is mitigated by utilising automated scoring via a software package that utilises a mathematical model of the human visual system based on measurements of signal-to-noise ratio (SNR) (Alsleem & Davidson 2012; Shet, Chen & Siegel 2011; Tapiovaara 2008). LCD analysis methods based on automated software provide quantitative evaluations of low contrast and small objects measurement of clinical images. Due to this automated approach, LCD analysis is considered a straightforward and direct method of image quality assessment (Bath 2010; Uffmann et al. 2004).

The aim of Chapter 3 is to evaluate methods of LCD detectability performance as tools of image quality assessment and image optimisation of digital radiography. Accordingly, the chapter will compare detectability performance among CR, IDR and DDR. In addition, this chapter will measure the performance of radiographers' observation on image quality optimisation and evaluate their LCD detectability in different digital radiography systems compared with software scoring as the gold standard.

The studies of this chapter have only evaluated the effects that resulted from a change in the radiographic factors of kVp and mAs. Whilst it is understood that radiation dose also changes with a change in kVp and mAs (Schaefer-Prokop et al. 2008; Veldkamp, Kroft & Geleijns 2009; Williams et al. 2007), it was felt that clinicians better understand changes in radiographic factors and hence would then be able to relate these changes to image quality. As such, the radiation dose measurements were not recorded.

To satisfy the aims of this chapter with respect to Phase 1 of this project, three studies were conducted which are discussed in three separate sections. In Section 1 of Phase 1, the influence factors of LCD detectability performance are evaluated based on software image scoring. In Section 2 of Phase 1, these factors are evaluated using radiographer image scoring. Section 3 of Phase 1 is a comparison between software and radiographer scoring results.

3.2 Section 1 of Phase 1: Evaluation of LCD factors based on software image scoring

In this section, the influences of exposure factors, namely kVp and mAs, on LCD detectability performance of digital radiography were evaluated based on automated LCD analyses results. The quality measure of detectability performance is called the inverse image quality figure (IQF_{inv}), which can be calculated by using automated scoring software. Thijssen et al. (1989) found that the image quality figure (IQF) is directly related to the square root of the entrance dose. The higher the IQF_{inv}, the better the detectability performance and hence the image quality.

The study of this section aimed to demonstrate the value of LCD as a measure to discriminate between systems and exposure conditions. Accordingly, the LCD detectability performance across three different digital radiography systems was compared. This was accomplished by measuring the changes to IQF_{inv} values in three areas: firstly when using different mAs levels, secondly when altering kVp settings and thirdly when using different digital radiography systems.

3.2.1 Materials and methodology

Phantom model (CDRAD phantom)

The CDRAD type 2.0 phantom (Artinis Medical Systems, Zetten, Netherlands) was used for the low contrast-details objects. The CDRAD phantom is 26.5 x 26.5 cm in size with 1 cm thickness of Plexiglas plate. It contains 225 drilled holes of varying depths (0.3–8.0 mm) and different diameters (0.3–8.0 mm), so that the CDRAD phantom has circular discs

with varying contrast levels and diameter sizes (Figure 2.9 in Chapter 2). The 225 circular details are arranged in 15 columns and 15 rows. Each row has 15 holes of exactly the same diameter but different contrast levels due to the gradually varying depths of the holes. Each column has 15 holes with exactly the same contrast level but different diameters. The first three rows contain only one detail per square (Figure 2.9 in Chapter 2) while the remaining 12 rows contain two identical details per square with the same hole depth and diameter. One detail is located in the centre of the square and the second detail is located in a randomly chosen corner (Pascoal et al. 2005; Uffmann et al. 2004).

The CDRAD phantom was inserted between 10 cm thickness of Perspex sheets, with 5 cm thickness of Perspex above and 5 cm underneath the phantom (Figure 3.1). The Perspex is used to simulate attenuation of the anatomical region of an additional 10 cm of soft tissue and provides a homogenous scatter source (Pascoal et al. 2005; Uffmann et al. 2004).
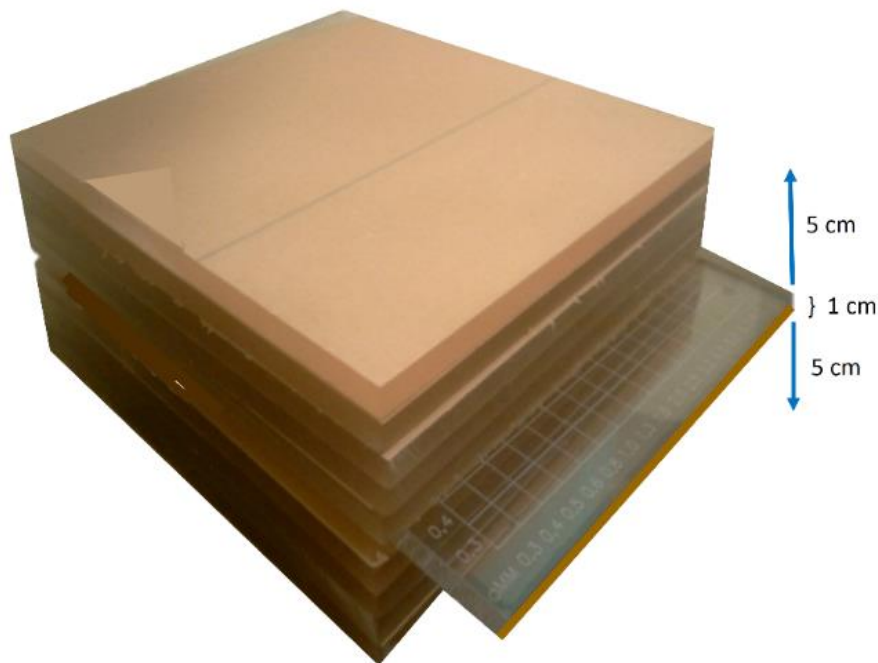
Figure 3.1   CDRAD phantom is inserted in the middle of 10 cm thickness of Perspex.

Detector types

Digital radiographs of the CDRAD phantom were obtained using three systems: CR, IDR and DDR. The specifications of these systems are provided in Table 3.1. The table also shows detective quantum efficiency (DQE) of each system. Quality assurance tests of the performance of x-ray units—including half value layer (HVL), linearity and reciprocity, and accuracy and reproducibility—were undertaken and all units passed all tests (Appendix 2).

Table 3.1   Specification of digital radiographic systems

System type	CR	IDR	DDR
Product name	AGFA/CR 75.0 /IP CDMD 4.1	Carestream DRX-1C	Shimadzu RADspeed Safire
Tube	Trex TM65	Varian A-192	Shimadzu
Focal spot	Large (1.2mm)	Large (1.2 mm)	Large (1.2mm)
Detector material	The phosphor (BaFBrx I1-x)	CsI scintillator	Amorphous selenium 1000 μm
Pixel size	150 μm/pixel (6 pixels/mm)	139 μm	150 μm
Detector size/type	350 x 430 mm IP code 38	350 x 430 mm FPD	432 x 432 mm FPD
Anti-scatter grid	Bucky table 8:1 103/inch	Bucky table 8:1 115/inch	Bucky table 10:1 100/inch
Resolution	Standard: 3.4lp/mm High: 5.0 lp/mm	3.6 lp/mm	3.3lp/mm
DQE DQE(1lp/mm) DQE(2lp/mm)	20% to 30% 18% 9%	60% to 80% 50% 35%	40% 55% 40%
QA tests	Pass	Pass	Pass

Image acquisition

The CDRAD phantom and 10 cm Perspex sheets were imaged at various values of tube voltage (80, 90, 100 and 110 kVp) and tube current levels (1, 2, 4 and 8 mAs). The eight mAs setting was only used with 80 kVp (Table 3.2). The size of the collimation area was

fixed. FDD was maintained at a fixed distance of 100 cm. The Bucky grid table was used for all images. Three images of the CDRAD phantom at each exposure setting were acquired from each system (CR, IDR and DDR). The soft copy images were coded and saved on CD-ROMs as image files in DICOM format (Table 3.3).

Table 3.2   Exposure values of CDRAD phantom images of each system

Thickness 10 cm, FFD 100cm with bucky, large focal spot												
kVp	80				90			100			110		
mAs	1	2	4	8	1	2	4	1	2	4	1	2	4

Table 3.3   The codes of different exposure factors images from different systems

Image exposure factors		Image codes		
kVp	mAs	CR system	IDR system	DDR system
80	1	CR-80/1	IDR-80/1	DDR-80/1
80	2	CR-80/2	IDR-80/2	DDR-80/2
80	4	CR-80/4	IDR-80/4	DDR-80/4
80	8	CR-80/8	IDR-80/8	DDR-80/8
90	1	CR-90/1	IDR-90/1	DDR-90/1
90	2	CR-90/2	IDR-90/2	DDR-90/2
90	4	CR-90/4	IDR-90/4	DDR-90/4
100	1	CR-100/1	IDR-100/1	DDR-100/1
100	2	CR-100/2	IDR-100/2	DDR-100/2
100	4	CR-100/4	IDR-100/4	DDR-100/4
110	1	CR-110/1	IDR-110/1	DDR-110/1
110	2	CR-110/2	IDR-110/2	DDR-110/2
110	4	CR-110/4	IDR-110/4	DDR-110/4

Image scoring

The CDRAD analyser software, version 2.1.9 (Artinis Medical Systems, Zetten, Netherlands), was used to score the images. The CDRAD analyser is dedicated software developed specifically for CDRAD phantom images and designed to provide quantitative analysis of image quality. At each of the 255 matrix locations, the software determines if a difference between the object and background exists. The Welch Satterthwaite test (Student t-tests with Welch correction) is applied in order to determine whether a certain LCD combination was detected or not (Pascoal et al. 2005). An a priori difference of means (APD) is also applied to allow a valid comparison of automated scores obtained from images stored with different bit-depth (Pascoal et al. 2005). The CDRAD analyser was used to calculate the IQF_{inv} values using Equation 2.1 in Chapter 2 (Pascoal et al. 2005; Thijssen et al. 1989). All image sets—each consisting of three images with identical exposure factors—were evaluated by the CDRAD analyser software.

Statistical analysis

Gaussian distributed was used to test the distribution normality of the scores on each variable. The Gaussian distribution, which is also called normal distribution, is a function that tests the probability of whether the scores on each variables real fall between any two real limits. The dependent scores of IQF_{inv} values appear to be reasonably and normally distributed. A two-way between-groups analysis of variance (ANOVA) using the Statistical Package for the Social Sciences (SPSS) software was conducted in data analysis. The two-way ANOVA is statistics test used to examine the influence of different categorical independent variables on one dependent variable. The two-way ANOVA is used when there

is more than one independent variable and multiple observations for each independent variable. The two-way ANOVA can determine the main effect of contributions of each independent factor and also can identify if there is a significant interaction effect between different independent factors on one dependent factor. Student t-tests, at an Alpha value of 0.05 is conducted as a part of the two-way ANOVA calculations to determine significance. So that, the two-way ANOVA test was used to determine the impact of the exposure factors including kVp and mAs and the effects of the different radiography system on the values of IQF_{inv}. This test also used to explore if there is a significant interaction effect between these factors (Pallant 2013). Tukey Honest Significant Difference (HSD) test was also conducted. Tukey HSD is a post-hoc test as it is performed after an analysis of variance, the two-way ANOVA test. The Tukey HSD test was used to determine which groups in the sample differ. Even though the two-way ANOVA can indicate whether groups in the sample differ, it cannot determine which groups differ. While the two-way ANOVA was used to determine if there is significant difference among the groups, the Tukey HSD test was used to determine groups in differ significantly (Pallant 2013).

3.2.2 Results

The average IQF_{inv} value of the three images of same exposure factors from each system (CR, IDR and DDR) were calculated and are shown in Table 3.4, which also shows the variance of the IQF_{inv} values of the three images.

Table 3.4   IQF$_{inv}$ values of the images (these values are the average of three identical exposures)

kVp	mAs	CR images		IDR images		DDR images	
		Mean	SD	Mean	SD	Mean	SD
80	1	3.033	0.45	3.987	0.20	4.903	0.45
80	2	4.073	0.31	4.717	0.26	4.980	0.23
80	4	4.327	0.29	5.317	0.13	4.987	0.23
80	8	4.427	0.36	5.333	0.22	5.263	0.12
90	1	4.673	0.35	5.457	0.19	5.723	0.33
90	2	4.963	0.11	5.853	0.18	6.003	0.31
90	4	5.087	0.15	6.533	0.32	6.010	0.33
100	1	5.393	0.49	6.813	0.38	6.127	0.16
100	2	5.427	0.55	6.883	0.39	6.360	0.24
100	4	5.847	0.45	7.117	0.33	6.660	0.22
110	1	5.920	0.44	7.523	0.49	6.667	0.46
110	2	6.210	0.27	7.523	0.16	6.710	0.08
110	4	6.623	1.04	7.630	0.06	7.140	0.26

Changes to IQF$_{inv}$ when using different mAs levels

The relationship between mAs levels and IQF$_{inv}$ values at fixed kVp were evaluated and are shown in Figures 3.2 to 3.4. Figure 3.2 shows an example of typical results: as mAs increased, the IQF$_{inv}$ values increased.
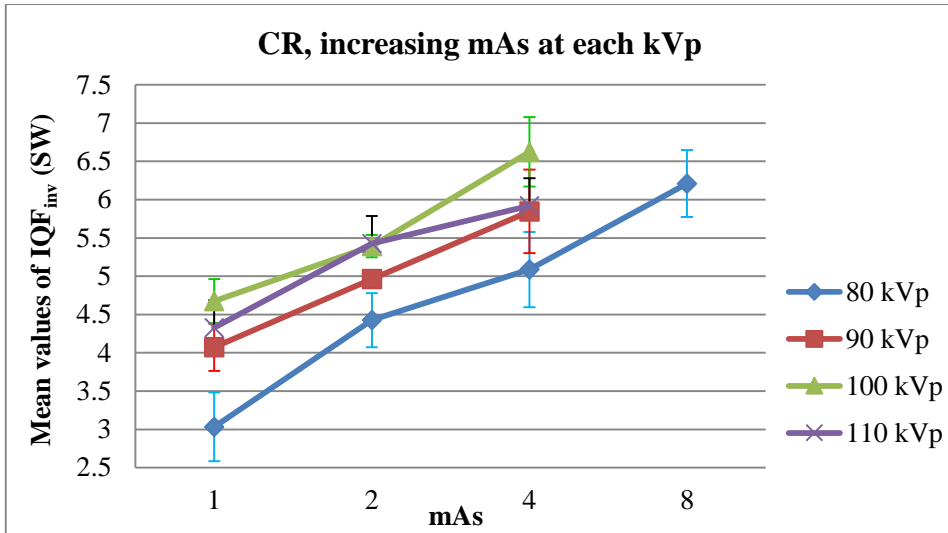
Figure 3.2   IQF$_{inv}$ values increase as mAs increases at each kVp setting with CR.
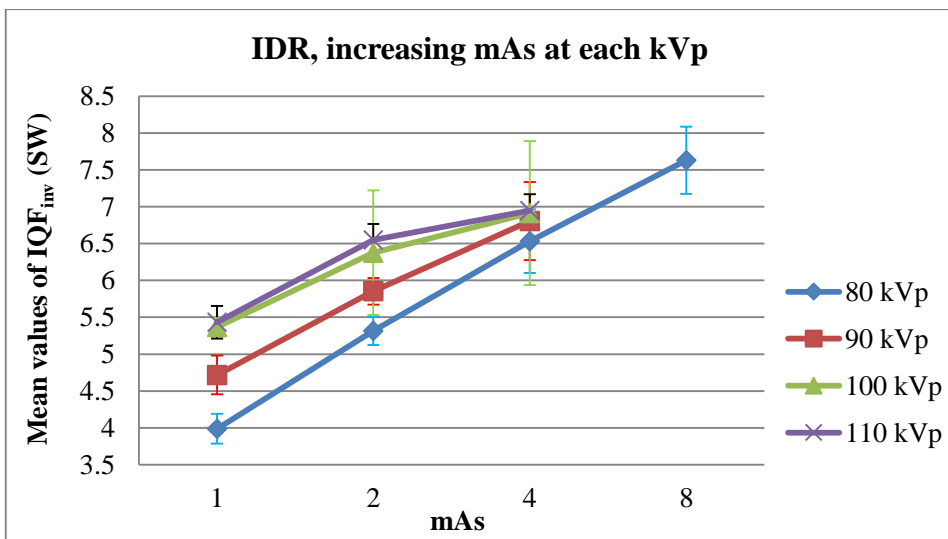
Figure 3.3   IQF$_{inv}$ values increase as mAs increases at each kVp setting with IDR.
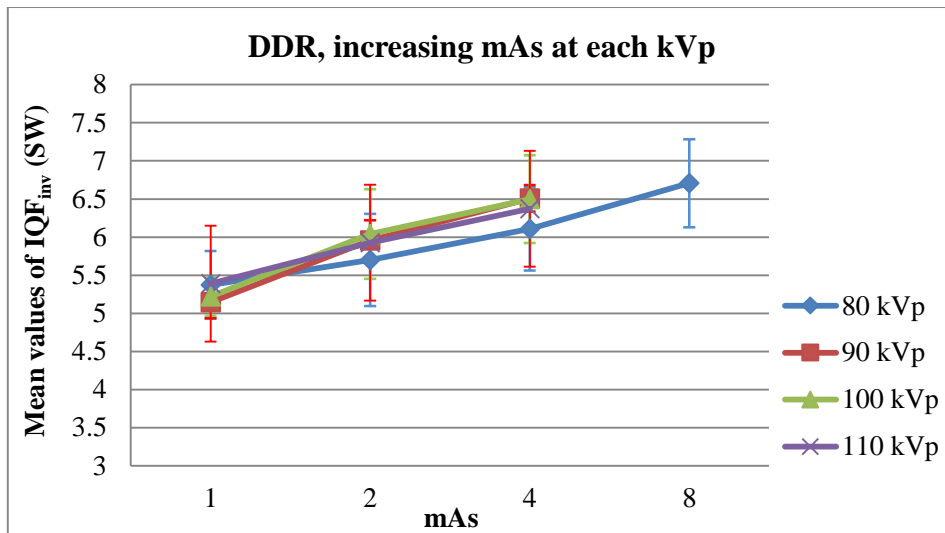
Figure 3.4 IQF$_{inv}$ values increase as mAs increases at each kVp setting with DDR.

When comparing mean IQF$_{inv}$ values resulting from changes in the mAs when a fixed kVp was used, there were significant differences in mean IQF$_{inv}$ ($p < 0.05$) when increasing the mAs and seeing a resultant increase in the IQF$_{inv}$ values (Table 3.5). The Tukey HSD test also indicated that the mean of IQF$_{inv}$ values for 1 mAs was significantly ($p < 0.01$) different from the 2, 4 and 8 mAs groups. There were several exceptions to these results, however, when no significant increase to IQF$_{inv}$ occurred due to an increase of mAs. These were:

- when using CR, at 100 kVp with 1 and 2 mAs increase ($p = 0.082$)

- when using DDR, at 110 kVp with 1 and 2 mAs increase ($p = 0.054$).

69

Table 3.5   Differences (p values, Student t-tests) between images when altering mAs within kVp groups (based on IQF$_{inv}$ values from software)

kVp	mAs	Sig. (p values, Student t-tests)		
		CR images	IDR images	DDR images
80	1	Ref	Ref	Ref
80	2	0.006	0.001	0.034
80	4	0.003	0	0.008
80	8	0	0	0.007
90	1	Ref	Ref	Ref
90	2	0.027	0.001	0.006
90	4	0.002	0.001	0.002
100	1	Ref	Ref	Ref
100	2	0.082	0.005	0.004
100	4	0.004	0.001	0
110	1	Ref	Ref	Ref
110	2	0.017	0.02	0.054
110	4	0.046	0.009	0.01

Changes to IQF$_{inv}$ when using different kVp settings

The relationships between kVp and the IQF$_{inv}$ values were evaluated, with the results of these relationships shown in Figures 3.5 to 3.7. At all mAs settings, higher kVp settings generally resulted in higher IQF$_{inv}$ mean values in CR and IDR. However, there was a decline in IQF$_{inv}$ when the kVp increased from 100 to 110 kVp in CR. In DDR, there were small changes in IQF$_{inv}$ values with increasing kVp, as shown in Figure 3.7.
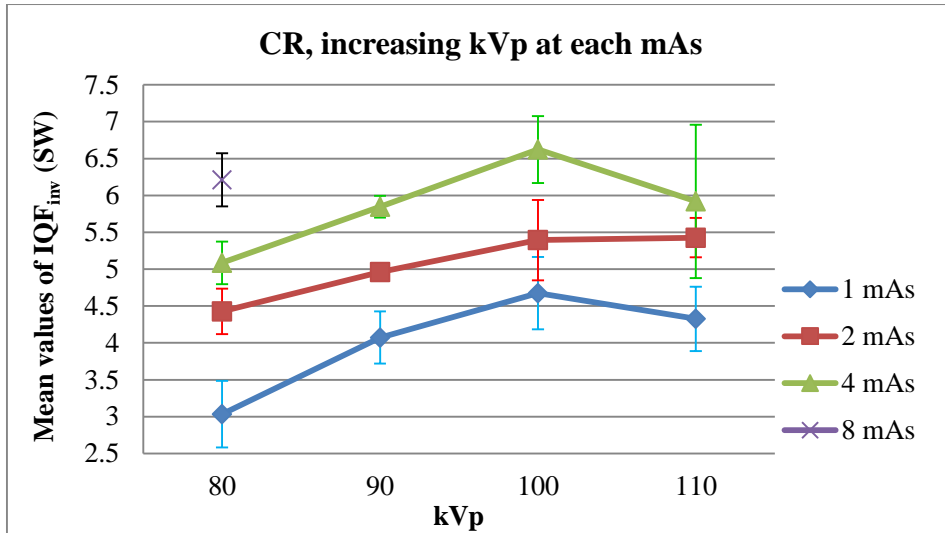
Figure 3.5   Effects of increasing kVp at each mAs level on IQF$_{inv}$ values in CR. (Note the change in IQF$_{inv}$ values for CR with 4 and 8 mAs at 100 and 110 kVp.)
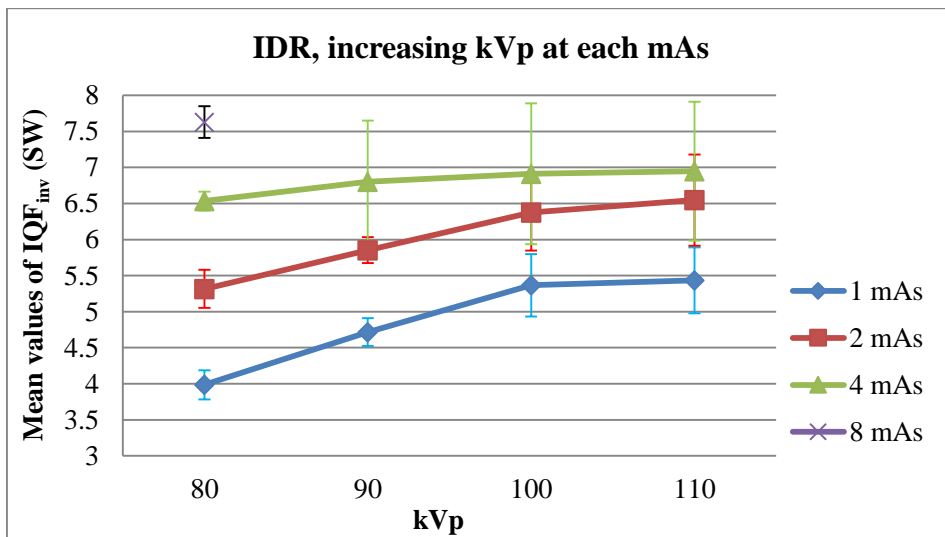
Figure 3.6   Effects of increasing kVp at each mAs level on IQF$_{inv}$ values in IDR. (Note the change in IQF$_{inv}$ values with 1 and 4 mAs at 100 and 110 kVp.)

71
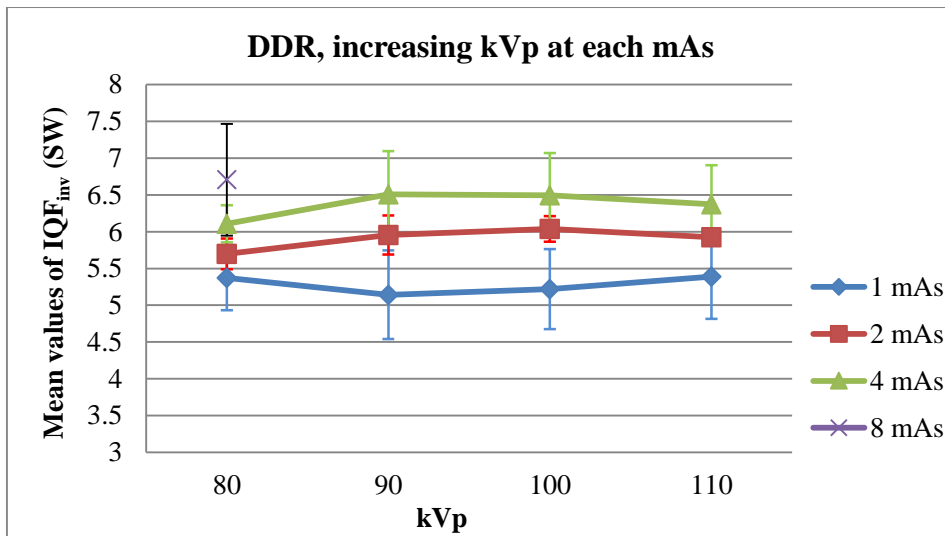
Figure 3.7   Effects of increasing kVp at each mAs level on IQF$_{inv}$ values in DDR. (Note the change in IQF$_{inv}$ values with 1 mAs at 90 and 100 kVp and the change with 2 and 4 mAs at 90, 100 and 110 kVp.)

There were significant differences in mean IQF$_{inv}$ (p <0.05) when comparing mean IQF$_{inv}$ values resulting from changes in the kVp with fixed mAs in CR (Table 3.6). The one exception was between the images of 80 and 110 kVp at 4 mAs ($p < 0.156$). When IDR and DDR were used, the expected effect of changing kVp (i.e. an increase in the IQF$_{inv}$ values) was not always seen (Table 3.6). Indeed, the differences in IQF$_{inv}$ values resulting from changes in the kVp were insignificant ($p > 0.267$) at 4 mAs in IDR and at all mAs levels in DDR. For all radiographic systems, when two subject Anova was used, there was no significant differences between IQF$_{inv}$ values of the images ($p = 0.781$) when mAs was kept constant and kVp was varied. There was also no significant difference ($p = 0.770$) when mAs was kept constant and kVp was varied in each radiographic system. The Tukey HSD post-hoc test was conducted and, when evaluating all radiographic systems, there were no significant differences between 80 and 90 kVp ($p = 0.889$) and between 100 and 110 kVp ($p = 0.909$).

Table 3.6   Differences (*p* values, Student t-tests) between images when altering kVp within mAs groups (based on IQF$_{inv}$ values from software)

kVp	mAs	Sig. (*p* values, Student t-tests)		
		CR images	IDR images	DDR images
80	1	ref	ref	ref
90	1	0.017	0.005	0.311
100	1	0.006	0.008	0.362
110	1	0.012	0.008	0.485
80	2	ref	ref	ref
90	2	0.033	0.022	0.129
100	2	0.038	0.027	0.048
110	2	0.007	0.026	0.089
80	4	ref	ref	ref
90	4	0.013	0.32	0.179
100	4	0.008	0.286	0.377
110	4	0.156	0.267	0.324

Changes to IQF$_{inv}$ when using different radiographic imaging systems

The relationships between different radiographic systems and IQF$_{inv}$ values were evaluated for images with the same exposure factor. Figures 3.8 to 3.15 display the results that show these relationships. IDR had higher IQF$_{inv}$ values than CR in all cases and DDR in most cases. DDR had higher IQF$_{inv}$ than IDR only at low exposure kVp settings, mainly at 80 or 90 kVp at mAs. DDR had higher IQF$_{inv}$ values than CR in most cases.
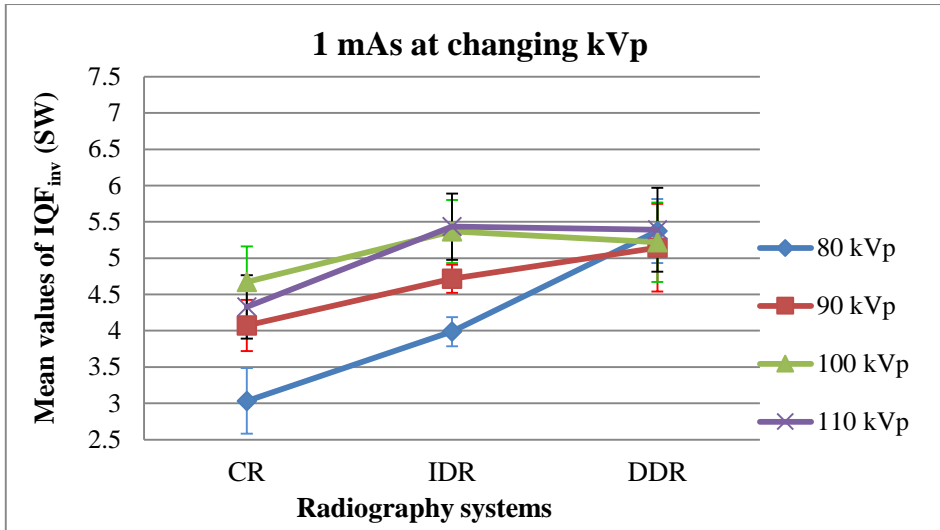
Figure 3.8   Average IQF$_{inv}$ values at 1 mAs for each system. (Note the superiority of DDR at 80 and 90 kVp.)
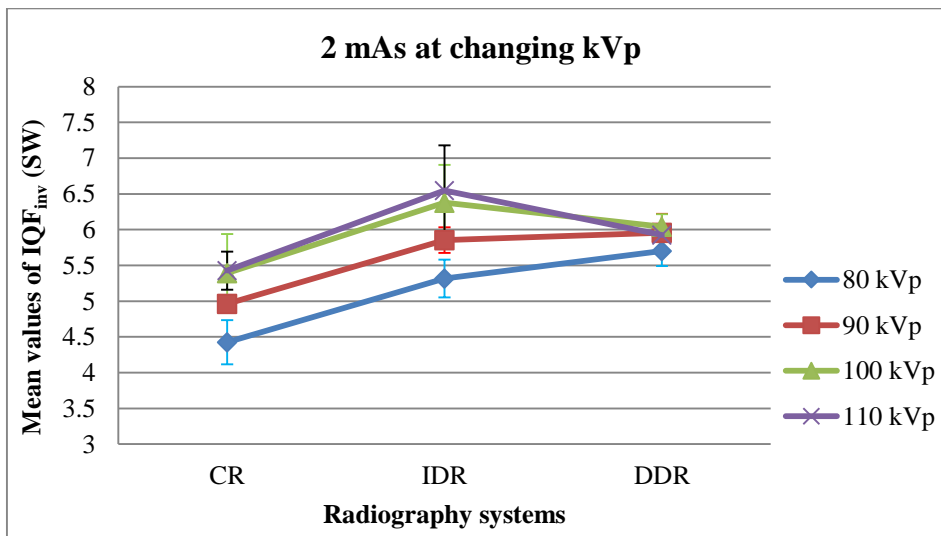
Figure 3.9   Average IQF$_{inv}$ values at 2 mAs for each system. (Note the superiority of DDR at 80 and 90 kVp and the superiority of IDR at 100 and 110.)
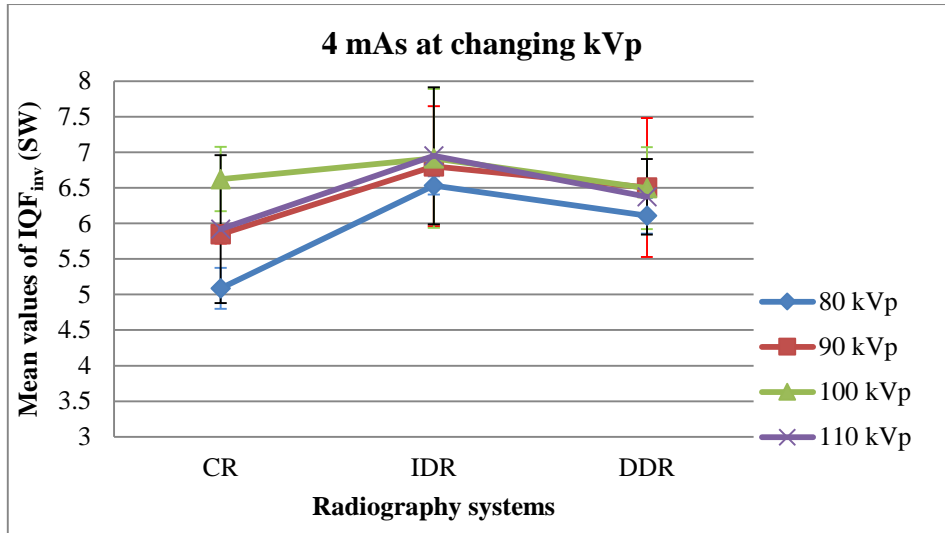
Figure 3.10   Average IQF$_{inv}$ values at 4 mAs for each system show the superiority of IDR.
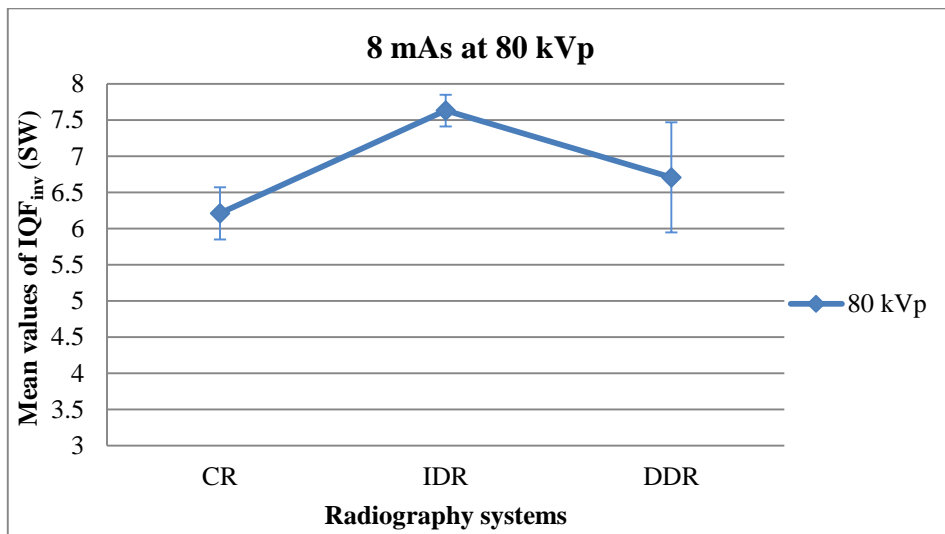
Figure 3.11   Average IQF$_{inv}$ values at 8 mAs for each system show the superiority of IDR.
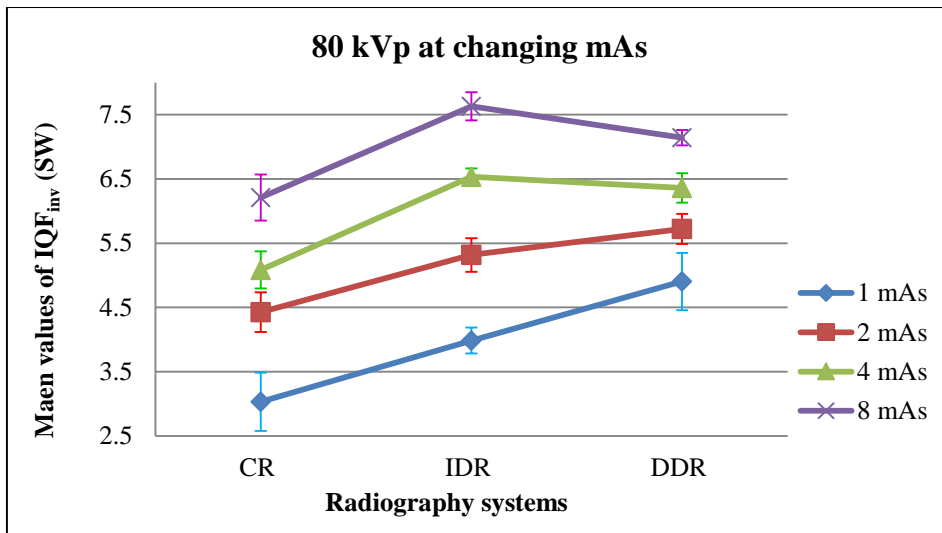
Figure 3.12   IQF$_{inv}$ mean values at 80 kVp for each radiography system show the superiority of DDR at 1 and 2 mAs and IDR at 4 and 8 mAs.
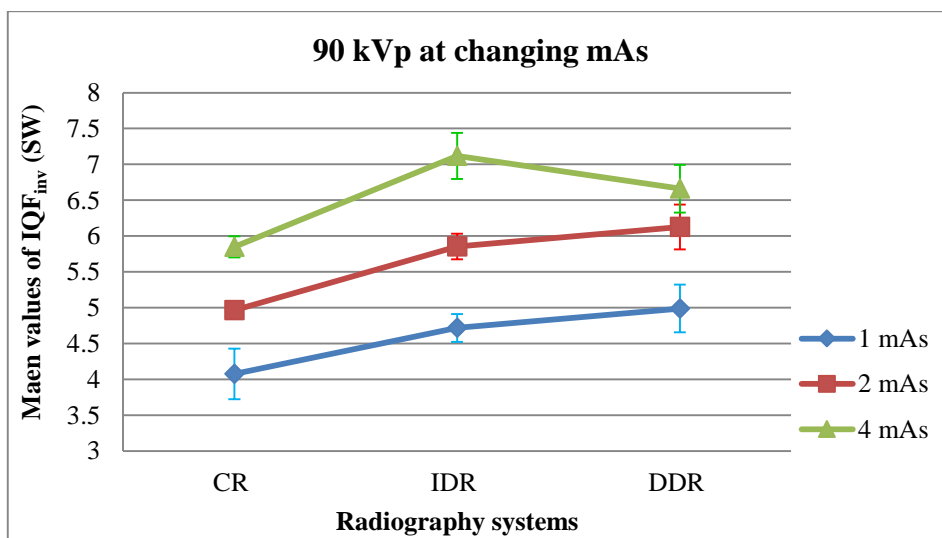
Figure 3.13   IQF$_{inv}$ mean values at 90 kVp for each radiography system show the superiority of DDR at 1 and 2 mAs and IDR at 4 mAs.
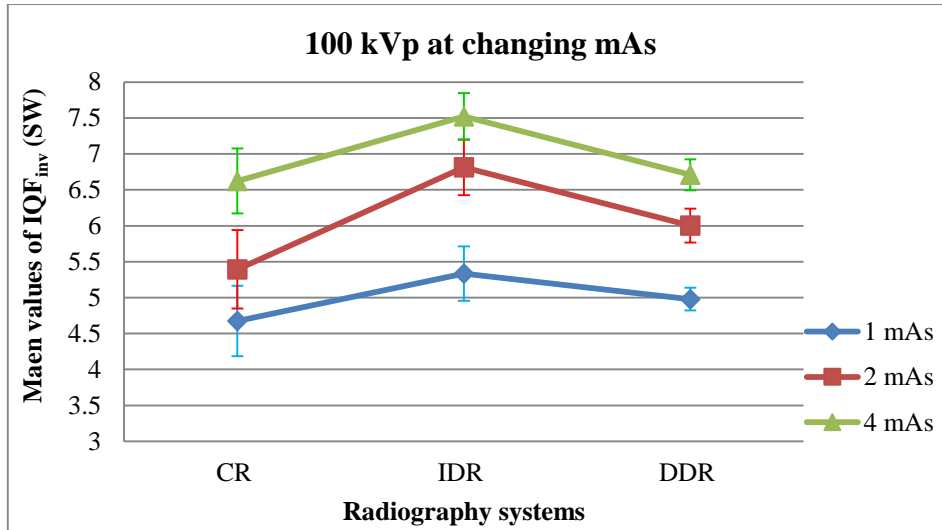
Figure 3.14 IQF$_{inv}$ mean values at 100 kVp levels for each radiography system show the superiority of IDR at all mAs levels.
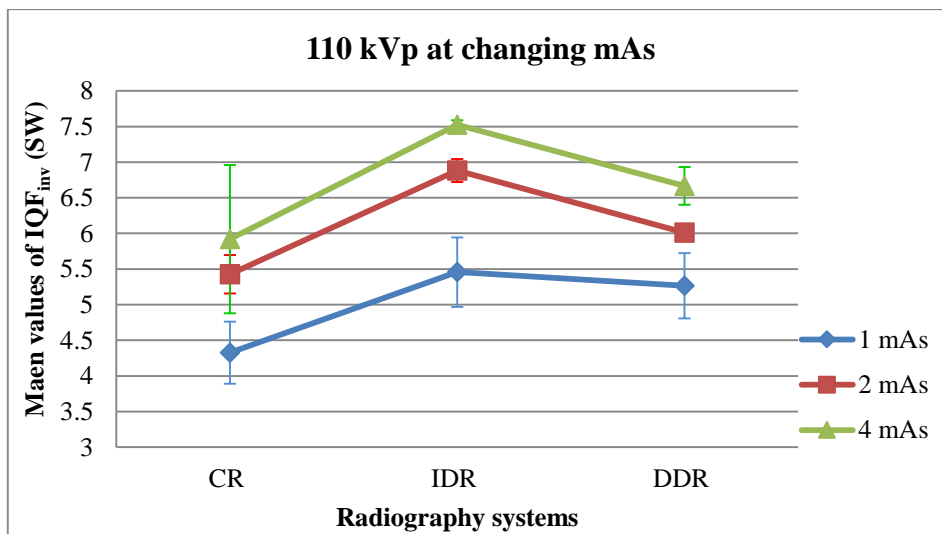
Figure 3.15 IQF$_{inv}$ mean values at 110 kVp for each radiography system show the superiority of IDR at all mAs levels.

Differences between images from different radiography systems were evaluated to measure any significant changes between them (Table 3.7). IDR and DDR had significantly higher IQF$_{inv}$ than CR at different exposure factors in most cases (Table 3.7). The differences between IDR and DDR were mostly insignificant. The Tukey HSD test indicated that the

mean of IQF$_{inv}$ values for each system was significantly different from either of the other systems ($p < 0.01$).

Table 3.7   Comparing (p values, Student t-tests) between systems' images (differences between images of same exposure factors)

kVp	mAs	Sig. (p values, Student t-tests)		
		CR x IDR	IDR x DDR	DDR x CR
80	1	0.022	0.024	0.003
80	2	0.01	0.058	0.002
80	4	0.002	0.169	0.002
80	8	0.005	0.022	0.026
90	1	0.035	0.156	0.016
90	2	0.003	0.14	0.004
90	4	0.004	0.082	0.015
100	1	0.069	0.116	0.205
100	2	0.011	0.027	0.087
100	4	0.025	0.018	0.392
110	1	0.02	0.322	0.031
110	2	0.002	0.002	0.034
110	4	0.058	0.016	0.176

3.2.3   Discussion

When calculating the mean IQF$_{inv}$ values for each image, there was minimal variance between individual images of the same kVp and mAs setting for each digital radiography recording system (Table 3.4). This shows a high consistency of the x-ray units and recording systems used.

Changes to IQF$_{inv}$ when using different mAs levels

It was expected that the increased photon count from the higher mAs would result in increased SNR and thus increased detectability performance. High noise level images

increase the risk of diagnostic detail loss (Uffmann & Schaefer-Prokop 2009), and therefore a higher radiation dose should improve detectability performance (Figures 3.2 to 3.4).

Changes to IQF$_{inv}$ when using different kVp settings

Increasing the kVp has two effects on the x-ray beam: it increasing the average photon energy of the beam and increases the number of photons in the beam (Carlton & Adler 2012). Lowering the kVp increases x-ray attenuation and consequently the subject contrast is improved (Geijer, Norrman & Persliden 2009; Launders et al. 2001; Spahn 2005). Whilst this is well understood, the ability to visualise this contrast change in the image was not seen. When using digital recording systems, changing the kVp setting had insignificant effect on the detectability of objects, particularly in DDR and at higher mAs settings in IDR. An example of this is seen in Figure 3.7 with DDR. At the various mAs settings, when changing the kVp, the IQF$_{inv}$ essentially did not change.

Changes to IQF$_{inv}$ when using different radiographic imaging systems

IDR had higher IQF$_{inv}$ values than CR and DDR, particularly at higher exposure kVp settings. This reflects the stronger DQE of IDR (0.6-0.8) compared with that of DDR (0.4) and CR (0.2-0.3) (Gomi et al. 2006; Neitzel 2005). Cesium iodide doped with thallium (CsI:TI), which is used in IDR systems for fluorescence, is an excellent x-ray photon absorber due to its high atomic number (Z= 53) (Achenbach). The use of needle-like structures of CsI reduces light spreading in the scintillators—similar to regular CR systems—meaning that a thicker layer can be utilised to maximise detection efficiency (Abe et al.). The different design principles of CR, IDR and DDR detectors are attributed as the reason behind the differences between them. DDR detectors are potentially less

susceptible to conversion noise compared to IDR detectors, as they require no light-to-charge conversion (Samei 2003b). DDR also has better performance than IDR at the higher spatial frequencies, as DDR systems show less blurring of the image signal (Veldkamp, Kroft & Geleijns 2009). One of the contributing factors to these results is the absorption efficiency of each system at various photon energies. Materials used in IDR have low energy k-edges and generally greater absorption efficiency at all energies compared with materials used in CR and DDR. The weaker DQE of DDR versus IDR detectors reflects the lower x-ray absorption efficiency of a-Se compared with CsI:Tl (American Association of Physicists in Medicine 2006; Neitzel 2005).

Due to absorption efficiency, it is suggested that DDR detectors are less suitable for chest imaging because they suffer from a lower dose efficiency, particularly for vascular and interstitial structures and infiltrates in the lung (Schaefer-Prokop et al. 2008). Using alternative photoconductor materials—such as polycrystalline compounds instead of a-Se—might conceivably lead to DDR detectors with DQE performance competitive with current indirect conversion detectors (noise-aliasing and other technical problems not withstanding) (Cowen, Kengyelics & Davies 2008). These materials—which include PbI_2, HgI_2 and PbO—promise 50-100% greater x-ray absorption efficiency than an equivalent thickness of a-Se plus a greater yield of signal electrons (Kasap et al. 2011).

These results suggest that the evaluation method of LCD detectability performance based on automated software is a reliable tool to measure the effects of exposure factors on image quality and to compare between different radiography systems. This approach has the potential to evaluate and optimise the image quality and provide a deeper understanding of exposure factor effects on various CR, IDR and DDR systems. However, the validity of this method may be influenced by the absence of human's observation. Automated software

may be not a good representative of human eye. Therefore, the validity of this method should be examined.

3.2.4   Conclusion

Increasing mAs in all digital imaging systems generally improves detectability performance. However, there is a direct relationship between mAs and the number of x-ray photons produced (and hence the dose to patients) so caution is needed when considering this approach to improve the detectability of objects in a digital radiograph. Changing the kVp setting typically did not show significant change to the IQF_{inv} (or, by extension, to the detectability of objects in a digital radiograph), particularly in DDR and at higher mAs settings in IDR. This shows that a change in the average photon energy of the x-ray beam—and the resultant change in subject contrast—is not being seen in the digital radiograph. An increase in kVp, without a change in mAs, is known to increase the number of x-ray photons produced; this increase also had no significant effect on object detectability. The use of kVp to change radiographic or image contrast when using the film/screen recording system is well known, although this is now not the case when using digital radiographic systems. Both IDR and DDR show better detectability performance than CR, and IDR has better detectability performance than DDR only at higher mAs settings and at higher kVp settings (100 and 110 kVp). The differences between them are significant only at high exposure factors (100 or 110 kVp and 2 or 4 mAs), as DDR shows better detectability performance with lower exposure factors than IDR. The selection of an imaging system should now also be considered based on typical radiographic examinations. The effects of exposure factors on the image quality of different radiography systems are not similar: IDR has better detectability performance when using high kVp while DDR has better noise handling

capability at lower radiographic factors. The limitation of this study is that only one manufacturer of each type of radiographic system was tested. Furthermore, only one thickness (being 10 cm of Perspex) was examined. Radiation dose and beam filtration are important factors in determining the dose delivered by each system, although these were not measured (and/or considered) in the present study. Further research is needed to fully evaluate the effects on diagnostic ability when changing kVp, mAs or the digital recording systems. Because different combinations of mAs and kVp produce different doses, radiation dose should be measured in further studies.

The automated tool of LCD detectability performance is reliable evaluation method of image quality. However, the experiments in Section 1 of Phase 1 are purely based on software results. In order to examine the validity of these results and to emphasise the effectiveness of automated LCD detectability performance, the experiments should also be conducted based on human observation and scoring. Therefore, Section 2 of Phase 1 will evaluate the influence factors of LCD detectability performance based on the scoring events of radiographers.

3.3   Section 2 of Phase 1: Evaluation of LCD factors based on radiographers' scoring results

In the previous section, Section 1 of Phase 1, the method of LCD detectability performance as a tool of image quality optimisation was evaluated based on software image scoring. The effects of exposure factors on image quality (in terms of IQF_{inv}) were also evaluated based on automated scoring results. However, to effectively examine the validity of the LCD detectability evaluation method, human observers should be involved in the experiments.

There were several reasons why radiographers were selected to represent the human element for this section of the study. Firstly, radiographers bear the responsibility for image optimisation and radiation reduction to patients, and should therefore carefully and appropriately select a combination of exposure and other radiographic parameters to produce optimum quality of the radiographic image while maintaining the lowest dose radiation to the patient. Radiographers also have the responsibility for equipment performance monitoring and image quality evaluation (The International Society of Radiographers and Radiological Technologists 2004).

The current section of this study (Section 2 of Phase 1) aimed to assess the evaluation method of LCD detectability performance based on the scoring results of observers. The effects of exposure factors on LCD detectability performance of images (in terms of IQF_{inv} values) were also evaluated based on radiographer assessments. Consequently, this section of the study also aimed to examine the detectability performance of radiographers.

3.3.1 Materials and methodology

The methodology and materials required to produce images are identical to the previous section of this phase of the study. Therefore, the images that were used in the current section were selected from the images that were acquired and used in the study of Section 1 of Phase 1. One image (out of the three images of identical exposure parameters) was selected to be scored by radiographers, represented by the shaded images in Table 3.8. This option was chosen due to limitations with the amount of images able to be scored, plus the number of available radiographers. The images were coded in such a way as to keep them unidentified in terms of exposure factors and

radiography system. While there was no significant difference between the scores made by the software, the selection of the images was also based on the highest IQF_{inv} values of scoring results. The soft copy images were saved on CD-ROMs as images files in DICOM format.

Table 3.8   The codes of the images

kVp/mAs	CR system			IDR system			DDR system		
80/1	A1a	A1b	A1c	B1a	B1b	B1c	C1a	C1b	C1c
80/2	A2a	A2b	A2c	B2a	B2b	B2c	C2a	C2b	C2c
80/4	A3a	A3b	A3c	B3a	B3b	B3c	C3a	C3b	C3c
80/8	A4a	A4b	A4c	B4a	B4b	B4c	C4a	C4b	C4c
90/1	A5a	A5b	A5c	B5a	B5b	B5c	C5a	C5b	C5c
90/2	A6a	A6b	A6c	B6a	B6b	B6c	C6a	C6b	C6c
90/4	A7a	A7b	A7c	B7a	B7b	B7c	C7a	C7b	C7c
100/1	A8a	A8b	A8c	B8a	B8b	B8c	C8a	C8b	C8c
100/2	A9a	A9b	A9c	B9a	B9b	B9c	C9a	C9b	C9c
100/4	A10a	A10b	A10c	B10a	B10b	B10c	C10a	C10b	C10c
110/1	A11a	A11b	A11c	B11a	B11b	B11c	C11a	C11b	C11c
110/2	A12a	A12b	A12c	B12a	B12b	B12c	C12a	C12b	C12c
110/4	A13a	A13b	A13c	B13a	B13b	B13c	C13a	C13b	C13c

Image display

A three megapixel diagnostic quality colour liquid crystal display monitor (LCDM) (Eizo Radioforce R-31, Japan) was used to display the images to be scored by the radiographers. The monitor was bought new and it has been calibrated as part of purchase process. All radiographers (from different hospitals) used the same monitor and the viewing and lighting conditions were approximated for each hospital. The room light and conditions were maintained as per a reporting room environment.

Image scoring method (radiographers scoring)

Ethical approval for this project was obtained through the RMIT University Human Ethics Committee (Approval number ABSEHAPP 11) (Appendix 3). The soft copy images (from the CR, DDR and IDR) were de-identified—as to the modality and exposure factors—and then scored by radiographers, who were provided with the images saved on a CD-ROM as DICOM files. Each CD-ROM included thirty-nine images, with thirteen images from each system (Table 3.8). Forty-two radiographers from different hospitals were invited to score the images, with each image scored six times by six different radiographers. Each radiographer scored six images (two images from each system), except for six radiographers who scored only three images (one image from each system). Each of these six radiographers scored the same images, although the images were scored in a different order (Table 3.9). Radiographers scored the images independently during their break times during working days.

Table 3.9   Image scoring distribution between the radiographers

Radiographers codes	The images (De-identified codes were used for radiographers, see Table 3.8)		
R1, R8, R15, R22, R29 and R36	CR-80/1	IDR-80/1	DDR-80/1
	CR-80/2	IDR-80/2	DDR-80/2
R2, R9, R16, R23, R30 and R37	CR-80/4	IDR-80/4	DDR-80/4
	CR-80/8	IDR-80/8	DDR-80/8
R3, R10, R17, R24, R31 and R38	CR-90/1	IDR-90/1	DDR-90/1
	CR-90/2	IDR-90/2	DDR-90/2
R4, R11, R18, R25, R32 and R39	CR-90/4	IDR-90/4	DDR-90/4
	CR-100/1	IDR-100/1	DDR-100/1
R5, R12, R19, R26, R33 and R40	CR-100/2	IDR-100/2	DDR-100/2
	CR-100/4	IDR-100/4	DDR-100/4
R6, R13, R20, R27, R34 and R41	CR-110/1	IDR-110/1	DDR-110/1
	CR-110/2	IDR-110/2	DDR-110/2
R7, R14, R21, R28, R35 and R42	CR-110/4	IDR-110/4	DDR-110/4

The radiographers were provided with scoring instruction and scoring sheets (Appendices 4 and 5). The radiographers were asked to indicate the location of the second spot in each square for each fixed diameter. In other words, radiographers were asked to indicate the location of the visible corner cylinder/disc in the image on each square of each row. Correct indication of the location confirms that the disc was really seen, not just guessed. The viewing conditions, including the phantom background level and display contrast enhancement factor, were chosen to optimise image appearance. Radiographers were instructed that they could alter the image brightness and contrast using the window level and width as much as they wanted, in order to optimise their personal viewing of the images. The monitor was situated in an environment similar to that used when reporting images is undertaken. Based on the completed image scoring forms by radiographers, the IQF_{inv} for each image was manually calculated.

Calculation of IQF_{inv}

The completed forms of image scoring by radiographers were then reviewed according to the manual of the CDRAD analyser (Appendix 6). The IQF_{inv} value was then calculated for each image using Equation 2.1 in Chapter 2. The smallest visible depth (C_i) against the smallest visible diameter (D_i) was determined for each row (i). The value of C_i*D_i for each row is the smallest detected depth. By summing up the value of C_i*D_i at each row, and by dividing 100 by the result, the IQF_{inv} values were measured for each scored image.

Statistical analysis

The same statistical tests that were used to analyse the results in the previous section (Section 1 of Phase 1) were also applied in this study. Gaussian distributed was used to test the distribution normality of the scores on each variable and to identify if whether the scores on each variables real fall between any two real limits. The scores of IQF_{inv} which is the dependent variable appear to be normally distributed. A two-way ANOVA using SPSS software was conducted in data analysis. The two-way ANOVA is statistics test used to examine the influence of different categorical independent variables on one dependent variable. The two-way ANOVA was used to determine the impact of the exposure factors including kVp and mAs and the effects of the different radiography system on the values of IQF_{inv} and to identify if there are a significant differences between the different factors. Student t-tests, at an Alpha value of 0.05 is conducted as a part of the two-way ANOVA calculations to determine the significance differences (Pallant 2013). Tukey HSD was also conducted to determine which groups differ significantly (Pallant 2013).

3.3.2 Results

The IQF_{inv} value of each image—that was scored by six radiographers from each exposure group for CR, IDR and DDR—was calculated and the results are shown in Table 3.10. This table also shows IQF_{inv} value image variance between the six radiographers.

Table 3.10   IQF$_{inv}$ values of the images based on radiographers scoring

kVp	mAs	CR images		IDR images		DDR images	
		Mean	SD	Mean	SD	Mean	SD
80	1	1.43	0.24	1.66	0.31	1.55	0.09
80	2	1.50	0.26	2.23	0.31	1.69	0.17
80	4	2.05	0.75	3.59	1.28	2.43	0.39
80	8	2.20	0.67	3.89	1.07	2.67	0.68
90	1	1.66	0.75	2.05	0.39	1.73	0.31
90	2	1.75	0.77	2.67	0.60	1.96	0.41
90	4	2.20	0.59	2.87	0.38	1.97	0.16
100	1	1.50	0.08	2.14	0.31	1.80	0.48
100	2	1.89	0.37	3.09	0.50	1.98	0.33
100	4	2.11	0.67	3.52	0.61	1.94	0.21
110	1	1.92	0.54	2.58	0.82	1.86	0.25
110	2	1.90	0.38	3.24	1.26	2.02	0.16
110	4	1.81	0.79	2.56	0.75	1.93	0.09

Changes to IQF$_{inv}$ when using different mAs settings

The relationships between mAs and IQF$_{inv}$ values were evaluated, and Figures 3.16 to 3.18 display the results that show these relationships. Based on the scoring results of the radiographers, higher mAs settings generally resulted in higher IQF$_{inv}$ mean values, with few exceptions. One notable exception was that, for all systems, there was no improvement in IQF$_{inv}$ values when mAs increased from 2 to 4 at 110 kVp.
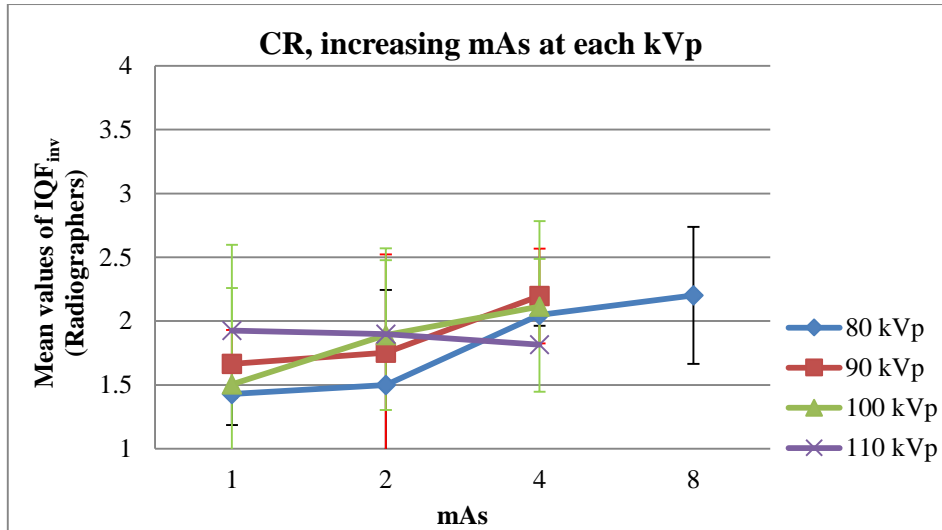
Figure 3.16   IQF$_{inv}$ values generally increase as mAs increases at each kVp setting, excluding 110 with CR.
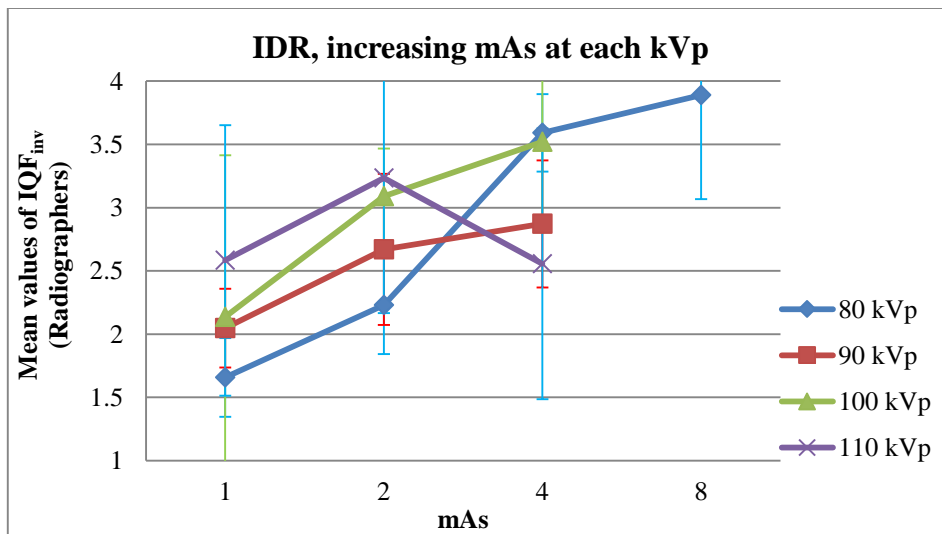
Figure 3.17   IQF$_{inv}$ values increase as mAs increases at each kVp setting with IDR. (Note the change in IQF$_{inv}$ at 110 when mAs increases from 2 to 4.)
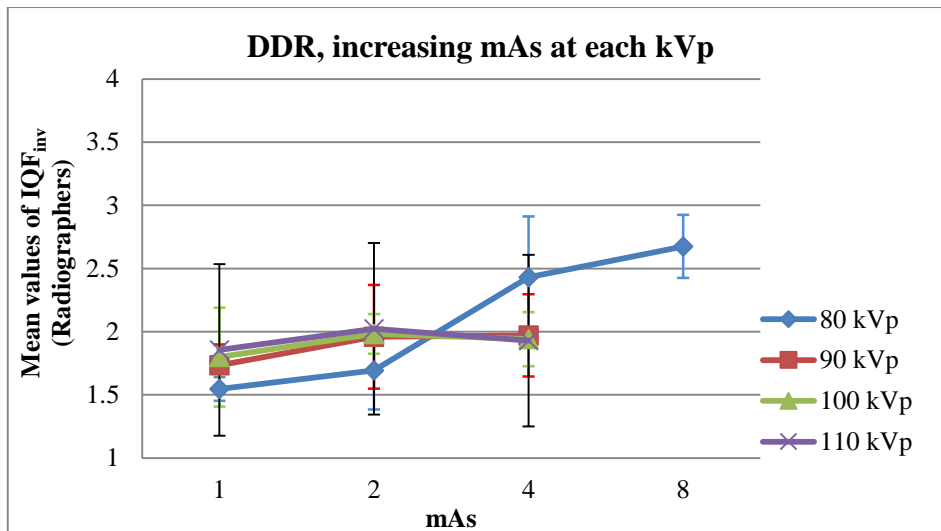
Figure 3.18   IQF$_{inv}$ values increase as mAs increases at each kVp setting with DDR except when mAs increases from 2 to 4 at 90.100 and 110 kVp.

With CR, there were mostly insignificant differences in mean IQF$_{inv}$ (when increasing the mAs and seeing a resultant increase in the IQF$_{inv}$ values). The significant differences were only between 1 and 8 mAs at 80 kVp ($p = 0.019$), between 1 and 2 mAs at 100 kVp ($p = 0.024$) and between 1 and 4 mAs at 100 kVp ($p = 0.039$) (Table 3.11). With IDR, there were significant differences in IQF$_{inv}$ values when mAs increased at fixed kVp. There were exceptions, however, such as at 110 kVp, where there were insignificant changes with increasing mAs (Table 3.11). In DDR, when mAs increased, there were significant increases in IQF$_{inv}$ values only at 80 kVp (Table 3.11). The Tukey HSD test indicated the 1 mAs group differed significantly ($p > 0.04$) from either of the other mAs groups.

Table 3.11   Differences (*p* values, Student t-tests) between images when altering mAs within kVp groups (based on IQF$_{inv}$ values from radiographers)

kVp	mAs	Sig. (*p* values, Student t-tests)		
		CR images	IDR images	DDR images
80	1	Ref	Ref	Ref
80	2	0.324	0.005	0.047
80	4	0.052	0.006	0.001
80	8	0.019	0.001	0.005
90	1	Ref	Ref	Ref
90	2	0.423	0.03	0.155
90	4	0.101	0.002	0.07
100	1	Ref	Ref	Ref
100	2	0.024	0.002	0.231
100	4	0.039	0.001	0.266
110	1	Ref	Ref	Ref
110	2	0.461	0.157	0.102
110	4	0.392	0.477	0.262

Changes to IQF$_{inv}$ when using different kVp settings

The relationships between kVp and the IQF$_{inv}$ values were evaluated, and Figures 3.19 to 3.21 display the results that show these relationships. At 1 and 2 mAs settings, higher kVp settings generally resulted in higher IQF$_{inv}$ mean values in CR. There was a decline in IQF$_{inv}$ value when the kVp increased from 90 to 100 kVp at 1 mAs and there was very small change when kVp increased from 100 to 110 kVp at 2 mAs in CR. At 4 mAs, IQF$_{inv}$ values increased with increasing kVp from 80 to 90 kVp and then declined with higher kVp in CR.

In IDR, higher kVp settings resulted in higher IQF$_{inv}$ mean values at 1 and 2 mAs settings. At 4 mAs, the IQF$_{inv}$ increased when kVp increased to 90 then declined with higher kVp (Figure 3.20). In DDR, when the kVp increased to 90, IQF$_{inv}$ values increased at 1 and 2 mAs and declined at 4 mAs. There were limited changes in IQF$_{inv}$ when kVp increased from 90 to higher kVp at all mAs levels (Figure 3.21).
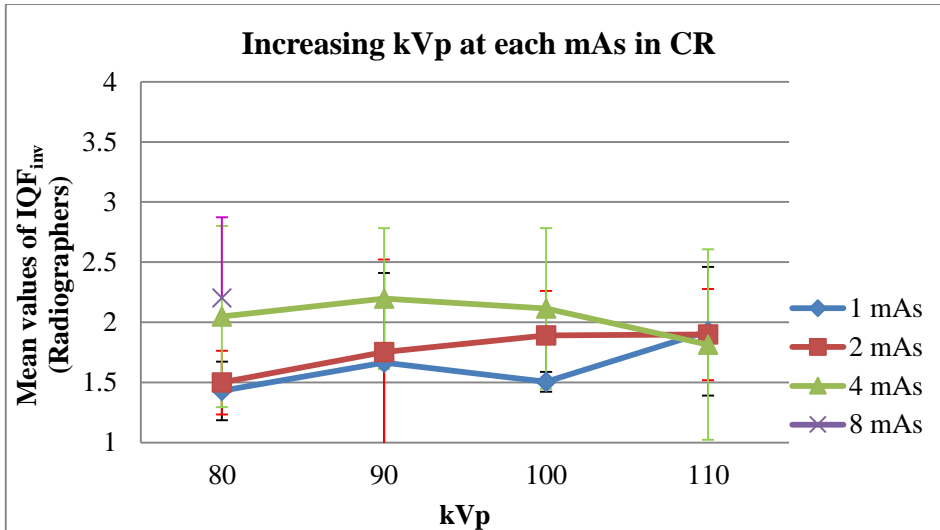
Figure 3.19   There were mostly increases in IQF$_{inv}$ mean values when kVp increased at fixed mAs. (Note the decline in IQF$_{inv}$ at 100 kVp with 1 mAs at 100 and 110 kVp with 4 mAs.)
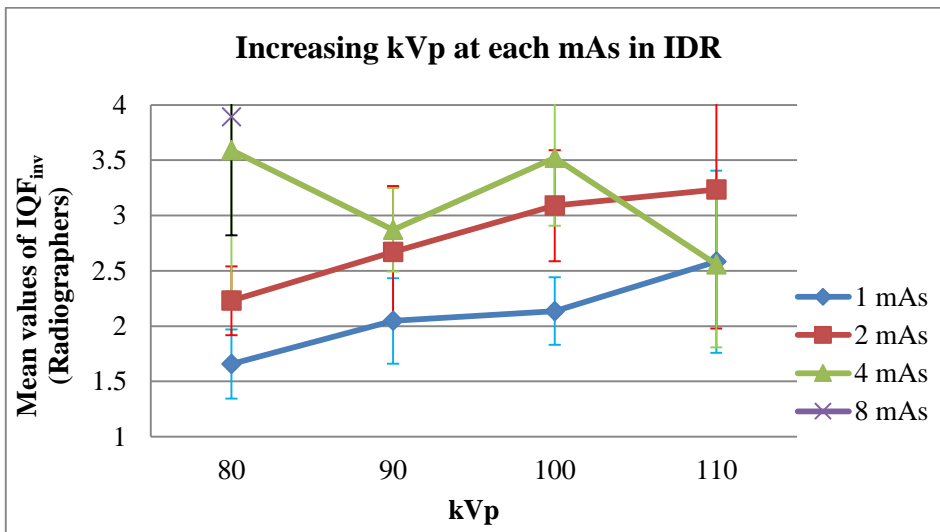
Figure 3.20   In IDR, at 1 and 2 mAs, the higher kVp was the higher mean values of IQF$_{inv}$. (Note the changes in IQF$_{inv}$ at 4 mAs with increasing kVp.)
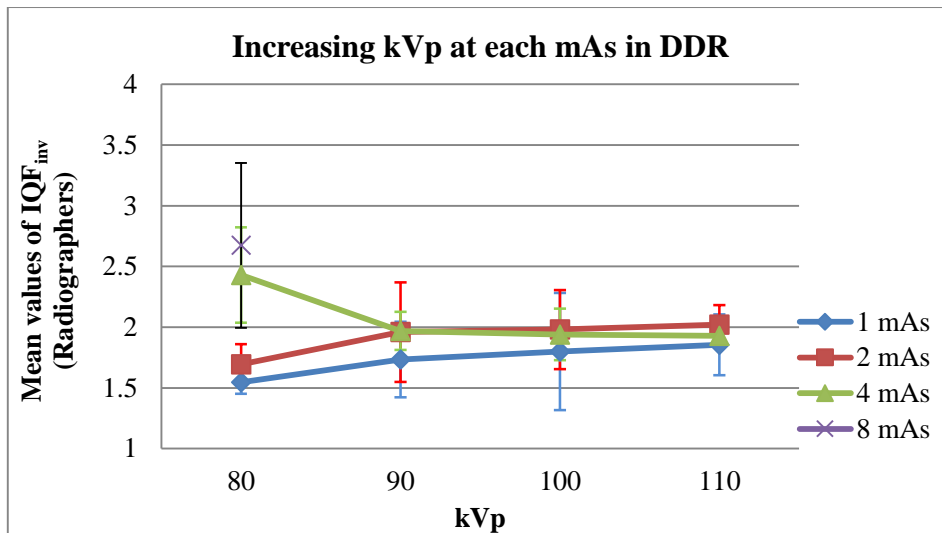
Figure 3.21   In DDR, IQF$_{inv}$ mean values increased when kVp increased to 90, at 1 and 2 mAs and declined at 4 mAs. (Note the changes in IQF$_{inv}$ values when kVp increased from 90 to higher kVp at all mAs levels.

In CR, the significant changes in IQF$_{inv}$ values were at 1 mAs when kVp increased to 110 ($p = 0.039$) and at 2 mAs when kVp increased to 100 or to 110 (p= 0.032) (Table 3.12).

In IDR, there were significant changes in IQF$_{inv}$ values with increasing kVp at 1 mAs ($p <$ 0.41) and when kVp increased from 80 to 100 at 2 mAs ($p = 0.004$). At 4 mAs, there were insignificant changes in IQF$_{inv}$ values with increasing kVp (Table 3.12).

In DDR, the significant changes in IQF$_{inv}$ mean values were when the kVp increased from 80 to 110 at 1 mAs ($p = 0.015$), when kVp increased to 100 or to 110 at 1 mAs ($p = 0.048$ and 0.003), and when kVp increased at 4 mAs ($p < 0.016$) (Table 3.12).

From the above discussion, the IQF$_{inv}$ values did not change significantly with increasing kVp at 4 mAs in CR and IDR, and significantly reduced in DDR based on the scoring results of radiographers. In CR, kVp had less effect on IQF$_{inv}$ values than in other systems.

The Tukey HSD test indicated that the 80 kVp group generally did not differ significantly ($p > 0.51$) from either of the other kVp groups.

Table 3.12   Differences (p values, Student t-tests) between images when altering kVp within mAs groups (based on IQF$_{inv}$ values from radiographers)

kVp	mAs	Sig. (p values, Student t-tests)		
		CR images	IDR images	DDR images
80	1	Ref	Ref	Ref
90	1	0.245	0.041	0.102
100	1	0.25	0.011	0.131
110	1	0.039	0.021	0.015
80	2	Ref	Ref	Ref
90	2	0.238	0.074	0.093
100	2	0.032	0.004	0.048
110	2	0.032	0.053	0.003
80	4	Ref	Ref	Ref
90	4	0.355	0.117	0.016
100	4	0.437	0.454	0.014
110	4	0.307	0.063	0.011

Changes to IQF$_{inv}$ when using different radiographic imaging systems

The relationships between the radiographic system and IQF$_{inv}$ values were evaluated, and Figures 3.22 to 3.29 display the results that show these relationships. The images of IDR had higher IQF$_{inv}$ values than CR and DDR at the various kVp settings and different mAs levels (Figures 3.22 to 3.29). The images of DDR mostly had higher IQF$_{inv}$ values than that of CR.
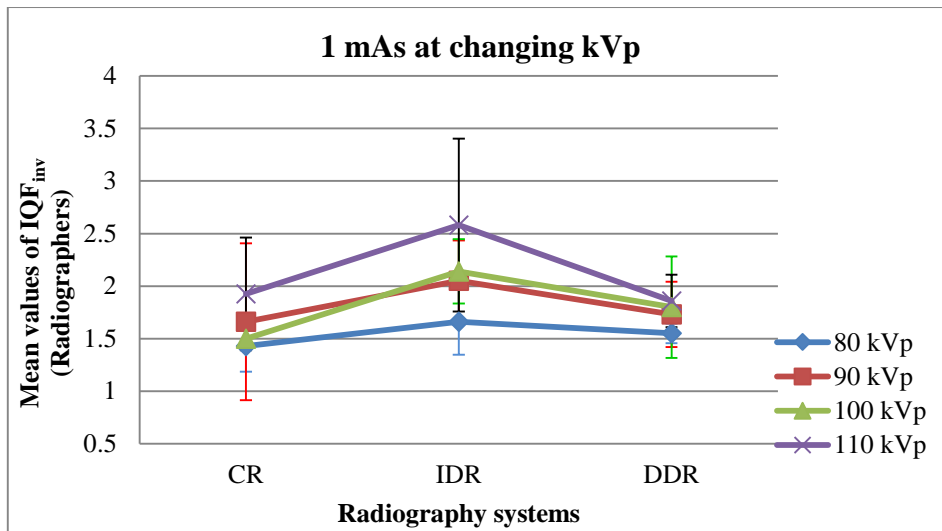
Figure 3.22   At 1 mAs, IDR had higher IQF_{inv} values with each kVp setting than CR and DDR. DDR had slightly higher IQF_{inv} than CR, except at 110 kVp.
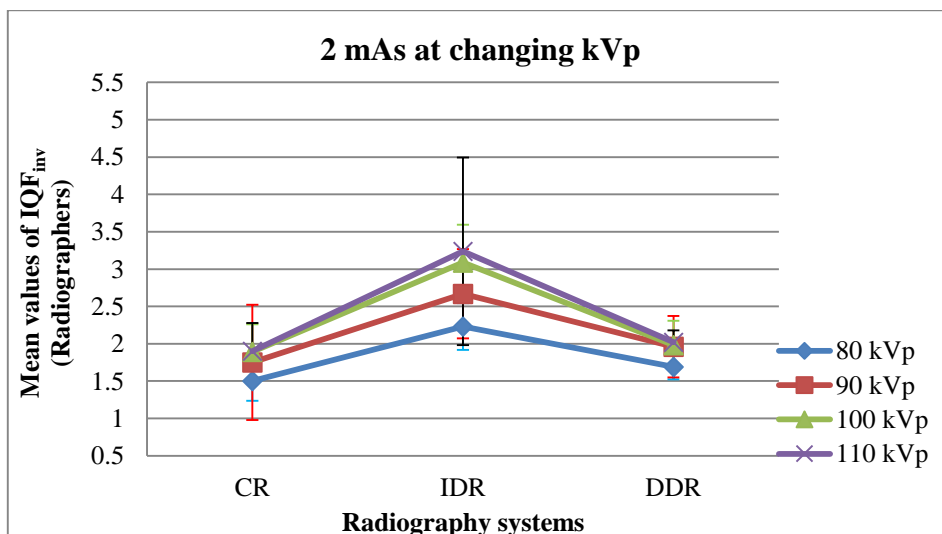
Figure 3.23   At 2 mAs, IDR had higher IQF_{inv} values with each kVp setting than CR and DDR. DDR had slightly higher IQF_{inv} than CR.
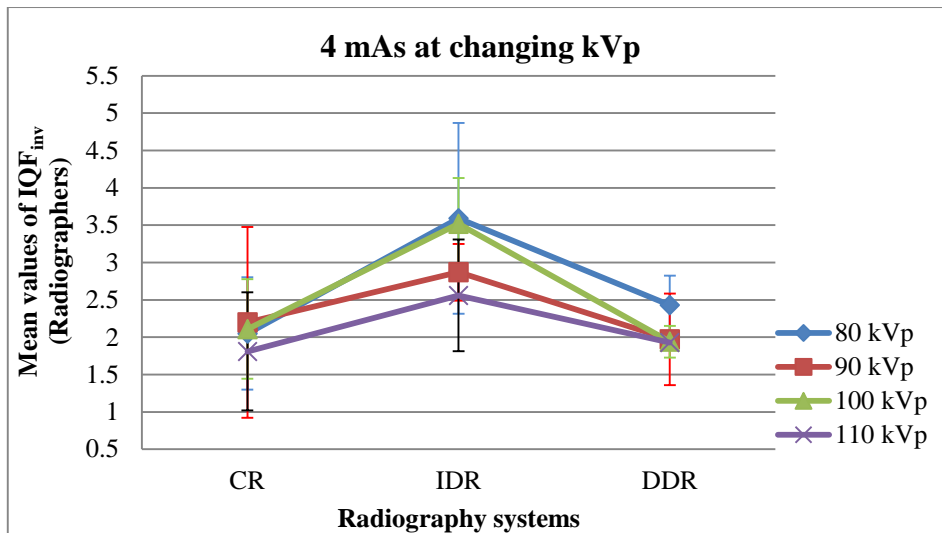
Figure 3.24   At 4 mAs, IDR had higher IQF_{inv} values with each kVp setting than CR and DDR. DDR had slightly higher IQF_{inv} than CR, only with 80 and 110 kVp.
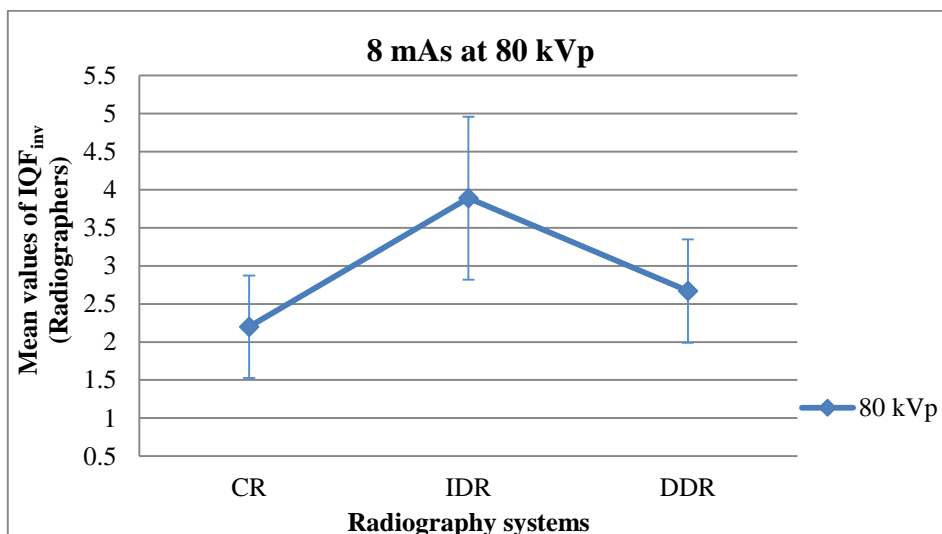
Figure 3.25   At 4 mAs, IDR had higher IQF_{inv} values with each kVp setting than CR and DDR. DDR had slightly higher IQF_{inv} than CR.
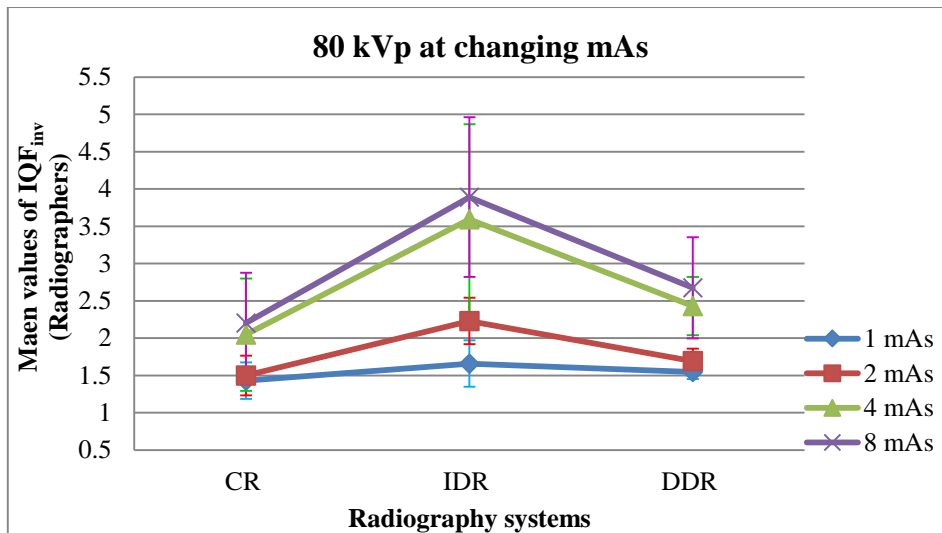
Figure 3.26 With 80 mAs, IDR had higher IQF$_{inv}$ values at each mAs level than CR and DDR. DDR had higher IQF$_{inv}$ than CR at all mAs levels.
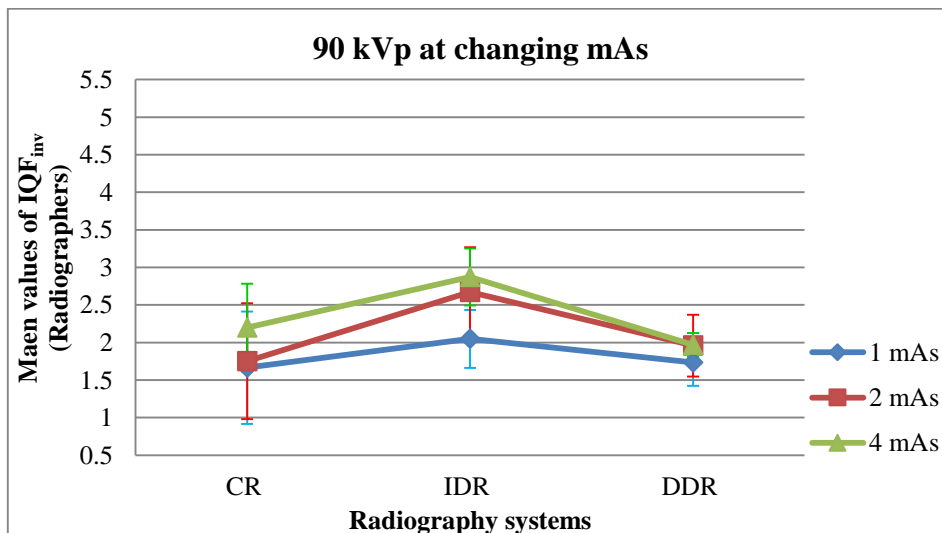
Figure 3.27 With 90 mAs, IDR had higher IQF$_{inv}$ values at each mAs level than CR and DDR. DDR had higher IQF$_{inv}$ than CR at 1 and 2 mAs levels.
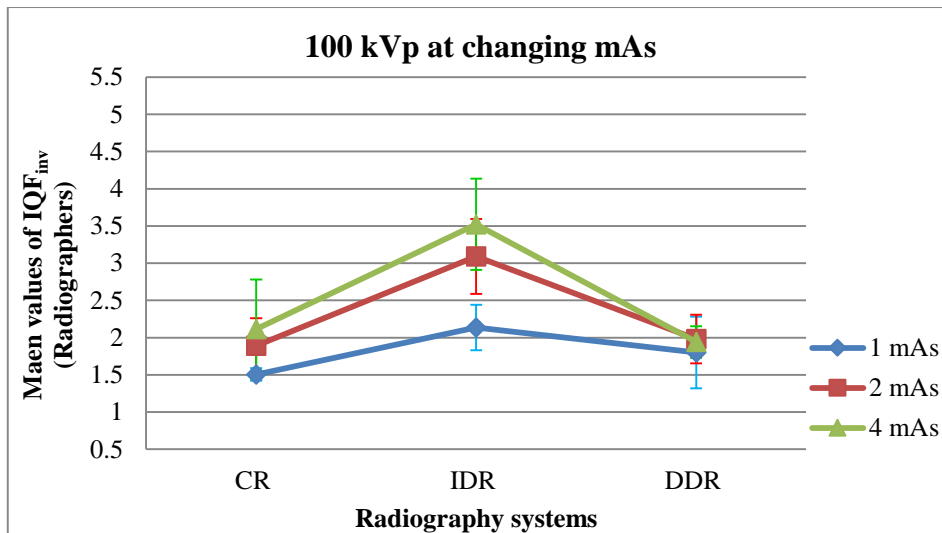
Figure 3.28 With 100 mAs, IDR had higher IQF_{inv} values at each mAs level
than CR and DDR. DDR had higher IQF_{inv} than CR at 1 and 2 mAs levels.
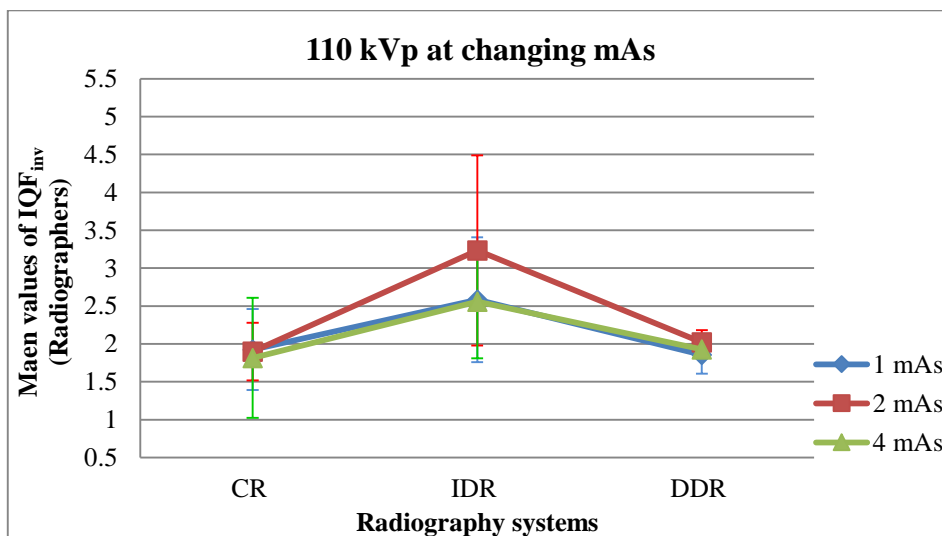
Figure 3.29 With 110 mAs, IDR had higher IQF_{inv} values at each mAs level
than CR and DDR. DDR had slightly higher IQF_{inv} than CR at all mAs levels.

Differences between images were also evaluated to measure any significance between them (Table 3.13). The differences in IQF_{inv} values between the images of IDR and other systems were mostly significant, particularly at 2, 4 and 8 mAs (Table 3.13). The differences between IQF_{inv} values of DDR and CR were insignificant all of the time (Table 3.13). The

Tukey HSD test indicated that the mean of IQFinv values for IDR was significantly different from either of the other systems (p <0.01) but CR was not differ significantly (p <0.38) from DDR.

Table 3.13   Comparing between systems' images differences (*p* values, Student t-tests) between images of same exposure factors

kVp	mAs	Sig. (*p* values, Student t-tests)		
		CR x IDR	IDR x DDR	DDR x CR
80	1	0.096	0.215	0.159
80	2	0.001	0.003	0.083
80	4	0.017	0.039	0.151
80	8	0.018	0.023	0.127
90	1	0.15	0.076	0.42
90	2	0.023	0.02	0.288
90	4	0.021	0.001	0.197
100	1	0.001	0.093	0.1
100	2	0.001	0.001	0.332
100	4	0.002	0	0.283
110	1	0.068	0.042	0.391
110	2	0.023	0.033	0.243
110	4	0.063	0.049	0.37

3.3.3   Discussion

Changes to IQF$_{inv}$ when using different mAs settings

The higher mAs levels generally improved the IQF$_{inv}$ values, as higher radiation dose from the higher mAs increased photon count, which would in turn result in increased SNR and thus increased detectability. However, high noise level images also increase the risk of diagnostic detail loss (Alsleem & Davidson 2012; Uffmann & Schaefer-Prokop 2009).

Changes to IQF$_{inv}$ when using different kVp settings

As mentioned previously in Section 1 of Phase 1, changing the kVp setting (when using digital recording systems) had an insignificant effect on the detectability of objects. Examples of this are seen in Figures 3.19 and 3.21, with CR and DDR. At the various mAs settings, when changing the kVp, the IQF$_{inv}$ values essentially did not change. However, there were inconsistent changes in IQF$_{inv}$ values when kVp increased at 4 mAs in IDR (Figure 3.20).

Changes to IQF$_{inv}$ when using different radiographic imaging systems

As discussed previously in Section 1 of Phase 1, the different design principles of CR, IDR and DDR detectors are attributed as the reason behind the differences in IQF$_{inv}$ values for images of each system.

The results suggest that evaluation method of LCD detectability performance based on radiographers' image assessments is a valid tool to examine the effects of exposure factors on image quality and to compare between different radiography systems. This approach has the potential to assess and optimise the image quality of digital radiography. This approach has the potential to provide a deeper understanding of exposure factor effects on various CR, IDR and DDR systems. However this method may be affected and limited by larger radiographers' number required and longer time. Hence the reliability of this method should be tested.

3.3.4 Conclusion

LCD detectability performance based on the observation of radiographers is a valid tool of image quality evaluation and optimisation and systems performance comparison. Higher mAs generally resulted in higher IQF_{inv} in all systems based on the scoring results of radiographers. Overall, kVp has less effect on IQF_{inv}, which reflects the fact of that kVp is not the dominant factor of final image contrast in digital radiography. The IDR system has significantly higher LCD detectability performance than other systems, while DDR and CR have comparable LCD detectability performance. Radiographers were generally sensitive to increasing mAs, where the higher mAs levels improved the IQF_{inv} values of the images. The linearity of radiographers' results—to the extent that higher mAs images had better IQF_{inv} values—were more consistent with IDR images than CR and DDR images.

While LCD detectability performance based on the observation of radiographers can be used for image quality optimisation and systems performance comparison, it is also essential to examine the reliability of the radiographers' results. This can be assessed by comparing their scoring results with software scoring results as the gold standard. Therefore, in the next section (Section 3 of Phase 1), LCD detectability performance based on the observation of radiographers will be evaluated. Accordingly, the validity and the effectiveness of automated LCD detectability performance based on software scoring will also be assessed.

3.4 Section 3 of Phase 1: Comparing the results from software and radiographers

In the previous two sections (Sections 1 and 2 of Phase 1), LCD detectability performance as a tool of image quality evaluation and optimisation was tested based on software scoring and radiographers' assessments. The effects of exposure factors on image quality (in terms of IQF_{inv} values) were assessed. The current study (Section 3 of Phase 1) aimed to examine the validity and effectiveness of the objective approach of the LCD detectability performance method based on automated software. The study also aimed to evaluate the reliability and the practicality of the subjective approach of the LCD detectability performance method based on the observation of radiographers. Software and radiographer assessment results were compared to examine the effectiveness and efficiency of LCD detectability performance as an optimisation tool. This section also aimed to measure detectability performance of radiographers. Correlation, assessment and measurement of differences were performed between the scoring performance of radiographers and software to evaluate the detectability performance of the radiographers.

3.4.1 Materials and methodology

The results from Sections 1 and 2 of Phase 1 were used to compare and contrast the results—and the implications of these results—between radiographers and software at different levels and contexts.

Statistical analysis

The statistical test of Pearson correlation coefficients was used to provide a numerical summary of the direction and the strength of the linear relationship between the mean scoring results of software and the average assessment results of radiographers. Pearson correlation coefficients which can range from -1 to +1 indicates whether there is a negative or positive correlation according to the sign and provides information on the strength of the relationship according to the value. While +1 indicates a perfect positive correlation, -1 indicates a perfect negative correlation and 0 indicates no relationship between the two variables (Pallant 2013). The correlation between detectability performance results—of radiographers compared with software analyser scoring—was performed for all images from different systems. Analysis of IQF_{inv} values was undertaken to determine if significant differences existed between the mean scoring results of software and the average assessment results of radiographers. Student t-tests, at an Alpha value of 0.05, were used for this purpose (Pallant 2013).

3.4.2 Results

In terms of detectability performance, there exists a positive correlation ($r = 0.558$) between radiographers and the software analyser. In most cases, IQF_{inv} values from radiographers' assessments and software scoring results were influenced similarly when changing systems and/or exposure factors. The average values of IQF_{inv} results from radiographers and software both showed that IDR and DDR had better detectability performance than CR, and that IDR had better detectability performance than DDR. However, there were significant differences ($p < 0.001$) between the assessments of radiographers versus software scoring. While the mean of IQF_{inv} values that were scored by software was 5.75,

the mean was only 2.19 for the images that were scored by radiographers. Figures 3.30 to 3.32 show the differences of the IQF_{inv} scoring values between software and radiographers for images of same exposure factors and same radiography system.
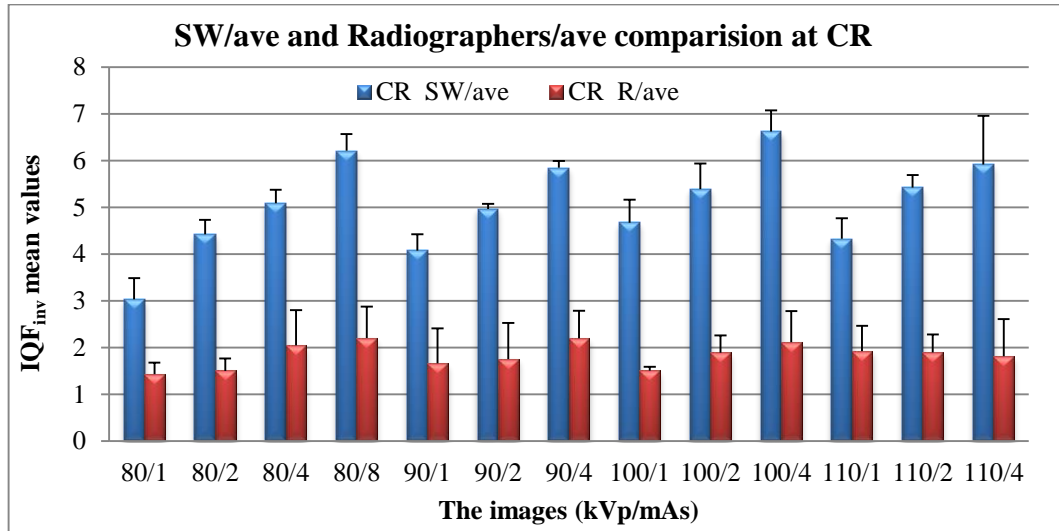
Figure 3.30 IQF_{inv} values from software are significantly higher than that from radiographers in CR systems. The values of IQF_{inv} for same images (scored by software and radiographer) increased with higher mAs particularly at 80, 90 and 100 kVp.
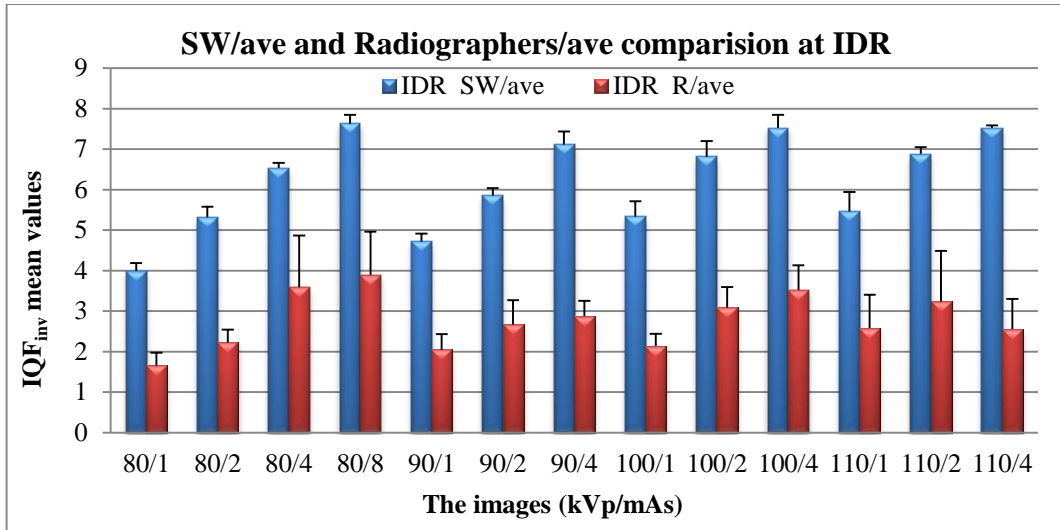
Figure 3.31 IQF$_{inv}$ values from software are significantly higher than those from radiographers in an IDR system. The values of IQF$_{inv}$ for same images (scored by software and radiographer) increased with higher mAs at each kVp.)Note the trend of IQF$_{inv}$ between 2 and 4 mAs at 110 kVp.
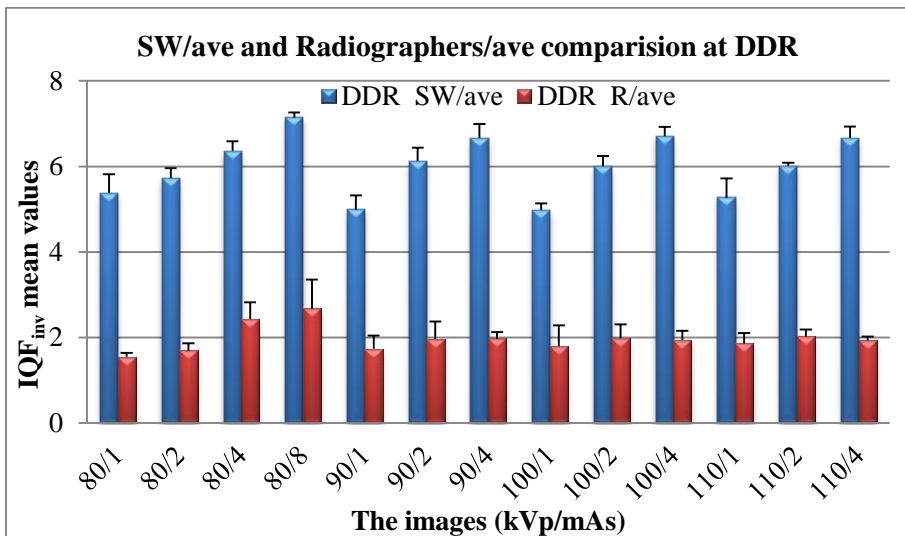
Figure 3.32 IQF$_{inv}$ values from software are significantly higher than that from radiographers in IDR system. The values of IQF$_{inv}$ for same images (scored by software and radiographer) increased with higher mAs at 80 kVp. Note the trend of IQF$_{inv}$ between 2 and 4 mAs at 90, 100 and110 kVp.

3.4.3 Discussion

Even though there were significant differences between IQF_{inv} values of the scoring results for radiographers compared with software, there was a positive correlation coefficient between them. The average scoring results of radiographers agreed with the scoring results of the software with respect to the IDR system having better detectability performance than other systems (although there were inter-radiographer differences). The radiographers and software also agreed that DDR has better contrast-detail detectability than CR. Several studies support this finding (Borasi et al. 2003; Cowen, Kengyelics & Davies 2008; Giovanni et al. 2006; Gomi et al. 2006; Neitzel 2005; Samei & Flynn 2003; Veldkamp, Kroft & Geleijns 2009), which reflects the strength of IDR (0.6-0.7) compared with that of DDR (0.4) and CR (0.2-0.3) (Borasi et al. 2003; Gomi et al. 2006; Neitzel 2005; Samei & Flynn 2003).

Software rescoring variation and inter-radiographer differences

When each image was analysed by the software several times to calculate its IQF_{inv} value, the same value was obtained (Table 3.4). To estimate inter-radiographer differences, the coefficient variation was calculated for each image that was scored by six radiographers. The inter-radiographer differences were lower in the DDR images than CR and IDR. Only two images of DDR have a coefficient variation above the mean (Figure 3.33).

An example of radiographer differences is seen in Figure 3.34, which shows results from two images: CR-80/1 and CR-80/2. The software IQF_{inv} scores were 3.033 and 4.427 respectively. Radiographers' scores significantly differed from the software ($p < 0.001$) and there were differences between themselves when scoring the same images. Importantly,

this also highlights that, in this example, one radiographer (R1) scored CR-80/2 lower when the software scored that image higher than an image of lower mAs (CR-80/1).

A further example of individual radiographer differences is shown in Figure 3.35. Radiographer R9's results showed that CR has better detectability performance than DDR, differing from the other five radiographers who scored the same images. The average results of radiographers—and the scoring results of software—showed that DDR has better LCD detectability performance than CR. Other such similar examples were noted in the radiographer results and shown in Figures 3.36 to 3.41.

Hendee and Ritenour (2002) also found that there were inter-observer variations, in addition to *intra*-observer variations (i.e. disagreement with a previous reading by the same observer). This can be explained by the fact that observers' performance is influenced by several factors. For example, the problem of 'not seeing' includes the limitations in human eye-brain visual system and distraction (Giger, Chan & Boone 2008). Observer fatigue while reading electronically displayed images is another cause (Krupinski & Berbaum 2009).
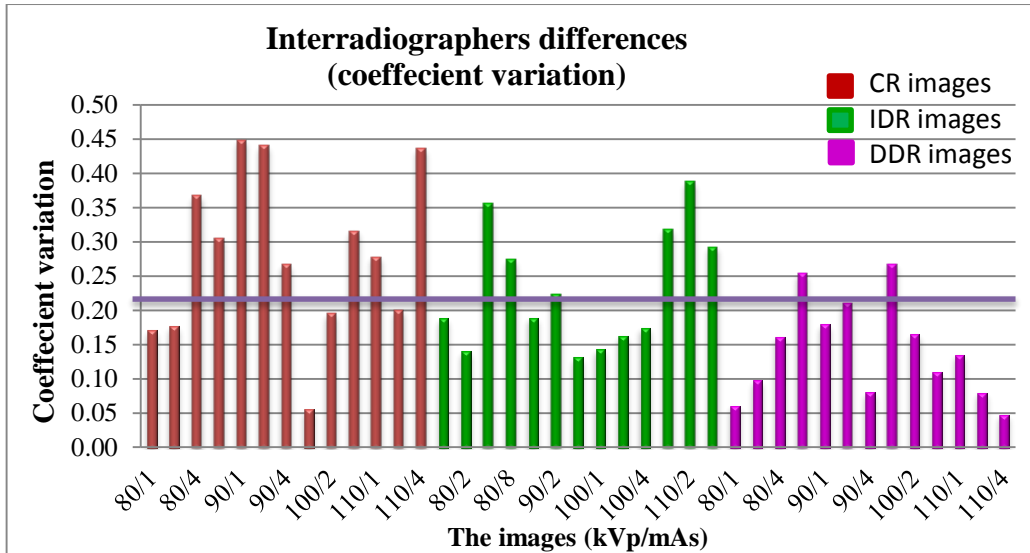
Figure 3.33   The differences between radiographers who score the same image in comparison with the average radiographer results and software scoring results in different systems. The inter-radiographer differences are lower in DDR.
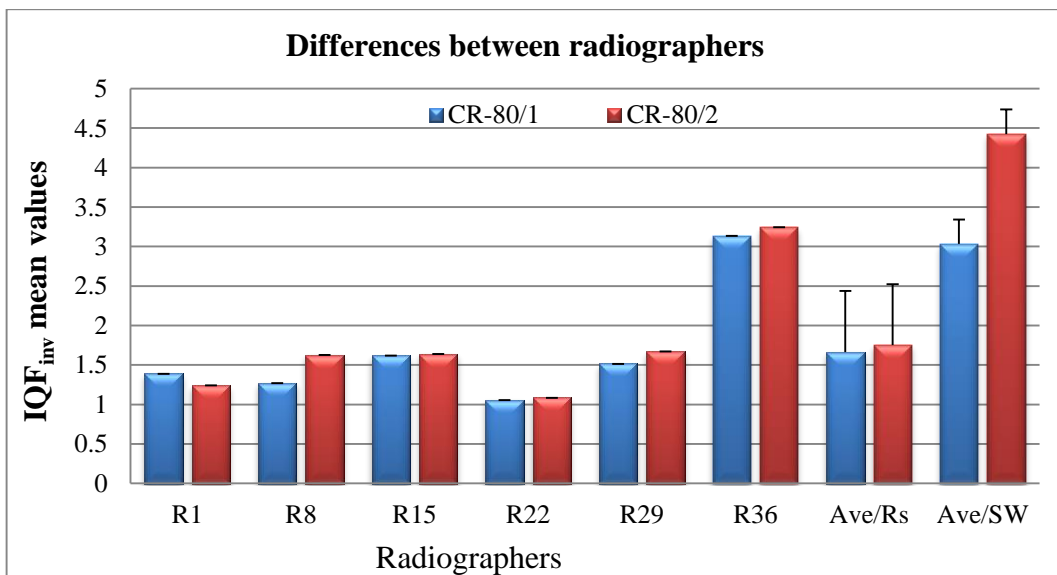
Figure 3.34   IQF$_{inv}$ values of CR-80/1 and CR-80/2 images (according to the software scoring) were significantly different to the average radiographer scoring. There are also differences between radiographers themselves when scoring the same images. (Note the results from R1 who scored CR-80/2 lower when the software scored that image higher than an image of lower mAs, that of CR-80/1)
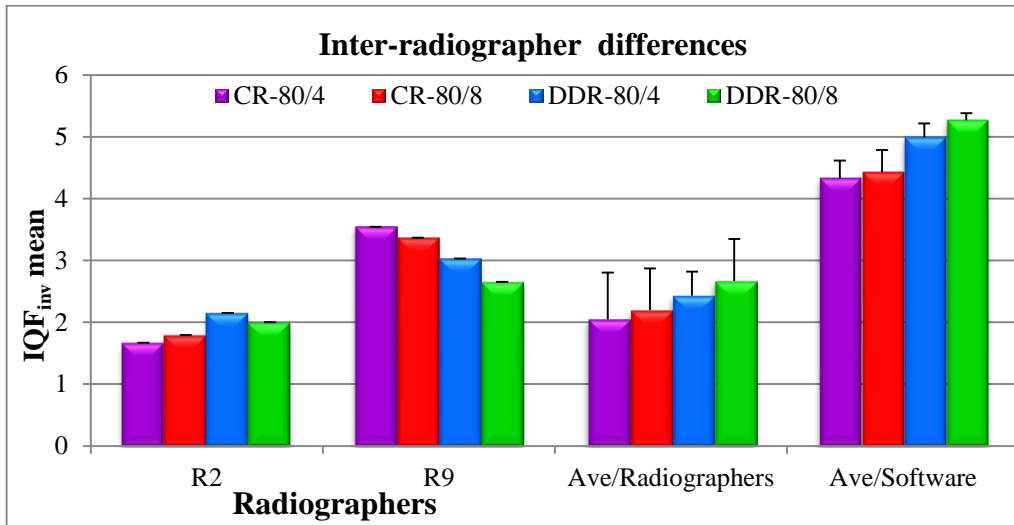
Figure 3.35   Results of some radiographers who scored the same images differ from that of software and radiographers' average results. The results of Radiographer R9 do not match with Radiographer R2, the average radiographers results or the software, as their scoring results in DDR had better detectability performance than CR.
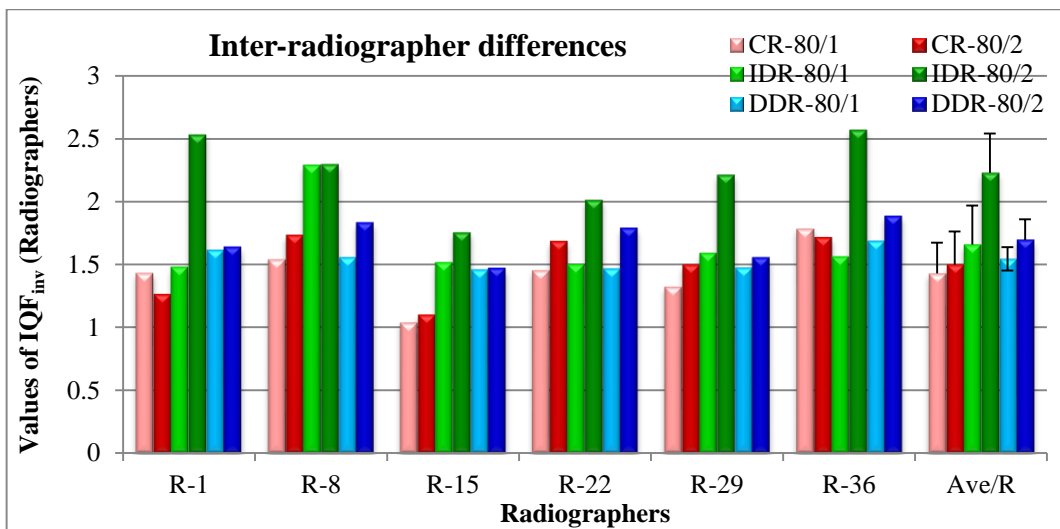
Figure 3.36   Results of some radiographers who scored the same images differ from that of software and radiographers' average results. The results of Radiographers R-1 and R-36 at CR images do not match with other radiographers and the average of radiographers. The average radiographers' results shows that CR-80/2 has better detectability performance than CR-80/1.
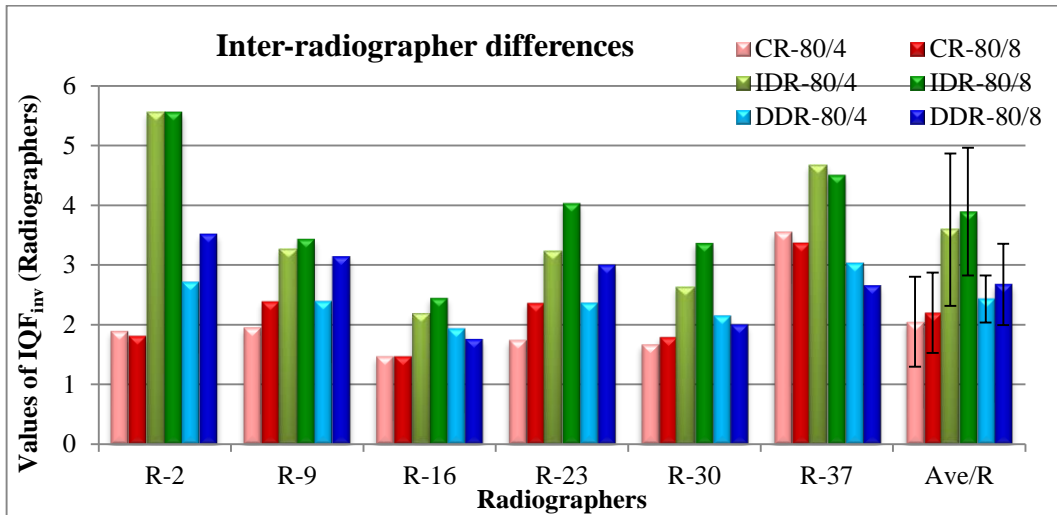
Figure 3.37   Results of some radiographers who scored the same images differ from that of software and radiographers' average results. The results of Radiographer R-37 do not match with other radiographers and the average of radiographers. For each system's images, the average radiographers' results show that higher mAs scores better and DDR images score better than CR images. However, R-37 shows the opposite.
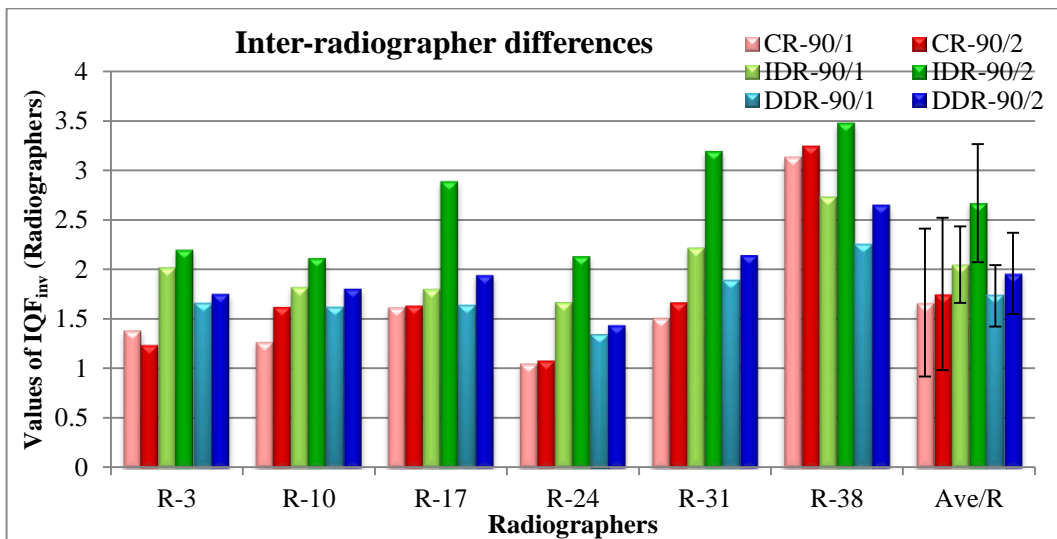
Figure 3.38   Results of some radiographers who scored the same images differ from that of software and radiographers' average results. The results of Radiographer R-3 do not match with other radiographers for CR images. The results of Radiographer R-38 also do not match with other radiographers and the average radiographers result as they show that DDR images have better scoring than CR images.

110
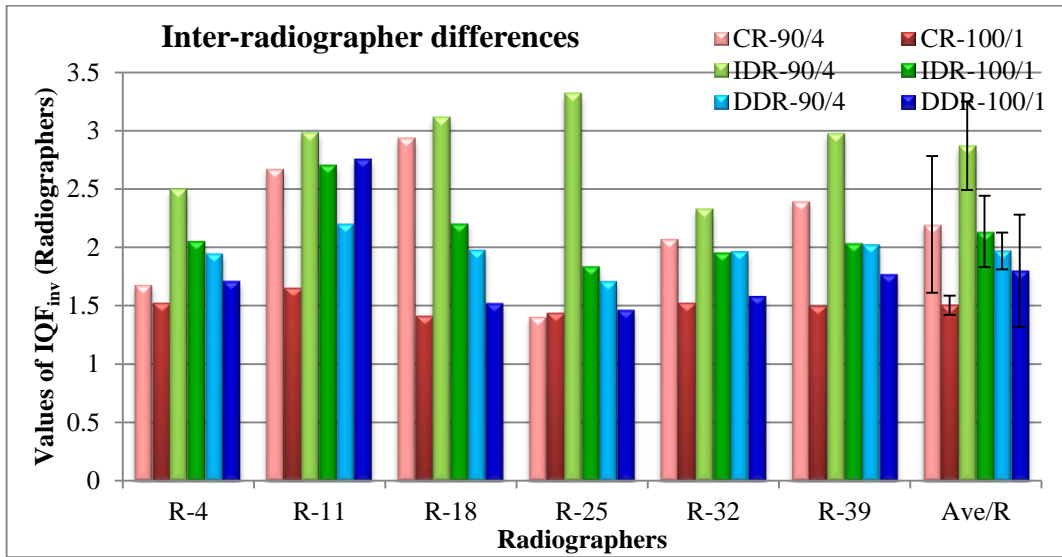
Figure 3.39   Results of some radiographers who scored the same images
differ from that of software and radiographers' average results. The results of
Radiographer R-11 do not match with other radiographers and the average
radiographers' results for DDR images. Their scoring results for DDR-90/4
show better detectability performance than for DDR-100/1.
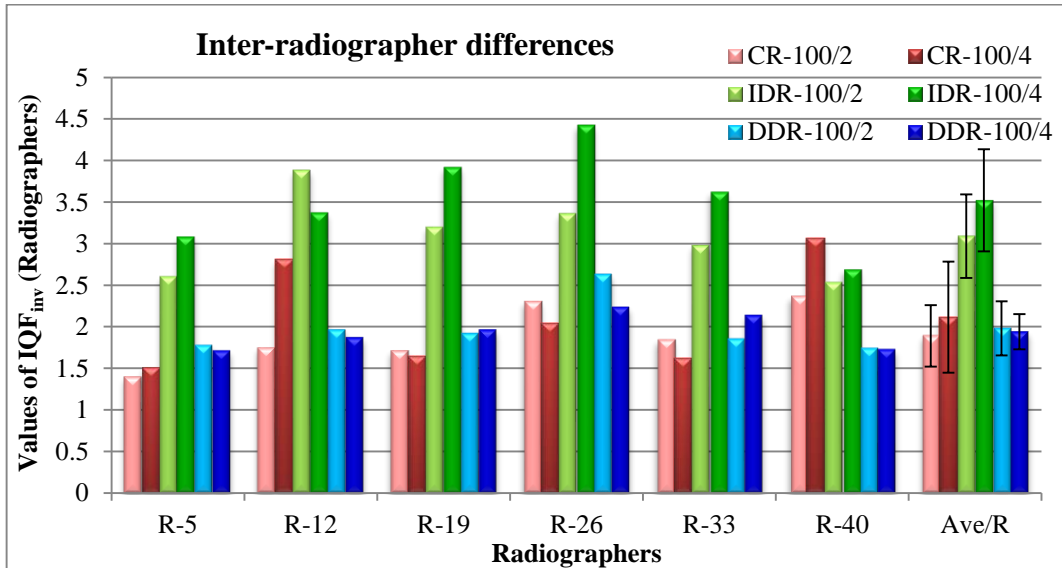
Figure 3.40   Results of some radiographers who scored the same images
differ from that of software and radiographers' average results. For CR
images, the results of Radiographer R-19, R-26 and R-33 do not match with
other radiographers and the average radiographers' results.

111
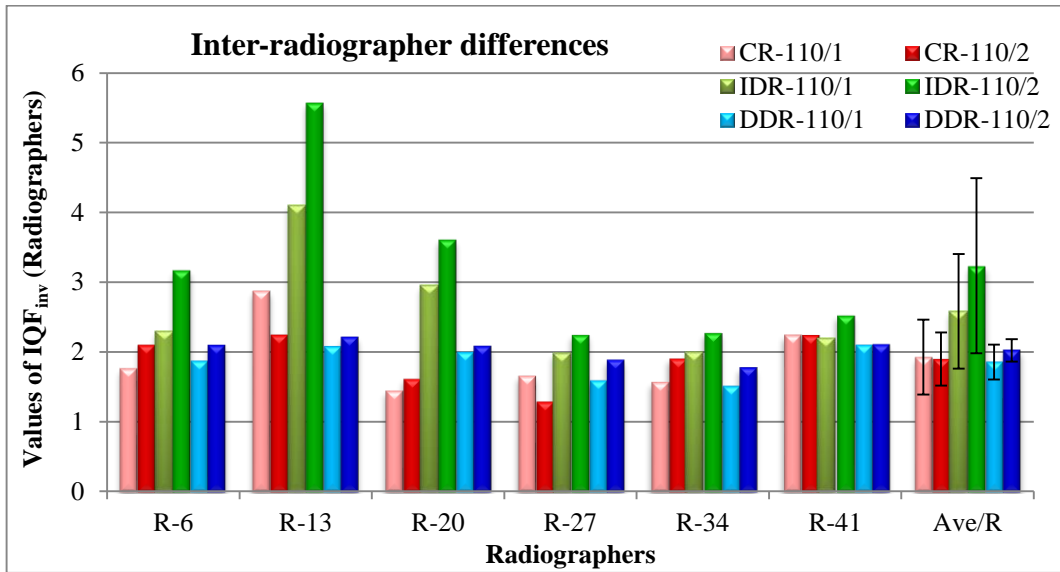
Figure 3.41   Results of some radiographers who scored the same images differ from that of software and radiographers' average results. For CR images, the results of Radiographer R-6, R-20 and R-34 do not match with other radiographers and the average radiographers' results.
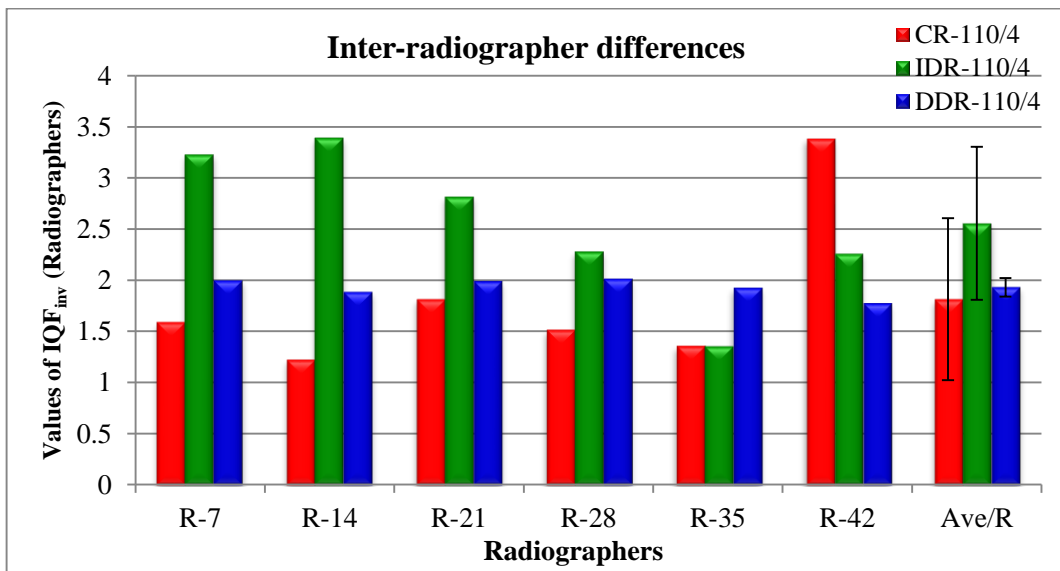
Figure 3.42   Results of some radiographers who scored the same images differ from that of software and radiographers' average results. The results of Radiographer R35 and R42 do not match with other radiographers and the average results, particularly for CR and IDR images.

3.4.4   Conclusion

The scoring performance of radiographers was compared with that of the software analyser, and both showed that IDR has better detectability performance than DDR and CR. However, software was much easier and faster, and offered higher validity than radiographers. In contrast, the reliability of radiographers' scoring results was hampered by inter-radiographer variability, which was lower in DDR than IDR and CR. In addition, the evaluation procedures based on radiographers required many radiographers to reduce human subjectivity and increase result reliability. Therefore, the subjective approach that involves human observers is time-consuming and cumbersome, meaning that the evaluation approach of LCD detectability based on human scoring is not ideal for routine image quality evaluation and optimisation. Generally, the ability of radiographers to detect LCD in an image is low compared with software scoring results. It is therefore recommend that, in order for radiographers to improve their LCD detectability, they should undergo further clinical practice/training in image viewing. This is an important area in their studies, as radiographers bear the responsibility of image quality optimisation. The limitations of this study include the fact that more radiographers could have been included to increase the reliability of the scoring results and to obtain more accurate results. Also, information about the radiographers—such as age, qualifications and experience—was not considered in this study. Such information could provide a deeper understanding about radiographers' detectability performance.

3.5 Overall conclusion

LCD detectability performance based on automated software image scoring is an effective tool for image quality assessment and image optimisation of digital radiography. This approach has the potential to provide a deeper understanding of exposure factor effects on various CR, IDR and DDR systems. Overall, mAs is the dominant factor of LCD detectability performance (compared with kVp) in digital radiography, and higher mAs generally resulted in better detectability performance in all digital imaging systems.

The IDR system has better detectability performance than CR and DDR (with better detectability performance at higher kVp), while DDR has better noise handling capability at lower exposure factors. The influences of exposure factors—of different radiography systems in terms of detectability performance—are not similar. While the results from radiographers led to similar results as the software, the approach based on radiographers' scoring is time-consuming and cumbersome, and therefore impractical for routine image quality assessment and optimisation. LCD detectability performance based on automated software is much easier and faster, and has higher validity and reliability than the human-based approach. By extension, it would appear that radiographers require more training to improve their ability in assessing the detectability performance of LCD. Further studies are suggested to test the different manufacturers of each type of radiographic system. Furthermore, different thicknesses of Perspex should be examined to represent different organ sizes. Radiation dose and beam filtration should also be considered in future studies. In Chapter 4, LCD detectability performance in computed tomography (CT) will be evaluated based on the literature.

Chapter 4 Low contrast-detail detectability of CT

4.1 Introduction

Computed tomography (CT) is a digital imaging system used to produce axial slices of a scanned object by rotating a thin beam of ionising radiation around the object and reconstructing an image using computers (Kalender & Khadivi 2011; Seeram 2009; Sprawls 1995). CT slice images allow the user to see inside the scanned object without cutting or opening it. The main advantage of CT is to improve low contrast-detail, or to be able to differentiate anatomical objects of low contrast from each other. CT eliminates the superimposition of tissue details outside the interest area (Sprawls 1995), and axial CT slice images can be also reconstructed to be a volume or a three-dimensional image (Kalender & Khadivi 2011; Seeram 2009; Sprawls 1995). Indeed, CT imaging technology is rapidly developing (Ledenius et al. 2009). With the introduction of multiple detector CT (MDCT), dual source CT (DSCT) and flat-panel detector CT (FDCT), the range of CT examinations has increased enormously. As a result of this increase in range, the number of CT exams has also increased (Fishman 2007; Kato et al. 2002). Recent developments of CT scanners have also improved the quality of CT images (Kalender & Khadivi 2011).

CT image quality parameters include spatial resolution, contrast resolution, temporal resolution, noise and artefacts. The current advanced technology of MDCT has improved contrast and temporal resolutions significantly, even though spatial resolution—particularly in-plane spatial resolution—has not markedly improved (Kalender & Khadivi 2011; Paul et al. 2010; Sun et al. 2008).

The highest radiation dose from medical imaging modalities is from CT scans (Brenner & Hricak 2010; Hayton et al. 2010), meaning that the radiation dose delivered to patients is

still the main concern in CT scan examinations. As a result, dose reduction has become a very important goal in CT applications (Brenner & Hricak 2010; Mahesh 2009). Despite this, there remain trade-offs between image quality and dose. The higher the dose contributing to the image, the lower image noise and hence the better visualisation of low contrast structures. Detecting low contrast-details and lesions are primarily limited by noise, which can be reduced by increasing radiation dose (Goldman 2007; Seibert 2004). Several studies have shown that there is still misdiagnosis—or loss of information—in CT images, as the pathologic lesions/details may be misdiagnosed or not detected by interpreters (Imai et al. 2009; Kalender & Khadivi 2011; Miller et al. 2010; Paul et al. 2010; 2005a; Peldschus et al. 2005b; Sun et al. 2008). Consequently, there is an imperative need for image quality evaluation and optimisation, and radiation dose reduction for CT images.

Several methods are used to evaluate imaging performance and image quality. Detective quantum efficiency (DQE), receiver-operating characteristics (ROC), visual grading characteristics (VGC) and low contrast-detail (LCD) detectability performance are all commonly used methods (Bath 2010; Cowen, Kengyelics & Davies 2008). CT scanners— of different manufacturers, various models and different algorithmic software—add further complexity to image quality optimisation (Ledenius et al. 2009). However, several authors state that LCD detectability performance is the most appropriate method to optimise image quality and to examine the potential of radiation dose reduction (Alsleem & Davidson 2012; Baker et al. 2012).

Since the common task of diagnostic CT scan images is the visual detection of lesions, LCD detectability performance is an important measure of image quality (Wunderlich & Noo 2008). LCD detectability performance is usually measured by using LCD phantoms, which contain cylindrical objects of a range of different sizes and contrast levels (Suess,

Kalender & Coman 1999; Zarb, Rainford & McEntee 2010). The evaluation method of LCD detectability performance has the potential to examine image optimisation and to assess the potential of dose reduction of imaging systems (Alsleem & Davidson 2012; Hamer et al. 2003). Recognising and understanding the factors that influence the detectability performance of different CT scan systems is a fundamental concern in effectively implementing this method.

This chapter aims to review and discuss the image quality parameters of CT images and the factors that influence these parameters. It also aims to discuss and evaluate the different image quality evaluation methods that are used to measure CT image quality, plus discuss advantages and limitations of each method. Accordingly, the factors that control the evaluation method of LCD detectability performance, the topic of this project, will be discussed. Therefore, the current chapter (Chapter 4) includes four main sections. Firstly, the physics of different CT types will be briefly described. Secondly, image quality parameters will be discussed. Thirdly, the evaluation methods of image quality will be explained. Finally, the factors that affect LCD detectability performance will be discussed. The results from the first and third sections of this chapter have been published (Appendix 1b) (Alsleem & Davidson 2013).

4.2 CT scanner systems

Today, CT scanners are of different types and models (Figure 4.1). The first CT scanners were commercially available in the 1970s, and since then this imaging technology has grown in popularity. Since the introduction of helical or spiral CT, which was invented in 1989, CT has seen a constant succession of innovations. Development of CT scanner

technology continued with MDCT. Four detector MDCT (4-MDCT) was introduced in 1998. Advances in MDCT scanning continued with the introduction of more detectors of MDCT (Kalender & Khadivi 2011; Seeram 2009). At the time of writing, MDCT scanners were offering up to 320 slices (Kalender & Khadivi 2011). DSCT, which uses two different x-ray tubes in a single CT unit, is a relatively new technique of CT imaging technology (Achenbach, Anders & Kalender 2008). FDCT is a CT technique under development to improve the quality of CT images (Gupta, R et al. 2008).
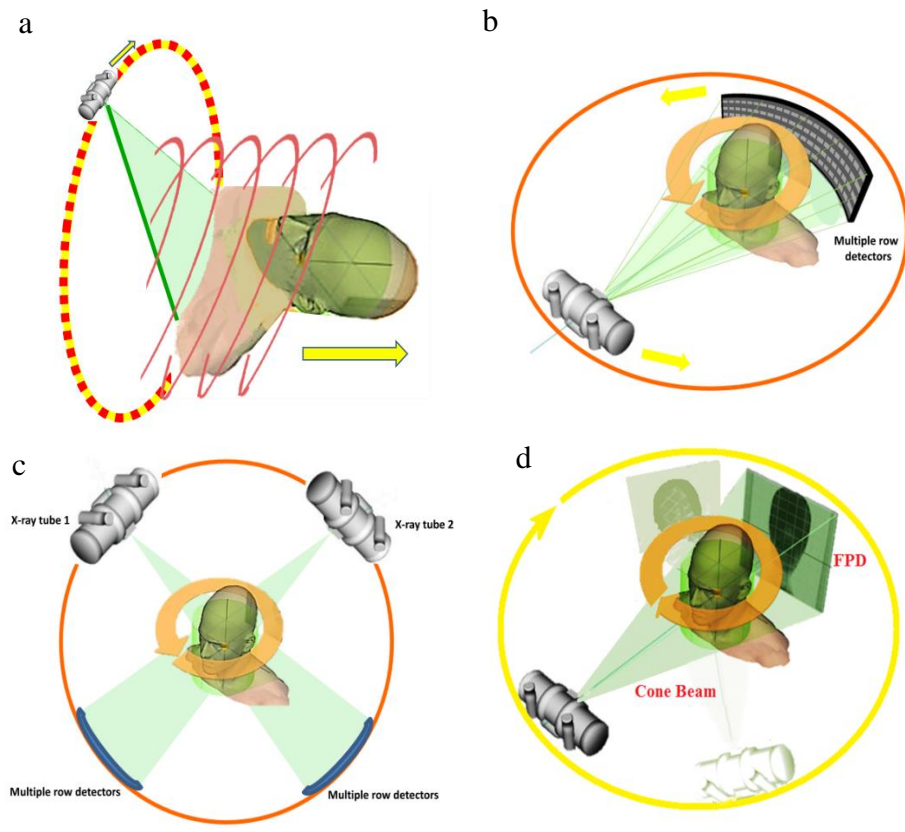
Figure 4.1   Spiral CT single slice, helical CT scanner with single row detector (a). MDCT scanner with multiple row detectors (b). DSCT scanner with two x-ray tubes (c). FDCT scanner with flat-panel detector (d), modified from (courtesy of Exxim Computing Corp) (EXXIM Computing Corporation).

118

Spiral CT (single slice CT)

Spiral CT scanners involve continuous patient translation and continuous radiation exposure during both the rotation of the x-ray tube and the acquisition of data (Figure 4.1a). Therefore, a shorter period of time is required to obtain a volume data set in comparison with conventional CT scanners. The detector of the spiral CT scanners includes one row of detector elements, which means that one slice is produced at a time; hence the spiral CT scan is sometime called a single CT scanner (Kalender & Khadivi 2011; Seeram 2009).

Multiple detector CT (MDCT)

MDCT is a spiral CT scanner with more than 1 row of detector elements. MDCT may have 4, 16, 64, 256 or 320 detector rows. Hence, MDCT scanners are able to generate many slices simultaneously, depending on the number of detector rows. With MDCT, scans can be completed in seconds or in a sub-second period (Figure 4.1b). In addition, recent MDCT can provide isotropic (the voxel depth, Z, is the same for pixel's X and Y dimensions) resolution and cross-sectional reconstruction in arbitrary planes (Bardo & Brown 2008; Hurlock, Higashino & Mochizuki 2009).

Dual source CT (DSCT)

DSCT has two x-ray tubes, which are arranged at 90° offset in a single gantry (Figure 4.1c). The two tubes and detectors are operated simultaneously. Hence, a one-quarter rotation of the gantry is sufficient to collect the data necessary for one image. Accordingly, the gantry rotation time of 330 ms provides an effective scan time of 83 ms in the centre of rotation.

DSCT offers the advantage of exposing the patient to two different energy spectrums (Achenbach, Anders & Kalender 2008; Kalender & Khadivi 2011).

Flat-panel detector CT (FDCT)

A recent development of CT technology is FDCT (Figure 4.1d), which utilises flat-panel detectors (FPDs) instead of the multiple detector rows in MDCT (EXXIM Computing Corporation) (Gupta, R et al. 2008; Kalender & Khadivi 2011).

4.3 Image quality parameters

Several parameters characterise the quality of CT images. Resolution (which includes spatial resolution, contrast resolution and temporal resolution), noise and artefacts are the main parameters of image quality (Bourne 2010; Goldman 2007). These parameters and their influence factors are fully discussed later in this chapter and are summarised in Figure 4.1. There are also other measures used to characterise image quality, including linearity and uniformity, which are briefly discussed.

Figure 4.2   Parameters of image quality an.d the influence factors of each parameter

4.3.1   Resolution

Image resolution is the essential feature of image quality. Resolution is the ability of the medical imaging process to discriminate between two objects in the image. Good image resolution clarifies accurate anatomic structures and details within the image. Resolution comprises three main categories: spatial resolution, contrast resolution and temporal resolution (Bourne 2010). Spatial resolution is the ability to discriminate between small objects with large differences in densities. Contrast resolution is the ability to discriminate

between objects with close differences in densities (Goldman 2007). Temporal resolution is the ability to discriminate between objects with respect to time (Bourne 2010).

4.3.1.1 Spatial resolution

Spatial resolution refers to the ability of an imaging system to discriminate between small objects that are close together (Seeram 2009). The size of pixels and the spacing between them define the maximum spatial resolution of digital images. The smaller the pixel sizes, the higher is the spatial resolution. However, this is not always true, because spatial resolution is influenced by other causes, such as blur factors (Bourne 2010; Chotas, Dobbins & Ravin 1999).

Two aspects are considered to explain and measure the spatial resolution of CT scan images, namely in-plane resolution (the so-called X/Y plane) and longitudinal or cross-plane resolution (the Z plane). The ability of CT scanners to resolve different sets of bars of lead (or other dense materials), where each set has a certain line pair per millimetre, measures in-plane spatial resolution. On the other hand, the slice sensitivity profile is used to describe cross-plane spatial resolution (Hsieh 2009).

A- In-plane spatial resolution factors

In-plane spatial resolution is the resolution in the X/Y direction. The in-plane spatial resolution is affected by scanner geometry and the reconstruction algorithm (Hsieh 2009).

The main physical influences of in-plane spatial resolution are the x-ray focal spot size and shape, the distance between the source and the iso-centre, the distance between the detector

and the source, and the detector cell size. The iso-centre is the point where the x-ray beams intersect while the gantry is rotating during beam-on. Appropriate geometric parameters are essential to acquire CT images with proper spatial resolution and noise performance (Hsieh 2009).

The x-ray tube of most CT scanners has two x-ray focal spots: a small spot and a wide spot. Better spatial resolution can be obtained by utilising a smaller focal spot size; however, the smaller the focal spot is the less x-ray flux can be delivered, which increases image noise (Hsieh 2009; Seeram 2009). X-ray flux is the total photons per unit of time passing through per unit area (Gupta, A 2013).

The reconstruction procedures of the CT image include reconstruction algorithms, the reconstruction field of view (RFOV), the display field of view (DFOV), the sampling rate and the sampling interval. The sampling rate or sampling frequency is the number of samples per unit of time taken from a continuous signal to make a discrete signal. The sampling interval or the sampling period is the time between samples. The mathematical procedures of image reconstruction, including conversion and back projections, affect in-plane spatial resolution. The image is sharpened; blur is removed by applying conversion algorithms or kernel to correct the frequency contents of the projections before back projection. Therefore, the convolution algorithms/kernel modify the appearance and the resolution of image structures. Various algorithmic conversions are used for different applications of anatomic structures. For example, sharpener algorithms are applied to emphasise bony structures, including extremities and the inner ear, and smoother algorithms are used to emphasise soft tissue and brain (Seeram 2009). Higher spatial resolution can be achieved by applying the bone algorithms. However, the improvement of spatial resolution is often accompanied by higher image noise (Hsieh 2009).

In-plane spatial resolution is also affected by RFOV, which is the size of the scanned field of view (SFOV) that is reconstructed to produce the final image. The RFOV determines the maximum diameter of the reconstructed image and generally ranges between 12 and 50 cm. RFOV is the essential determining factor of pixel size which is equal to RFOV divided by matrix size (Seeram 2009). For example, a pixel size of 0.98 mm is required to cover an image matrix of 512×512, with RFOV of 50 cm. Selecting RFOV size determines how much of the total raw data available will be used to reconstruct the image. The smaller the SFOV, the smaller the size of pixels. Hence, the information is distributed among smaller pixels and less information is contained in each pixel. Small object reconstruction and visualisation require an adequate small sampling interval (Hsieh 2009). Increasing RFOV increases the amount of data to be included. However, increasing RFOV also increases the pixel size, and hence more information obtained from the patient is packed into each pixel. As a result, in-plane resolution is reduced. The image pixel size should be small enough to support spatial resolution; however, too small a an image pixel will degrade spatial resolution and may exclude relevant areas from the visible image (Singh & Kalra 2012). RFOV can be changed by post-processing if raw data are available (Hsieh 2009).

B- Longitudinal or cross-plane resolution factors

Cross-plane spatial resolution is the term used for the resolution in the Z direction. Before the introduction of MDCT, slice thickness simply influenced the cross-plane resolution in CT. However, cross-plane resolution of MDCT images is affected by additional influences, such as the interpolation reconstruction algorithms, the reconstruction intervals, the size of the detector element and pitch. Pitch is the table feed per single rotation for an MDCT scanner (Mahesh 2009).

Slice thickness

Slice thickness is the depth of the voxel (Z-axis). Compared with the display field or matrix size, slice thickness plays a larger role in spatial resolution. Thinner slices have two influences on spatial resolution. Firstly, they reduce the amount of objects and tissues averaged together. As such, the slice thickness selection is essential to control volume averaging, which occurs when CT numbers of two or more different tissue types are averaged in a particular pixel, and hence affect the spatial resolution. Reducing slice thickness limits the degree of volume averaging (which can also occur in the X/Y direction) in CT images. Secondly, thinner slices increase the noise in the image if the exposure factors are not adjusted to compensate for the limitation of photons due to increased collimation (Kalra 2008; Mahesh 2009).

The thickness of slice selection, particularly in MDCT, is limited by the detector element size. The reconstructed slice thickness cannot be smaller than the detector elements used in the CT scanner (Mahesh 2009). In non-isotropic CT scanners, when the depth of the voxel is longer than the pixel's X and Y dimensions, the depth will be longer than either pixel's dimensions, as the slice thickness increases even with a large matrix and a small field of view. Slice width cannot be smaller than the detector element width, which is a main reason why there has been rapid improvement in detector technology to develop thinner and thinner detector assemblies (Mahesh 2009).

The pitch is also a limiting factor in image thickness and the effectiveness of the interpolation. The lower the pitch, the smaller the Z-gap of the helix pattern representing the Z-sampling spacing of the projection data used in the interpolation, and hence the

greater the interpolation effectiveness and the better the image quality. In CT, the Z-sampling efficiency, volume coverage speed, slice profile and image artefacts should be considered in the pitch selection. Larger pitch is required to increase volume coverage speed selection, and smaller pitch is selected to improve slice profile and image artefacts (Hu 1999).

Interpolation algorithms are used to reconstruct the data of spiral CT, and the Z-filtering (or Z-axis resolution) reconstruction algorithms are used to handle and reconstruct the data of multi-detector rows. Reconstruction algorithms are essential in MDCT, because of the table translation and displacement of multiple detector rows. The closer the Z-location to the measurement-to-slice location, the greater the contribution of measurements from all detector rows, and hence the more accurate the image reconstruction. The trade-offs of the slice thickness versus image noise and artefacts can also be controlled (Hu 1999).

The scan parameters—including mAs, beam collimation and pitch—and the Z-filtering reconstruction algorithms influence slice profile. The Z-filtering reconstruction enables the practitioner to generate multiple image sets from a single scan. However, Z-filtering reconstruction algorithms may cause image noise and artefacts, which means that the practitioners should select image thickness according to application requirements (Hu 1999).

C- Other Factors Affecting Spatial Resolution

Detector blurs (in plane and cross plane)

The blur that results from a detector is called detector un-sharpness. Spatial resolution basically depends on physical detector characteristics (Chotas, Dobbins & Ravin 1999), such as the width of the detector, detector aperture, matrix size, pixel size and the spacing between detector elements, each of which are factors of spatial resolution loss (Seeram 2009). The smaller size of detector elements represents superior spatial resolution. However, a small detector cell size reduces the dose efficiency of the system, as the effective detector area reduces (with smaller cell size) because of the cell gaps and post-patient collimator. The size of detector elements and focal spot should be properly balanced to avoid the drop-off of dose efficiency and/or the increase of image noise (Hsieh 2009).

Location of different x-ray absorptions within a detector element may be indistinguishable because all the x-ray photons contribute to a single quantity. Hence, when the image structures of a patient are smaller than the size of a single element of the detector, they are smeared out and their contrast is reduced (unless they are inherently high contrast objects). For example, when micro calcification is smaller than an element, it may be recognised as a calcification, since its attenuation properties are so diverse from the other tissue in the element (Williams et al. 2007).

The size of the detector element limits the reconstructed slice thickness in MDCT, as the slices cannot be reconstructed to be smaller than the dimension of the detector elements (Mahesh 2009).

The efficiency of the detector is influenced by the septa, the narrow strips between detector element spaces that are utilised to isolate the elements from each other and treat scatter

radiation that may contribute to the final detector signal. The geometric efficiency of the detector is determined by the ratio between the active area of the detector array and the whole radiation area of the detector. The material type of the detector construction, and the properties of the detector's absorption and conversion, control the sensitivity and the efficiency of the detector elements (Mahesh 2009).

Detector un-sharpness is also referred to as scatter radiation, fluorescence or photoelectric interactions within the image receptor when photon energy is dissipated. Blur can also be caused when all or part of the photon energy is deposited somewhere in the detector other than the original point of entry. Another source of blur is when a portion of scattering secondary energy carriers is absorbed by the detector (Hsieh 2009; Mahesh 2009; Samei 2003b).

Patient factors

Subject un-sharpness (also referred to as object blur) may be caused by object size, shape or structural composition. Motion un-sharpness is the most problematic un-sharpness factor caused by the patient. When motion occurs, the boundaries of patient structures are shifted from their actual position during image processing. Consequently, the structure boundaries in the image are blurred. Motion that originates from the anatomic region being imaged can be either a voluntary action of the patient or an involuntary physiologic process. The influences of involuntary motion—such as heartbeats and bowel peristalsis—can be eliminated or minimised by utilising very short examination times (Hsieh 2009; Samei 2003b).

4.3.1.2 Contrast resolution

Contrast resolution—sometimes called tissue resolution—refers to the ability of an imaging system to discriminate between objects with small density differences and/or differentiate small attenuation variety on an image (Williams et al. 2007). Contrast resolution determines the capability of the image system to discriminate subtle structures in organs being examined (Hendee & Ritenour 2002), and is measured and reported in terms of LCD detectability performance. Contrast resolution can be inherited by recording the information of interest with sufficient resolution intensity to discriminate low contrast structures of interest from the background (Bourne 2010; Mahesh 2009). While the first step of the digitisation is sampling in space, which affects the spatial resolution, the second step is the quantisation in signal intensity, which influences the contrast resolution or the gray-scale bit depth (Krupinski et al. 2007).

Contrast resolution is affected by tube collimation, radiation dose, noise, scatter radiation, beam filtration, detector properties and algorithmic reconstruction (Goldman 2007). It is also influenced by x-ray photon flux which is affected by tube current (Mahesh 2009). A noisy or inhomogeneous background makes it hard to distinguish two lesions with minor density differences (Park, H et al. 2009). Contrast resolution of the final image is influenced by subject contrast, detector sensitivity, reconstruction algorithm, slice thickness and image display (Mahesh 2009).

Subject contrast

CT subject contrast originates from differences in the physical density of tissue, which causes differential attenuation for Compton scatter (Goldman 2007). The anatomical and

physiological characteristics of the region being imaged are considered the intrinsic factors of image contrast: known as intrinsic, subject, object or patient contrast. Low intrinsic contrast tissues have very subtle differences in composition. The physical properties of atomic number, physical density differences among different tissues, and patient thickness all influence intrinsic (or subject) contrast (Hendee & Ritenour 2002).

Image contrast can be enhanced by selecting careful exposure techniques for specific tissues—and certain purposes—to obtain the desired information. It can be also improved by introducing enhancement substances or contrast media into the body. Contrast media alters the subject contrast of the tissue by changing its photon attenuation properties from those of the surrounding structures, and hence different signals are provided (Hendee & Ritenour 2002).

Detector properties

The characteristics of the detector play an important role in producing contrast resolution in the final image. The performance of the detector is described by DQE, which is used to assess the ability of the detector to transfer a signal and to characterise the noise associated with the detector (Pascoal et al. 2005). The ability of detectors to reproduce and preserve the information contained in the incident x-ray signal is an essential factor that influences contrast resolution (Bath 2010; Tsai, Lee & Matsuyama 2008).

Reconstruction and processing effects

Reconstruction algorithms and parameters, including slice thickness and post-processing applications, can also influence contrast resolution. For example, reconstructing images by combining thin slices into thicker slices enhances the contrast resolution (Mahesh 2009).

Slice thickness

Slice thickness is a factor in CT that increases image noise and hence deteriorates the contrast resolution of CT images. When slice thickness is reduced, the number of detected photons will reduce as well. In the same way, doubling slice thickness will also double the detected photons (Goldman 2007). As such, thicker slice reconstructions are recommended to improve contrast resolution, although a result of this may be that spatial resolution is reduced. With the introduction of MDCT, however, contrast resolution can be improved without compromising spatial resolution (Mahesh 2009).

Post-processing application

The window level and window width settings are used to display the image control contrast resolution of CT images. These settings determine how the actual measurements of tissue attenuation are converted into a gray-scale appearance. Narrow widths are more useful for showing soft tissues, and wide window widths can be used to provide an accurate demonstration of bone (Sprawls 1992). Noise appearance in the image is reduced with a wider window, but this also reduces the contrast appearance of the image (Hsieh 2009).

Display aspects

Viewing environment and conditions—such as room lighting and light reflecting from other display monitors—can affect image display quality and hence contrast resolution. It can be improved by using zooming and roaming display functions to achieve a correspondence between the display pixel matrix and the detector element matrix, so that resolution limitations of partially displayed monitor images can be avoided. Moreover, contrast resolution can be enhanced by maintaining uniform display luminance throughout the entire image. Bit depth resolution, which controls the luminance quantification of soft copy display, is recommended to be large in order to prevent the loss of contrast-details or the appearance of contour artefacts (Krupinski et al. 2007).

The contrast resolution of CT images can be measured with phantoms containing different low contrast objects, or a range of different CT numbers of different sizes. LCD detectability performance of the CT level is shown in terms of linear attenuation coefficient percentage. For example, 1% contrast means that the variance of CT numbers between the object and its background is 10 Hounsfield Unit (HU) (Mahesh 2009).

4.3.1.3 Temporal resolution

The photons that carry information have finite speed and take a certain period to be recorded by the detectors. Temporal resolution refers to the measurement accuracy and precision with respect to time (Bourne 2010; Taguchi & Anno 2000), and determines the

ability and efficiency of any imaging system to deliver image detail in the shortest period of time (Taguchi & Anno 2000).

Recent applications of CT studies, particularly CT fluoroscopy and cardiac imaging, increase the importance of the temporal resolution specifications of CT systems. CT fluoroscopy, which is used primarily for interventional procedures, relies on near real-time feedback from the presented images on the monitor to guide the practitioner in introducing the interventional instrument to the correct orientation and depth. On the other hand, cardiac CT scanning relies on the freezing of the cardiac motion. Even though these two applications emphasise different aspects of temporal resolution, they both demand better temporal CT resolution (Hsieh 2009).

Temporal resolution can be improved by several methods. First, temporal resolution is improved by increasing the scan speed, which eliminates or reduces motion influences. The second method is the use of reconstruction algorithms that use less than a full rotation of projection data for reconstruction. Half-scan algorithms with a view range of 180 degrees are the most commonly used algorithms. Temporal resolution can be improved by 40% with an algorithm of 220 degrees for typical CT scanner geometry. The third method to improve temporal resolution is the use of a physiological gating device for cardiac imaging. Even though this method does not directly improve the temporal resolution, it assists in reducing the motion impacts of the heart. The fourth method is to increase the scan coverage. Commercially available CT scanners (with 320 MDCT) can cover the entire heart, up to 16 cm, in a single rotation. DSCT that utilises two x-ray tubes improves the temporal resolution by the factor of two (Mahesh 2009; Seeram 2009).

4.3.2 Noise

Noise is un-useful information (Sprawls 1995) that is recognised by the grainy appearance of an image—or 'salt-and-pepper' pattern (Goldman 2007)—and is produced by the statistical fluctuation of value from pixel to pixel. Image noise relates to the numbers of x-ray photons that are logged in each pixel. The noise level is explained by the standard deviation, a measure of how spread out the pixels' values are. The lower the standard deviation, the higher the accurate average pixel value (Samei 2003b; Tapiovaara 2008). Goldman (2007) categorised the sources of noise into three types: quantum noise, electronic or detector noise, and computational or quantisation noise.

Quantum noise

Quantum noise is determined by the number of x-ray photons that are detected. The scanning techniques (including kVp and mAs), time, slice thickness, pitch, scan speed and umbra-penumbra ratio are the main factors of quantum noise. The percentage of photons that are detected (and converted to useful signals) is also determined by the scanner efficiency, including DQE and detector geometry. Noise can be reduced by increasing scanning technique (mAs and kVp), although this will also increase the radiation dose to patients. Thicker slices and slower scan speed will also reduce image noise, although thick slices may degrade the quality of the volume image and increase the partial volume effect. Slower scan speed may increase the effects of patient motion artefacts and reduce organ coverage. Therefore, understanding these trade-offs is essential in order to adjust these factors effectively to combat noise (Hsieh 2009).

Anatomical structure size, decreasing pixel size and scatter radiation are also factors that cause quantum noise. Any disturbing anatomic background variability is often called anatomical noise (Tapiovaara 2008).

The inherent physical limitations of the system

The second source of noise is created by the inherent physical limitations of the system. This kind of noise can originate from the detector's photodiode, the data acquisition system, x-ray translucency of the scanned object, scattered radiation, and many other factors (Hsieh 2009). Detector or receptor noise, which is also called electronic noise, is produced because of a non-uniform response to a uniform x-ray beam (Sprawls 1995). This type of noise has a fixed correlation to locations on the receptor; therefore, it is called fixed pattern noise. Fixed pattern noise can be largely eliminated in digital imaging systems through post-processing stages. Additionally, defects in the receptor's elements, which may have occurred during the manufacturing process, can form unrelated structures in the image, creating noise (Williams et al. 2007).

Image generation noise

Image generation processes are the third source of noise in CT images. This noise originates from different areas, including reconstruction algorithms and parameters, in addition to the effectiveness of calibration. Reconstruction kernels, reconstruction FOV, image matrix size, and post-processing technique selection can also affect noise level. For example, reconstruction algorithms for high-resolution reconstruction kernels will increase the noise

level in the images. Many post-processing techniques or image filtering techniques have been developed to suppress noise and preserve fine structures in the original image (Hsieh 2009).

Quantisation noise occurs during the digitisation process or during translation of the analogue output voltage of detectors to discrete pixel values (Williams et al. 2007).

4.3.3 Artefacts

An artefact is any error or distortion in the image that is not related to the organs or objects being examined (Morgan & Miller 1983). Artefacts degrade image quality, hide pathologic tissues and lead to misdiagnosis. Artefacts originate from various sources and form in different situations. The main causes of artefacts are geometric inconsistencies, blurring, inaccurate CT numbers, motion, metallic objects, out-of-field effects, edge gradient effects, high-low frequency interfaces, equipment malfunctions and sampling errors.

There are different categories of artefacts (Barrett & Keat 2004): physics-based artefacts, patient-based artefacts, scanner-based artefacts, and spiral and cone beam artefacts. Physics-based artefacts—including beam hardening, photon starvation, volume averaging and under-sampling—produce from the data acquisition process. Patient-based artefacts originate from the presence of metallic materials, patient motion and incomplete projections. Scanner-based artefacts—such as ring artefacts—are caused by imperfections in scanner function. There are also different patterns of artefact that degrade the quality of CT scan images. Most of the mentioned artefacts appear as streaks, shading or stair-step artefacts. Spiral and cone beam artefacts occur in the images of helical scanners,

particularly MDCT and FDCT scanners (Barrett & Keat 2004). The most common artefacts are briefly discussed in next paragraphs.

Beam hardening

Beam hardening artefacts occur when high-density structures absorb the low energy photons of the x-ray incident beam and leave the high-energy photons in the transmitted beam to strike the detectors. This increases the effective energy of the photon beam when it passes through the object being imaged. When the photons strike bone (high-density structures) then traverse over brain tissues (low densities structures), lower energy photons are absorbed. Consequently, a thick streak artefact appears across the region being scanned. For example, beam hardening artefacts occur in the area between the bone and soft tissue when the posterior fossa is imaged (Barrett & Keat 2004).

Metallic object artefacts

Metallic object artefacts occur when the objects being imaged contain metallic material such as dental fillings or prosthesis. Metallic materials cause a streaking effect on an image because such materials exceed the attenuation values that CT system can faithfully image. CT number scales have been expanded (to much higher than bone CT number) to include objects that have a CT number as high as 4,000 (Barrett & Keat 2004).

Edge gradient streak

Edge gradient streak artefacts occur when the edges of a sharp high-density object interface with a smooth surface such as the edges between bone and soft tissues. For example, this artefact occurs on pelvis CT images (in the area of the ischia spines), due to a high frequency structure interfacing with adjacent muscle tissues (a low frequency structure). As a result, a thin black streak artefact arises from the edge of the bone. Edge gradient streak artefacts also emanate from a thin biopsy needle, although they generally originate from within an anatomical part and are not always straight line streak artefacts (Barrett & Keat 2004).

Motion artefacts

Motion artefacts are produced by any movement that occurs during body scanning and image reconstruction, and cause streaking lines and blurring that degrade the image information of the body organ being imaged (Barrett & Keat 2004). The efficiency of image reconstruction depends on the ability of the computer to position attenuation values into the corresponding location of pixels. While the computer performs the mathematical reconstruction algorithm to produce the image, motion blur may be caused by any movement that prevents the computer from placing an attenuation value onto the image displaying matrix. The image reconstruction system is therefore unable to solve and process these inconsistencies in attenuation.

Equipment malfunctions—such as tube-arching faults, electrical defects and detector errors—produce artefacts. Tube arching malfunctions create many streaks that look like a

lightning storm. Straight black line streaks, particularly on scout images, arise generally from malfunctioning detectors (Barrett & Keat 2004).

Volume averaging

The partial volume effect—or volume averaging—occurs when a particular pixel is occupied by two or more different tissue types. The CT numbers of these tissues are averaged in that pixel. For example, if one pixel contained two different tissues that had CT numbers of 100, and 200, the ROI measurement of that pixel would be approximately 150. The tissues are averaged which produce a number that is inconsistent with the three tissues that were evaluated. Partial volume averaging is always present and can never be eliminated. Utilising smaller section thicknesses or smaller displayed views may increase the accuracy of CT numbers (Barrett & Keat 2004).

Ring artefacts

A ring or a number of rings that appear on CT images—and superimposed on the structures being scanned—are called ring artefacts. Ring artefacts are mainly caused by misaligned and/or miscalibrated detectors; this error occurs in rotate–rotate CT scan systems, where the x-ray tube and detector array rotate at the same time. Any shifting in the tube, which is physically connected to the detectors, can cause misalignment of the CT system and consequently non-uniform information as ring artefacts occur on the image (Barrett & Keat 2004).

The above discussed parameters are judged objectively (statistical measurement) and/or subjectively (human observation) to measure the level of image quality (Tapiovaara 2008). In order to improve image quality, parameters should be manipulated to optimise the image quality for certain purposes and specific regions, as these parameters are not independent (Goldman 2007).

Other image quality parameters

4.3.4 Image consistency and uniformity

The consistency and uniformity of CT scan images measure the accuracy of the CT number. The consistency of the CT number implies that the CT numbers of the reconstructed phantom image should not vary when that phantom is scanned at different times, with different slice thicknesses and/or in the presence of other objects (Hsieh 2009). CT number uniformity implies that the CT number measurement of phantom images should not change when changing location of the selected ROI or by shifting the phantom position relative to the iso-centre of the scanner (Hsieh 2009; Seeram 2009). In other words, uniformity is a measure of the homogeneity or heterogeneity of the CT image of a uniform phantom (Cierniak 2011). Uniformity is the homogeneity of the HU value of water over time (Kalender & Khadivi 2011).

CT value scale is defined by the HU value of water, which is zero HU, and the HU value of air, which is -1000 HU. Uniformity is evaluated by regularly measuring the CT value of water using a particular water phantom. The range of 4 HU to 2 HU values of water is an acceptable CT value of water for different measures over time (Kalender & Khadivi 2011).

The CT number may change significantly with different reconstruction algorithms. Each reconstruction kernel should be utilised for the specific clinical applications (Hsieh 2009).

4.3.5 Linearity

Linearity defines the relationship of the CT number values assigned to objects representing different types of tissue to be imaged, compared to the linear attenuation coefficients measured at the average energy of the scanner (Cierniak 2011; Seeram 2009).

Linearity is essential to routinely examine the accuracy of the CT numbers for each material. It is measured by using a phantom of several materials of different compositions and linear attenuation coefficients, with known CT numbers, placed in different locations throughout the phantom. Calibration or further action is required if the linearity deviates more than 5 HU from the known CT number value of each material within the phantom (Kalender & Khadivi 2011).

Plastic materials (with attenuation values between those for polyethylene and Plexiglas) can be used to adequately cover the range of fat to soft tissue attenuation in order to examine the linearity of CT images. It is important to point out that there are wide variations in density in certain plastics. Therefore, the density for any plastic sample should be determined to accurately calculate the linear attenuation coefficients of each plastic being used (Judy et al. 1977).

4.3.6 Radiation dose and image quality

Two main perspectives are considered to approach radiation dose reduction. Firstly, dose reduction can be achieved by improving some aspects of image quality. This can be by implementing radiation dose reduction techniques, optimising the scanners and scanning techniques, and improving data processing and image reconstruction (Yu et al. 2009). Secondly, determining the appropriate image quality required for each imaging purpose and specific diagnostic task, so that the image can be obtained with a tolerable noise level and adequate spatial resolution. For example, with CT imaging of high contrast structures—such as the detection of polyps from a background consisting of air in CT colonography—higher noise level and lower radiation dose is allowed without sacrificing diagnostic confidence (De Crop et al. 2012). On the other hand, the detection and imaging of low contrast lesions—such as CT examinations of brain and liver/pancreas—require lower noise level and thus higher dose. Hence, the diagnostic task determines the appropriate target image quality and thus the allowed noise and radiation levels that are controlled by scanning parameters such as tube current, scan time, pitch and tube potential. However, this is a challenging task owing to the complexity of clinical imaging studies such as the preference variations among interpreters and the performance differences among scanners. Although there are guidelines and standards for image quality requirements, they are detailed for only a very few examinations.

The main challenge with reducing radiation dose is the image noise. Noise in CT has two principal sources: quantum noise and electronic noise. The quantum noise is determined by the number of photons collected by the detector. The electronic noise is the result of fluctuation in the electronic components of the data acquisition system. When the number of photons is reduced to the level where the detected signal is as small as signal from

142

electronic noise, the image quality will be significantly degraded. Photon starvation artefacts occur in low-dose situations, or when the patient size is large with limited photon flux. It is desirable to reduce the level of electronic noise in order to improve the image quality in low-dose examinations, which requires the refinement of all electronic components in the x-ray detection system (Yu et al. 2009).

The main parameters that control radiation dose in CT imaging systems are patient size, exposure factors (including kVp and mA), time, pitch factor, slice thickness, collimation, scanner systems and scanning mode, reconstruction algorithms and image processing applications (Figure 4.2).

Figure 4.3   The factors of radiation dose in CT scan imaging.

Patient size

Smaller bodies, such as children and thin adults, attenuate fewer x-ray photons. The dose at the skin of smaller children is almost the same dose at their body centre, whereas for

adults it is two to three times less. Therefore, exposure parameters of mAs, kVp and pitch should be reduced for smaller patients (Strang & Dogra 2006).

kVp and mAs

The quality of the x-ray beam and its penetrating ability are influenced by kVp. However, the dose to the patient may be increased with increasing kVp if other exposure factors are not adjusted. For example, the dose to the patient will be increased by approximately 40% when kVp is raised from 120 to 140, if all other parameters remain the same. The quantity of photons of the x-ray beam is determined by mAs. Therefore, the higher the mAs is the greater the dose to the patient; however, lower image noise is attained (Strang & Dogra 2006). Utilising the technique of automatic exposure control (AEC) automatically adjusts exposure parameters to maintain a preselected image signal-to-noise ratio (SNR) for certain exams regardless of patient size. AEC aims to reduce the dose that may be delivered by over-exposure (Strang & Dogra 2006).

Pitch and slice thickness

Pitch, which is the table movement per single rotation for a multi-slice scanner, is inversely proportionate to the dose. When the pitch is doubled, as an example, the dose will be halved. However, the image noise increases when the pitch is increased. Increasing scan length also increases the effective dose to the patient, as more organs are affected (Strang & Dogra 2006).

Thinner slices are accompanied by more noise, as they are reconstructed from fewer data than thick slices. Consequently, more doses are required to keep the image noise reasonable. Hence, thin slices are accompanied by higher doses (Strang & Dogra 2006). Collimation is also a factor in radiation dose that determines the x-ray beam width. The overlap or over-beaming is associated with narrower collimated beams. As a result, radiation dose to patients increases (Strang & Dogra 2006).

Reconstruction algorithm and image processing

Current reconstruction algorithmic techniques are a promising strategy for noise and artefacts reduction. These techniques have the potential to reduce radiation dose as they reduce image noise and different artefacts. Iterative reconstruction algorithmic techniques can be used to reduce radiation doses in small or intermediate-sized patients while maintaining diagnostically adequate noise (Marin et al. 2011).

The iterative reconstruction techniques have recently been used—instead of filtered back-projection (FBP)—to process and reconstruct CT images. Iterative reconstruction algorithms are statistical reconstruction measurements of image reconstruction, and they require higher computational capabilities compared to analytical methods such as FBP. The iterative reconstruction process consists of three main steps: the artificial raw data is created, then the artificial and measured raw data are compared and an updated image is computed, which is then back-projected to the current volumetric image. The three steps are repeated iteratively, forming the iterative reconstruction loop. The final volumetric image is produced once the loop is terminated (Beister, Kolditz & Kalender 2012).

There are several iterative techniques which are implemented in clinical CT. ASIR (Adaptive statistical iterative reconstruction) was developed and established by GE Healthcare in 2008. In 2009, GE Healthcare implemented a more complex model-based iterative reconstruction method called VEO. Siemens implemented IRIS (image reconstruction in image space) in 2009 and have recently introduced SAFIRE (sinogram affirmed iterative reconstruction), which is a reconstruction technique that works in both the raw data and image space. Philips introduced their iterative reconstruction, iDose, in 2009 (Beister, Kolditz & Kalender 2012; Marin et al. 2011). Iterative reconstruction processes are performed either from the image data alone, from projection data alone or from both the projection and image data. While the IRIS used the image data alone, the ASIR, SAFIRE and iDose used both the projection and image data (Marin et al. 2011).

Scanner model and scanning mode

Patient dose varies considerably depending on CT manufacturer, model, reconstruction algorithms and techniques utilised. MDCT, which is recent and widely used, increases the radiation dose to the patient because of the penumbrae at the edges of the beam. The penumbrae result from the over-beaming phenomenon used to cover a wide-ranging field. While penumbrae irradiate the patient, their data are not used in image reconstruction (International Commission on Radiological Protection 2007).

Dual source CT is one of the current technical developments in MDCT. Using two radiation sources in this system reduces exposure time to half. Therefore, the system has the potential to reduce the radiation dose to the patient (Achenbach, Anders & Kalender 2008; Flohr, G

et al. 2006). Development of 320-MDCT systems contributes to further dose reduction to patients (Khan et al. 2011; Zhang et al. 2011).

Scan modes—such as normal scan (when the slice reconstructed from the data is acquired in a full 360-degree rotation), over-scan or under-scan—also control radiation doses to patients. Moreover, angled gantry scans deliver more radiation doses to patients than axial scans (International Commission on Radiological Protection 2007).

Filters—that are used for beam shaping (such as wedge filters and bow-tie filters) or for removing soft or low-energy x-rays (such as additional flat filters)—reduce the dose gradually, towards the edges of the radiation field and to the skin. Organs that are located in the direct radiation beam acquire the highest dose. Organs that are not in the field of the collimated beam still receive doses from scatter radiation. Generally, the closer the organs are to the primary radiation source, the higher the acquired dose is (Strang & Dogra 2006).

The measure units of dose in CT examination

The measures of patient dose in CT are the computed tomography dose index (CTDI) and dose-length product (DLP). CTDI is measured in polymethyl methacrylate phantoms (or models that mimic human tissue) as it is difficult to measure in a real patient. CTDI is attained from a CTDI phantom for a single axial scan, and is determined by three measures: the CTDI (100), weighted CTDI (CTDIw) and volume CTDI (CTDIvol). The CTDI (100) is the absorbed dose measured under the area field between two symmetric points that are at +50 and −50 mm from the centre (Kalender & Khadivi 2011).

The CTDIw measures the variation in absorbed radiation within the scanned region, which is about two times higher at the peripheral areas than at the centre of the field of view (Equation 4.1) (Mahesh 2009). CTDIvol is the estimate of average dose that the patient acquires over the entire scan volume (Equation 4.2) (Mahesh 2009).

$$CTDIw = \left(\frac{1}{3}\right) CTDI\ (100) centre\ + \left(\frac{2}{3}\right) CTDI\ (100)\ peripheral \quad \textit{Equation 4.1}$$

$$CTDIvol\ = \frac{CTDIw}{pitch\ factor} \quad \textit{Equation 4.2}$$

DLP is the effective dose, which is related to probable biologic harm of the radiologic exam, associated with average patient dose over entire scan volume multiplied by the scan length. DLP can be measured by using Equation 4.3 (Mahesh 2009).

$$DLP\ =\ CTDIvol\ \times\ scan\ length \quad \textit{Equation 4.3}$$

Optimum image quality relies on the balancing of the image quality and patient dose and depends on the region being studied and the case being examined. To optimise image quality, its parameters (as mentioned previously) should be manipulated and altered according to the purpose of the examination with respect to patient dose. Moreover, image quality can be optimised by eliminating or reducing the influences of image degradation factors (Kalender & Khadivi 2011; Seeram 2009).

4.4 Image quality evaluation methods

Image quality in CT should be routinely evaluated to ensure the images represent the true attenuation value or HU of the fine and/or low contrast-details of body tissues (Mansson 2000; Zarb, Rainford & McEntee 2010). The main types of evaluation tools of CT image quality and scanner performance include physical parameters evaluation methods,

diagnostic performance assessments and psychophysical tests (discussed previously in Chapter 2). The physical evaluation methods—such as DQE, modular transfer function (MTF) and SNR—are the primary objective measurements of scanner imaging performance. Diagnostic performance-based evaluation methods include VGC and ROC, which are usually performed by radiologists or radiographers. Psychophysical tests—such as the LCD detectability method—are the evaluation tools based on appropriate phantoms to measure different image quality parameters. The images of these phantoms are assessed by observers (Zarb, Rainford & McEntee 2010).

The detectability performance of LCD is measured by using a phantom that contains cylindrical objects of different attenuation coefficients and diameter sizes. This evaluation method would be ideal to investigate the effects of dose- or noise-reduction techniques on diagnostic-quality images because the detectability performance of LCD is the major challenge with these techniques. The detectability performance of LCD is influenced by noise texture, the contrast between the lesion and its background, lesion size, exposure factors and spatial resolution (Baker et al. 2012). It is also affected by the reduction of slice thickness, which increases quantum noise (Brooks & Di Chiro 1976). Furthermore, reconstruction algorithms and the display window and level also affect LCD detectability performance (Goodenough & Weaver).

There are two main ways to measure LCD detectability performance of CT images: subjectively by observers and quantitatively or objectively by software that is used to measure the CNR.

Use of observers in evaluation of quality

Observers, radiographers or radiologists are asked to score the CT images of the LCD phantom by identifying the discs of different HU number and diameter sizes that they can detect (as discussed in Chapters 2 and 3). LCD detectability—and other evaluation methods that involve human observers—may become time consuming, costly and strenuous. Such methods may also be unreliable, as they suffer from human subjectivity. The results of these methods may be biased as the observer is using a known phantom beforehand. As a result, subjective measurements are not a good choice to evaluate the low contrast detectability in constancy control of CT (Thilander-Klang et al. 2010). As an alternative to subjective assessments, different objective methods are recommended (Verdun et al. 2002), such as the contrast-to-noise ratio (CNR) measurement method (by using computer software), which was suggested to objectively assess LCD detectability in CT.

Contrast-to-noise ratio (CNR)

The detection of a lesion depends on its contrast to the surronding area, and also on the noise level in that image. These two aspects are describend in a metric-combining parameter, namely CNR (Xia 2007), which is a main parameter that determines how well an object is displayed. The higher the CNR, the higher the possibility of detecting small objects. CNR is determined by the differences in CT numbers between a lesion and its background area, in relation to the noise defined by the standard deviation of CT values of the background (Rubin & Rofsky 2012). CNR—which is influenced by the pitch and reconstructed slice thickness—determines small low contrast detectability (Verdun et al. 2002). As such, the values of CNR for different discs/objects (in phantom images measured

150

by software) are used as image quality indicators (Verdun et al. 2002). According to the Rose model of human vision, the detectability of high contrast objects is not affected by quantum mottle or image noise as much as low contrast object detection is affected (Kanal et al. 2011).

According to Smith (1997), the human eye can detect a minimum contrast (the contrast difference between the object/lesion and background) of 0.5% to 5%, or 20 to 200 shades of grey between the blackest black and the whitest white. Baker et al. (2012) found that the objects were identified 92% of the time when the noise was less than the attenuation difference between the object and background. The detection of objects reduced when the noise was greater than the attenuation difference between object and background (Baker et al. 2012).

Schindera et al. (2012) found that increasing the contrast from 20 to 35 to 50 HU (attenuation/contrast differences of 4.1%, 48.8%, and 92.4% respectively) in the tumour yielded a significant increase in detectability ($p < 0.001$). The detectability for the 10 and 14 mm tumour also increased significantly as the contrast difference between the tumour and liver tissue increased from 20 to 35 HU ($p < 0.01$). However, the detectability of tumour lesions of 10 and 14 mm did not significantly increase when the contrast differences between the tumour lesions and liver tissue increased from 35 to 50 HU ($p < 0.733$ and $p > 1.0$, respectively). Hence, the contrast between objects and background tissue should be optimised to improve lesion detectability while maintaining lower radiation dose (Schindera et al. 2012).

According to Hasegawa et al. (1982), 3.5, 5.64 and 6.48 mm object diameter sizes can be identified at 20, 15 and 10 HU differences respectively. Baker et al. (2012) suggested that a low contrast object diameter size of 5 mm or smaller within a liver can be detected at

contrast differences greater than 10 to 15 HU—with ideal scanning parameters (thin reconstructed slice, optimal dose and optimal reconstruction kernel)—but they have not found published literature supporting their assertion.

A study conducted by Kanal et al. (2011)—using a 64-MDCT scanner (Light Speed VCT XT, GE Healthcare) and phantom (model 061, CIRS)—showed that the detectability of a low contrast object of 6.3 mm and at 20 HU below background was 91% at a noise index of 5–9. The detectability decreased up to 61% at a noise index of 23–2 (Baker et al. 2012). CNR is not a reliable indicator of LCD detectability because it does not consider spatial resolution and noise spatial correlation (Baker et al. 2012). MDCT at collimation less than 5 mm did not improve the low contrast detectability of liver lesions by human readers (Haider et al. 2002; Verdun et al. 2002). Verdun et al. (2002) found that the mean CNR measurements correlated significantly to the subjective scores. Object diameter sizes of 5, 7 and 9 mm can be 100% detected when they have CNRs of at least 1.0, 0.8 and 0.6 respectively (Verdun et al. 2002).

Up to 5 mm slice thickness, CNR increases as slice thickness increases for polyps ranging from 5 to 10 mm. It also increases with slice thicknesses up to 3.75 mm for polyps smaller than 5 mm. CNR decreases with slice thicknesses larger than 5 mm for 5 to 10 mm polyps and with slice thicknesses larger than 3.75 mm for polyps smaller than 5 mm. However this is applicable only on high contrast CT studies—such as CT colonography—where the polyps' tissues are outlined by air. Therefore, the results of this study may not be correct for low contrast CT studies such as live CT examinations (Sundaram et al. 2003).

Huda et al. (2004) found that CNR can be improved by increasing kVp. Their study results suggested that CNR for muscle, fat lesions and iodine lesions could be improved by 130%, 100% and 25% respectively for adults when kVp increased from 80 to 140. However,

maintaining the CNR at a constant level, the radiation dose to the patient would also be increased. CNR reduces with larger patient size.

Even though Baker et al. (2012) suggested that CNR of LCD objects may be helpful in evaluating new reconstruction techniques, Reiser, Lu and Nishikawa (2012), in their recent study, found that CNR is not an appropriate performance metric for evaluating the potential of dose reduction with different reconstruction algorithms. In addition, CNR does not consider background noise correlations (Reiser, Lu & Nishikawa 2012).

In breast CT, CNR is independent of lesion size (Xia 2007). SNR takes into acount the size of lesions and is related to the CNR and the radical value of pixel numbers occupied by that lesion. The minimum SNR which determines the human detection of a low contrast object is based on its size and CNR (Hanson 1977). According to the Rose criterion, the detectable lesion size of 1 mm has an SNR of 5 (Hasegawa, B 1991). Since the SNR increases linearly with the lesion's diameter, it can be used to solve the limitation of CNR by applying Equation 4.4 (Xia 2007). SNR and CNR were also calculated according to Equations 4.5 and 4.6 (Heyer et al. 2007).

$$SNR = CNR \; x \; N^{\frac{1}{3}} \qquad\qquad \textit{Equation } 4.4$$

Where N is the number of pixels occupied by lesion

$$SNR = \frac{SI_{MPV}}{BN} \qquad\qquad \textit{Equation } 4.5$$

$$CNR = \frac{SI_{MPV} - muscle \; SI}{BN} \qquad\qquad \textit{Equation } 4.6$$

Where SIMPV is mean SI of pulmonary vessel and BN is background noise

Computer-model observers were suggested to predict human visual detectability performance in noisy images. These models seem to be very useful tools to investigate the influence of acquisition and reconstruction parameters and the effects of object size and

shape on the detectability in CT (Eckstein, Abbey & Bochud 2000). However, to the knowledge of the researcher, software model observers dedicated to evaluate the detectability performance (with an LCD CT phantom) are not yet commercially available, although several studies have suggested such models.

4.5 Factors affecting LCD detectability

LCD detectability performance of CT scanners and images is influenced by several factors, including CT system specification, mAs, kVp, slice thickness, pitch, beam collimation, and image processing and visualisation. These factors should be adjusted to optimise image quality, in terms of LCD performance, in order to lower image noise and maintain lower radiation dose (Figure 4.4).
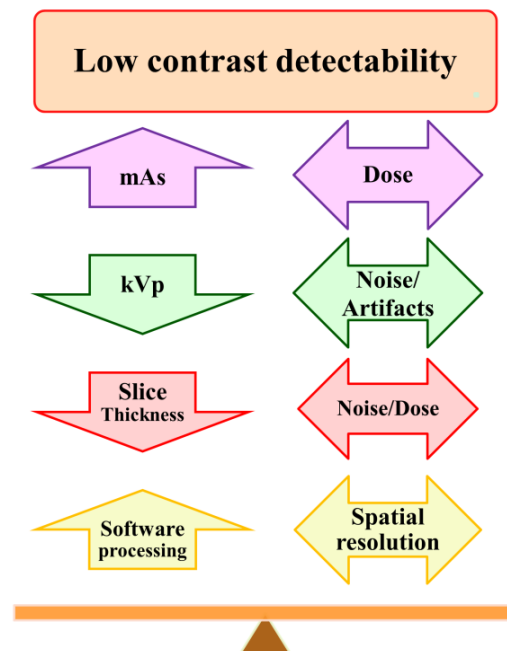
Figure 4.4   Detectability performance can be optimised by balancing
between the adjusted protocol parameters (mAs, kVp, slice thickness/pitch
and software processing) and tolerated noise and artefacts while maintaining
low radiation dose.

4.5.1 Scanner systems and detector properties

CT scanners are of different systems and models; each has its own performance ability according to its properties and specifications (Figure 4.1). The criteria of CT systems fundamentally emphasises noise features and hence influences LCD detectability performance of the produced images (Faulkner & Moores 1984). Indeed, scanner specifications largely determine image blur/resolution. For example, the size of the focal spot and single detector element are the main sources of blur (Hsieh 2009). The system's imaging area coverage and gantry rotation time also affect detectability performance of CT scanners (Mahesh 2009; Seeram 2009). Consequently, the effects of imaging factors on LCD detectability performance of different systems, models and manufacturers are not the same. Even though the latest generation of CT scanners are suggested to have better image quality, they still have limitations that may influence detectability performances of LCD. The following discussion shows that different CT systems and scanners have different LCD detectability performance (Figure 4.4).

The imaging of coronary arteries is still challenging with single slice spiral CT. The image quality is deteriorated by biphasic motion artefacts even with gating and/or with slow heart rates (Hurlock, Higashino & Mochizuki 2009). The image quality of CT studies are improved and enhanced, however, with the introduction of MDCT. Compared to single slice CT, MDCT systems have larger area coverage, faster scanners and smaller detector element sizes. Spatial resolution becomes much higher with MDCT scanners (Bardo & Brown 2008; Hurlock, Higashino & Mochizuki 2009); the entire chest can be scanned with 1 mm slices and within one breath-hold. These scanners also use enhanced reconstruction algorithms and advanced image processing. The accuracy of CT image interpretation and pathology diagnostic are improved with MDCT, as MDCT scanners have much higher

sensitivity and specificity to detect pathologies—particularly cardiovascular diseases—than single slice CT (Hurlock, Higashino & Mochizuki 2009). Thinner slices can be obtained by using thinner detector rows; spatial resolution improves with thinner slices and hence the effects of partial volume average and calcium artefacts can be minimised. Examination time can be also reduced with faster gantry rotation and wider detector area coverage. Temporal resolution is improved with faster scanners and hence the effects of motion artefacts can be reduced (Hurlock, Higashino & Mochizuki 2009). With more detector row scanners, stair-step artefacts (Figure 4.5) are almost eliminated, particularly with 64-MDCT and above. Stair step artefacts occur around the edges of structures in the volume or multiplanar reformatted images, and particularly when a wide collimation is used or when no overlapping scanning is selected (Barrett & Keat 2004).

With the introduction of 256-MDCT, 128 mm of anatomy can be covered with 0.5 mm slices. The number of channels in the radial axis has been increased in this scanner, and it is able to image fine structures with isotropic resolution. Cardiac imaging—which is a most challenging task because of the heart-beating motion and tiny coronary artery structures—is extensively improved with 256-MDCT scanners. They provide higher image quality and have higher potential for radiation dose reduction compared with previous MDCT scanners. 256-MDCT scanners can also provide more accurate and quicker diagnoses (Hurlock, Higashino & Mochizuki 2009). Fusing the images with CT angiography examinations, which allows morphologic and functional assessment, is also possible with 256-MDCT (Hsiao, Rybicki & Steigner 2010).

The 320-MDCT—which includes 320 detector rows—is a recent development of MDCT. This scanner has shorter gantry rotation time (350 ms) and wider area coverage of anatomy (160 mm) compared with previous MDCT scanners. Accordingly, the 320-MDCT is able

to achieve complete coverage of the heart within a single rotation, without table movement (Hurlock, Higashino & Mochizuki 2009; Kitajima et al. 2011). Volumetric imaging of the entire heart is completed within one cardiac cycle (Hsiao, Rybicki & Steigner 2010). The temporal resolution is also improved with the wider area coverage and faster gantry rotation. The motion effects of heart structures on CT images and radiation dose to patients can also be significantly reduced with the higher temporal resolution that is offered by 320-MDCT (van der Wall et al. 2012). Likewise, Khan et al. (2011) found that the 320-MDCT has the capability to significantly reduce radiation doses delivered to patients compared with the 64-MDCT at the same image quality. The assessment of smaller coronary vessels (up to 1.5 mm) and the detection of small volume plaque, are possible with 320-MDCT scanners (Paul et al. 2010).

MDCT scanners have several disadvantages and limitations. Several types of artefacts are generated by MDCT systems, including artefacts with multi-planar and three-dimensional reformation approaches in MDCT. Zebra artefacts, which appear as faint stripes, may also occur on the image (Figure 4.6) (Barrett & Keat 2004). Additional artefacts on images may be produced from interpolation methods which were developed with spiral scanning (Romans 2011). The interpolation reconstruction algorithms methods are used to generate projections in a single plane. The projections are processed in a spiral motion around the patient, and do not lay in a single plane because of the continuous motion of the table and x-ray tube (Mahesh 2009). The higher pitch, and/or the number of detector rows, are the more significant effects of interpolation artefacts. Interpolation of artefacts lead to misdiagnosis as this artefacts cause inaccuracies in CT number assessment (Romans 2011).

Another limitation of MDCT scanners is the use of wider beam collimation, which can deteriorate the image quality (Romans 2011). More detector rows require wider collimation

of the x-ray beam, which then becomes cone-shaped. Therefore, a new image reconstruction technology, using cone beam algorithms, is used in MDCT. This technology causes cone beam artefacts that negatively affect the image quality (Romans 2011) and occur when the data—which is collected from each detector during gantry rotation—does not correspond to them ideal flat plane, but instead to the volume contained between two cones. Cone beam artefacts are similar to those caused by partial volume around off-axis structures (Barrett & Keat 2004). The effects of cone beam artefacts increase with the greater divergence of cone beams (Romans 2011); these artefacts are more pronounced for the outer detector rows than for the inner rows (Barrett & Keat 2004).

In addition, the current MDCT scanners do not improve in-plane spatial resolution. Current reconstruction methods are focused on cross-plane spatial resolution, not on spatial resolution with the two-dimensional image plane (Kalender & Khadivi 2011; Paul et al. 2010).
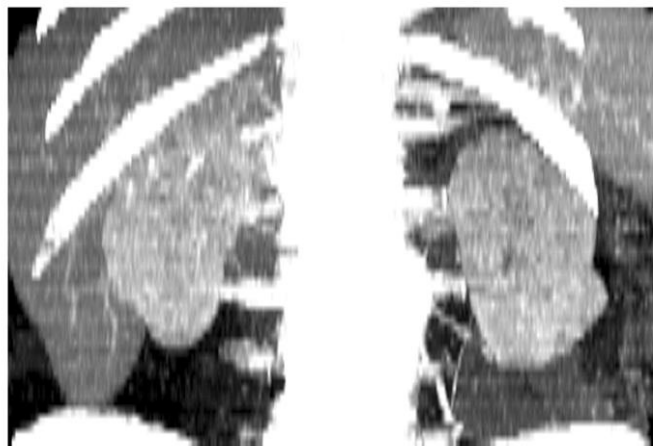
Figure 4.5   Sagittal reformatted CT image obtained with 5 mm collimation and a 5 mm reconstruction interval shows stair-step artefacts (Barrett & Keat 2004).
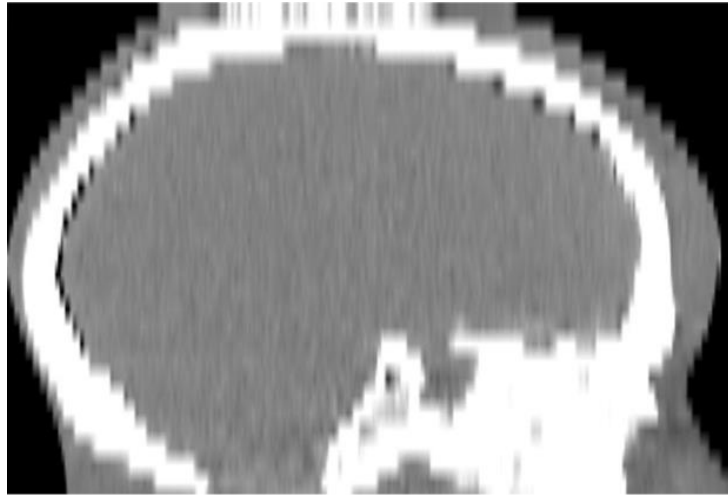
Figure 4.6   CT image obtained with helical shows zebra artefacts (Barrett & Keat 2004).

In DSCT, the exposure time can be reduced by a factor of two (Figure 4.4C) (Achenbach, Anders & Kalender 2008), and the temporal resolution can therefore be increased by the same factor (Achenbach, Anders & Kalender 2008; Flohr, G et al. 2006; Hurlock, Higashino & Mochizuki 2009). However, DSCT has similar disadvantages to recent MDCT, in terms of the intrinsic limitations of the CT image reconstruction matrix and spatial resolution (Barreto et al. 2008).

FDCT has the capability of high-spatial resolution volumetric imaging and dynamic CT scanning, and is promising for diagnostic and interventional clinical procedures (Gupta, R et al. 2008). FDCT has a wide coverage (Z-axis) flat-panel detector (FPD), which allows imaging of entire organs—such as heart or brain—in one axial scan. Moreover, FDCT can provide ultra-high spatial resolution, as the FPD mostly consists of 200 μm or less detector element size. The FDCT detector with 150-μm element size can provide spatial resolution up to 150×150 μm. FDCT scanners also have superior spatial resolution compared to MDCT scanners. MDCT provides spatial resolution only up to approximately 400 μm in plane and approximately 500 μm in the Z-axis direction. The two-dimensional FPD allows

159

imaging at any arbitrary angle. Thinner sections can be acquired with FDCT using similar radiation doses to MDCT (Gupta, R et al. 2008).

FDCT has lower contrast resolution images and longer scanning time compared with MDCT. The FDP of FDCT scanners utilises a slow caesium iodide scintillator, which limits the projection acquisition time to 100 frames per second. In comparison, the acquisition time of MDCT is 900 to 1200 projections during a single 0.5 second rotation (Gupta, R et al. 2008).

4.5.2   mA/mAs and radiation dose

Radiation dose has a linear relationship with mAs. Higher mAs means higher radiation dose, which in turn translates to higher signals and lower noise. Image quality is improved with reducing the noise and increasing the SNR, although this typically implies a greater radiation dose to the patient. For example, increasing SNR by a factor of 1.4 requires a doubling of the radiation dose. The high radiation dose techniques are not recommended; the acceptable radiation dose is determined by clinical requirements and purposes (Figure 4.7) (von Falck, Galanski & Shin 2010). Radiation dose to the patient can be reduced by reducing mAs, but this increases image noise and consequently the CNR is reduced. The visibility of structures is also negatively influenced by the reduction of x-ray quanta (Funama et al. 2005; Toth 2012). Furthermore, spatial resolution may also be influenced by the radiation dose and there is an ongoing trade-off between these factors (Ozgun et al. 2005). As stated, the diagnostic purpose and clinical task being performed should determine the acceptable level of trade-offs in image quality (Seibert 2004) .

The detectability performance of LCD is improved by increasing the mAs to reduce the noise. However, mAs should be adjusted to minimise the radiation dose while maintaining optimum LCD detectability performance.
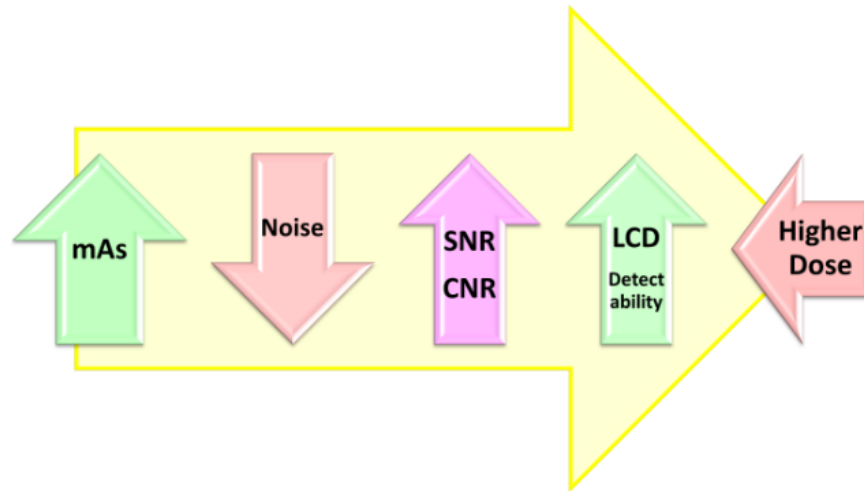
Figure 4.7   The relationship between mAs, noise, SNR, CNR and the LCD detectability is illustrated. Increasing mAs reduces noise and increases SNR and CNR and, as a result, LCD is improved. However, increasing mAs increases the radiation dose to the patient.

4.5.3   kVp

Lower kVp essentially improves subject contrast. Low kVp increases photoelectric interactions and consequently the attenuation level is improved. As a result, the image contrast is enhanced and detail visualisation is improved (Ertl-Wagner et al. 2004; Seibert 2004). However, subject contrast must not be confused with displayed contrast that can be modified on the displayer monitor.

Godoy et al. (2010) found that the subjective quality of the image was lower at 140 kVp than at 80 kVp images, even though the measured image noise was higher in the lower kVp

161

images. This result highlights the fact that the image quality is determined more by SNR and CNR than image noise. Further, Funama et al. (2005) found using 90 kVp improved CNR more than selecting 120 kVp. They suggested that that lower kVp could improve CNR. The image quality is not reduced by the noise, with low kVp due to the higher SNR and higher attenuations (Figure 4.8) (Godoy et al. 2010; Marin et al. 2010; Schindera et al. 2008).

Lowering the kVp does reduce the radiation dose to the patient when other exposure factors are fixed, even though the radiation dose is not linear with kVp (Seibert 2004). Funama et al. (2005) found that, by reducing the kVp from 120 to 90, the radiation dose can be reduced by 29% without affecting the CNR. Another study conducted by Zhang et al. (2011) also suggested that 100 kVp in 320-MDCT can reduce the radiation dose to patients without deteriorating image quality compared with 120 kVp.

The total energy flux is reduced with the lower kVp technique, if other exposure factors are not adjusted. Hence, the image noise increases and leads to reduction in image quality and diagnostic accuracy (Ertl-Wagner et al. 2004; Godoy et al. 2010; Huda, Scalzetti & Levin 2000; Seibert 2004). Low energy beams—such as 80 kVp—may cause beam hardening for some types of artefacts (Seibert 2004). A new adaptive filter can be used to suppress that image noise produced from the low kVp selection (Huda, Scalzetti & Levin 2000). kVp should be selected based on the patient's cross-section diameter and according to the examination purposes. Therefore, 80 kVp is recommended for small children and 140 kVp is recommended for obese patients (Kalender & Khadivi 2011). , in their multi-reader study, examined the impacts of various kilovoltages—80, 120 and 140 kVp, while keeping other exposure factors the same—on the image quality of vessel delineation of cranial MDCT images. The researchers concluded that the higher voltages are better to show

vessels close to bone and subsegmental arteries, as the high kVp has greater effects (Ertl-Wagner et al. 2004).

According to the above, the interdependence of LCD detectability and radiation dose on kVp is very complex. The kVp should be adjusted to be low enough to increase contrast resolution in order to improve detectability performance of LCD. However, at the same time, kVp should be kept high enough to reduce the noise. Patient size and diagnosis purposes should be considered in kVp selection to optimise LCD performance.
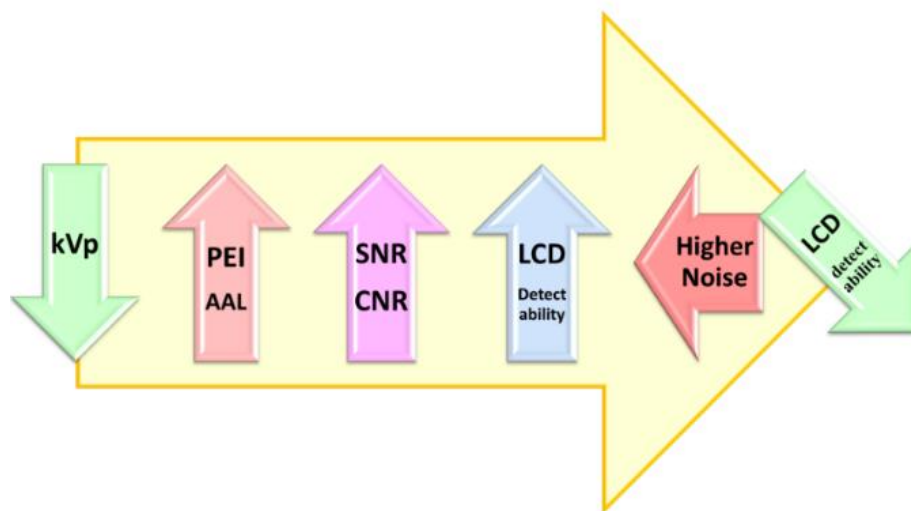
Figure 4.8   The relationship between kVp, SNR, CNR, noise and LCD detectability is illustrated. Appropriately lowering kVp increases photoelectric interaction (PEI) and the attenuation level (AAL), which leads to an increase in SNR and CNR, and hence LCD performance is improved. However, the noise level increases with excessively lowering kVp and/or if the other exposure factors are not adjusted.

4.5.4   Slice thickness, pitch and/or beam collimation

Thinner slices provide higher resolution, and MDCT is routinely used to acquire sub-millimetre slices and, recently, isotropic image data sets. Through-plane partial-volume averaging effects are also minimised with thinner slices, although noise will be increased and consequently LCD detectability performance is degraded (von Falck, Galanski & Shin 2010). Moreover, exposure factors should be increased to reduce image noise, but this will increase the radiation dose to patient (Figure 4.9) (Seibert 2004; von Falck, Galanski & Shin 2010).

The resultant noise from thin slice thickness should be reduced to improve LCD detectability performance. This can be achieved by increasing the dose to increase SNR, using soft reconstruction algorithmic kernels, applying appropriate data filters, utilising sliding-thin-slab averaging or by adjusting window width and level settings. Using a sliding-thin-slab averaging algorithm, with thin-section scanning during image reconstruction, can reduce the effects of through-plane partial-volume averaging by the retrospective generation of thicker sections. Hence, the detectability of LCD objects is improved (von Falck, Galanski & Shin 2010).

Over-ranging and over-beaming, which are associated with slice thickness selection, also increase radiation dose to patients. Over-ranging occurs when additional gantry rotations are automatically performed by the scanner to acquire enough data for image construction. The rotation number increases with increasing collimation, when increasing slice thickness in the primary reconstruction and/or when increasing pitch (Theocharopoulos et al. 2007; van der Molen & Geleijns 2007).

Over-beaming occurs when the actual profile beam collimation widens to be larger than the nominal beam widths used to keep uniform distribution of radiation across the detector bank. Beam collimation is determined by changing the number of active detectors, or their length, in MDCT (Theocharopoulos et al. 2007). Over-beaming is due to the resultant penumbra effect. It increases the radiation dose and can be reduced by selecting larger slice thicknesses or by using more channels. The effect of penumbra, which explains the over-beaming, depends on the type of MDCT scanner. Over-beaming effects are lower in 16-MDCT scanners compared with 4-MDCT (Theocharopoulos et al. 2007). There is a trade-off between the advantages of nearly isotropic voxels, which determine the spatial resolution, and the disadvantages of radiation dose or image noise when selecting slice thickness (von Falck, Galanski & Shin 2010).
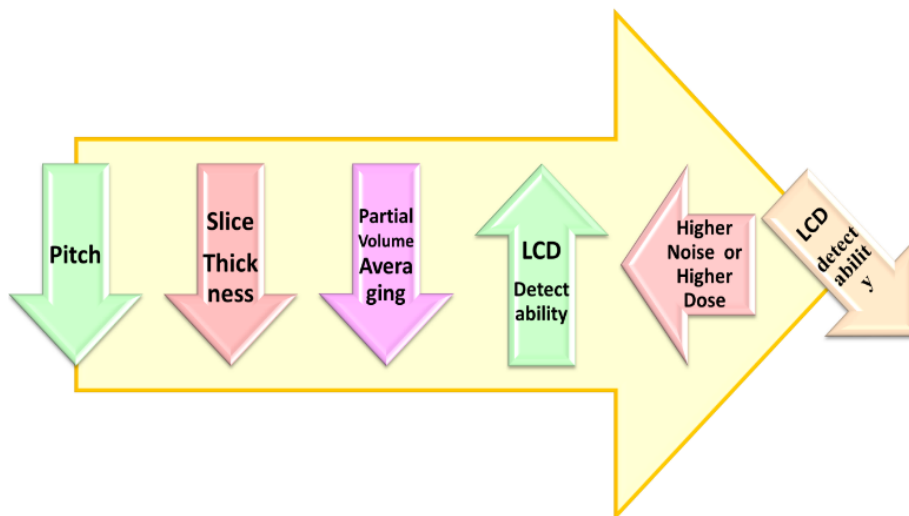
Figure 4.9   The relationship between pitch, slice thickness, noise and LCD detectability is illustrated. Selecting lower pitch allows production of thinner image slices. Thinner image slices reduce the problem of partial volume averaging and hence the LCD is improved. However, thinner slices increase image noise, which in turn deteriorates LCD if the radiation dose is not increased.

From above, selecting slice thickness—according to the diagnostic purposes—is fundamental to acquiring higher LCD detectability performance while maintaining desired spatial resolution and lower radiation dose.

4.5.5   Image reconstruction and processing and visualisation

CT images that are in digital form can be processed, manipulated and modified by computer algorithms. Density values, histograms and other tissue parameters can also be acquired at any time for digital CT images. Image post-processing applications—including three-dimensional reconstruction, multi-planar reformatting, software-assisted lesion detection and quantification—improve LCD detectability performance (Kalender & Khadivi 2011; Rubin 2003). The original axial images can be reformed to different orientation views, including coronal, sagittal and oblique planes. CT images can also be reconstructed from two-dimensional images to three-dimensional displays, four-dimensional animated studies, virtual endoscopic views, and interactive manipulation of image volumes. Specific tissues are now possibly detected by automated determination of advanced image processing approaches (Kalender & Khadivi 2011).

In comparison with FBP, iterative reconstruction techniques display impressive improvements in image quality and noise reduction (Beister, Kolditz & Kalender 2012; Marin et al. 2011; Winklehner et al. 2011). Iterative reconstruction algorithms are more capable of dealing with missing data or irregular sampling; higher flexibility in the scan geometry is also provided by iterative techniques, as many various trajectories are possible because there is no explicit expression that an inverse transform is required (Beister, Kolditz & Kalender 2012). In addition, iterative methods can help avoid artefact results

based on approximations, since these methods represent a more intuitive and natural way of image reconstruction (Marin et al. 2011).

Selecting appropriate soft reconstruction kernels is essential to improve the LCD detectability while maintaining low radiation doses to patient (Bissonnette, Moseley & Jaffray 2008; Yoo et al. 2006). LCD detectability improvement increases diagnostic accuracy (Bissonnette, Moseley & Jaffray 2008); incorrect or inappropriate selection of reconstruction algorithm filters can degrade image quality and reduce diagnostic reliability (Flohr, T et al. 2005).

Unfortunately, the properties of different settings of reconstruction algorithms are not standardised and vary greatly between vendors and scanner types. Hence, there is no general recommendations that can be applied for the optimum setting selections (Bissonnette, Moseley & Jaffray 2008). There are trade-offs between selection of a specific reconstruction algorithm and the desired spatial resolution with the tolerated image noise (Goldman 2007).

Displayed contrast of CT images can be modified and improved by appropriately adjusting the window level and window width. The window level determines the centre CT number value displayed by the range of gray-scale. The window width determines that gray-scale range of CT number values. The window level and window width settings dictate how the actual measurements of tissue attenuation are converted into a gray-scale image. They are adjusted according to tissue properties and diagnostic purposes. While a narrow window width is used to precisely visualise soft tissues, wide window widths are selected to accurately demonstrate the bone width (Barnes 1992).

The display factors of digital images—including monitor type, displayer resolution, image size, monitor brightness, display function and room illumination—influence LCD detectability performance (Yamaguchi et al. 2010). Cathode-ray tube (CRT) monitors and liquid-crystal display monitors (LCDM) are commonly available display monitors of medical images. LCDMs are increasingly used in medical imaging departments for their inherent advantages (Samei, Ranger & Delong 2008), as they provide wider dynamic range than CRT monitors. LCD detectability performance can be improved by using high-resolution LCDM. The interactive adjustment of brightness and contrast of digital images can also improve the detectability of LCD (BacherSmeetsDe Hauwere, et al. 2006). The main limitation of LCDM is that the contrast resolution is decreased significantly when the monitor is seen from angulated views (Samei, Ranger & Delong 2008).

Visualising low contrast features requires high display contrast, which can be achieved by increasing the contrast of the monitor. Higher monitor contrast can be acquired by reducing window width as far as possible without loss of diagnostic information of the image (Warren 1984).

According to the above, the detectability performance of LCD can be improved by utilising correct image reconstruction algorithms and appropriate image processing applications. Proper monitors and visualising conditions are essential to obtain higher LCD detectability performance.

4.6 Conclusion

The factors affecting the LCD performance of different CT scanner systems were discussed in this chapter. Indeed, the factors that affect the level of LCD detectability, and hence the image quality, are complex and interwoven. They also do not exactly affect image quality—from one scanner to another and from system type to another—in the same manner. These factors are the ultimate key to optimising image quality in terms of LCD detectability performance, while achieving the goal of lower radiation doses. For some factors, the LCD detectability performance of CT is inherent to the system type and unit specification and cannot be controlled by radiographers. However, radiographers play an essential role in improving system performance and image quality by effectively controlling and adjusting protocol parameters. Radiographers need to have a great understanding of the various CT scanner systems in order to improve the image quality while maintaining lower radiation doses. Further studies of contrast-detail performance are required to more deeply understand the influences of exposure factors on image quality and radiation dose.

Even though the automated LCD detectability evaluation methods are an effective tool to optimise image quality in radiography, similar approaches are not commercially available for CT. The available objective evaluation method in CT to examine LCD is CNR measurement. In Chapter 5, this approach will be evaluated to assess its efficiency as a measure of LCD detectability performance and image quality optimisation.

Chapter 5 Evaluation of contrast-detail in CT based on CNR measurements and available LCD phantom

5.1 Introduction

The dramatic increase in the number of computed tomography (CT) scanners has raised the importance of radiation dose reduction for CT studies (Kalender & Khadivi 2011). While advancement of CT technology has led to an improvement of disease diagnosis, the downside is the corresponding radiation dose (Berrington de Gonzalez et al. 2009). Patients may also receive overdose from CT studies as a result of inappropriate protocol parameters (Martinsen et al. 2010). Furthermore, Martinsen et al. (2010) found that there are wide differences in the amount of radiation dose and image quality between different manufacturers and scanner models that fulfil similar diagnostic purposes. Consequently, the American Association of Physicist in Medicine (AAPM) has recommended reasonable scan protocols for common CT examinations, for different manufacturers and models to ensure appropriate image quality with lower radiation dose (Martinsen et al. 2010). Indeed, radiation dose can be reduced further without losing relevant diagnostic image details (Martinsen et al. 2010). Because of the trade-off between dose and image quality, image quality should be optimised with the aim to acquire an adequate diagnostic image for specific clinical indication while ensuring lowest possible radiation dose to patient (Smith-Bindman 2010). CT image quality optimisation should be regularly evaluated, and scanner performance regularly assessed, in order to meet this dual aim.

Methods that are used to evaluate scanner performance and image quality of CT were discussed in Chapter 4. It is suggested that low contrast-detail (LCD) detectability performance could be the most appropriate method to optimise image quality (Alsleem & Davidson 2013; Hernandez-Giron et al. 2011; Pascoal et al. 2005).

The most significant challenge is that low dose techniques deteriorate LCD detectability performance, particularly in abdomen examinations (Baker et al. 2012). For instance, neoplastic liver disease is commonly manifested as low-attenuation lesions within a background of slightly higher attenuation normal tissue (Baker et al. 2012). LCD detectability must be maintained with any dose-reduction strategy (Alsleem & Davidson 2013; Baker et al. 2012). Therefore, the LCD detectability performance evaluation method is an essential tool to optimise the parameters of CT protocols of different CT manufacturers, models and studies (Alsleem & Davidson 2013; Hernandez-Giron et al. 2011). The factors that influence LCD detectability performance of different CT systems were determined and discussed in Chapter 4. Two main methods—subjective and objective approaches—are available to measure LCD of CT images (see Chapter 4). The subjective approach is based on human observation and the objective is based on quantitative measurements of contrast-to-noise ratio (CNR) (Alsleem & Davidson 2013). Due to the subjectivity of human observers, an objective approach to measuring LCD performance may be preferred.

This chapter aims to evaluate the influences of exposure factors—mainly kVp, mAs and slice thickness—on the LCD of CT scanners. The method used to evaluate these influences was based on CNR measurements of the objects visualised in the Catphan® 600 phantom images. In addition, this chapter aims to compare between different CT scanners in terms of CNR values of phantom objects. Accordingly, the studies of this chapter aim to evaluate the evaluation method based on CNR values, in order to measure the detectability performance of LCD of CT images for different CT scanners.

5.2 Materials and methodology

5.2.1 Phantom model

A CT phantom, the Catphan® 600 (Phantom Laboratory, Cambridge, NY), was used for this phase of the project. The phantom is made from solid-cast materials and is constructed from modules of 15 mm in diameter. Each module is designed to evaluate specific concerns associated with performance potential of multi-detector CT (MDCT). An LCD phantom module, CTP515, was included in the phantom and also used in the study (see Figure 5.1). The phantom module is made of several sets of cylindrical low contrast objects, located on two levels. This module of the phantom contains contrast objects which are 40 mm long in the z-axis with various diameters (2, 3, 4, 5, 6, 7, 8, 9 and 15 mm) and three contrast levels 0.3%, 0.5% and 1%. The objects which are located at the outer level were chosen for the study, including objects with sizes of 5 to 15 mm at 1% contrast level, 6 to 15 mm at 0.5% contrast level and 7 to 15 mm at 0.3% contrast level. The three different contrast level objects were used to examine the effects of object size on CNR. The objects selected for the experiments of this phase of the project were 1% contrast level objects for two reasons. Firstly, the researcher was able to measure that the CNR of a 5 mm size object was only at 1% contrast level, and 6 mm size object was measured only at 1% and 0.5% contrast level. Secondly, the data was very large and difficult to control when objects of all contrast levels were considered. Limiting the data to one contrast level therefore enhanced the accuracy of the results. The phantom was always positioned in the centre of the gantry.
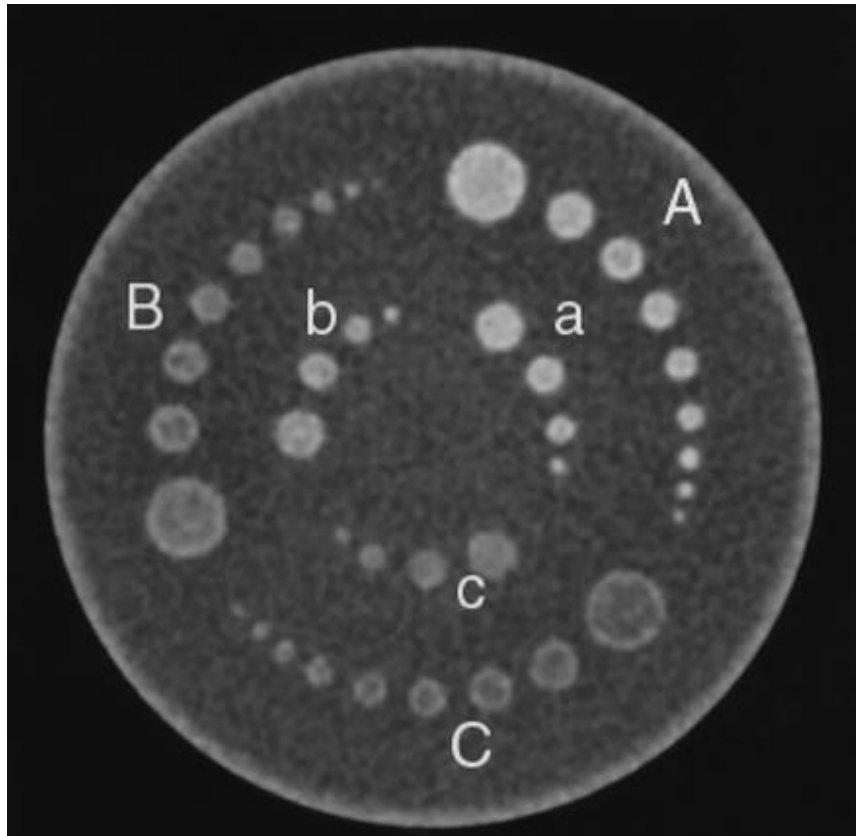
Figure 5.1   Phantom low contrast module. The low contrast objects are placed in six different regions (i.e., A, B, C, and a, b, c). The objects placed in regions A, B, and C were long cylindrical objects of 2, 3, 4, 5, 6, 7, 9 and 15 mm in diameter. The objects in region A/a, B/b, and C/c have contrast differences with the background of 1%, 0.5% and 0.3% respectively.

5.2.2   CT scanners

Three MDCT scanners, a 16-MDCT system (LightSpeed, GE Healthcare), a 64-MDCT system (LightSpeed VCT, GE Healthcare) and an 80-MDCT system (Aquilion Prime 80, Toshiba, America Medical Systems Inc.) were used in this study (Table 5.1). All systems were regularly serviced and maintained under maintenance contracts. This ensured that the performance of the scanners were in agreement with manufacturer specifications.

Table 5.1   CT scanners' specifications

	16-MDCT	64-MDCT	80-MDCT
Manufacturer	GE Healthcare	GE Healthcare	Toshiba
Product name	LightSpeed 16	LightSpeed VCT 64	Aquilion Prime 80
detector row no.	16 x 912	64 x 912	80 x 896
Detector Type	Solid-state polycrystalline ceramic scintillator	Solid-state Ceramic Detectors	Solid-state Gd2O2S
detector cell size	0.625 mm	0.625 mm	0.5 mm
Area coverage	20 mm	40 mm	40 mm
gantry aperture	70 cm	70 cm	78 cm
Reconstruction algorithm	Filtered back projection - 2D back projection	GE property volume recon 2D back projection	Filtered back projection
X-ray tube anode	HiLight ceramic	HiLight ceramic	Tungsten, molybdenum, graphite
Tube heat capacity	6.3 MHU	8 MHU	7.5 MHU
Fastest rotation	0.5 seconds	0.35 Sec	0.35 Sec
Maximum scan technique	440 mA at 120 kV	700 mA 140 kVp 120 sec	600 mA 135 kVp 100 sec
Focal spot size	0.7 x 0.6 0.9 x 0.7	0.6 x 0.7 0.9 x 0.9	0.9 x 0.8 1.6 x 1.4

5.2.3   Image acquisition

The LCD module of the phantom was centred in the scanner gantry. All measurements were performed by using two tube voltage selections of 80 and 120 kVp with different mAs, section thicknesses and reconstruction algorithms (see Table 5.2). Each series of images was repeated three times. The field of view (FOV) was set to 360 mm for 16- and 64-MDCT images and 240 mm for 80-MDCT images for the data acquisitions. The scans were reconstructed using three different reconstruction algorithms: standard, soft and lung. The impacts on CNR of different reconstruction algorithms and object contrasts, in combination with object size, were examined, as were the effects on CR of kVp, mAs and slice thickness on CNR. The soft reconstruction images and 1% contrast level objects were

used to examine the effects of kVp, mAs and slice thickness, in order to minimise the large amount of data.

Table 5.2 Protocol parameters of images acquisition

kVp	80, 120	
mAs	10 , 20, 50, 100, 200	
Slice thicknesses	For 80-MDCT	0.5, 1, 2, and 5 mm
	For 16- and 64-MDCT	0.625, 1.25, 2,5 and 5
Reconstruction algorithms	soft tissue, standard and lung	

5.2.4   CNR calculation and MATLAB software

The Hounsfield Unit (HU) of each selected object (outer level objects), background HU and the standard deviation of noise were measured (Figure 5.2), and algorithms were developed using MATLAB (version 7.14, MathWorks, Massachusetts) to calculate CNR (Appendix 7). The algorithms were then applied to each image, and the CNR for each object was calculated using Equation 5.1 (Heyer et al. 2007). The standard deviation of the mean CNR was also calculated.

$$CNR = \frac{CT\ value\ (object) - CT\ value\ (background)}{SD\ (noise)} \qquad \textit{Equation 5.1}$$
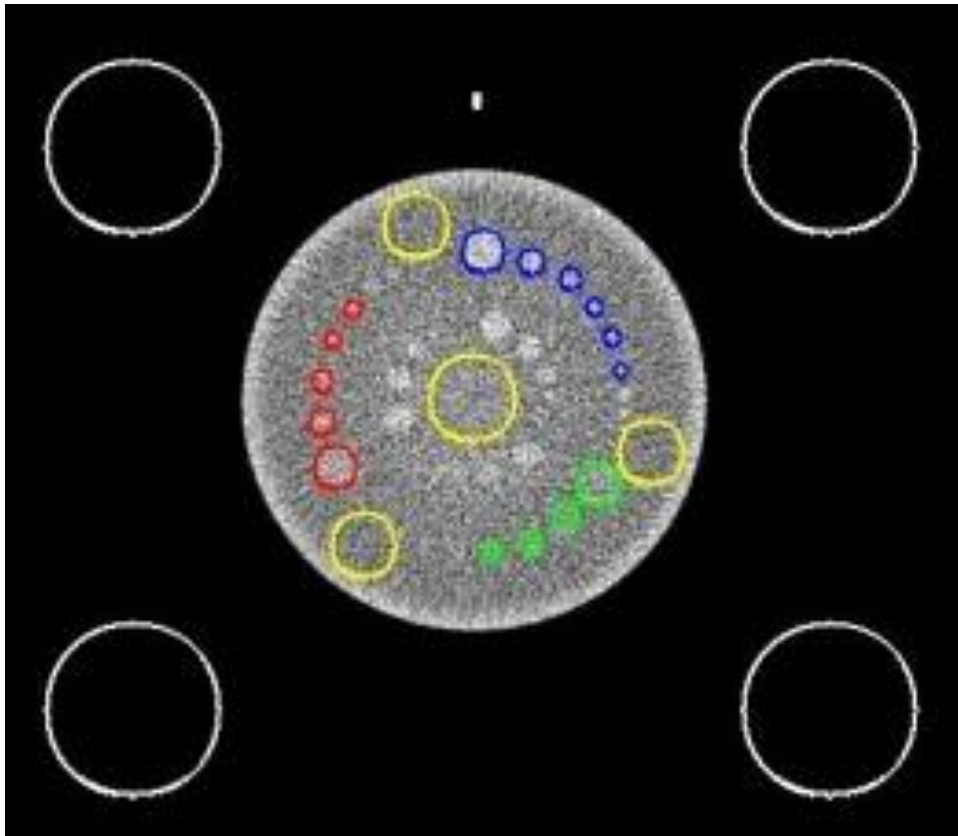
Figure 5.2   CT image of Catphan® 600 phantom. The largest circles, white colour outlined, are the areas of noise measurement which is the standard deviation of the CT values (in HU) of scan scope of outside phantom, yellow outlined circles are the areas of the mean of the CT values (in HU) from the background material of the phantom, and blue, red and green colour outlined circles are areas of the mean of CT values of objects under evaluation with the background of 1%, 0.5% and 0.3% respectively.

5.2.5   Statistical analysis

Gaussian distributed was used to test the distribution normality of the scores on each factor. The Gaussian distribution tests the probability of whether the scores on each variables fall between two real limits (Pallant 2013). The scores of CNR, which is the dependent variable, appear to be normally distributed. A two-way between-groups analysis of variance (ANOVA) using the Statistical Package for the Social Sciences (SPSS) software was

conducted for data analysis. The two-way ANOVA statistics test was used to examine the influence of different CT protocol parameters including reconstruction algorithms, kVp, mAs slice on CNR values of each image and each of its objects. The impact of other factors such as object size, object contrast level and scanner type on CNR values were also examined by conducting the two-way ANOVA test. It is used to determine the main effect of contributions of each independent factor. The two-way ANOVA test was also used to determine if significant differences existed between kVp groups exposed at the same mAs and slice thickness, between mAs groups at the same kVp and slice thickness and between slice thickness groups at the same kVp and mAs. This test also used to explore if there is a significant interaction effect between these factors. Student t-tests, at an Alpha value of 0.05 is conducted as a part of the two-way ANOVA calculations to determine if significance differences exist between different groups (Pallant 2013).

5.3 Results

The results of the different reconstruction algorithm images—and the object with various contrast levels—are shown in Figures 5.3 to 5.5. The results from the soft reconstruction algorithm images and objects of 1% contrast level are presented in Table 5.3 and 5.4.

Table 5.3   CNR mean values of the images at 80 kVp. The mean values are obtained from the average of three identical exposures.

kVp	mAs	16-MDCT			64-MDCT			80-MDCT		
		Slice thickness (mm)	Mean	SD	Slice thickness (mm)	Mean	SD	Slice thickness (mm)	Mean	SD
80	10	0.625	0.24	0.18	0.625	0.26	0.29	0.5	-0.02	0.20
80	10	1.25	0.52	0.31	1.25	0.42	0.32	1	0.17	0.25
80	10	2.5	0.09	0.18	2.5	0.42	0.28	2	0.17	0.16
80	10	5	0.18	0.24	5	0.56	0.22	5	0.19	0.17
80	20	0.625	0.07	0.21	0.625	0.52	0.43	0.5	0.11	0.25
80	20	1.25	0.16	0.13	1.25	0.60	0.33	1	0.23	0.17
80	20	2.5	0.28	0.18	2.5	0.68	0.30	2	0.29	0.15
80	20	5	0.50	0.21	5	0.89	0.23	5	0.52	0.19
80	50	0.625	0.32	0.38	0.625	0.61	0.39	0.5	0.27	0.21
80	50	1.25	0.33	0.28	1.25	0.88	0.19	1	0.39	0.20
80	50	2.5	0.33	0.28	2.5	1.06	0.26	2	0.39	0.16
80	50	5	0.94	0.16	5	1.53	0.23	5	0.72	0.15
80	100	0.625	0.74	0.30	0.625	1.04	0.36	0.5	0.29	0.15
80	100	1.25	0.92	0.36	1.25	1.29	0.34	1	0.57	0.13
80	100	2.5	0.99	0.21	2.5	1.74	0.37	2	0.67	0.14
80	100	5	1.31	0.19	5	2.19	0.27	5	0.91	0.17
80	200	0.625	0.83	0.34	0.625	1.20	0.25	0.5	0.53	0.14
80	200	1.25	1.09	0.20	1.25	1.51	0.26	1	0.61	0.19
80	200	2.5	1.50	0.38	2.5	2.14	0.34	2	0.98	0.12
80	200	5	1.96	0.28	5	3.11	0.39	5	1.42	0.17

Table 5.4   CNR mean values of the images at 120 kVp. The mean values are obtained from the average of three identical exposures.

kVp	mAs	16-MDCT			64-MDCT			80-MDCT		
		Slice thickness (mm)	Mean	SD	Slice thickness (mm)	Mean	SD	Slice thickness (mm)	Mean	SD
120	10	0.625	0.35	0.36	0.625	0.57	0.30	0.5	0.06	0.21
120	10	1.25	0.56	0.28	1.25	0.77	0.34	1	0.36	0.24
120	10	2.5	0.49	0.21	2.5	0.92	0.29	2	0.24	0.19
120	10	5	0.58	0.24	5	1.14	0.34	5	0.35	0.20
120	20	0.625	0.49	0.36	0.625	0.71	0.38	0.5	0.23	0.16
120	20	1.25	0.60	0.40	1.25	1.13	0.33	1	0.34	0.16
120	20	2.5	0.77	0.32	2.5	1.34	0.35	2	0.43	0.25
120	20	5	1.02	0.21	5	1.60	0.32	5	0.65	0.26
120	50	0.625		0.46	0.625	1.09	0.43	0.5	0.37	0.19
120	50	1.25	1.07	0.42	1.25	1.65	0.34	1	0.46	0.27
120	50	2.5	1.11	0.25	2.5	1.91	0.38	2	0.69	0.18
120	50	5	1.56	0.22	5	2.54	0.22	5	1.05	0.23
120	100	0.625	0.98	0.31	0.625	1.39	0.32	0.5	0.64	0.24
120	100	1.25	1.37	0.29	1.25	2.10	0.25	1	0.67	0.15
120	100	2.5	1.77	0.40	2.5	2.71	0.31	2	1.02	0.29
120	100	5	2.51	0.25	5	3.48	0.27	5	1.33	0.31
120	200	0.625	1.27	0.29	0.625	2.17	0.47	0.5	0.80	0.28
120	200	1.25	1.55	0.27	1.25	2.69	0.35	1	1.01	0.24
120	200	2.5	2.33	0.34	2.5	3.64	0.26	2	1.35	0.24
120	200	5	3.17	0.43	5	5.14	0.33	5	1.87	0.40

The effects of object size on CNR value were firstly examined. Object size effects—in combination with scanner types, reconstruction algorithms, object contrast levels or mAs— were also examined. The effects of the reconstruction algorithms, kVp, mAs and slice thickness on CNR values were then evaluated. The performance of different scanners based on CNR values was finally compared.

Effects of object sizes on CNR

The effects of the size of the objects, with 1% contrast level, on CNR values were evaluated at different MDCT scanners, different reconstruction algorithms, different object contrast levels, and different mAs selections (Figures 5.3 to 5.12). These figures show that the effect of object sizes at different reconstruction algorithms, contrast levels or mAs selections were limited on CNR values.

There were generally insignificant differences in CNR mean values between objects of different sizes in all scanners ($p > 0.1$) (Table 5.5). However, there were significant differences ($p = 0.021$) between 5 and 8 mm object sizes of 1% contrast levels in 16-MDCT (Figure 5.4). In 64-MDCT, there were insignificant differences in CNR values between objects sizes all the time (Figure 5.5). In 80-MDCT, there were significant differences in CNR values between a 5 mm object and 15, 8 and 7 mm objects ($p = 0.001$, 0.044 and 0.001 respectively) (Figure 5.6).
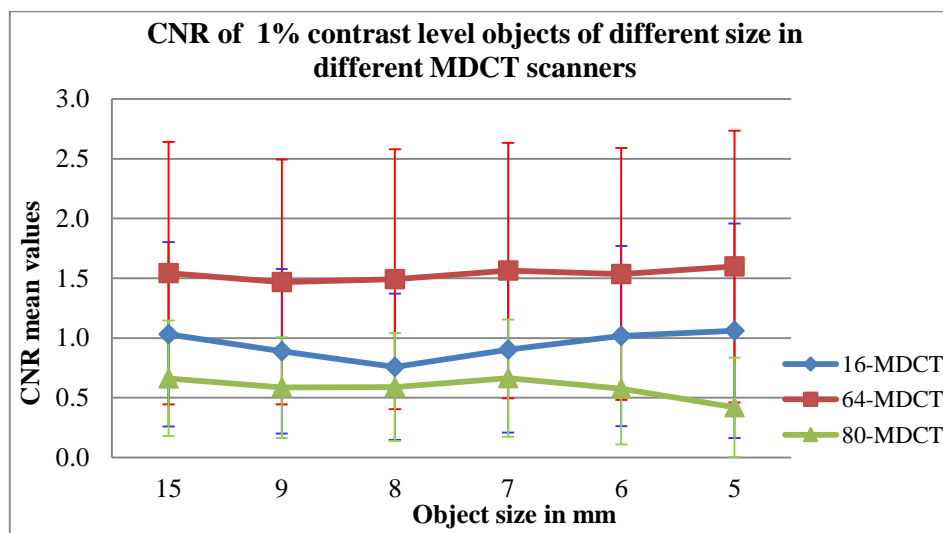
Figure 5.3   Limited effects of the size of 1% contrast levels objects on CNR values for all CT scanners. (Note the change in CNR values for 16-MDCT with 8 mm objects size and for 80-MDCT with 5 mm objects size.)

180
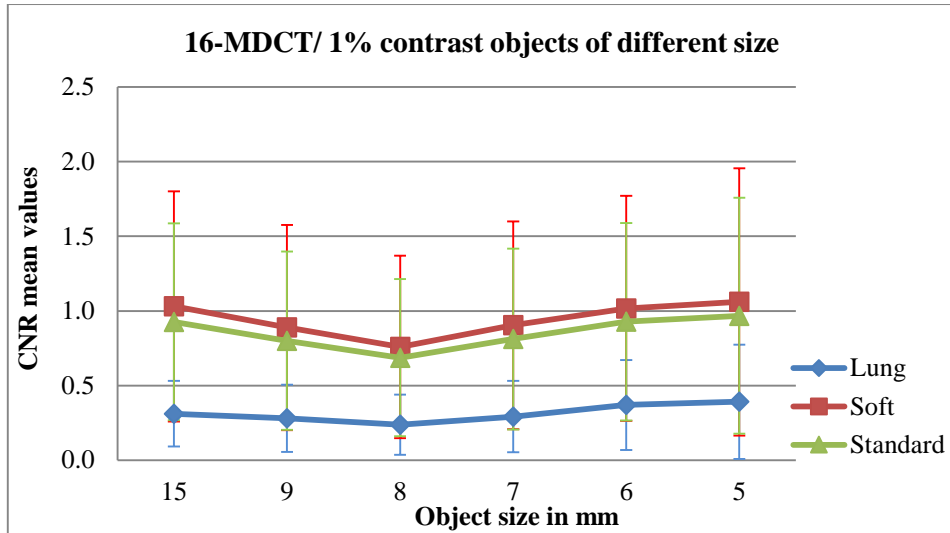
Figure 5.4   Effects of 1% contrast level object sizes are limited on CNR values for the 16-MDCT scanner with different image reconstruction algorithms. Note the change in CNR values for 9, 8 and 7 mm objects sizes, particularly with soft and standard reconstruction images.
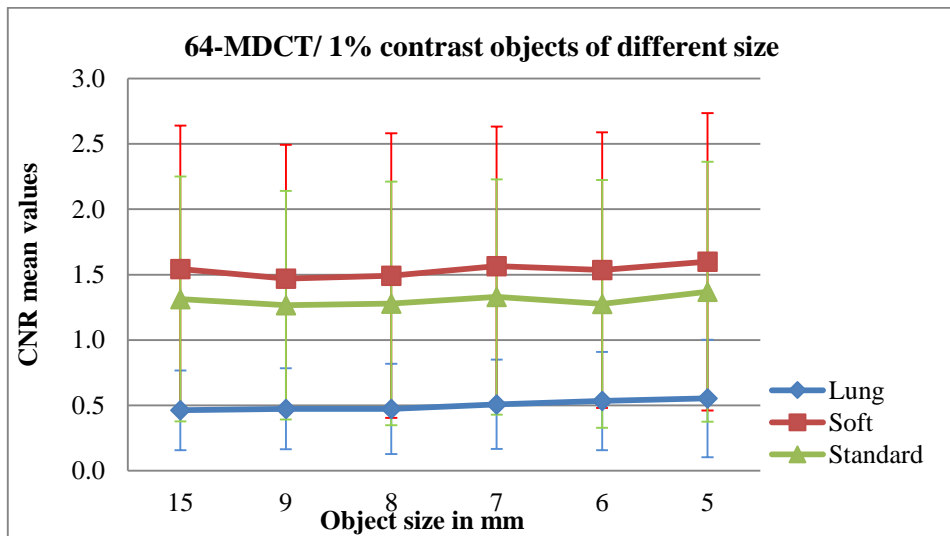
Figure 5.5   Effects of 1% contrast level object sizes are limited on CNR values for the 64-MDCT scanner with different image reconstruction algorithms.
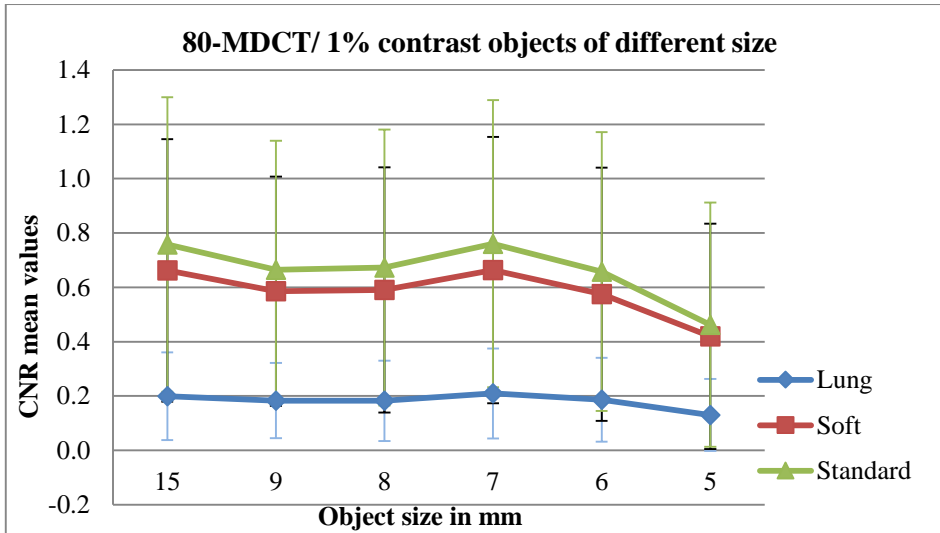
Figure 5.6   Effects of 1% contrast level object sizes are generally limited on CNR values for the 80-MDCT scanner with different image reconstruction algorithms. (Note the change in CNR values with 5 mm objects size.)
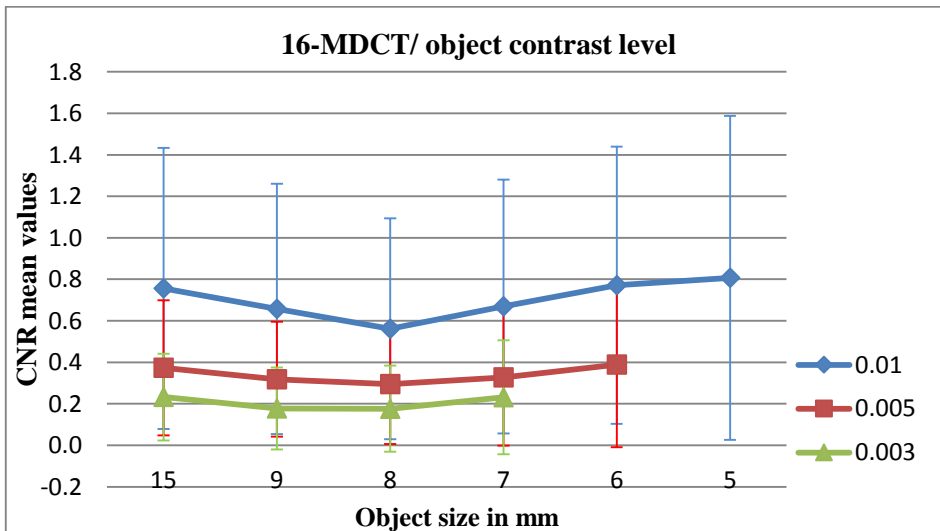
Figure 5.7   Effects of different contrast level object sizes are generally limited on CNR values for the 16-MDCT scanner. (Note the change in CNR values with 8 mm objects size for 1% contrast level group.)
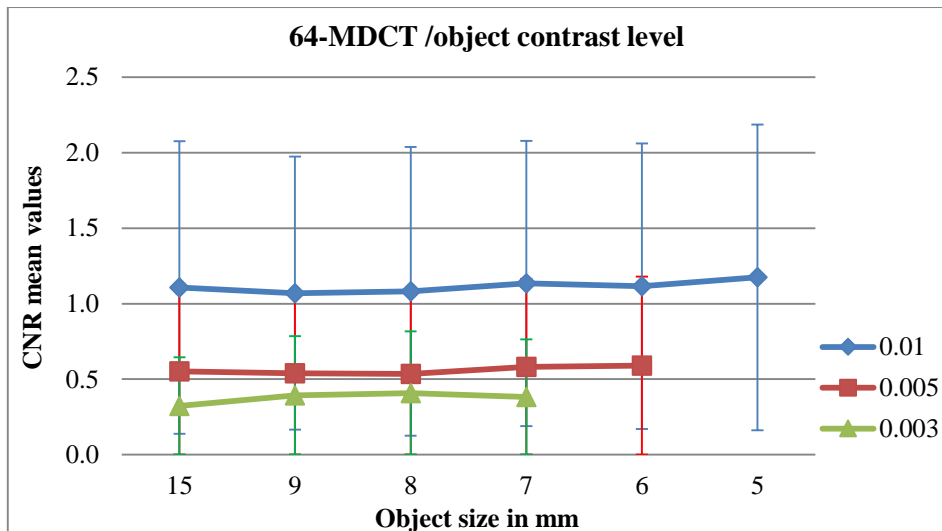
Figure 5.8 Effects of different contrast level object sizes are generally limited on CNR values for the 64-MDCT scanner.
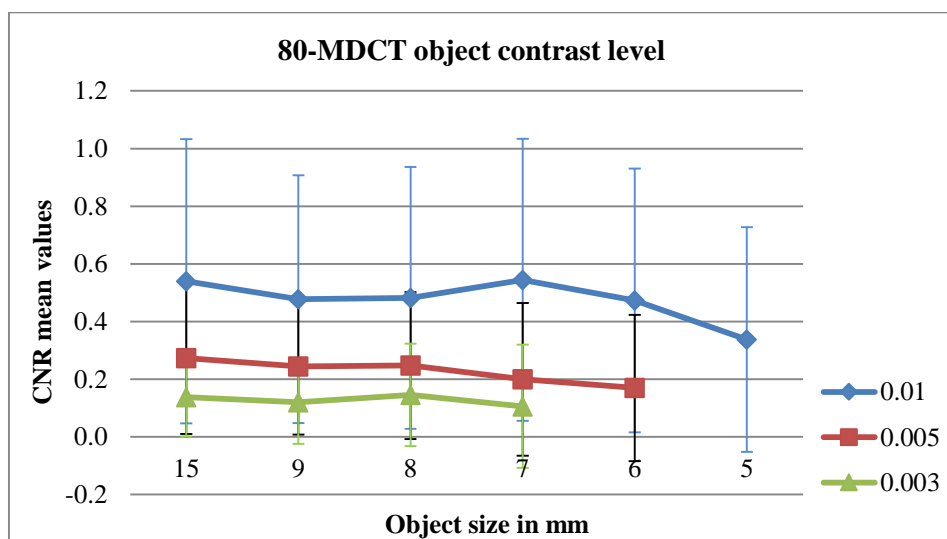
Figure 5.9 Effects of different contrast level object sizes are generally limited on CNR values for the 80-MDCT scanner. Note the change in CNR values with 5 mm objects size for 1% contrast level group.
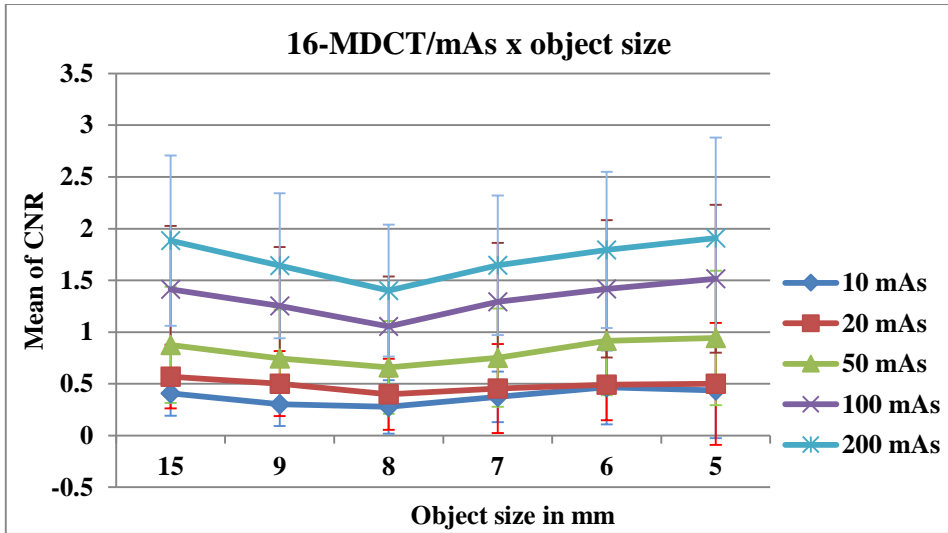
Figure 5.10   Effects of level object sizes at different mAs are limited on CNR values for the 80-MDCT scanner. (Note the change in CNR values with 8 mm objects particularly at high mAs levels.)
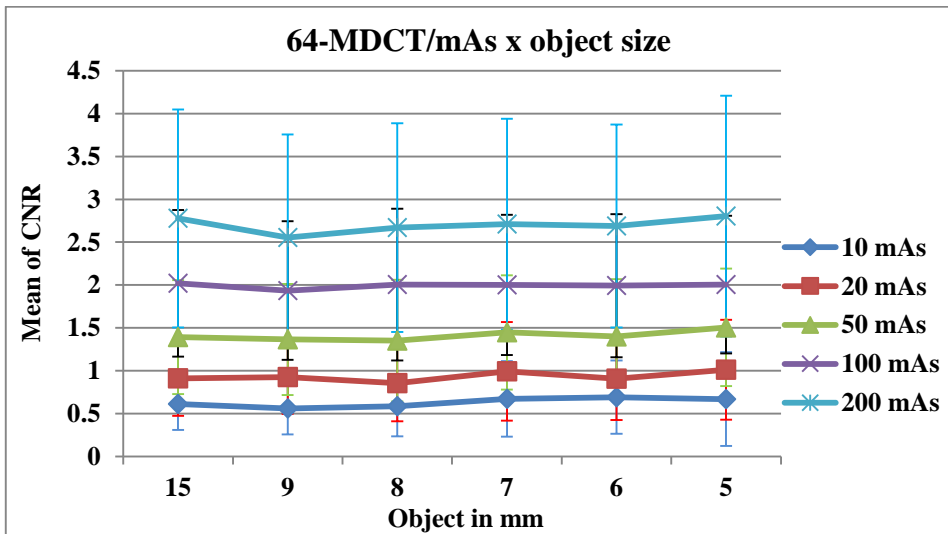
Figure 5.11   Effects of level object sizes at different mAs are limited on CNR values for the 64-MDCT scanner.

184
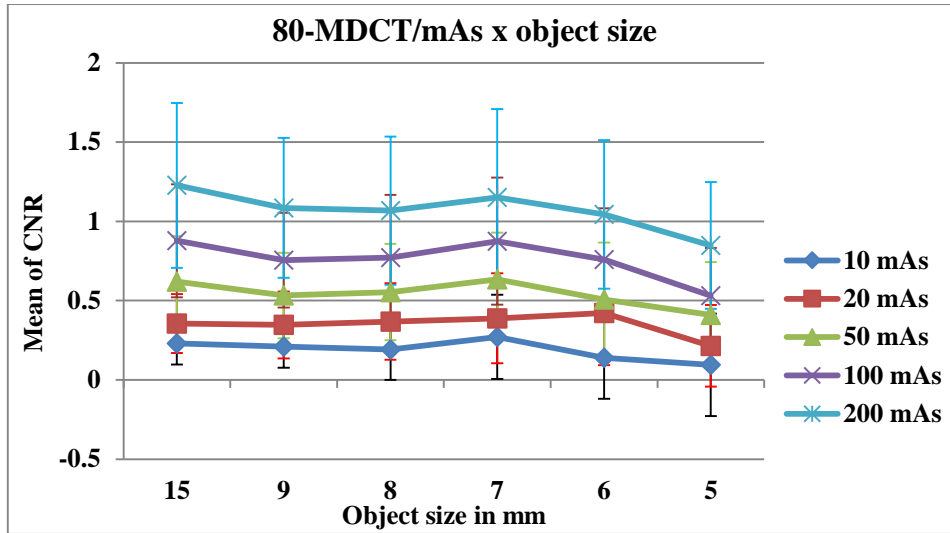
Figure 5.12   Effects of level object sizes at different mAs are limited on CNR values for the 80-MDCT scanner. (Note the change in CNR values with 5 mm objects particularly at high mAs levels.)

Table 5.5   The differences of CNR values (*p* values, Student t-tests) between different object sizes at 1% contrast in each CT scanners

Object size	Object sizes	Sig. (*p* values, Student t-tests)		
		16-MDCT	64-MDCT	80-MDCT
5	6	0.989	0.99	0.005
	7	0.228	0.999	0
	8	0	0.905	0.001
	9	0.145	0.799	0.002
	15	0.998	0.994	0
6	7	0.601	1	0.309
	8	0.004	0.998	0.999
	9	0.459	0.987	1
	15	1	1	0.333
7	8	0.308	0.982	0.537
	9	1	0.937	0.467
	15	0.472	1	1
8	9	0.436	1	1
	15	0.002	0.997	0.566
9	15	0.339	0.979	0.495

185

Effect of image reconstruction algorithms on CNR

In 16-MDCT and 64-MDCT, the CNR values for soft tissue reconstruction images were significantly higher than those of lung reconstruction images ($p < 0.001$). Soft tissue reconstruction images also had significantly higher CNR values than standard reconstruction images in 16-MDCT and 64-MDCT ($p = 0.011$ and $p < 0.001$ respectively). In 80-MDCT, however, standard reconstruction images had significantly higher CNR values than other algorithmic reconstruction images ($p < 0.001$) (Figure 5.13).
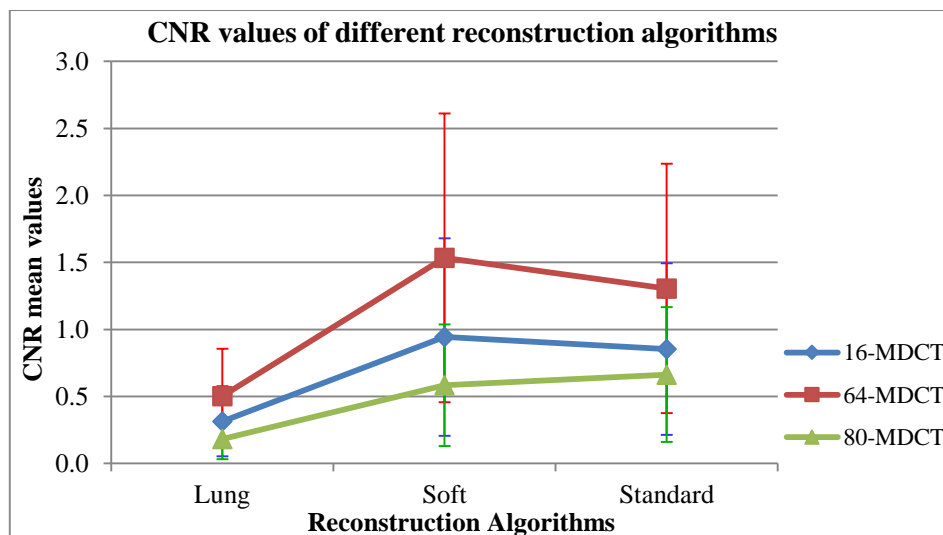
Figure 5.13   Soft reconstruction algorithm images had significantly higher CNR values than other images in 16-MDCT and 64-MDCT, while in 80-MDCT the standard reconstruction algorithm images were significantly higher CNR values than other images.

Effect of kVp on CNR

The use of higher kVp generally resulted in better CNR in all CT scanners (Figures 5.14 to 5.17). There were significant improvements in CNR values when the kVp increased from 80 to 120 (Table 5.6). However, there were insignificant differences between CNR values

at 80 and 120 kVp with 10 mAs and 0.625 mm ($p = 1$) in 16-MDCT. At 100 mAs with

0.625, there was also insignificant change in CNR values ($p = 0.894$) when the kVp

increased to 120. In 64-MDCT, there were significant improvements in CNR values when

the kVp increased from 80 to 120, the only exception being at 20 mAs and 0.625 mm slice

thickness ($p < 0.639$). In 80-MDCT, there were insignificant improvements in CNR at 10

and 20 mAs with all slice thicknesses when the kVp increased from 80 to 120. At 50 mAs,

with 0.5 and 1 mm slice thicknesses, there were insignificant improvements in CNR ($p =$

0.51 and 0.77 respectively) when the kVp increased from 80 to 120. There were also

insignificant differences in CNR values between 80 and 120 kVp at 100 mAs with 0.5 mm

slice thickness ($p = 0.81$).
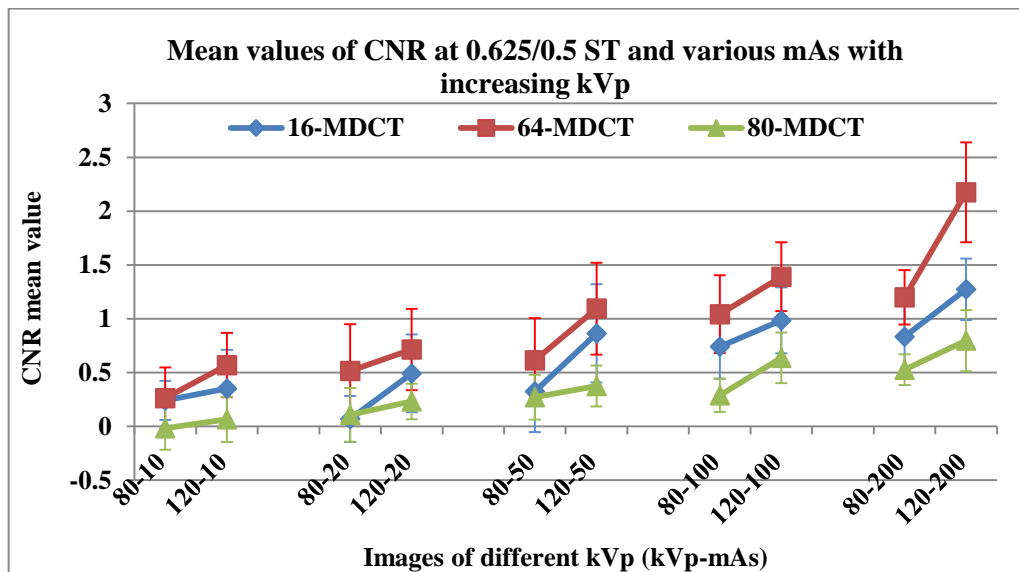
Figure 5.14   Higher kVp resulted in higher CNR values with 0.625/0.5 mm
slice thickness images for all CT scanners. (Note the change in CNR values
with low mAs levels.)

187
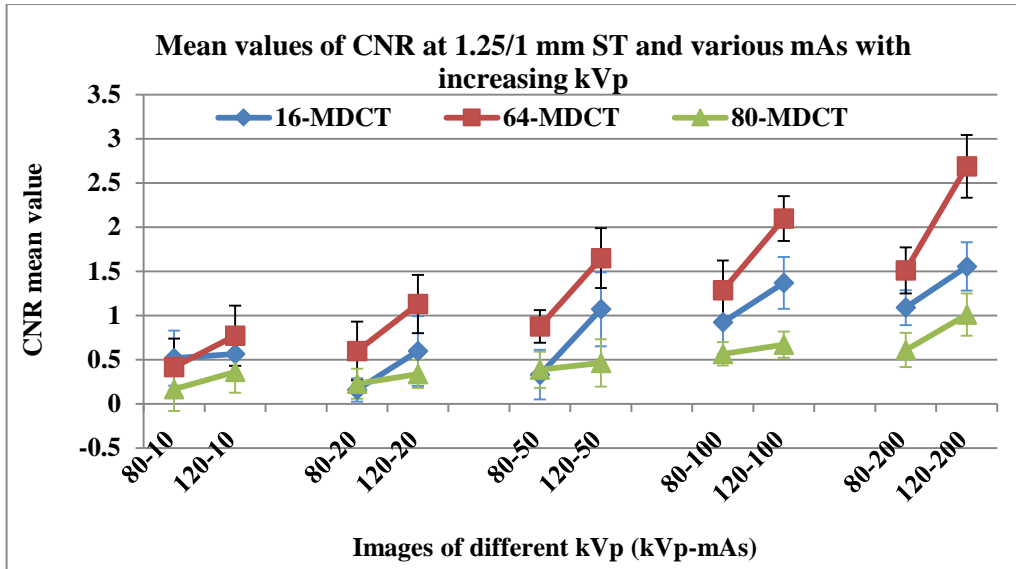
Figure 5.15   Higher kVp resulted in higher CNR values with 1.25/1 mm slice thickness images for all CT scanners.
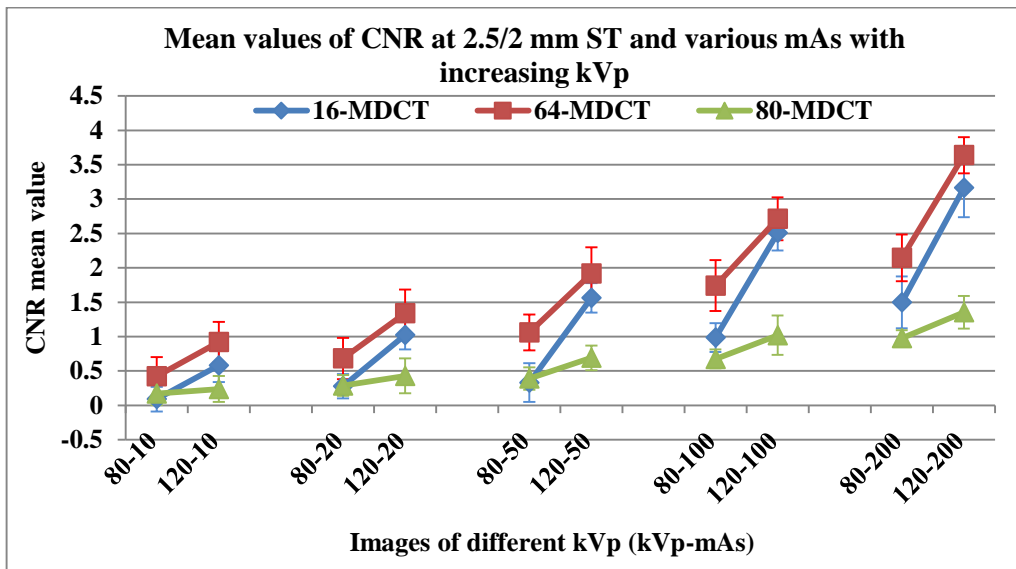
Figure 5.16   Higher kVp resulted in higher CNR values with 2.5/2 mm slice thickness images for all CT scanners.

188
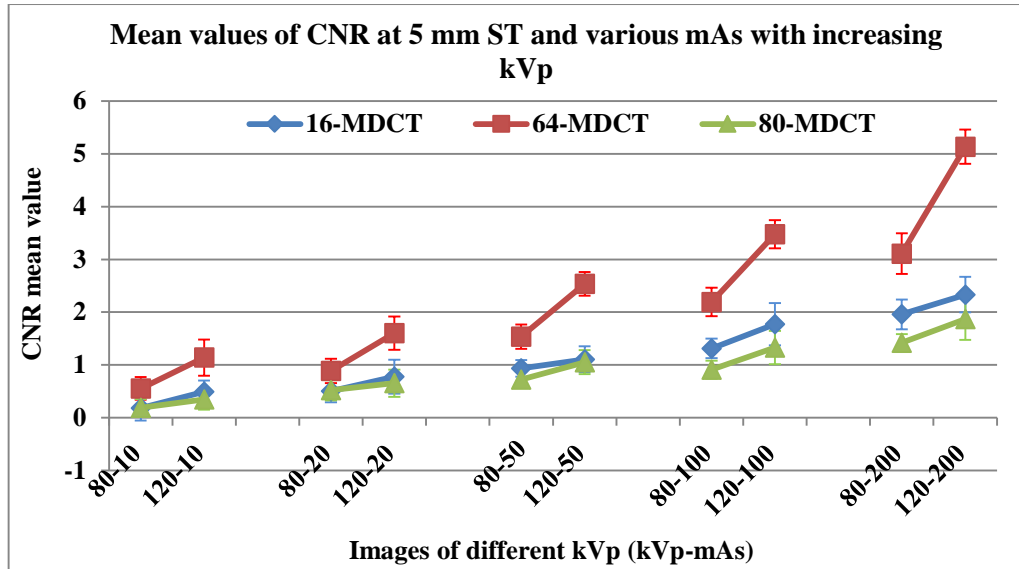
Figure 5.17   The higher kVp is, the higher CNR values with 5 mm slice thickness images for all CT scanners.

Table 5.6   The difference (p values, Student t-tests) between the images of same mAs and slice thicknesses with changing kVp in each CT scanner

(J) Image code (kVp-mAs-slice thickness)	(I) Image code (kVp-mAs-slice thickness)	Sig. (*p* values, Student t-tests)		
		16-MDCT	64-MDCT	80-MDCT
80-10-0.625/0.5	120-10-0.625/0.5	1.000	0.050	0.923
80-10-1.25/1	120-10-1.25/1	1.000	0.011	0.082
80-10-2.5/2	120-10-2.5/2	0.024	0.000	0.973
80-10-5	120-10-5	0.031	0.000	0.254
80-20-0.625/0.5	120-20-0.625/0.5	0.011	0.639	0.603
80-20-1.25/1	120-20-1.25/1	0.005	0.000	0.734
80-20-2.5/2	120-20-2.5/2	0.000	0.000	0.449
80-20-5	120-20-5	0.000	0.000	0.508
80-50-0.625/0.5	120-50-0.625/0.5	0.000	0.000	0.769
80-50-1.25/1	120-50-1.25/1	0.000	0.000	0.949
80-50-2.5/2	120-50-2.5/2	0.000	0.000	0.000
80-50-5	120-50-5	0.000	0.000	0.000
80-100-0.625/0.5	120-100-0.625/0.5	0.894	0.024	0.000
80-100-1.25/1	120-100-1.25/1	0.004	0.000	0.810
80-100-2.5/2	120-100-2.5/2	0.000	0.000	0.000
80-100-5	120-100-5	0.000	0.000	0.000
80-200-0.625/0.5	120-200-0.625/0.5	0.005	0.000	0.018
80-200-1.25/1	120-200-1.25/1	0.002	0.000	0.000
80-200-2.5/2	120-200-2.5/2	0.000	0.000	0.000
80-200-5	120-200-5	0.000	0.000	0.000

Effect of mAs on CNR values

The use of higher mAs levels generally resulted in better CNR values—particularly at greater slice thicknesses—in all CT scanners (Figures 5.18 to 5.23). There were mostly significant improvements in CNR values when the mAs increased from 10 to 20, 50, 100 or 200 (Table 5.7). However there were insignificant differences in CNR values between 10 and 20 mAs, particularly at lower kVp and thinner slice thicknesses ($p > 0.1$) in all CT scanners. In 16-MDCT, there were insignificant differences between 10 and 50 mAs at 80 kVp with 0.625 and 1.25 mm slice thicknesses ($p = 0.914$ and 0.244 respectively). At 120 kVp, there were insignificant differences in CNR values between 10 and 20 mAs at 120 with 0.625, 1.25 and 2.5 mm thicknesses ($p = 0.76$, 1 and 0.6 respectively). In 64-MDCT, there were insignificant differences between the images with 10 and 20 mAs at 120 kVp and slice thickness of 0.625 mm ($p = 0.781$). In 80-MDCT, there was insignificant differences between the images with 10 and 50 mAs at 120 kVp and 1.25 mm slice thickness ($p = 0.643$).
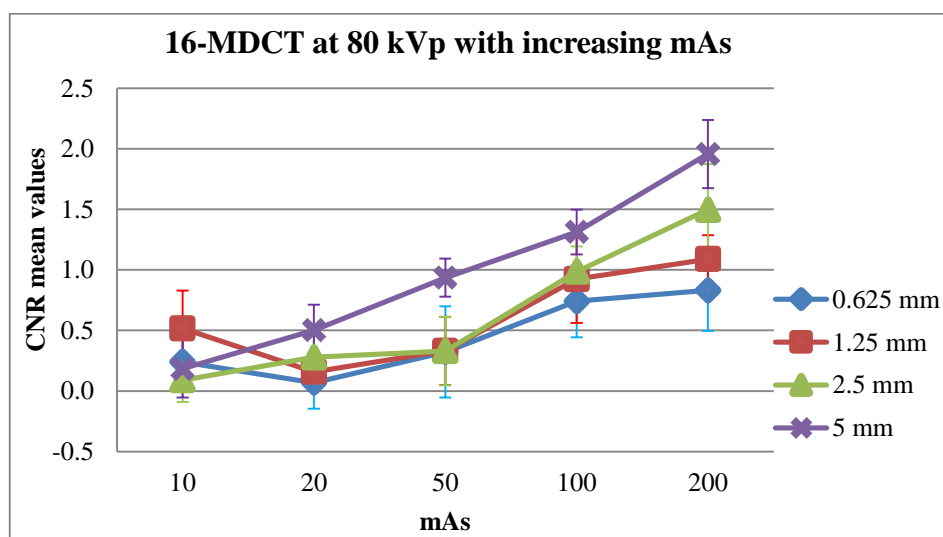
Figure 5.18   Higher mAs resulted in higher CNR values at 80 kVp with different slice thickness images for the 16-MDCT scanner. (Note the change in CNR values when the mAs increased from 10 to 20 mAs at 0.625 and 1.25 mm slice thickness images.)
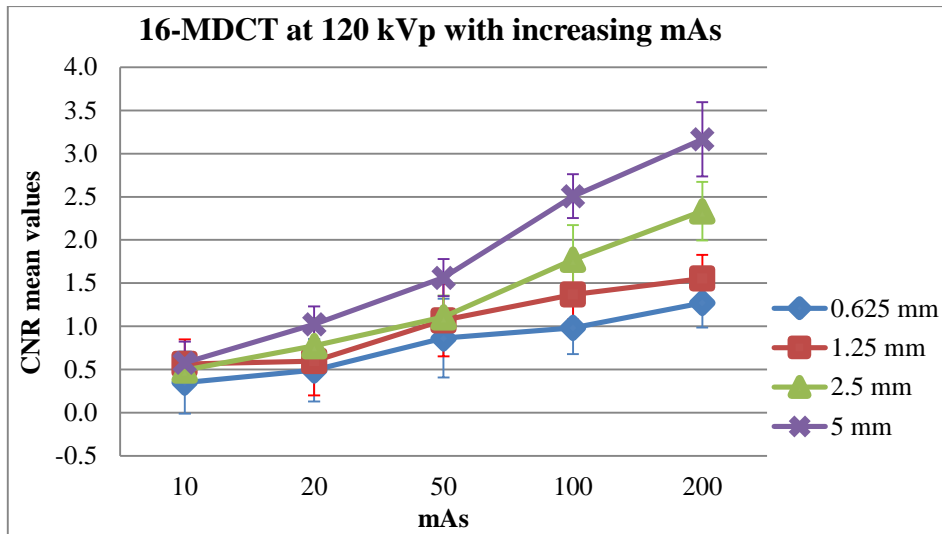
Figure 5.19 Higher mAs resulted in higher CNR values at 120 kVp, with different slice thickness images for the 16-MDCT scanner.
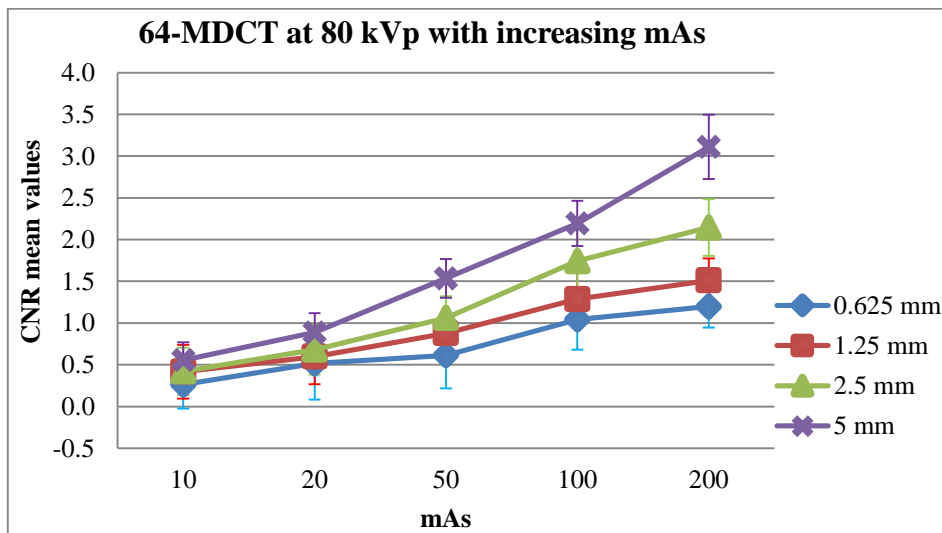
Figure 5.20   Higher mAs resulted in higher CNR values at 80 kVp with different slice thickness images for the 64-MDCT scanner.
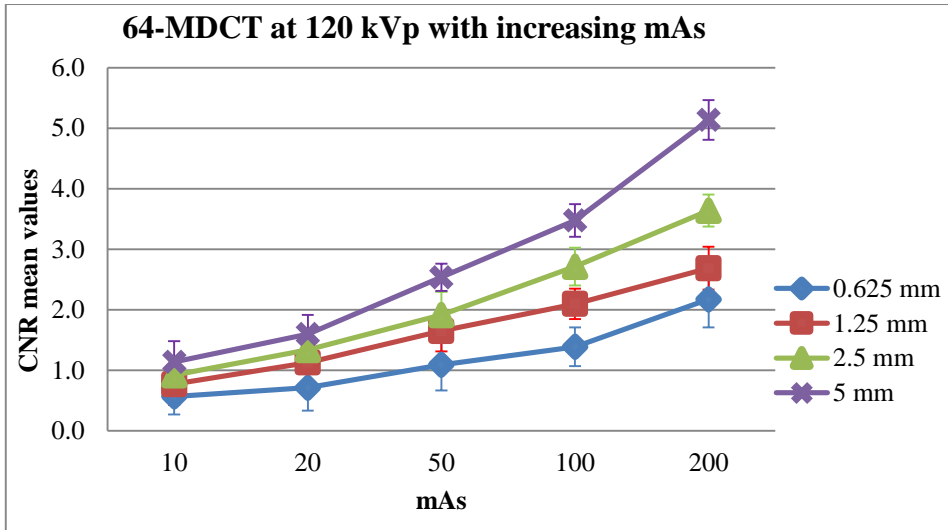
Figure 5.21   Higher mAs resulted in higher CNR values at 120 kVp with different slice thickness images for the 64-MDCT scanner.
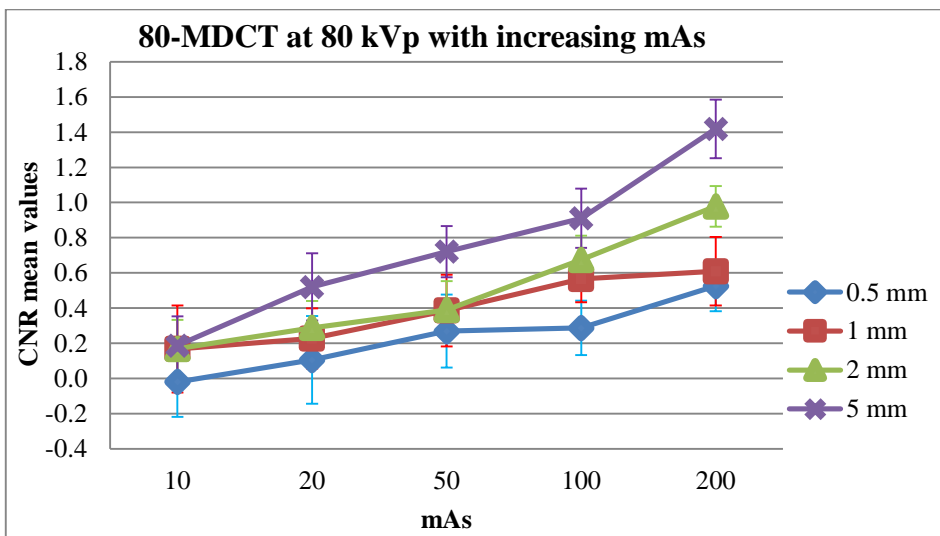
Figure 5.22   Higher mAs resulted in higher CNR values at 80 kVp with different slice thickness images for the 80-MDCT scanner.
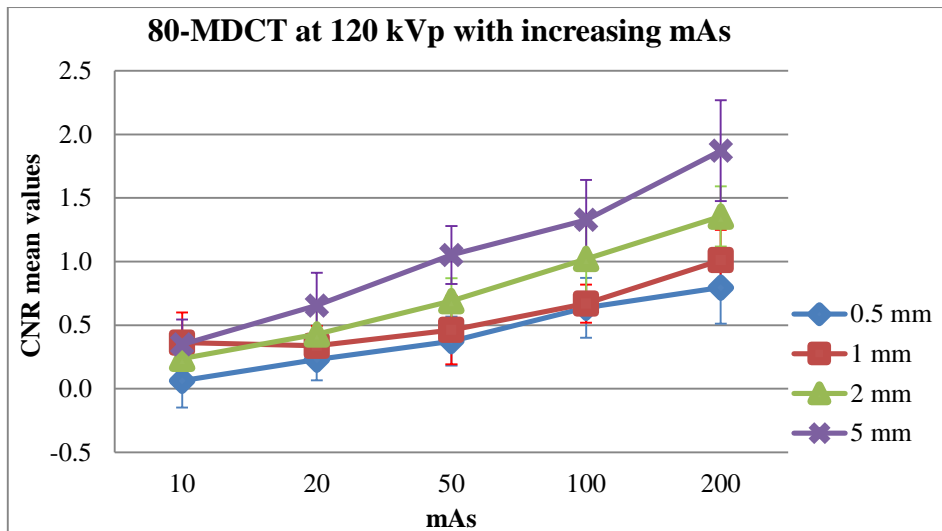
Figure 5.23   Higher mAs resulted in higher CNR values at 120 kVp with different slice thickness images for the 80-MDCT scanner. (Note the change in CNR values when the mAs increased from 10 to 20 mAs at 1 mm slice thickness images.)

Table 5.7   The difference (*p* values, Student t-tests) between the images of same kVp and mAs with changing mAs in each CT scanners

Image code kVp-mAs-ST	Image code kVp-mAs-ST	Sig. (*p* values, Student t-tests)		
		16-MDCT	64-MDCT	80-MDCT
80-10-0.625/0.5	80-20-0.625/0.5	0.395	0.203	0.310
	80-50-0.625/0.5	0.914	0.029	0.000
	80-100-0.625/0.5	0.000	0.000	0.000
	80-200-0.625/0.5	0.000	0.000	0.000
80-10-1.25/1	80-20-1.25/1	0.001	0.347	0.886
	80-50-1.25/1	0.244	0.000	0.009
	80-100-1.25/1	0.000	0.000	0.000
	80-200-1.25/1	0.000	0.000	0.000
80-10-2.5/2	80-20-2.5/2	0.188	0.099	0.120
	80-50-2.5/2	0.047	0.000	0.000
	80-100-2.5/2	0.000	0.000	0.000
	80-200-2.5/2	0.000	0.000	0.000
80-10-5	80-20-5	0.000	0.004	0.000
	80-50-5	0.000	0.000	0.000
	80-100-5	0.000	0.000	0.000
	80-200-5	0.000	0.000	0.000
120-10-0.625/0.5	120-20-0.625/0.5	0.760	0.781	0.166
	120-50-0.625/0.5	0.000	0.001	0.001
	120-100-0.625/0.5	0.000	0.000	0.000
	120-200-0.625/0.5	0.000	0.000	0.000
120-10-1.25/1	120-20-1.25/1	0.998	0.012	0.997
	120-50-1.25/1	0.000	0.000	0.643
	120-100-1.25/1	0.000	0.000	0.000
	120-200-1.25/1	0.000	0.000	0.000
120-10-2.5/2	120-20-2.5/2	0.060	0.002	0.109
	120-50-2.5/2	0.000	0.000	0.000
	120-100-2.5/2	0.000	0.000	0.000
	120-200-2.5/2	0.000	0.000	0.000
120-10-5	120-20-5	0.000	0.000	0.017
	120-50-5	0.000	0.000	0.000
	120-100-5	0.000	0.000	0.000
	120-200-5	0.000	0.000	0.000

Effect of slice thickness on CNR

The use of thicker slices generally resulted in better CNR in all CT scanners (Figures 5.24 to 5.29). There were mostly significant improvements in CNR values when the slice thickness increased from 0.625/0.5 to 1.25/1, 2.5/2 or 5 mm (Table 5.8). In 16-MDCT,

there was insignificant difference between the images with 0.625 and 1.25 mm slice thicknesses at 20, 50 and 100 mAs with 80 kVp and at 10, 20, 50 and 200 mAs with 120 kVp. There were also insignificant difference between the images with 0.625 and 1.25 mm slice thicknesses at 20, 50, 100 and 200 mAs with 80 kVp and at 10, 20, 50 and 200 mAs with 120 kVp. There were also insignificant differences between the images with 0.625 and 2.5 mm slice thicknesses at 10 and 50 mAs with 80 kVp and at 10, 20 and 50 mAs with 120 kVp. There were also insignificant differences between the images with 0.625 and 5 mm slice thicknesses at 10 mAs with 80 and 120 kVp (Table 5.8).

In 64-MDCT, there were insignificant differences in CNR values between 0.625 and 1.25 and between 0.625 and 2.5 mm slice thicknesses with 10 and 20 mAs at 80 kVp. There was also insignificant differences between images of 0.625 and 1.25 mm slice thicknesses at 100 mAs and 80 kVp ($p = 0.138$). There was also insignificant differences between images of 0.625 and 1.25 mm slice thicknesses at 10 mAs and 120 kVp (Table 5.8).

In 80-MDCT, the insignificant differences were between the images with 0.5 and 1 mm thicknesses at 20, 50 and 200 mAs and 80 kVp. There were also insignificant differences between images with 0.5 and 2 mm thicknesses at 50 mAs and 80 kVp. There was also insignificant differences between images of 0.5 and 1 mm slice thicknesses at 20, 50, 100 and 200 mAs and 120 kVp. There were also insignificant differences between images with 0.5 and 2 mm thicknesses at 10 mAs and 120 kVp (Table 5.8).
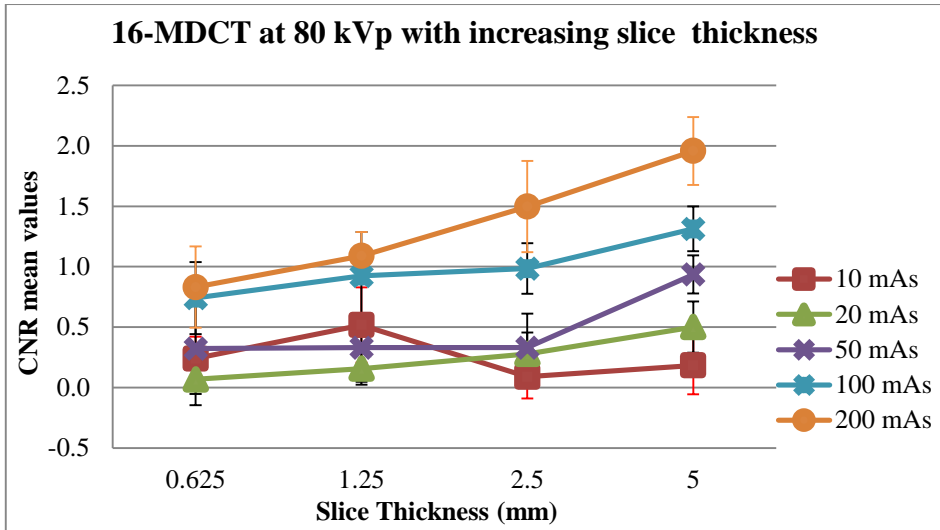
Figure 5.24 Thicker slice images resulted in higher CNR values at 80 kVp with different mAs levels for the 16-MDCT scanner. (Note the change in CNR values at 0.625/0.5 and 1.25 mm slice thickness images with 10 and 50 mAs.)
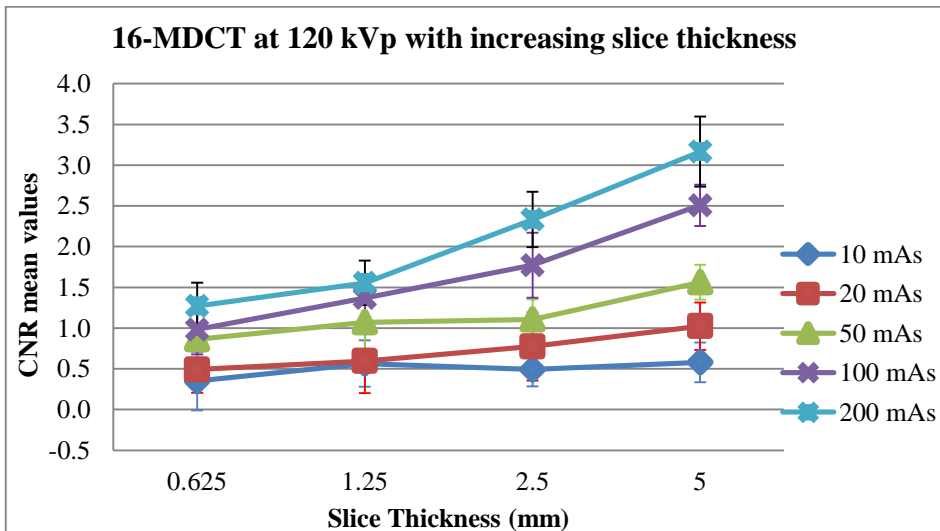
Figure 5.25 Thicker slice images resulted in higher CNR values at 120 kVp with different mAs levels for the 16-MDCT scanner. (Note the change in CNR values at 10 mAs at different slice thickness images.)
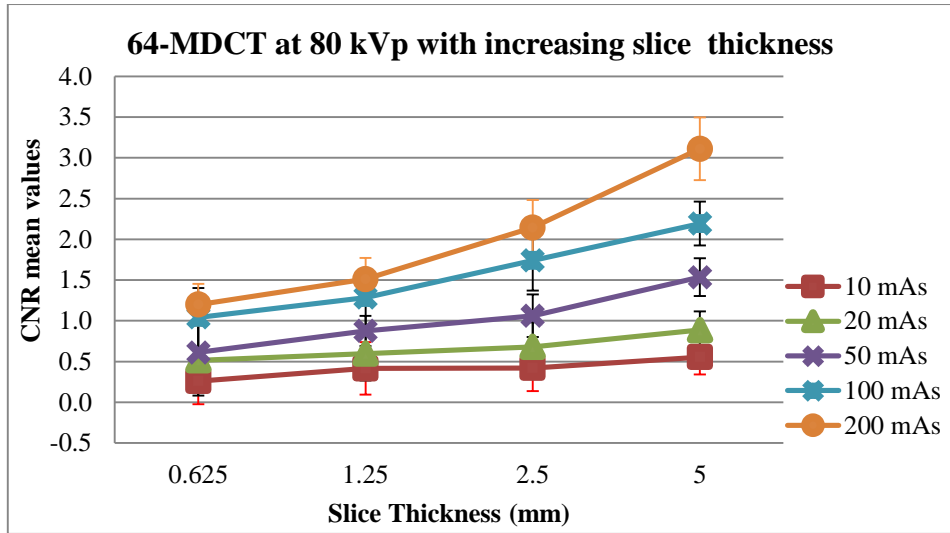
*Figure 5.26   Thicker slice images resulted in higher CNR values at 80 kVp
with different mAs levels for the 64-MDCT scanner.*
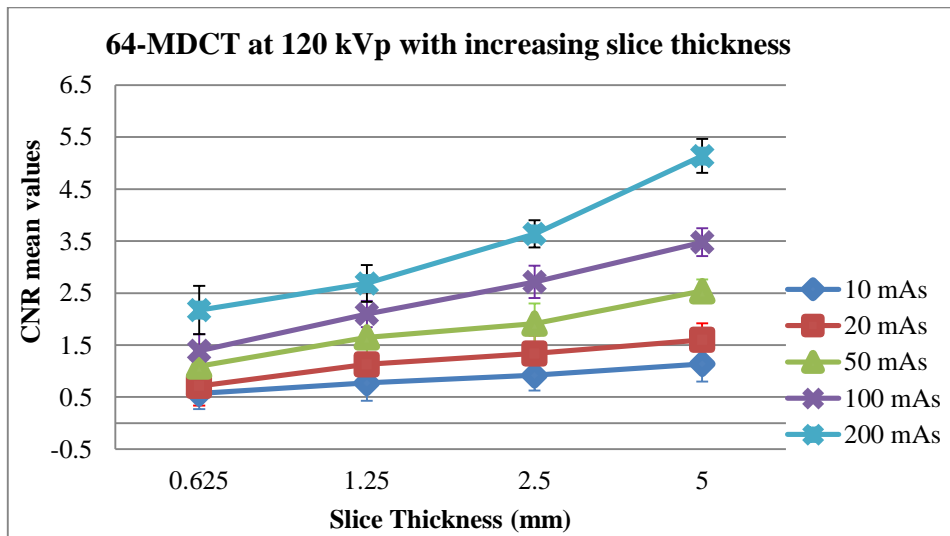
*Figure 5.27   Thicker slice images resulted in higher CNR values at 120 kVp
with different mAs levels for the 64-MDCT scanner.*
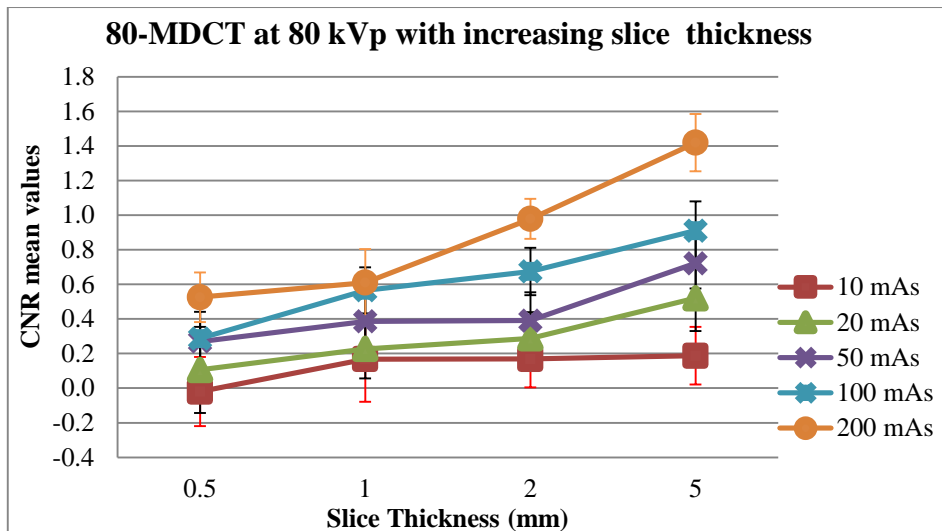
Figure 5.28 Thicker slice images resulted in higher CNR values at 80 kVp with different mAs levels for the 80-MDCT scanner. (Note the change in CNR values at 10 mAs between 1, 2 and 5 mm slice thickness images and the change in CNR values at 50 mAs between 1 and 2 mm slice thickness images.)
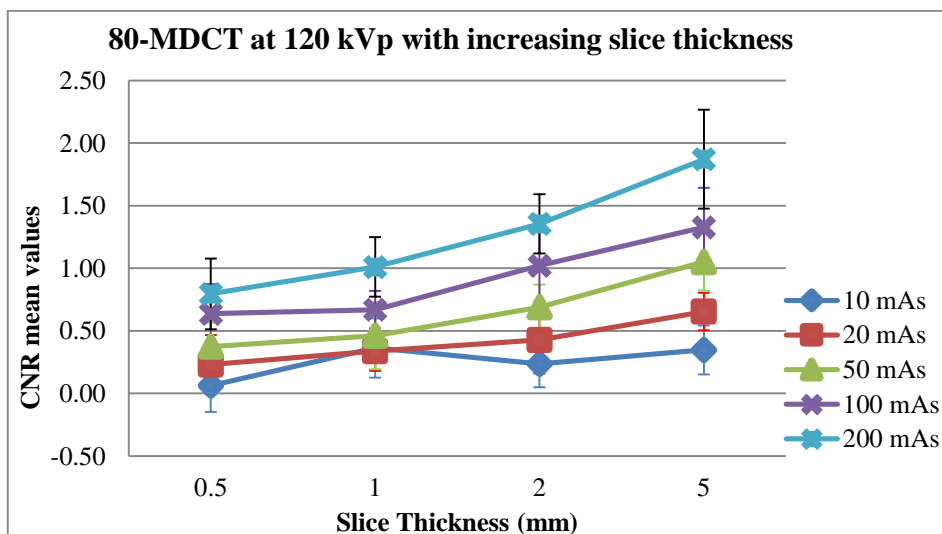
Figure 5.29   Thicker slice images resulted in higher CNR values at 120 kVp with different mAs levels for the 80-MDCT scanner. (Note the change in CNR values at 10 mAs between 1, 2 and 5 mm slice thickness images.)

Table 5.8   The difference (*p* values, Student t-tests) between the images of same kVp and mAs with changing slice thicknesses in each CT scanners

(I) Image code	(J) Image code	Sig. (*p* values, Student t-tests)		
		16-MDCT	64-MDCT	80-MDCT
80-10-0.625/0.5	80-10-1.25/1	0.004	0.348	0.029
	80-10-2.5/2	0.227	0.325	0.028
	80-10-5	0.888	0.012	0.013
80-20-0.625/0.5	80-20-1.25/1	0.480	0.878	0.246
	80-20-2.5/2	0.006	0.441	0.032
	80-20-5	0.000	0.007	0.000
80-50-0.625/0.5	80-50-1.25/1	1.000	0.029	0.228
	80-50-2.5/2	1.000	0.000	0.200
	80-50-5	0.000	0.000	0.000
80-100-0.625/0.5	80-100-1.25/1	0.193	0.138	0.000
	80-100-2.5/2	0.044	0.000	0.000
	80-100-5	0.000	0.000	0.000
80-200-0.625/0.5	80-200-1.25/1	0.065	0.020	0.384
	80-200-2.5/2	0.000	0.000	0.000
	80-200-5	0.000	0.000	0.000
120-10-0.625/0.5	120-10-1.25/1	0.108	0.229	0.000
	120-10-2.5/2	0.424	0.008	0.070
	120-10-5	0.075	0.000	0.001
120-20-0.625/0.5	120-20-1.25/1	0.773	0.003	0.434
	120-20-2.5/2	0.058	0.000	0.035
	120-20-5	0.000	0.000	0.000
120-50-0.625/0.5	120-50-1.25/1	0.291	0.000	0.633
	120-50-2.5/2	0.166	0.000	0.000
	120-50-5	0.000	0.000	0.000
120-100-0.625/0.5	120-100-1.25/1	0.003	0.000	0.980
	120-100-2.5/2	0.000	0.000	0.000
	120-100-5	0.000	0.000	0.000
120-200-0.625/0.5	120-200-1.25/1	0.067	0.000	0.139
	120-200-2.5/2	0.000	0.000	0.000
	120-200-5	0.000	0.000	0.000

Comparison study between scanners based on CNR values

Based on CNR value measurements, 64-MDCT generally showed superior performance compared with other CT scanners (Figures 5.29 to 5.38). 16-MDCT showed higher CNR values than 64-MDCT only at 80 kVp and 10 mAs with 1.25 mm slice thickness (Figure

5.29). 16-MDCT generally showed better performance than 80-MDCT, although 80-MDCT had better CNR values than 16-MDCT at 80 kVp and 10 mAs with 2.5/2 mm slice thickness, at 80 kVp and 20 mAs with different slice thickness and at 80 kVp and 50 mAs with 2.5/2 slice thickness (Figures 5.29 to 5.31).

There were significant differences between 16-MDCT and 64-MDCT scanners, with some exceptions: at 80 kVp and 10 mAs with 0.625 or 1.25 mm slice thicknesses, and at 120 kVp and 50 mAs with 0.625 mm slice thicknesses (Table 5.9). There were also significant differences in CNR values between 16-MDCT and 80-MDCT at low exposure factors: at 80 kVp and 10 mAs with 2.5/2 or 5 mm slice thicknesses, at 80 kVp and 20 with different slice thickness, and at 80 kVp and 50 mAs with 0.625/0.5 and 1.25/1 mm slice thicknesses. The differences in CNR values between 64-MDCT and 80-MDCT were always significant.

64-MDCT did not only show significantly higher CNR than other scanners, but also demonstrated better linearity of CNR values improvement with the increases in kVp, mAs or slice thicknesses (Figures 5.14 to 5.28).
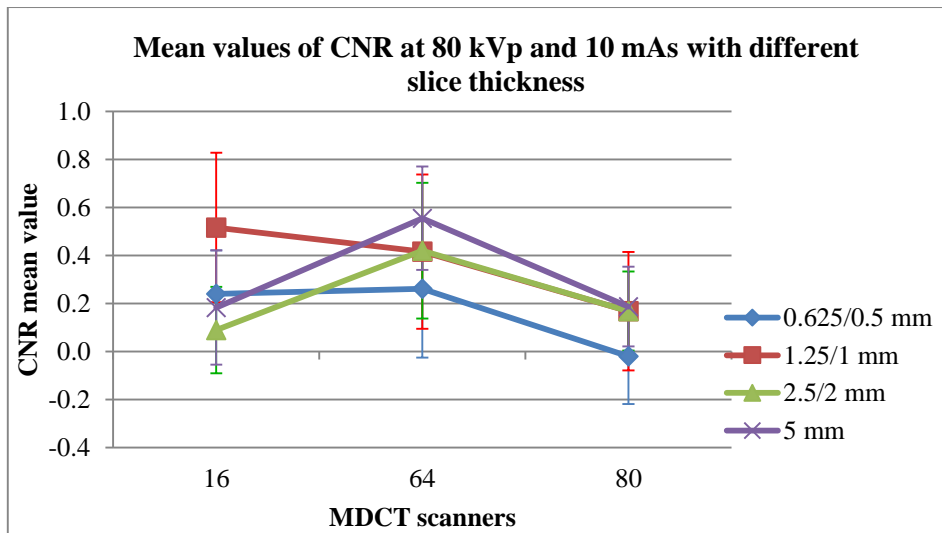
Figure 5.30   Average CNR values at 80 kVp and 10 mAs for each CT scanner show the superiority of 64-MDCT over other scanners and the superiority of 16-MDCT over 80-MDCT. (Note the change in CNR values using 16-MDCT at 1.25/1 and 2.5/2/2 mm slice thicknesses.)
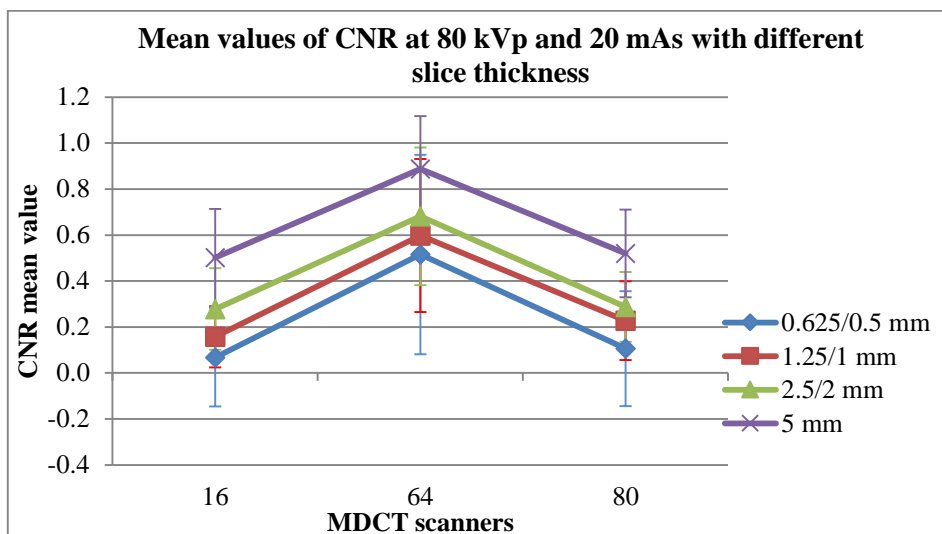
Figure 5.31   Average CNR values at 80 kVp and 20 mAs for each CT scanner show the superiority of 64-MDCT. 16-MDCT and 80-MDCT are comparable in terms of CNR values.

201
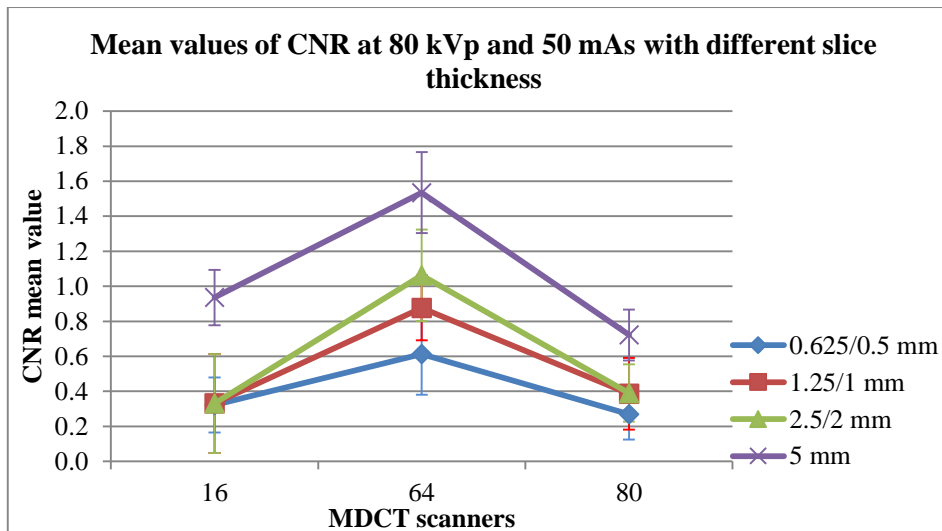
Figure 5.32   Average CNR values at 80 kVp and 50 mAs for each CT scanner show the superiority of 64-MDCT. 16-MDCT and 80-MDCT are comparable in terms of CNR values. (Note the difference of CNR values between 16-MDCT and 80-MDCT at 5 mm slice thicknesses.)
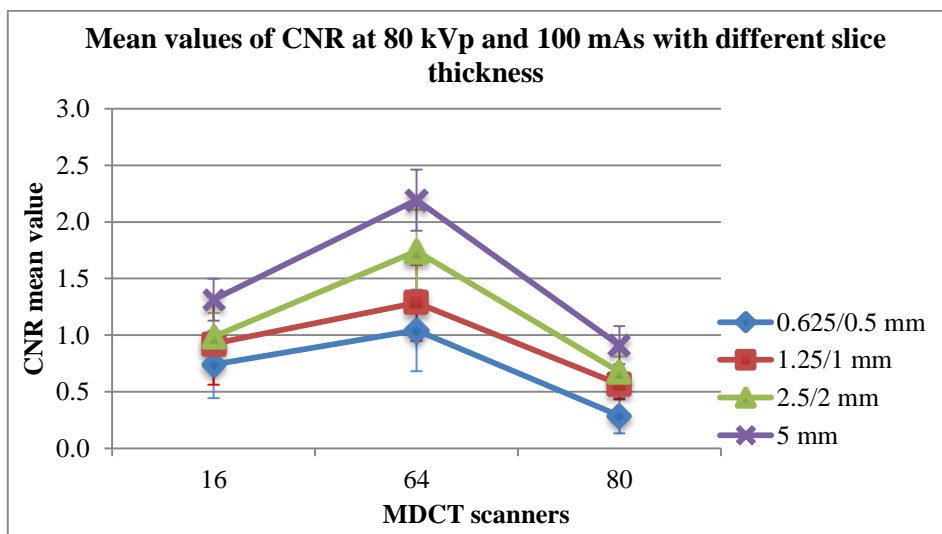
Figure 5.33   Average CNR values at 80 kVp and 100 mAs for each CT scanner show the superiority of 64-MDCT over the other scanners and the superiority of 16-MDCT over 80-MDCT.
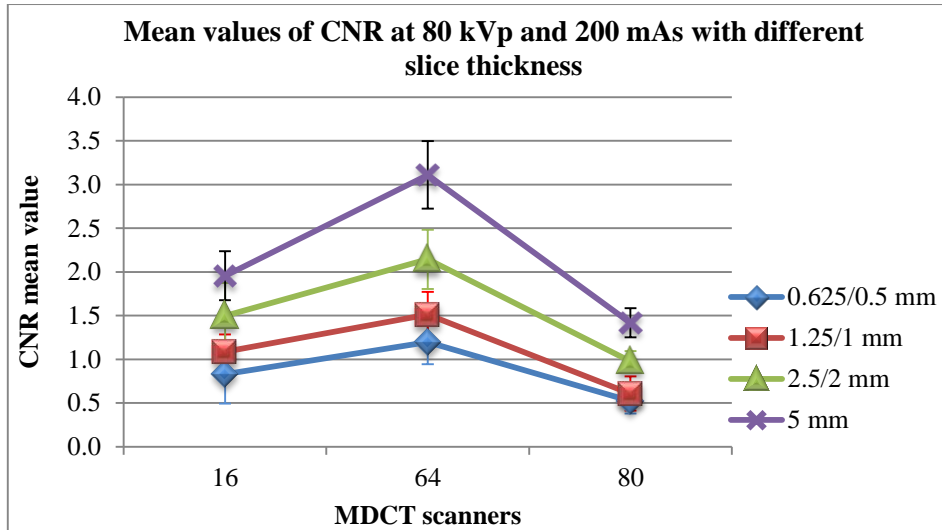
Figure 5.34   Average CNR values at 80 kVp and 200 mAs for each CT scanner show the superiority of 64-MDCT over the other scanners and the superiority of 16-MDCT over 80-MDCT.
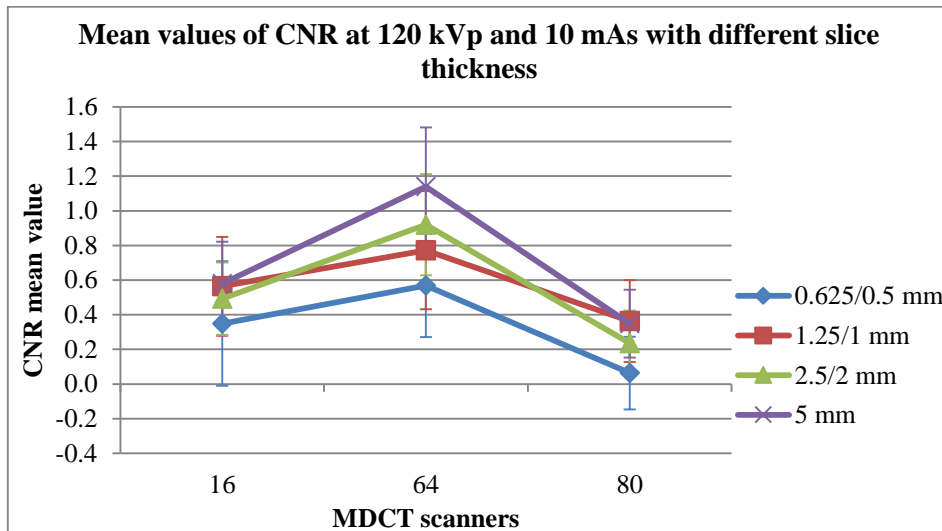
Figure 5.35   Average CNR values at 120 kVp and 10 mAs for each CT scanner show the superiority of 64-MDCT over the other scanners and the superiority of 16-MDCT over 80-MDCT. (Note the changes in CNR values with 16-MDCT and 80-MDCT at different slice thickness images.)
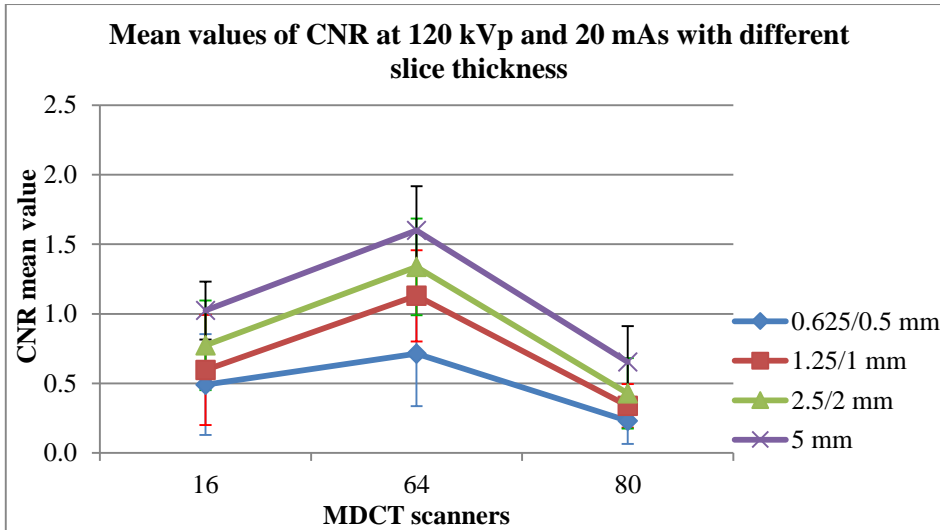
Figure 5.36 Average CNR values at 120 kVp and 20 mAs for each CT scanner show the superiority of 64-MDCT over the other scanners and the superiority of 16-MDCT over 80-MDCT.
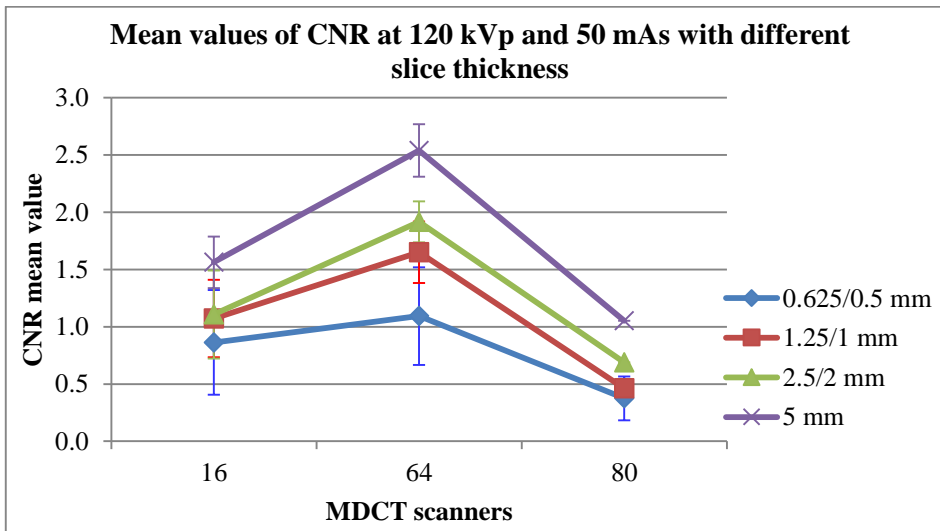
Figure 5.37 Average CNR values at 120 kVp and 50 mAs for each CT scanner show the superiority of 64-MDCT over the other scanners and the superiority of 16-MDCT over 80-MDCT.
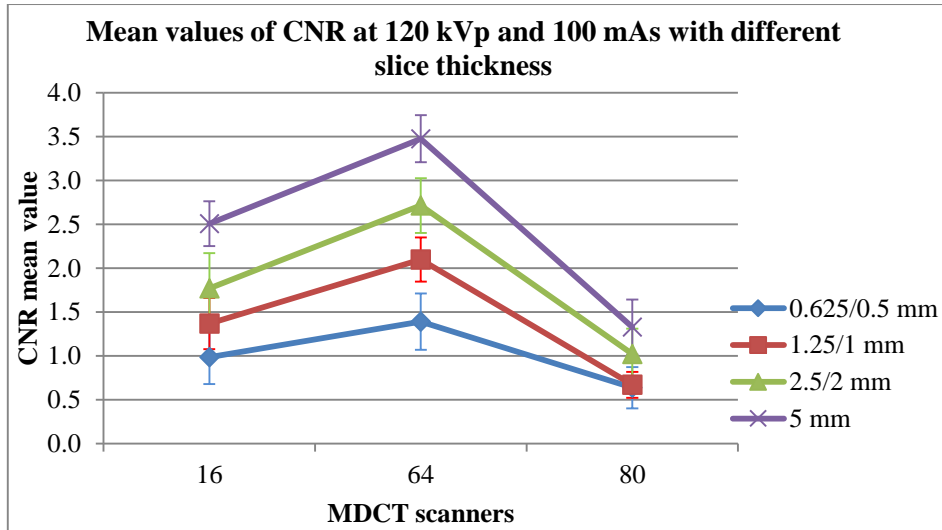
Figure 5.38   Average CNR values at 120 kVp and 100 mAs for each CT scanner show the superiority of 64-MDCT over the other scanners and the superiority of 16-MDCT over 80-MDCT. (Note the changes in CNR values with 16-MDCT and 80-MDCT at different slice thickness images.)
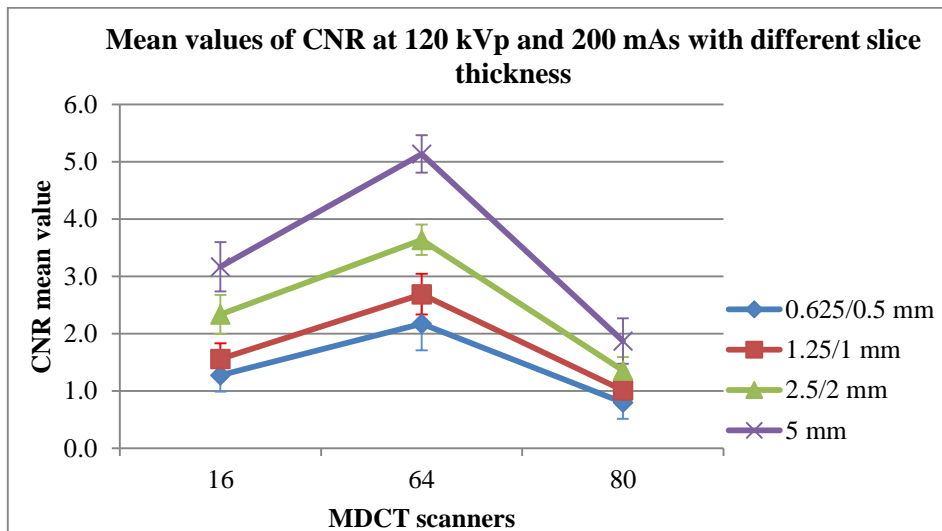
Figure 5.39   Average CNR values at 120 kVp and 200 mAs for each CT scanner show the superiority of 64-MDCT over the other scanners and the superiority of 16-MDCT over 80-MDCT.

Table 5.9 The differences (*p* values, Student t-tests) between the images of same factors and slice thicknesses from different CT scanners.

kVp	mAs	ST	Sig. (*p* values, Student t-tests)		
			16-MDCT x 64-MDCT	16-MDCT x 80-MDCT	64-MDCT x 80-MDCT
80	10	0.625/0.5	0.3961	< 0.001	0.0009
80	10	1.25/1	0.1735	0.0004	0.0069
80	10	2.5/2	< 0.001	0.0892	0.0015
80	10	5	0.0000	0.4788	0.0000
80	20	0.625/0.5	0.0003	0.3145	0.0009
80	20	1.25/1	0.0000	0.0905	< 0.001
80	20	2.5/2	0.0000	0.4316	0.0000
80	20	5	0.0000	0.3921	0.0000
80	50	0.625/0.5	0.0153	0.3027	0.0015
80	50	1.25/1	0.0000	0.2520	0.0000
80	50	2.5/2	0.0000	0.2208	0.0000
80	50	5	0.0451	< 0.001	0.0000
80	100	0.625/0.5	0.0050	0.0000	0.0000
80	100	1.25/1	0.0019	0.0004	0.0000
80	100	2.5/2	0.0000	0.0000	0.0000
80	100	5	0.0000	0.0000	0.0000
80	200	0.625/0.5	0.0004	0.0009	0.0000
80	200	1.25/1	0.0000	0.0000	0.0000
80	200	2.5/2	0.0000	0.0000	0.0000
80	200	5	0.0000	0.0000	0.0000
120	10	0.625/0.5	0.0276	0.0035	0.0000
120	10	1.25/1	0.0273	0.0140	< 0.001
120	10	2.5/2	0.0000	0.0002	0.0000
120	10	5	0.0000	0.0018	0.0000
120	20	0.625/0.5	0.0395	0.0051	0.0000
120	20	1.25/1	< 0.001	0.0086	0.0000
120	20	2.5/2	0.0000	0.0005	0.0000
120	20	5	0.0000	0.0000	0.0000
120	50	0.625/0.5	0.0635	0.0002	0.0000
120	50	1.25/1	0.0000	0.0000	0.0000
120	50	2.5/2	0.0000	0.0000	0.0000
120	50	5	0.0000	0.0000	0.0000
120	100	0.625/0.5	0.0002	0.0003	0.0000
120	100	1.25/1	0.0000	0.0000	0.0000
120	100	2.5/2	0.0000	0.0000	0.0000
120	100	5	0.0000	0.0000	0.0000
120	200	0.625/0.5	0.0000	0.0000	0.0000
120	200	1.25/1	0.0000	0.0000	0.0000
120	200	2.5/2	0.0000	0.0000	0.0000
120	200	5	0.0000	0.0000	0.0000

5.4 Discussion

The effects of object size on CNR value was tested from different aspects, including their effects in combination with scanner types, reconstruction algorithms, object contrast levels and mAs. The effects of reconstruction algorithms—kVp, mAs and slice thickness—on CNR values were then examined, and the performance of different scanners based on CNR values were compared and assessed.

The CNR values were significantly influenced by changing image reconstruction algorithms. While the values of CNR were significantly higher at soft tissue reconstruction images in 16- and 64-MDCT, CNR values were higher at standard reconstruction images than other algorithmic reconstruction images in 80-MDCT.

According to Kalender and Khadivi (2011), different algorithmic reconstruction kernels impose different typical pixel noise values, which are determined by simulation. For example, the typical pixel noise of soft kernel is 62.1 HU, while the typical pixel noise of standard and high-resolution kernels are 31.5 and 57.5 HU respectively at 1 mm slice thickness and 32 cm slice width. The noise level of CT images is the essential factor with respect to the detectability of LCD objects (Kalender & Khadivi 2011).

The results did not show any significant changes in CNR values between different object sizes, down to the smallest diameter (5 mm) that the researcher was able to measure. As discussed in Chapters 2 and 4, object detectability is not only determined by object contrast level but also by object size (Baker et al. 2012; Davidson 2007; Faulkner & Moores 1984). How to manage indeterminate small lesion such as nodules in CT lung screening has become a major concern. Even though the vast majority of extremely small nodules are benign, some of them will turn out to be cancers (MacMahon et al. 2005). Some small

lesions such as small cell carcinoma showed rapid growth, with a mean volume doubling time of 149 days (Hasegawa, M et al. 2000). Hence, the early intervention is essential to provide an opportunity for cure (MacMahon et al. 2005). Accurate assessment and exact determination of the size pulmonary nodules and other lesions are important in certain clinical settings. This allows to evaluate the effects of the chemotherapy and to detect lesion growth at follow-up of small pulmonary nodules, which may indicate malignancy (Wormanns et al. 2000). The evaluation method based on CNR value measurements is an inappropriate approach to assess the effects of object size on LCD detectability performance.

Higher kVp generally resulted in better CNR in all CT scanners. In particular, there were significant improvements in CNR values when the kVp increased from 80 to 120. The effects of kVp on image quality in terms of CNR values were as expected: increasing kVp increases photon penetration and the radiation dose when other exposure factors are fixed, even though the radiation dose is not linear with kVp. Consequently, the noise is reduced and the CNR is enhanced (Alsleem & Davidson 2013; Seibert 2004).

Higher mAs levels generally resulted in better CNR values, particularly at larger slice thicknesses. As expected, CNR is improved with increasing mAs, as the image noise is reduced. The radiation dose linearly increases with mAs (Funama et al. 2005; Toth 2012).

With thicker slices, CNR values generally increased. The influence of slice thickness on imaging performance of CT scanners was as expected, because thicker slices reduce image noise and hence image quality improves (von Falck, Galanski & Shin 2010). According to the above, there were insignificant differences in CNR values between 0.625/0.5 and 1.25/1 mm slice thicknesses at all mAs levels and between 0.625/0.5 and 2.5/2 mm slice thicknesses, particularly at low exposure factors. The noise increases with thinner slices if

the radiation dose is not increased (Alsleem & Davidson 2013; Seibert 2004; von Falck, Galanski & Shin 2010). However, thinner slice thicknesses provide high-resolution isotropic image data sets and hence through-plane partial-volume averaging effects are minimised and image post-processing are optimised (Kalender & Khadivi 2011; Rubin 2003).

Based on CNR value measurements, 64-MDCT showed superior performance when compared with other CT scanners, and 16-MDCT generally showed better performance than 80-MDCT (Figures 5.29 to 5.38). There were significant differences between 16-MDCT and 64-MDCT scanners. The detector properties and system specifications of each CT scanner determine its own imaging performance. For example, CT scanner manufacturers, models, scanner geometry, tube specifications and detector design characterise noise and image blur, which in turn all affect imaging performance and image quality (Alsleem & Davidson 2013; Faulkner & Moores 1984; Hsieh 2009; Mahesh 2009; Seeram 2009). This study is limited by the fact that only one scanner system of one manufacturer was included. In addition, the smallest size of phantom objects that the researcher was able to measure was 5 mm.

5.5 Conclusion

The objective LCD evaluation method based on CNR value measurements was sensitive to measure the effects of kVp, mAs and slice thicknesses on image quality. This method was also effective in evaluating the effects of different reconstruction algorithms and different contrast level objects on image quality based on CNR values. However, using this method of CNR measurement, with the Catphan® 600, the smallest object size measured was 5mm.

Objects below this size could not be measured with accuracy without measuring outside of the object so as to determine the object's mean CT value. As such, no significant CNR changes between different object sizes were seen. LCD detectability is not only determined by object contrast but also by object size. Therefore, this method is not an appropriate method to measure LCD detectability performance. This phantom design is also not able to evaluate an object of the same contrast and size at different location levels inside the phantom. This method is time consuming and burdensome as it requires analysis of an extremely large amount of data. In addition, validity of this method is relatively low as human observers were not included in the process. As a result, this method of using Catphan® 600 is not an appropriate tool for image optimisation purposes and routinely based evaluation. Meanwhile, a similar methodology to those used in planar radiography that was examined in Chapter 3 does not exist for CT. A new phantom and approach should be developed to assess LCD detectability of CT performance. The next chapter will discuss the newly designed phantom and a developed LCD evaluation approach adopted by the researcher.

Chapter 6 Development of the new contrast-detail phantom and dedicated software

6.1 Introduction

The low contrast-detail (LCD) of CT images is currently evaluated by two approaches: objective and subjective. The objective approach of the LCD evaluation method is based on statistical measurements of CNR (which were evaluated in Chapter 5) to examine its appropriateness to assess LCD detectability performance in CT. According to von Falck, Galanski and Shin (2010) and the results of Chapter 5, this objective approach allows users to analyse a larger number of data sets and avoids the subjectivity of approaches based on human observers. Based on the results of Chapter 5, the objective approach is considered an appropriate method to evaluate the effects of exposure factors and slice thickness on image quality. However, the results of Chapter 5 also showed that this approach suffers from several limitations. The objective approach was not an appropriate method when used to evaluate the effects of different object sizes on CNR values. The objective approach based on CNR measurements also has limited validity as it does not involve human observers. This approach does not directly measure detectability performance, but just measures CNR as a factor that influences the detectability performance of observers. Statistical LCD based on CNR measurements mainly measures the noise characteristics in a uniform portion of the phantom and does not consider the impact on the detectability of LCD objects in the post-processed images (Hsieh & Toth 2008). In addition, a consensus on methods of LCD detectability performance evaluation for CT with higher validity and reliability has not yet been achieved, despite the efforts that are being conducted by several institutions and expert researchers (Kalender & Khadivi 2011).

The subjective approaches are influenced by inter and intra-variable differences of human observer decisions (Keat & Edyvean 2003; Levison & Restle 1968; Thilander-Klang et al. 2010). The results of Chapter 3 also demonstrated the limitations of the subjective approach, including its low reliability and time consuming and cumbersome procedures. As such, subjective approaches to LCD evaluation are inappropriate as routine image evaluation and optimisation tools. A software analyser has been used to measure CT image quality in terms of LCD, but they still need the clinical validation (von Falck, Galanski & Shin 2010).

While the evaluation method of LCD detectability performance is well established in digital radiography, a similar method of image evaluation and quality optimisation of CT images is not available. The automated evaluation method of LCD detectability performance in planar radiography was evaluated in Chapter 3, and this approach could be translated to CT. The current methods and results of LCD measurement in CT are limited, not only by the applied approaches but also by available phantoms (Hsieh & Toth 2008). As discussed in Chapter 5, the current LCD phantoms are used to examine LCD detectability performance, but these phantoms are only useful when evaluating LCD of smaller organs, such as the head. The sizes of commercially available LCD phantoms are not appropriate to evaluate the detectability performance of larger organs such as the abdomen or chest. To be more generally useful, an LCD phantom should include a wider range of different object sizes, contrasts and locations. However, such phantom design and properties are currently not available.

To avoid the limitations of subjective approaches, LCD detectability performance should be objectively assessed by model observer software (Hernandez-Giron et al. 2011; Pascoal et al. 2005). Dedicated LCD analyser software should be developed and utilised with a new

proposed methodology. The results and the use of the automated analysing software, discussed in Chapter 3, suggests that the automated Artinis CDRAD analyser, and the resultant measurement of the inverse image quality figure (IQF_{inv}), is a fast, valid and reliable method to evaluate LCD detectability performance of digital radiography.

This chapter aims to describe properties, specifications and materials of the prototype LCD CT (CDCT) phantom that was designed and manufactured. The new phantom was manufactured in cooperation with Artinis Medical Systems, who were also responsible for the design and development of the commonly used CDRAD phantom and software analyser in planar imaging. The chapter also explains the new methodology of image quality evaluation in terms of CT inverse image quality figure ($CTIQF_{inv}$), which is based on IQF_{inv}. Dedicated software, which was developed in cooperation with Artinis, is also described in this chapter.

6.2 Designing and manufacturing

6.2.1 Phantom specification

The new CDCT phantom was designed by the researcher and manufactured by Artinis Medical Systems to meet the proposed methodology of LCD detectability performance in CT. The specifications and materials of the CDCT phantom design were considered from international and specialised organisations, especially the standards suggested by the American Society for Testing and Materials (ASTM) International (ASTM International ; Ramaseshan et al. 2008; Suess, Kalender & Coman 1999).

The CDCT phantom body is circular and built from solid materials, such as resins, for long-term stability and ease of handling. A circular design was chosen so there would be a

uniform path length of the x-ray phantom from all directions of the CT beam, and hence uniform attenuation in all directions across the CDCT phantom. The CDCT phantom is 32 cm in diameter; this size was selected as quality control phantoms used in the assessment of image quality, equipment performance and dose measurements in CT abdomen and chest examinations are also this size. The thickness of the phantom is 10 mm, which was selected due to manufacturing technically difficulties and the expense of inserting smaller 1 mm diameter objects into a phantom with greater than 10 mm depth.

The CDCT phantom design contains different cylindrical objects to allow realistic contrast resolution measurements; it contains eight objects of different sizes and different attenuation material. The diameter of the objects of the phantom are 1, 1.5, 2, 3, 4, 5, 6.5 and 8 mm. Materials of eight different attenuation and different Hounsfield Unit (HU) values were selected to produce eight different contrast levels and comprise various human tissues. These materials are briefly discussed in the section of material selection in this chapter. The materials enabled the measurement and testing of LCD detectability and visibility up to nearly 10 HU contrast differences between the objects and background. Each object of certain size and specific contrast is assigned in two location levels, peripheral and central.

Three sets of eight cylindrical shapes—with different diameter sizes and HU values—are arranged in the centre square and the outer region, with two more sets in the outer area and another in the centre region (Figure 6.1). As discussed in Section 4.3.6 of Chapter 4, objects of outer location receive radiation dose more than objects of centre location by a factor of two-thirds. As a result, the noise at the outer location is much lower than central location, and consequently the detectability performance is not the same at different location levels. Dose is a contributor to contrast and hence LCD needs to be evaluated in inner and outer

214

regions of the phantom (Kalender & Khadivi 2011). The positions of the cylindrical objects of the CDCT phantom were exchanged from central to outer orbits, so that each object of fixed size and HU where in the central area and in two different locations in outer area. The central objects of same HU values were arranged from large to small sizes. Each second column was flipped top to bottom, in order to increase the spaces between objects to avoid artefacts and signal interference. The diameters of cylindrical objects include eight sizes (Table 6.1). The number of different densities is eight. There are three notches to be used as reference points to position the phantom and determine images orientation.
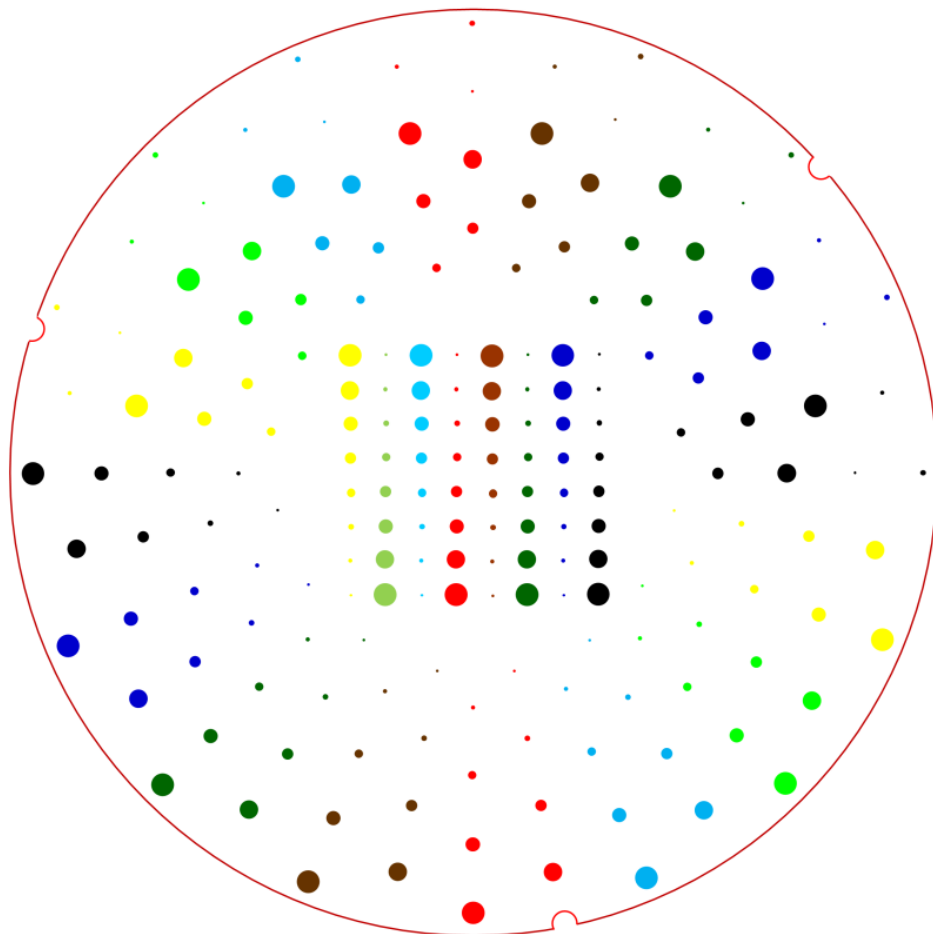
Figure 6.1   Schematic structure of new phantom.

Table 6.1   Diameter sizes of cylindrical objects in (mm)

Size (mm)	8	6.5	5	4	3	2	1.5	1
Objects	●	●	●	●	●	●	•	·

6.2.2   Material selection

Different polymers and plastic materials can attenuate x-ray beams at different rates. As such, different materials can be used to provide different HU values and hence contrast difference between the object and the background. The materials for inclusion in the CDCT phantom were selected to match attenuation and absorption properties in typical diagnostic examination (Brooks & Di Chiro 1976; Ramaseshan et al. 2008). The selected materials mimic attenuation characteristics of soft tissues, bone, fat and lung. The HU values of materials were suggested to be -1000, -100, -50, +25 , +50, +100, +400 and +1000 HU. The actual HU values of the materials used in the CDCT phantom are illustrated in Table 6.1.

The CDCT phantom's body is plastic water, manufactured by CNMC Company (www.cnmcco.com; USA), with a product code of PW-4010. Plastic water has attenuation characteristics similar to water (Hill, Kuncic & Baldock 2010), however also has mechanical strength and resilience (International Commission on Radiation Units and Measurements (ICRU) 1989; Ramaseshan et al. 2008; Suess, Kalender & Coman 1999).

Different materials of different HU values were used to represent different human tissues. Low density polyethylene (LDPE), acrylic, delrin and Teflon have -53.3, 129.6, 306.3 and 801.5 HU respectively. Other materials that with -47.9, 26.8 and 49.0 HU were prepared by the specialised company, QRM (Germany, Moehrendorf, http://www.qrm.de/).

Table 6.2   HU phantom materials

No	Symbol	Suggested HU	Tissue equivalent	Suggested materials		Used materials	
				Name	HU	Name	HU
0	Phantom body	0	Water	Plastic water (PW) DT *	0	PW, 4010 *	62.4
1	(yellow)	-1000	Air −1000	Air	-1000	Air	-907.3
2	(green)	-100	Fat	LDPE low density polyethylene C_2H_4 *	(-84 to -107)	LDPE *	-53.3
3	(blue)	-50		Polystyrene or polythene	-40 to -80		-47.9
4	(red)	+25	Soft tissue	Compound of (polyurethane + Teflon)			26.8
5	(brown)	+50	Soft tissue	Compound of (polyurethane ++ Teflon)			49.0
6	(dark green)	+100	Contrast +130	Acrylic ($C_5H_8O_2$) 120 *	+110 to +145	Acrylic *	129.6
7	(blue)	+400	Trabecular bone +300	Polyoxymethylene (Delrin) *	+320 to +430	Delrin *	306.3
8	(black)	+1000	Cortical bone ↑+600	Polytetrafluoroethylene (Teflon) *	+950 to +1050	Teflon *	801.5

* These items are commercial in confidence

The proposed phantom design, with suggested specifications, has been manufactured (Figure 6.2). Figure 6.3 shows CT images of the phantom. The distribution of object sizes and contrasts are on two different location levels; the colour-shaded orbits in Figure 6.4 demonstrate the two different locations. The numbers, inside the phantom's body, represent the object sizes (Figure 6.4). The numbers, located outside the phantom's body, represent the different contrast objects as explained in Table 6.2.
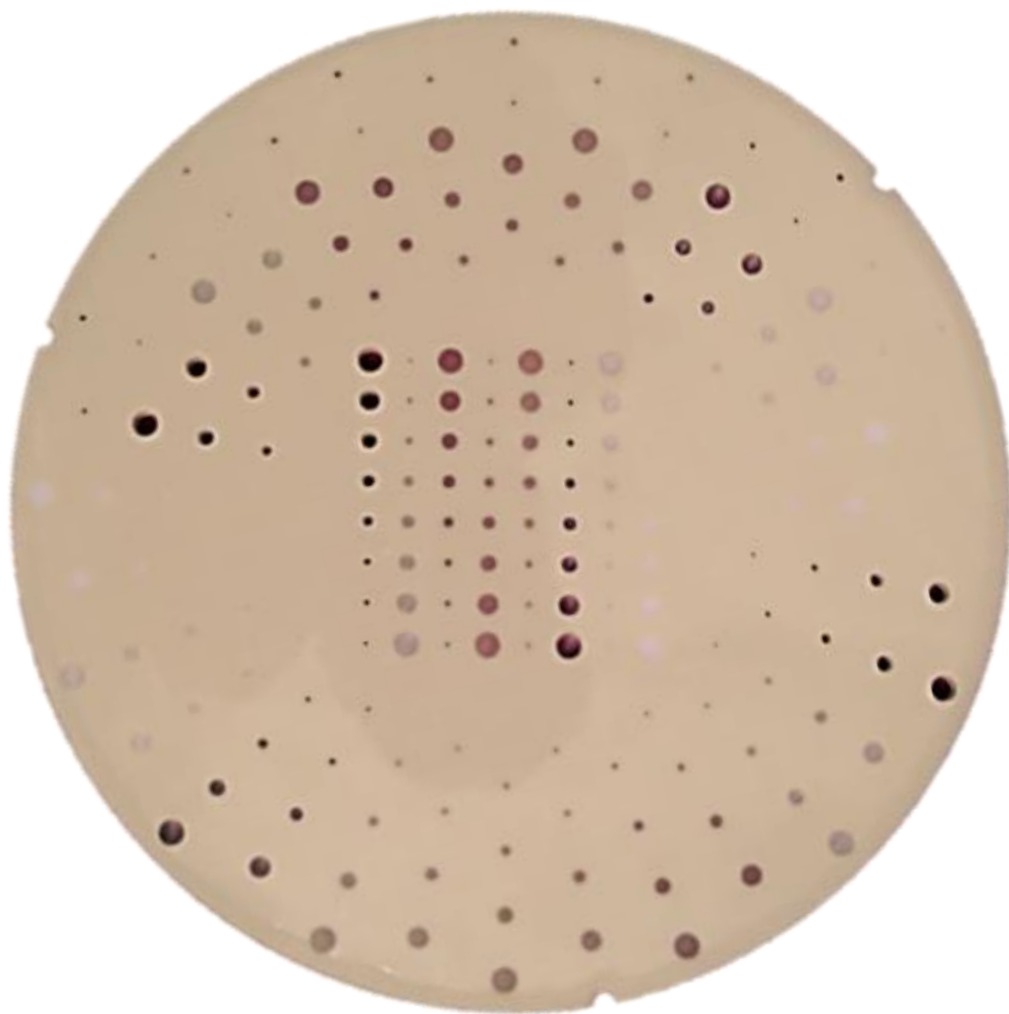
Figure 6.2   A photograph of the new CDCT phantom.
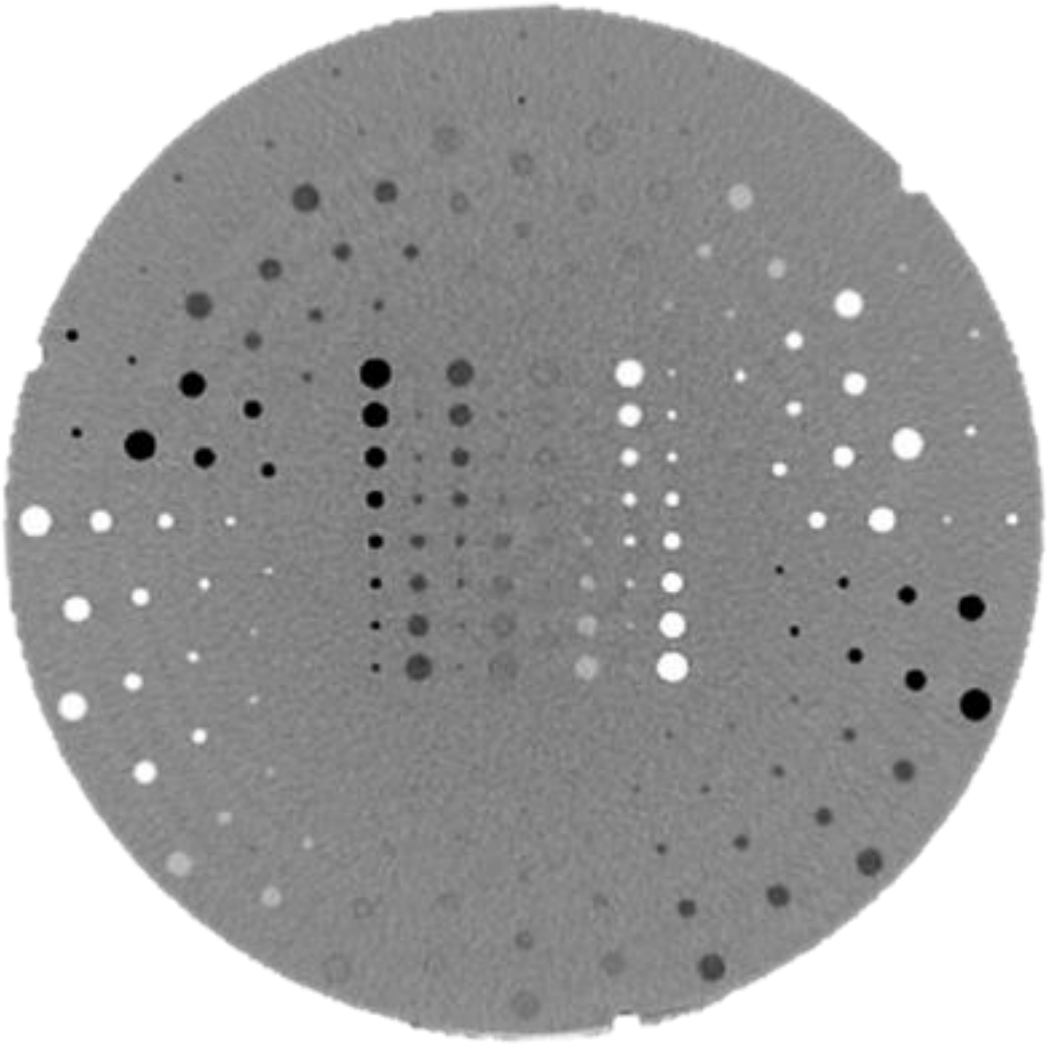
Figure 6.3   A CT image of CDCT phantom.
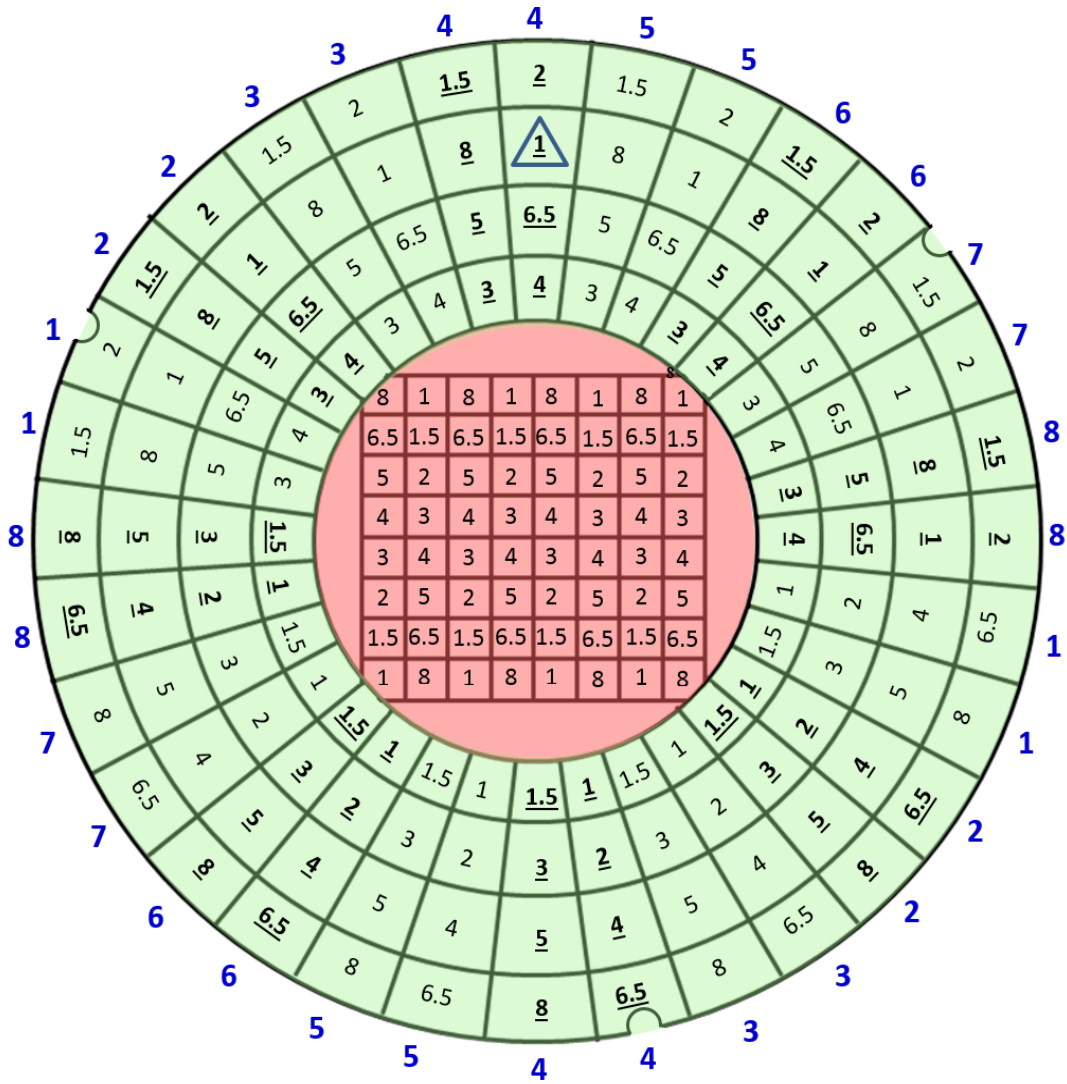
Figure 6.4   Numbers located inside the phantom design represent object sizes. Numbers located outside the phantom design represent the different contrast objects as explained in Table 6.1. The objects of different size and contrast are situated at two different locations; one set of objects are in the central square and two sets of objects are in the orbital area of the phantom.

6.3 Test consistency across CT platforms: (manufacture + kVp) of new contrast-detail phantom

The developed CDCT phantom was evaluated and tested to assess the phantom's conformity with the aimed specifications. The phantom was scanned using three different CT scanners and at two different kVp settings, 120 and 140, with a high mAs value of 200 and a slice thickness of 5 mm. High mAs settings and thick slices allow high x-ray photon numbers and hence improved the signal-to-noise ratio (SNR) and CNR in the images (Uffmann & Schaefer-Prokop 2009; Verdun et al. 2002; von Falck, Galanski & Shin 2010). With such settings, more accurate measurements of HU values will also be obtained. The largest object of each material type within the CDCT phantom, those of 8 mm diameter, were selected for the measurement of the HU values. HU values of the largest object were measured at three different locations of each object. The outer location included two objects of the same size and materials: the more peripheral object called outer and the other called middle. HU values of each object from each CT scanner and at each kVp setting were averaged. Detail are provided in Table 6.3.

Table 6.3 Evaluation of HU values of the objects and phantom consistency assessments

		8	7	6	5	4	3	2	1	
	Planed HU	1000	400	100	50	25	-50	-10	-1000	0.00
	Tissues	Cortical bone	Trabecular bone	Contrast				Fat	Lung	BG
Object size is 8 mm	Materials	Teflon	Delrin	Acrylic				LDPE	Air	Plastic water
16-MDCT-120kV-200mAs-5st	outer	745.01	282.19	121.90	51.24	37.94	-30.73	-25.82	-785.33	78.54
	middle	697.21	257.01	119.39	47.29	28.00	-39.04	-39.44	-811.73	47.18
	inner	560.73	220.23	37.82	-2.02	-41.3	-71.38	-88.27	-792.04	18.91
64-MDCT-120kV-200mAs-5st	outer	861.23	324.69	129.32	57.12	34.40	-36.32	-38.57	-930.08	75.59
	middle	859.31	321.01	134.38	56.95	36.20	-38.57	-40.38	-931.02	69.74
	inner	855.44	323.45	130.15	61.40	41.73	-43.93	-41.02	-936.35	69.35
64-MDCT-140kV-200mAs-5st	outer	868.39	326.63	130.84	53.88	35.13	-40.17	-41.28	-902.45	62.62
	middle	844.02	326.22	138.41	55.18	31.62	-39.15	-45.06	-918.73	58.94
	inner	834.86	330.63	133.75	47.75	36.92	-42.30	-44.31	-918.29	56.85
80-MDCT-140kV-200mAs-5st	outer	889.79	338.73	153.79	64.50	39.10	-47.29	-63.89	-960.39	80.71
	middle	854.41	323.58	141.66	49.85	20.75	-55.58	-65.06	-956.75	71.42
	inner	819.64	313.64	142.69	48.33	23.90	-56.23	-78.50	-944.67	64.54
80-MDCT-120kV-200mAs-5st	outer	799.33	309.61	152.33	55.53	28.81	-56.33	-60.20	-948.57	71.90
	middle	785.34	304.67	146.23	45.24	28.44	-63.04	-61.42	-934.12	57.13
	inner	748.14	292.21	132.08	42.21	20.16	-57.91	-66.78	-938.48	52.06
Average HU values		801.52	306.30	129.65	48.96	26.79	-47.86	-53.33	-907.27	62.36

6.4 CTIQF$_{inv}$ calculation

A measure of image quality using the CDCT phantom was needed. The method of calculation of the CTIQF$_{inv}$ was based on the methods used to calculate IQF$_{inv}$ in radiography (Equation 2.1). A method of measuring image quality in planar radiographic images of the CDRAD phantom (Figure 2.9), that of IQF$_{inv}$, was discussed in Chapter 2. Equation 2.1 explains the method that is used to calculate the IQF$_{inv}$.

In Equation 2.1, the object contrast is used. Contrast of the object in CT is determined by the attenuation characteristic or HU of the object and the surrounding background. Some materials are positive attenuators and others are negative attenuators compared to water,

and as such the objects are assigned positive and negative HU values. The contrast value was calculated by using Equation 6.1.

$$Ci = \frac{HUi - HUbg}{HUbg}$$ *Equation 6.1*

Where Ci is the absolute contrast value of the object, HUi is the HU value of the object of a particular contrast, and HUbg is the HU value of the background.

In the CDRAD phantom, all objects have the same material—air—although contrast is varied by changing the depth of the hole. All objects have differing diameters, however each object has a comparable influence to the IQF_{inv} score (Thijssen et al. 1989; Thijssen et al. 1988). The selection of the lowest visible object of each column determines the IQF_{inv} of that image. A change in the selection of the lowest visible step results in a change of the IQF_{inv} due to a linear increase/decrease of the contrasts and details ($Ci*Di$) (Table 6.4).

In the CDCT phantom, the objects do not have a linear increase/decrease in attenuation, and hence contrast to the phantom's background. As such, using the HU values—or a measure of contrast of the object's HU value to the phantom's background HU value—could not be used to determine the $CTIQF_{inv.}$. An additional issue in determining the method of calculating the $CTIQF_{inv}$ is that some objects have negative HU values and hence would have negative contrast values compared to the phantom's background.

Given these issues, the HU values to measure $Ci*Di$ of the CDCT phantom was not appropriate.

Table 6.4   The values of the CDRAD phantom objects of different contrast level and variable diameter size

Contra															
	0,3	0,4	0,5	0,6	0,8	1	1,3	1,6	2	2,5	3,2	4	5	6,3	8
0,3	0,0	0,1	0,1	0,1	0,2	0,	0,3	0,48	0,6	0,75	0,96	1,2	1,5	1,89	2,4
0,4	0,1	0,1	0,2	0,2	0,3	0,	0,5	0,64	0,8	1	1,28	1,6	2	2,52	3,2
0,5	0,1	0,2	0,2	0,3	0,4	0,	0,6	0,8	1	1,25	1,6	2	2,5	3,15	4
0,6	0,1	0,2	0,3	0,3	0,4	0,	0,7	0,96	1,2	1,5	1,92	2,4	3	3,78	4,8
0,8	0,2	0,3	0,4	0,4	0,6	0,	1,0	1,28	1,6	2	2,56	3,2	4	5,04	6,4
1	0,3	0,4	0,5	0,6	0,8	1	1,3	1,6	2	2,5	3,2	4	5	6,3	8
1,3	0,3	0,5	0,6	0,7	1,0	1,	1,6	2,08	2,6	3,25	4,16	5,2	6,5	8,19	10,
1,6	0,4	0,6	0,8	0,9	1,2	1,	2,0	2,56	3,2	4	5,12	6,4	8	10,0	12,
2	0,6	0,8	1	1,2	1,6	2	2,6	3,2	4	5	6,4	8	10	12,6	16
2,5	0,7	1	1,2	1,5	2	2,	3,2	4	5	6,25	8	10	12,	15,7	20
3,2	0,9	1,2	1,6	1,9	2,5	3,	4,1	5,12	6,4	8	10,2	12,	16	20,1	25,
4	1,2	1,6	2	2,4	3,2	4	5,2	6,4	8	10	12,8	16	20	25,2	32
5	1,5	2	2,5	3	4	5	6,5	8	10	12,5	16	20	25	31,5	40
6,3	1,8	2,5	3,1	3,7	5,0	6,	8,1	10,0	12,	15,7	20,1	25,	31,	39,6	50,
8	2,4	3,2	4	4,8	6,4	8	10,	12,8	16	20	25,6	32	40	50,4	64

Column header: Periodic increase in detail diameter (Di). Row header: Periodic increase in contrast level (Ci) of the detail.

The use of HU values of each object—or the contrast value that resulted from the HU values to calculate $CTIQF_{inv}$—need to be modified. The method of calculating the $CTIQF_{inv}$ should be based on the previous method used (Thijssen et al. 1989) to calculate IQF_{inv} such that no negative values of contrast could be used. Contrast in an image is absolute; that is, the object can be compared to the background or vice versa.

The absolute contrast value was calculated by using Equation 6.2.

$$Cia = \frac{HUi - HUbg}{HUbg} \qquad Equation\ 6.2$$

Where Cia is the absolute contrast value of the object, HUi is averaged HU of the object of a particular contrast from the 3 scanners and 2 kVp setting used on each scanner, HUbg is averaged HU of the phantom background from the 3 scanners and 2 kVp setting used on each scanner.

To use a similar approach to that used in determining the planar IQF_{inv}, the contrast or absolute contrast values should have equal weight in the $CTIQF_{inv}$ equation as the object

224

size. A means of achieving this goal was to linearly interpolate the Cia values between 1 and 8, giving them the same range of values as the smallest to largest objects. Equation 6.3 was used to calculate the linear interpolation values of the phantom objects of different contrast levels (Table 6.5).

$$Li = \frac{(Cia - Cla) \times (Lh - Ll)}{(Cha - Cla) + Ll}$$ *Equation 6.3*

Where Li is the linear interpolation value of object I, Cia is the absolute contrast value of object I, Cla is the absolute contrast value of the lowest Ca object, object #5. Lh is the linear interpolation of value of the highest Ca object, object #1. Ll is the linear interpolation of value of the lowest Ca object, object #5. Cha is the absolute contrast value of the highest Ca object, object #1.

Table 6.5   The linear interpolation values of the phantom objects of different contrast levels

Object #	HU (HUi)	Contrast value (Ci)	Absolute contrast value (Cia)	Linear interp.
5	49	-0.2	0.2	1
4	26.8	-0.6	0.6	1.19
6	129.6	1.1	1.1	1.45
3	-47.9	-1.8	1.8	1.82
2	-53.3	-1.9	1.9	1.86
7	306.3	3.9	3.9	2.94
8	801.5	11.9	11.9	7.11
1	-907.3	13.5	13.5	8
HUbg	62.4			

The CTIQF$_{inv}$ can then be calculated based on the method used to calculate IQF$_{inv}$. Equation 6.4 shows the method to obtain an increasing value of image quality as either Li,th or Di,th decrease. The smallest object (Di) in a column of objects of the same type of material (the Li column), that is detected are used to calculate Li,th x Di,th. It is calculated to measure the linear interpolation values of each size of particular contrast object level which are demonstrated in table 6.6.

$$CTIQF_{inv} = \frac{100}{\sum_{i=1}^{8} L_{i,th} * D_{i,th}} \qquad \text{Equation 6.4}$$

Where L$_{i,th}$ is threshold of the linear interpolation contrast values, and D$_{i,th}$ is threshold of details (sizes).

Table 6.6   The linear interpolation values of each size of particular contrast level object

Object # / interpolated value / Diameter (mm)	5	4		6	3	2	7	8	1
	1	1.19		1.45	1.82	1.86	2.94	7.11	8
1	1	1.19		1.45	1.82	1.86	2.94	7.11	8
1.5	1.5	1.78		2.18	2.72	2.79	4.41	10.66	12
2	2	2.37		2.91	3.63	3.72	5.88	14.22	16
3	3	3.56		4.36	5.45	5.58	8.82	21.33	24
4	4	4.75		5.81	7.26	7.44	11.76	28.44	32
5	5	5.93	7.27	9.08	9.31	14.70	35.55	40	
6.5	6.5	7.71		9.45	11.80	12.10	19.11	46.21	52
8	8	9.49		11.63	14.52	14.89	23.53	56.88	64

6.5   Software development

The software for CDCT was written and developed by Artinis to automate the measurement of CTIQF$_{inv}$ values. Equation 6.4 is used to calculate the CTIQF$_{inv}$ values. The CDCT phantom software principles are based on the contrast-detail (CDRAD analyser) software in radiography, previously discussed in Chapter 3. The software uses the Student t-tests with Welch correction (Welch Satterthwaite test) to determine whether or not the signal in an LCD object is equal to the signals from the surrounding background, plus an a priori difference of means (APD). The software measures CTIQF$_{inv}$ values for the two location regions—the inner and outer regions—in the image separately.

6.6 Conclusion

A new CDCT phantom was manufactured and dedicated software was developed and manufactured—according to developed design and suggested specifications—in cooperation with Artinis Medical Systems. The CDCT phantom and dedicated software analyser will be used as a new methodology of CT image evaluation and optimisation, designed to be an effective tool in quality control procedures. The validity and reliability of the new methodology based on the new CDCT phantom will be examined in Chapter 7.

Chapter 7 Validation of the new methodology of contrast-detail detectability performance

7.1 Introduction

The ability to detect small low contrast features in computed tomography (CT) images is one of the primary reasons that CT has become such an integral part of medical practice (Hsieh 2003). It allows subtle low contrast tumours and lesions to be detected in soft tissue that may not be apparent using other diagnostic x-ray imaging methods. Radiation dose is the main concern with CT examinations. There are trade-offs between the image quality and radiation dose, and therefore CT images should be evaluated and optimised. A new evaluation methodology of low contrast-detail (LCD) detectability performance has been developed for this purpose.

Chapter 6 discussed this new evaluation methodology, which was based on a newly designed low contrast-detail CT (CDCT) phantom. Dedicated software has also been developed to objectively assess the image quality and the imaging performance of CT scanners. The result of the previously discussed LCD detectability is a measure of image quality, the CT inverse image quality figure ($CTIQF_{inv}$). This new methodology measures the ability of identifying low contrast features at a low x-ray dose. Image quality optimisation, which is a main principle of radiation dose reduction, is the essential aim of this methodology (Toth 2012).

This chapter aims to examine the validity and reliability of this new evaluation methodology. This validity and reliability was evaluated by determining the LCD detectability performance of CT images of different protocol parameters and from three different multiple detector CT (MDCT) scanners. The chapter includes four study sections.

In the first section, Section 1 of Phase 4, the factors that affect LCD detectability performance of CT images were evaluated based on a prior knowledge. This section also included the material and methodology used to acquire the CT images of the CDCT phantom. In the second section, Section 2 of Phase 4, the factors that affect LCD detectability performance of CT images, as measured by $CTIQF_{inv}$, were evaluated using radiographers' assessments. In the third section of this chapter, Section 3 of Phase 4, the influence factors of LCD detectability performance of CT images, as measured by $CTIQF_{inv}$, were objectively evaluated using the dedicated software. A comparative study was performed in the fourth section, Section 4 of Phase 4, between the results of radiographer assessments and software scoring.

7.2 Prior knowledge and image acquisition methodology

7.2.1 Prior knowledge

The quality measure of LCD detectability performance of each image is the $CTIQF_{inv}$, which is calculated manually using Equation 6.4 in Chapter 6. Thijssen et al. (1989) found that the radiography inverse image quality figure (IQF_{inv}) is directly related to the square root of the entrance dose. Better LCD detectability performance CT images have higher $CTIQF_{inv}$ and hence better image quality. Validation of the $CTIQF_{inv}$ values was based on prior knowledge of CT image quality. CT image quality improves with increased x-ray photons reaching the detectors, assuming all other things remain the same, such as scanned object size and image reconstruction algorithm (Kalender & Khadivi 2011; Mahesh 2009; Seeram 2009). The values of $CTIQF_{inv}$ should increase with increasing CT exposure factors

and slice thicknesses. That is, increasing exposure factors will increase the number of photons that reach the detector, which should then result in an increase $CTIQF_{inv}$ values.

Setting higher mAs values results in a higher amount of photons produced, and therefore of radiation dose that reaches the detectors (Bushberg et al. 2012; Funama et al. 2005; Toth 2012). Higher radiation doses result in higher signals and lower noise. Increasing signals and reducing the noise improve signal-to-noise ratio (SNR) and contrast-to-noise ratio (CNR) (Funama et al. 2005; Toth 2012). As a result of increasing mAs, LCD detectability improves. However, high mAs techniques are not recommended as this increases the radiation dose to patient. The acceptable radiation dose should be determined by clinical requirements, so as to maintain optimum LCD detectability performance (Seibert 2004; von Falck, Galanski & Shin 2010).

As discussed in Chapter 4, the interdependence and relationship between LCD detectability performance and kVp is complex. Lower kVp techniques increase photoelectric interactions or attenuation and consequently subject contrast is improved (Ertl-Wagner et al. 2004; Seibert 2004). As a result, LCD detectability performance is also improved. CNR can also be improved with lower kVp, as the image quality is not reduced by the noise due to the higher CNR and higher attenuations (Godoy et al. 2010; Marin et al. 2010; Schindera et al. 2008).

On the other hand, lower kVp technique reduces the total energy flux if other exposure factors are not adjusted. As a result, image noise increases, which in turn reduces image quality in terms of LCD detectability performance (Ertl-Wagner et al. 2004; Godoy et al. 2010; Huda, Scalzetti & Levin 2000; Seibert 2004). In addition, lower kVp may cause some types of artefacts—particularly beam hardening—which in turn reduces LCD detectability performance (Seibert 2004).

An appropriate kVp level should be selected according to the size of the patient or organ to be scanned (Ertl-Wagner et al. 2004; Kalender & Khadivi 2011). The kVp should be adjusted high enough to reduce image noise but, at the same time, should be low enough to increase contrast resolution to improve LCD detectability performance.

As discussed in Chapter 4, even though thinner slices provide higher spatial resolution, noise increases with thinner image sections when other factors are kept the same. With thinner slices, a lower number of photons is received by the detectors, thus translating to an increase in noise and causing LCD detectability performance to degrade (von Falck, Galanski & Shin 2010). Higher exposure factors, for example mAs, are required with thinner slices to reduce image noise and improve LCD detectability. However, increasing exposure factors will increase radiation to patients (Seibert 2004; von Falck, Galanski & Shin 2010).

7.2.2   Materials and methodology of image acquisition

Phantom model (CDCT phantom)

The CDCT designed by the researcher and developed in cooperation with Artinis Medical Systems (Zetten, Netherlands) was used in this study. The CDCT phantom's diameter is 32 cm and thickness 1.2 cm. It is made of plastic water and includes 192 cylindrical objects of 10 mm length. The objects are of eight different sizes and eight different CT numbers. Three sets of the objects are situated in two different location levels of the phantom. Two sets are in an outer location and one is in an inner location. The full description of the CDCT phantom was given in Chapter 6, section 6.2, and its specifications were illustrated in Table 6.1, and in Figures 6.1 and 6.2.

MDCT scanners

CT images of the CDCT phantom were obtained from three different MDCT scanners. A 16-MDCT system (LightSpeed, GE Healthcare), a 64-MDCT system (LightSpeed VCT, GE Healthcare) and an 80-MDCT system (Aquilion Prime 80, Toshiba, America Medical Systems Inc.) were used in this study. The specifications of the scanners are listed in Table 5.1 in Chapter 5. The systems were regularly serviced and maintained under a maintenance contract which ensured that the scanners' performance was in agreement with manufacturer specifications.

Image acquisition

The CDCT phantom was centred and supported vertically in the CT gantry. All measurements were performed by using two kVp selections, four different mAs and three different slice thicknesses (Table 7.1). Each image series was repeated three times. All other parameters were maintained. The field of view (FOV) was set to 360 mm. The images were reconstructed using soft reconstruction algorithms.

Table 7.1   Protocol parameters of image acquisition

kVp	120 and 140	
mAs	50, 100, 150 and 200	
Slice thicknesses	For 80-MDCT	1, 2, and 5 mm
	For 16- and 64-MDCT	1.25, 2.5 and 5 mm
Reconstruction algorithms	Soft tissue	
FOV	360	

On viewing the resultant images, a deficit was noticed in the phantom. The wrong material had been used for one object. The object was 1 mm diameter in size and at the column of object contrast 4 in Table 6.3, and should have had a Hounsfield Unit (HU) value of 26.79. The small triangle shape in Figure 6.4 indicates wrong material was used for that object size.

7.3 Section 2 of Phase 4: Evaluation of LCD detectability performance of CT images based on radiographers' assessments

In this section the influences of protocol parameters—kVp, mAs and slice thickness—on LCD detectability performance of CT images were evaluated based on radiographers' evaluation results. This section, Section 2 of Phase 4, aims to validate the new methodology of CT image quality evaluation and to examine its efficacy and accuracy. This section also aims to examine the impacts of kVp, mAs and slice thickness on LCD detectability of CT images.

7.3.1 Scoring Methodology

Selected images

Eight CT images of the CDCT phantom—that were acquired from the 64-MDCT scanner (LightSpeed VCT, GE Healthcare)—were selected to be scored by the radiographers. The images were with two tube kVp selections (120 and 140 kVp), two mAs levels (100 and 200) and two slice thicknesses (1.25 and 5 mm).

Image Display

A three megapixel, diagnostic quality colour liquid crystal display monitor (LCDM) (Eizo Radioforce R-31, Japan) was used to display the images to be scored by radiographers from Australian hospitals. A five megapixel LCDM (Dome E5, NDS Surgical Imaging, USA) was used to display the images for the radiographers from the Saudi Arabian hospital. The room light and conditions were maintained as per a reporting room environment.

Image scoring method (radiographers scoring)

The soft copy CT images were scored by the radiographers. Ethical approval for this project was obtained through the RMIT University Human Ethics Committee (Approval number ABSEHAPP 11) (Appendix 8). The images were de-identified as to the exposure factors and slice thicknesses. The radiographers were provided with the images saved on a CD-ROM as DICOM files. The CD-ROM included eight images (details are provided in Table 7.2). Sixty-seven radiographers from different hospitals in Australia and Saudi Arabia were invited to score the images. Each radiographer scored the eight images, and did so independently during their break times during working days. The images were presented in different order to be scored by radiographers (Table 7.2).

The radiographers were provided with scoring instructions and image scoring sheets (Appendices 9 and 10). They were asked to indicate the image objects that they could detect in each corresponding square location of the scoring form. The viewing conditions, including display contrast factors, were adjusted to optimise image appearance. Radiographers were instructed that they could change the image brightness and contrast, and the window level and width, to optimise their personal viewing of the images.

Table 7.2 Image parameters, codes and scoring orders for each radiographer

Image parameters			Image code	Radiographers' code	Image scoring order
kVp	mAs	Slice thickness			
120	100	1.25	A	R1, R9, R17, R25, R33, R41, R49, R57, R66	A, B, C, D, E, F, G, H
120	100	5	B	R2, R10, R18, R26, R34, R42, R50, R58, R67	B, C, D, E, F, G, H, A
120	200	1.25	C	R3, R11, R19, R27, R35, R43, R51, R59	C, D, E, F, G, H, A, B
120	200	5	D	R4, R12, R20, R28, R36, R46, R52, R61	D, E, F, G, H, A, B, C
140	100	1.25	E	R5, R13, R21, R29, R37, R47, R53, R62	E, F, G, H, A, B, C, D
140	100	5	F	R6, R14, R22, R30, R38, R48, R54, R63	F, G, H, A, B, C, D, E
140	200	1.25	G	R7, R15, R23, R31, R39, R49, R55, R64	G, H, A, B, C, D, E, F
140	200	5	H	R8, R16, R24, R32, R40, R50, R56, R65	H, A, B, C, D, E, F, G

Calculation of CTIQF$_{inv}$

The forms were used to record the smallest objects of each contrast group that were viewed by radiographers. CTIQF$_{inv}$ values were then calculated for each image using Equation 6.4, with three values of CTIQF$_{inv}$ calculated for each scored image. The first CTIQF$_{inv}$ value was for the objects of outer location, the second was for those of centre location and the third was for the total locations which are the average value of outer and centre location values. The full description of the CTIQF$_{inv}$ calculation process is given in Chapter 6.

Statistical Analysis

Gaussian distributed was used to test the probability of whether the scores on each variables fall between two real limits (Pallant 2013). The scores of CTIQF$_{inv}$, which is the dependent variable, appear to be normally distributed. A two-way between-groups analysis of variance

(ANOVA) using the Statistical Package for the Social Sciences (SPSS) software was conducted to examine the influence of different CT protocol parameters including kVp, mAs and slice thickness on dependent the scores, which are $CTIQF_{inv}$ values of each image and each of its objects. The impact of object location factor was also examined by conducting the two-way ANOVA test. It is used to determine the main effect of contributions of each protocol factor. The two-way ANOVA test was also used to determine if significant differences exist between kVp groups exposed at the same mAs and slice thickness, between mAs groups at the same kVp and slice thickness and between slice thickness groups at the same kVp and mAs. Student t-tests, at an Alpha value of 0.05 is conducted as a part of the two-way ANOVA calculations to determine if significance differences exist between different groups (Pallant 2013).

7.3.2 Results

The results of radiographers' scoring for images of different parameters are shown in Table 7.3. There were significant differences ($p < 0.001$) between the images of different parameters based on $CTIQF_{inv}$ values. There were also significant differences ($p < 0.001$) in values between outer object locations and centre object regions for each CDCT phantom image.

Table 7.3 CTIQF$_{inv}$ mean values of the images. Each image has three mean readings, two for the two location levels, outer and centre, and one for the total of the image. The mean values were obtained from 67 radiographers

kVp	mAs	Slice thickness	Outer		Centre		Total	
			Mean	SD	Mean	SD	Mean	SD
120	100	1.25	2.075	0.28	2.17	0.3	2.1225	0.29
120	100	5	2.725	0.3	2.62	0.3	2.6725	0.3
120	200	1.25	2.43	0.245	2.49	0.3	2.4600	0.26
120	200	5	3.135	0.26	2.96	0.3	3.0475	0.29
140	100	1.25	2.17	0.27	2.28	0.3	2.2250	0.29
140	100	5	2.945	0.255	2.74	0.3	2.8425	0.29
140	200	1.25	2.665	0.28	2.46	0.3	2.5625	0.31
140	200	5	3.345	0.26	2.94	0.3	3.1425	0.34

The effects of protocol parameters—including kVp, mAs and slice thickness—on total image CTIQF$_{inv}$ values were evaluated. The effects of location levels of image objects on CTIQF$_{inv}$ mean values were also assessed. The reliability and validity of the new evaluation methodology based on radiographers' assessment were then evaluated. The results of these evaluation experiments are discussed in the following sections.

Effects of kVp on CTIQF$_{inv}$

The use of higher kVp generally resulted in better CTIQF$_{inv}$ values for the total image locations at all mAs levels and slice thicknesses (Figure 7.1). There were significant improvements ($p < 0.001$) in CTIQF$_{inv}$ values when the kVp increased from 120 to 140.
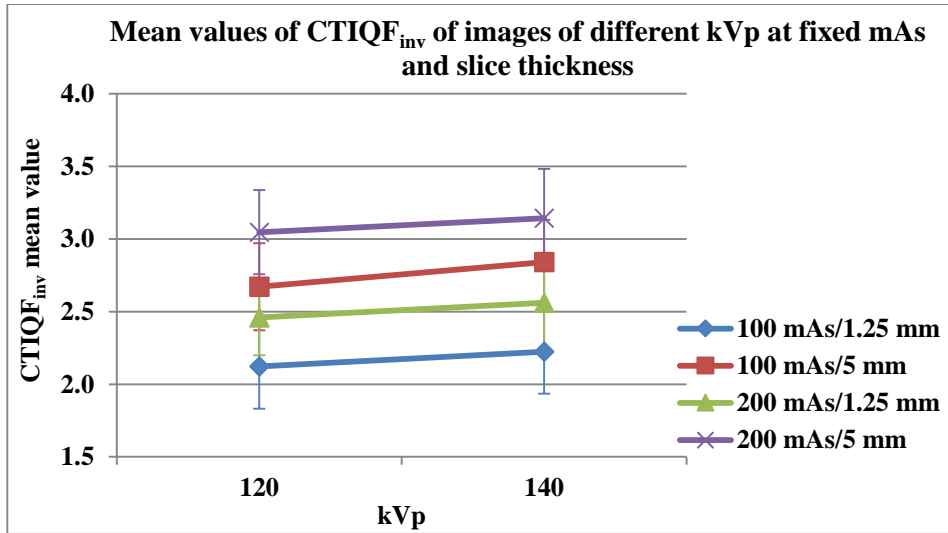
Figure 7.1 Higher kVp resulted in higher CTIQF$_{inv}$ values with different mAs levels and slice thicknesses.

Effects of mAs on CTIQF$_{inv}$ values

The use of higher mAs generally resulted in better CTIQF$_{inv}$ values for the total image locations at all kVp levels and slice thicknesses (Figure 7.2). There were significant improvements ($p < 0.001$) in CTIQF$_{inv}$ values when the mAs increased from 100 to 200.
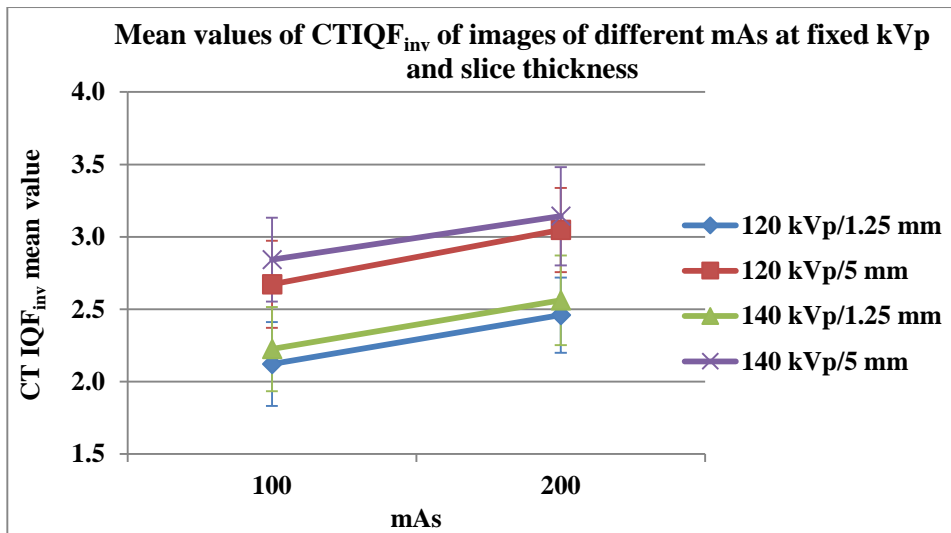
Figure 7.2   Higher mAs resulted in higher CTIQF$_{inv}$ values at different kVp selections with different slice thickness. There were also significant changes between the images when the mAs increased.

Effects of slice thickness on CTIQF$_{inv}$ values

The use of thicker slices generally resulted in better CTIQF$_{inv}$ values for the total image locations at all kVp and mAs levels (Figure 7.3). There were significant improvements ($p < 0.001$) in CTIQF$_{inv}$ values when the slice thickness increased from 1.25 to 5 mm at all kVp selections and mAs levels (Table 7.3).
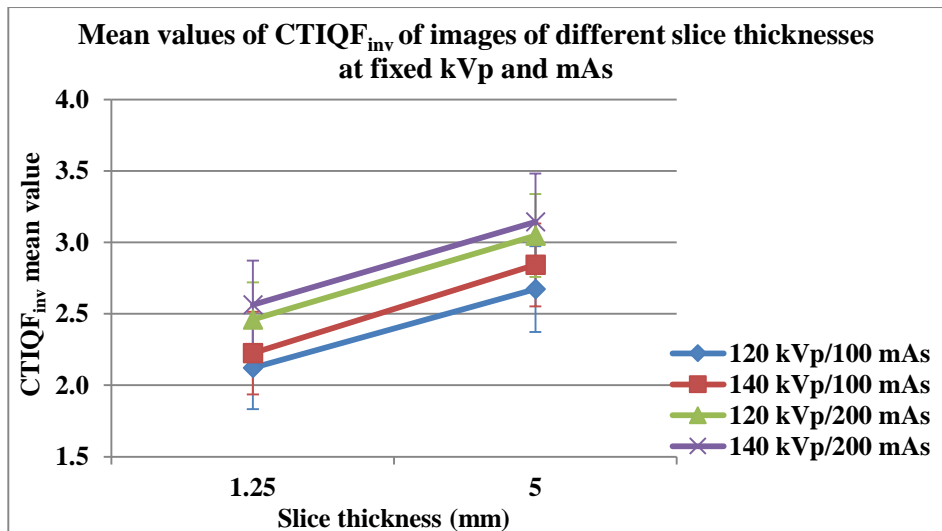
Figure 7.3   Thicker slice thicknesses resulted in higher CTIQF$_{inv}$ values at different kVp selections and mAs levels. There were also significant changes when the mAs increased.

The effects of object location levels on CTIQF$_{inv}$ mean values

CTIQF$_{inv}$ values of outer location objects were higher than centre location objects, particularly at 5 mm slice thickness with 200 mAs and at 5 mm slice thickness images (Figures 7.4 to 7.9). However, the centre location objects had higher CTIQF$_{inv}$ values than those in the outer location, at 1.25 mm slice thickness with 120 kVp and different mAs images (Figures 7.5 and 7.9).

The CTIQF$_{inv}$ values of outer and centre object locations were all the time significant ($p < 0.001$), with the outer object locations being greater than the centre locations.
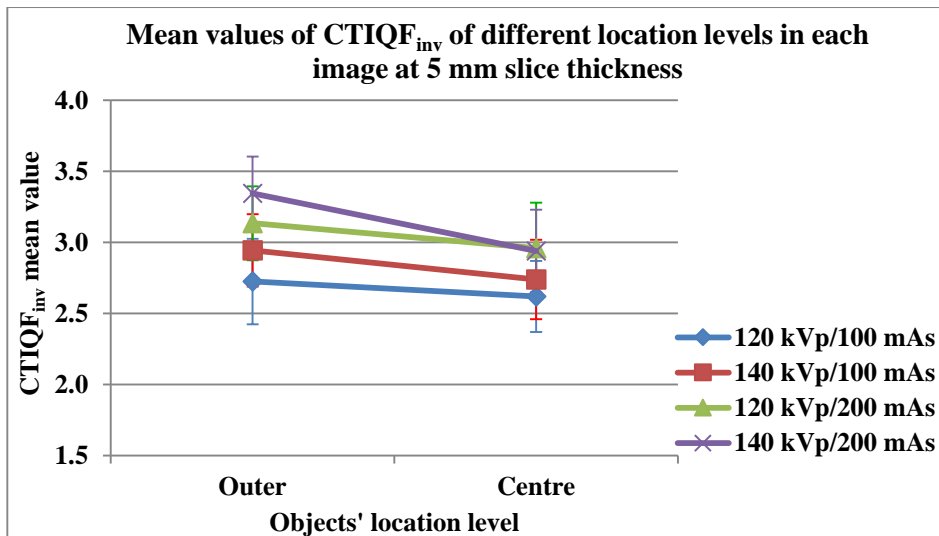
Figure 7.4   At 5 mm slice thicknesses, outer location objects had higher
CTIQF$_{inv}$ values with different kVp and mAs.
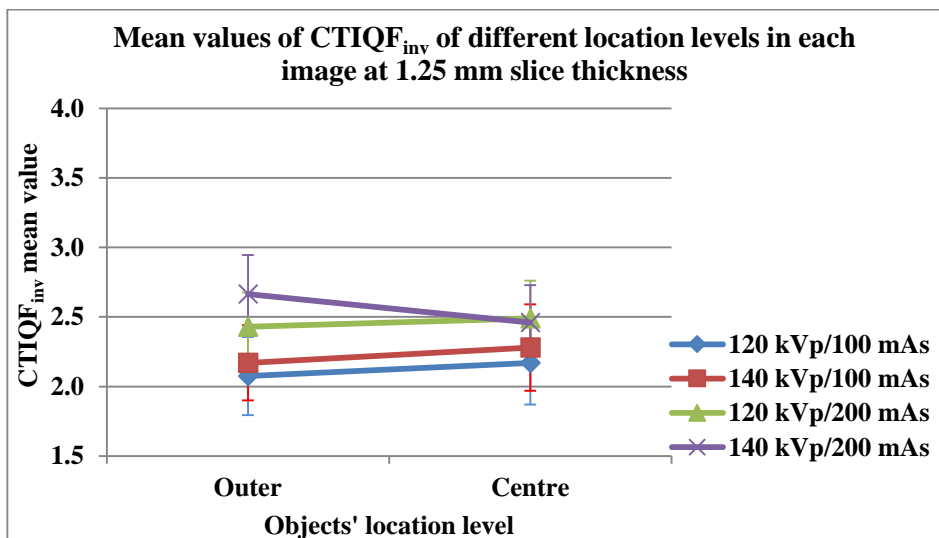
Figure 7.5   At 1.25 mm slice thicknesses, centre location objects had higher
had higher CTIQF$_{inv}$ values than outer location objects. However, at 140 kVp
and 200 mAs, the outer location objects had higher CTIQF$_{inv}$ values than
centrelocation.
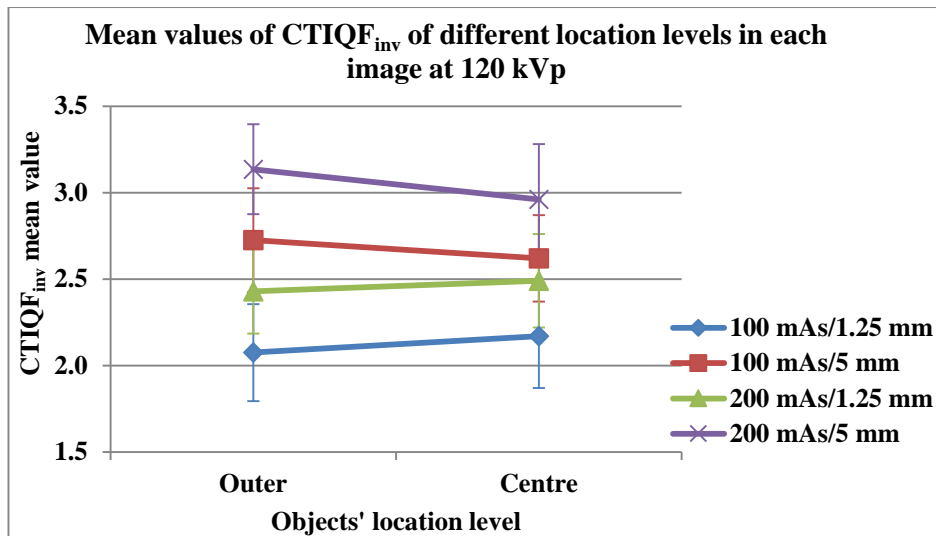
Figure 7.6   At 120 kVp, outer location objects had higher CTIQF$_{inv}$ values than centre location objects with thicker slice thicknesses. (Note the changes between location levels at thinner slice thicknesses.)
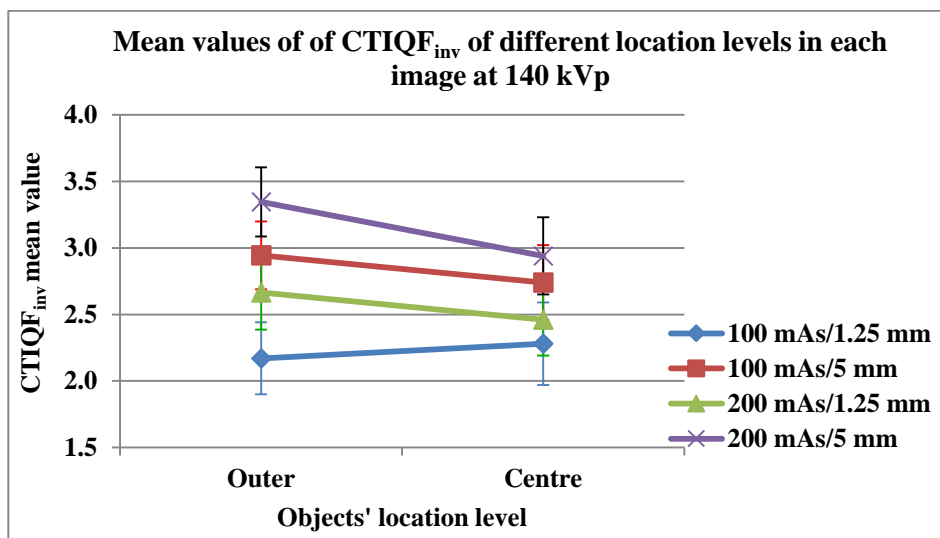
Figure 7.7 Outer location objects had higher CTIQF$_{inv}$ values at the images of 140 kVp. (Note the differences between outer and centre location levels at lower mAs and thinner slice thickness.)
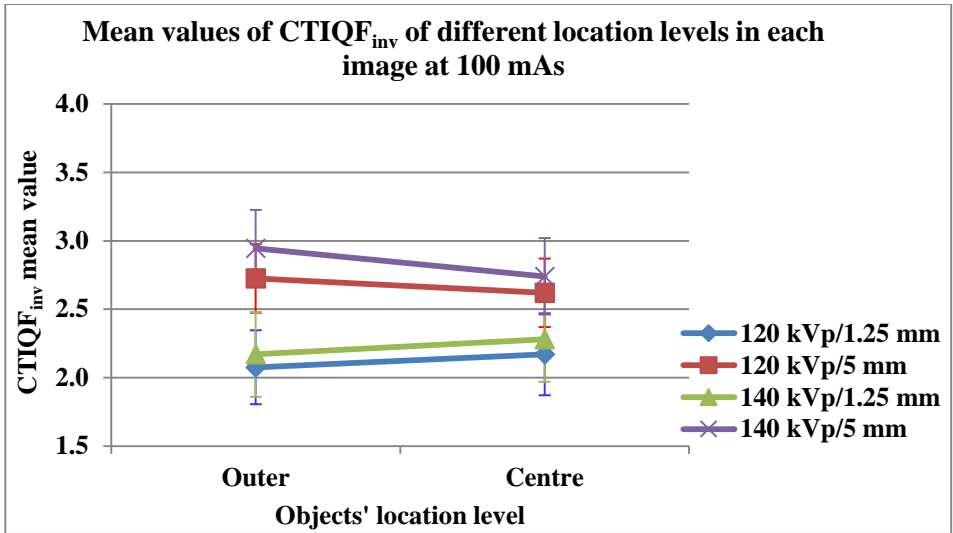
Figure 7.8   At 100 mAs, outer location objects had higher $CTIQF_{inv}$ values than centre location objects with thicker slice thicknesses and different kVp levels. However, at thinner slice thicknesses, the centre location level had higher $CTIQF_{inv}$ than outer location objects.
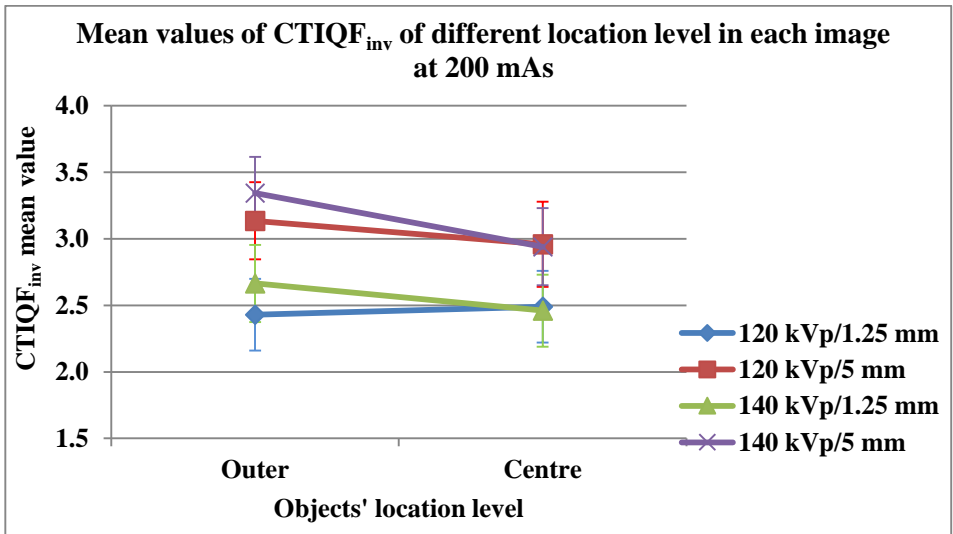
Figure 7.9   At 200 mAs, outer location objects had higher $CTIQF_{inv}$ values. (Note the changes between location levels at thinner slice thickness with lower kVp.)

7.3.3 Discussion

As previously mentioned, incorrect material was inserted in the phantom. The object size of this material was ignored in the calculation process of $CTIQF_{inv}$ values, particularly when the radiographer did not detect the larger size.

The effects of protocol parameters were evaluated, including kVp, mAs and slice thickness, in addition to the effects of location levels of image objects on $CTIQF_{inv}$ values. The effects of kVp, mAs and slice thickness on image quality, in terms of $CTIQF_{inv}$ values, were as expected. When these parameters were increased, $CTIQF_{inv}$ values increased. These results are supported by the literature (Fishman 2007; Hayton et al. 2010; Toth 2012), and by the results of Chapter 5. The radiation dose linearly increases with increasing mAs (Funama et al. 2005; Toth 2012), and higher radiation dose results in lower noise and hence better image quality. Even though the radiation dose is not linear with kVp, increasing the kVp increases the number of photons produced (when other exposure factors are fixed) and the number of photons reaching the detectors (given their higher average energy). As a result, image noise reduces. Consequently, image quality is enhanced with higher kVp and mAs (Alsleem & Davidson 2013; Seibert 2004). Thicker slice thickness reduces image noise as more photons reach the detectors and hence are included in the image. On the other hand, if the radiation is not increased, the noise increases with thinner slices (Alsleem & Davidson 2013; Kalender & Khadivi 2011; Seibert 2004; von Falck, Galanski & Shin 2010). With thinner slices, the quantum noise is pronounced in the MDCT images (Wedegartner et al. 2004). However, thinner slice thicknesses provide high-resolution isotropic image data sets and hence through-plane partial-volume averaging effects are reduced (Kalender & Khadivi 2011; Rubin 2003). Object detectability improves with increased photon numbers,

from higher kVp and mAs and from thicker thickness image slices (von Falck, Galanski & Shin 2010).

The effects of location levels of phantom images were mostly as expected, particularly at thicker slice thicknesses and higher kVp images. The peripheral object location of the phantom image had higher $CTIQF_{inv}$ values than the central object location. In other words, the detectability performance of outer object areas of phantom images is much higher than inner regions. According to Kalender and Khadivi (2011), the values of measured noise at the centre area of the 32 cm water phantom is almost double the noise values at peripheral areas, whether at the top or bottom, left or right. While the noise at the centre was 68.5 HU, the noise was only 34.2-35.3 HU at peripheral areas (Kalender & Khadivi 2011). It is well known that the higher noise, the lower detectability performance of LCD. In addition, the absorbed radiation dose at peripheral objects within the scanned region is higher than at the central object locations by a factor of two. Outer objects received 2/3 CT dose index in the area between +50 and −50 mm from the centre ($CTDI_{100}$), and the central objects received 1/3 $CTDI_{100}$ (Kalender & Khadivi 2011; Mahesh 2009; Seeram 2009) (for details see Equation 4.1). Because the outer object regions absorb more photons, the noise is lower at these areas than the central areas. Consequently, the details in the outer areas were better visualised than inner areas. In other word, the detectability performance of radiographers was better in outer locations of images.

Unexpectedly, the values of $CTIQF_{inv}$ in the centre object location for some images—particularly at thinner slice thicknesses with lower kVp and mAs—were higher than the outer object location, based on radiographers' scoring results. This can be explained by the fact that MDCT thin slice images of low contrast—such as liver lesions—do not require an increase in radiation dose because resultant noise in thinner sections is compensated by

improved lesion contrast (Wedegartner et al. 2004). In addition, radiographers might be confused between the real objects and the artefacts results from the higher noise conveyed with thinner thickness and lower kVp and mAs. The radiographers may have guessed at seeing noise as real detectable objects. Thilander-Klang et al. (2010) found that the observers required at least 50% of dose differences between images, in terms of mAs, to always recognise the differences between their LCD detectability performance.

The study of Thilander-Klang et al. (2010) also found that most observers rated the images of same mAs as unequal detectability performance. Some observers were not able to recognise the detectability performance differences between the different dose images, but also rated the images in wrong order, particularly at 25% dose difference or less (Thilander-Klang et al. 2010). The expert observers scored the images of 100 kVp as better detectability performance than 120 kVp, which can be explained by the fact that the maximum intrinsic contrast was at 100 kVp (Hernandez-Giron et al. 2011). This suggested that the errors of observers were not only caused by incorrect decisions, but also by their inability to distinguish small noise differences. Indeed, several studies suggested that subjective assessment of LCD detectability performance is unreliable due to the inter- and intra-observer differences and their rating errors (Hernandez-Giron et al. 2011; Tapiovaara & Sandborg 2004; Thilander-Klang et al. 2010).

7.3.4 Conclusion

The new methodology of LCD detectability performance is a valid and feasible tool to evaluate and optimise CT images based on the results of radiographers' assessment. The radiographers were sensitive to image quality changes, as measured by $CTIQF_{inv}$ mean

values, resulting from changing mAs, kVp and slice thickness. The radiographers were also sensitive to different object locations of phantom images, particularly at high exposure factors and thicker slice sections. This implies that the new methodology of LCD detectability performance, based on the new designed phantom, had high validity to measure image quality of CT and it would be an appropriate and effective tool to optimise the quality of CT images and to compare between different scanners. However, this approach is limited by human subjectivity, and by the fact that it is time consuming and there is limited data to be assessed. It is suggested that an automated approach for this methodology should be developed—to optimise its reliability and its appropriateness—and be implemented as a routine quality assurance procedure. The developed automated approach of new evaluation methodology will be evaluated in the next section.

7.4 Section 3 of Phase 4: Evaluation of LCD detectability performance of CT images based on software results

7.4.1 Introduction

In the previous section, Section 2 of Phase 4, the new methodology of LCD detectability performance as a tool of image quality evaluation and optimisation was subjectively evaluated based on radiographers' scoring. The results showed proof of concept of the new methodology of LCD detectability performance. The influences of protocol parameters—including kVp, mAs and slice thickness—on image quality in terms of $CTIQF_{inv}$ values were as expected, based on radiographers' scoring results. The radiographers' results showed $CTIQF_{inv}$ increases with increasing the levels of these protocol parameters. The results were consistent with the CT phantom's object location levels: the outer object

locations had better detectability than the centre areas, particularly in thicker images. Even though the new methodology showed reasonable validity as a tool of image quality assessment and optimisation, it suffered from subjectivity and was time consuming. In addition, this approach based on human observers does not help to assess large numbers of images. The reliability and practicality of the new method can be obtained by utilising an automated approach.

A recent study by Leng et al. (2013) concluded that the detectability performance of observer model approaches, based on automated software, were highly correlated with human observer performance. Park, S et al. (2005) found that objective approaches based on automated software had better and more efficient assessment of detectability performance than human observers, indicating that the automated software is the choice for image optimisation. This study also suggested that automated approaches of LCD detectability performance can be used to meaningfully optimise scan protocols and minimise radiation dose levels in the tasks of LCD detection and localisation (Leng et al. 2013). Hernandez-Giron et al. (2011) found that the software proved more sensitive than expert observers in detectability performance.

This section, Section 3 of Phase 4, aims to examine and validate the developed automated approach of the new LCD detectability performance method in terms of $CTIQF_{inv}$ values. This section also aims to assess the effects on LCD detectability performance of different object location levels in the image. This section also aims to compare three different MDCT scanners based on software scoring results.

7.4.2 Scoring methodology

Selected CDCT phantom images

All CT images of the CDCT phantom that were obtained from three different MDCT scanners were used in this study. Each image series included three images of same exposure factors and slice thickness, obtained from the same scanner. Table 7.1 shows the protocol parameters for each image series.

Image scoring

The images were scored by software to objectively calculate $CTIQF_{inv}$ values. The software requires accurate phantom location within the image, and the current version of the software cannot accurately detect the correct orientation and location of the phantom in the image. For this phase of the project, phantom location and orientation in the images was manually adjusted. The software uses a Welch Satterthwaite test (Student t-tests with Welch correction) with an added a priori difference of means (APD) to determine if a significant difference exists between the HU of the object and background. If the difference is statistically significant, the object is detected, otherwise it is ignored. When an object is not detected, the next larger object becomes the threshold object: the $D_{i,th}$ object in Equation 6.4. Each image was scored three times by the software.

Statistical Analysis

Gaussian distributed was used to test the probability of whether the scores on each variables fall between two real limits (Pallant 2013). The scores of $CTIQF_{inv}$, appear to be normally distributed. A two-way ANOVA using the SPSS software was conducted to examine the influence of different CT protocol parameters including kVp, mAs and slice thickness on $CTIQF_{inv}$ values of each image. The impact of CT scanner type was also examined by conducting the two-way ANOVA test. It is used to determine the main effect of contributions of each protocol factor. The two-way ANOVA test was also used to determine if significant differences exist between kVp groups exposed at the same mAs and slice thickness, between mAs groups at the same kVp and slice thickness, between slice thickness groups at the same kVp and mAs and between different CT scanners at same exposure parameters. The Student t-tests, at an Alpha value of 0.05 is conducted as a part of the two-way ANOVA calculations to determine if significance differences exist between different groups (Pallant 2013).

7.4.3   Results

The $CTIQF_{inv}$ values of the images of different exposure parameters and slice thicknesses, and from different MDCT scanners, are shown in Tables 7.4 and 7.5. Table 7.4 demonstrates $CTIQF_{inv}$ values for the outer object location level of the images, while Table 7.5 shows the $CTIQF_{inv}$ for the centre object location level. The $CTIQF_{inv}$ values for centre object location results, presented in Table 7.5, show significant inconsistency between expected and recorded results. Therefore, the $CTIQF_{inv}$ values of the image total location, which is the average $CTIQF_{inv}$ values of the outer and centre location levels, were not

recorded. The focus of this section, Section 3 of Phase 4, is only on the scoring results of

the outer location level of each image.

Table 7.4 Software scoring results of CDCT phantom images from different

MDCT scanners, $CTIQF_{inv}$ values of outer location, where each value is the

average of three images of same protocol parameters

kVp	mAs	16-MDCT			64-MDCT			80-MDCT		
		Slice thickness (mm)	Mean	SD	Slice thickness (mm)	Mean	SD	Slice thickness (mm)	Mean	SD
120	50	1.25	1.0400	< 0.001	1.25	1.0000	0.0173	1	1.1100	< 0.001
120	100	1.25	1.7800	< 0.001	1.25	1.5167	0.3060	1	1.2700	< 0.001
120	150	1.25	1.6700	< 0.001	1.25	1.8200	< 0.001	1	1.6867	0.0777
120	200	1.25	1.9200	< 0.001	1.25	1.8100	< 0.001	1	1.3700	< 0.001
120	50	2.5	1.4300	< 0.001	2.5	1.6100	< 0.001	2	1.0133	0.0751
120	100	2.5	1.9167	0.0808	2.5	1.7133	0.3926	2	1.7900	< 0.001
120	150	2.5	1.8600	< 0.001	2.5	1.4967	0.1848	2	1.7900	< 0.001
120	200	2.5	2.1400	< 0.001	2.5	1.3900	< 0.001	2	2.1200	< 0.001
120	50	5	1.8100	< 0.001	5	1.7000	< 0.001	4	1.6200	< 0.001
120	100	5	1.9170	0.0810	5	2.1300	0.4493	4	1.9300	< 0.001
120	150	5	2.0900	< 0.001	5	2.2600	< 0.001	4	2.0900	< 0.001
120	200	5	2.0300	< 0.001	5	2.23	0.0851	4	2.1900	< 0.001
140	50	1.25	1.0800	< 0.001	1.25	1.6333	0.0289	1	.7900	< 0.001
140	100	1.25	1.5300	< 0.001	1.25	2.0000	< 0.001	1	1.4600	< 0.001
140	150	1.25	2.2000	< 0.001	1.25	1.8300	< 0.001	1	1.6400	< 0.001
140	200	1.25	2.1900	< 0.001	1.25	2.2200	< 0.001	1	1.7200	< 0.001
140	50	2.5	1.8000	< 0.001	2.5	1.7500	< 0.001	2	1.4300	< 0.001
140	100	2.5	2.0200	< 0.001	2.5	2.0500	< 0.001	2	1.8300	< 0.001
140	150	2.5	1.7500	< 0.001	2.5	2.2600	0.0173	2	1.8900	< 0.001
140	200	2.5	2.0600	< 0.001	2.5	2.7100	< 0.001	2	2.2800	< 0.001
140	50	5	1.5600	< 0.001	5	2.2000	< 0.001	4	1.5800	< 0.001
140	100	5	1.9500	< 0.001	5	2.3	< 0.001	4	2.0200	< 0.001
140	150	5	2.3100	< 0.001	5	2.4100	< 0.001	4	2.1400	< 0.001
140	200	5	2.4000	< 0.001	5	2.3600	< 0.001	4	2.2100	< 0.001

Table 7.5 Software scoring results of CDCT phantom images of different MDCT scanners, CTIQF$_{inv}$ values of centre location.

kVp	mAs	16-MDCT			64-MDCT			80-MDCT		
		Slice thickness (mm)	Mean	SD	Slice thickness (mm)	Mean	SD	Slice thickness (mm)	Mean	SD
120	50	1.25	3.9900	< 0.001	1.25	1.1333	0.02887	1	0.9900	< 0.001
120	50	2.5	0.970	< 0.001	2.5	1.1200	< 0.001	2	0.8933	0.05774
120	50	5	1.3500	< 0.001	5	0.7000	< 0.001	4	0.7000	< 0.001
120	100	1.25	0.6800	< 0.001	1.25	1.1600	< 0.001	1	0.6600	< 0.001
120	100	2.5	1.1167	0.05774	2.5	1.1133	0.08083	2	0.6800	< 0.001
120	100	5	1.1167	0.05774	5	1.1100	0.09539	4	0.6800	< 0.001
120	150	1.25	0.6700	< 0.001	1.25	1.1100	< 0.001	1	0.7567	0.17010
120	150	2.5	1.0900	< 0.001	2.5	0.7000	< 0.001	2	1.0500	< 0.001
120	150	5	1.1200	< 0.001	5	1.0300	< 0.001	4	0.8700	< 0.001
120	200	1.25	0.6300	< 0.001	1.25	0.7000	< 0.001	1	0.6300	< 0.001
120	200	2.5	1.1600	< 0.001	2.5	1.2000	< 0.001	2	1.1400	< 0.001
120	200	5	0.6900	< 0.001	5	1.0033	0.26652	4	1.1200	< 0.001
140	50	1.25	0.9200	< 0.001	1.25	0.8467	0.30600	1	0.6700	< 0.001
140	50	2.5	1.0100	< 0.001	2.5	1.1100	< 0.001	2	1.1500	< 0.001
140	50	5	1.1700	< 0.001	5	0.7100	< 0.001	4	1.1000	< 0.001
140	100	1.25	0.6800	< 0.001	1.25	0.7400	< 0.001	1	1.2200	< 0.001
140	100	2.5	0.9700	< 0.001	2.5	0.7100	< 0.001	2	0.7200	< 0.001
140	100	5	1.1200	< 0.001	5	0.6700	< 0.001	4	0.8500	< 0.001
140	150	1.25	1.0700	< 0.001	1.25	1.1100	< 0.001	1	0.6200	< 0.001
140	150	2.5	1.0700	< 0.001	2.5	0.7433	0.17898	2	0.9500	< 0.001
140	150	5	1.0600	< 0.001	5	1.1000	< 0.001	4	0.9700	< 0.001
140	200	1.25	1.1800	< 0.001	1.25	0.6600	< 0.001	1	0.6300	< 0.001
140	200	2.5	0.8800	< 0.001	2.5	0.6400	< 0.001	2	0.7000	< 0.001
140	200	5	0.9800	< 0.001	5	1.0500	< 0.001	4	0.6200	< 0.001

Effects of kVp on CTIQF$_{inv}$

The use of higher kVp generally resulted in better CTIQF$_{inv}$ values from all CT scanners (Figures 7.10 to 7.12). In some cases there was a decline in CTIQF$_{inv}$ values when the kVp increased, particularly with thinner slice thicknesses. There were generally significant improvements in CTIQF$_{inv}$ values when the kVp increased from 120 to 140 in all CT scanners (Table 7.6).
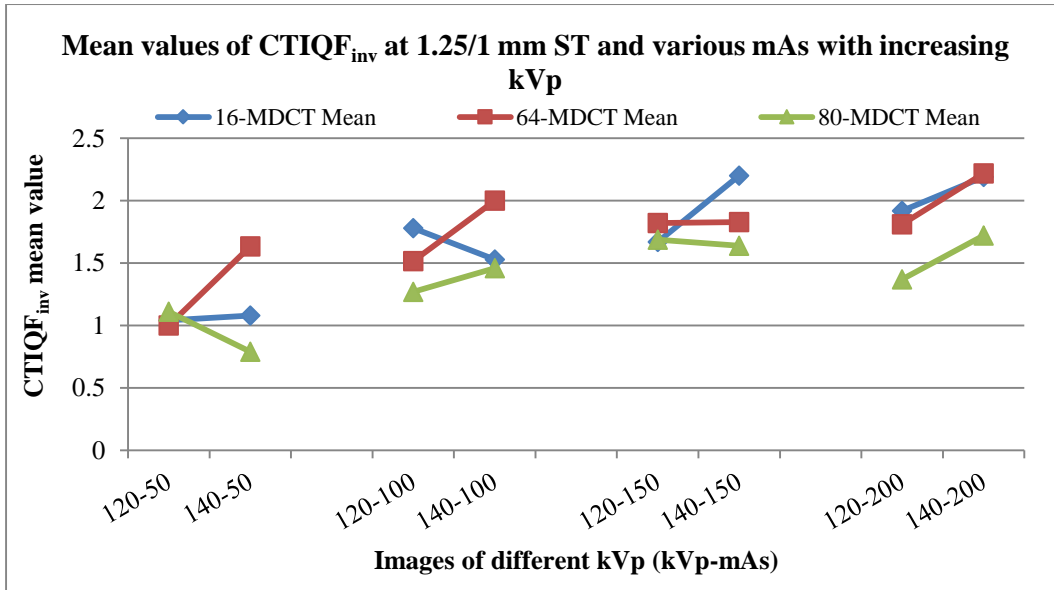
Figure 7.10 Higher kVp resulted in higher CTIQF$_{inv}$ values with 1.25/1 mm slice thickness images for all CT scanners. (Note the change in CTIQF$_{inv}$ values at 50 and 150 mAs in 80-MDCT and 16-MDCT, the change in CTIQF$_{inv}$ values at 100 mAs in 16-MDCT and the change in CTIQF$_{inv}$ values at 150 mAs in 64-MDCT and 80-MDCT.)
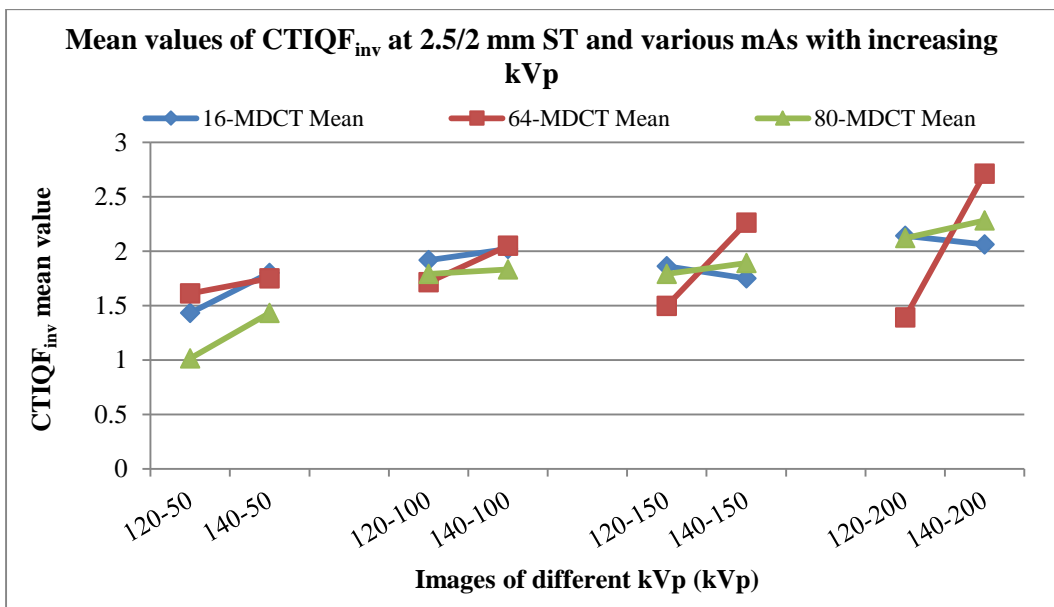
Figure 7.11 Higher kVp resulted in higher CTIQF$_{inv}$ values with 2.5/2 mm slice thickness images for all CT scanners. (Note the change in CTIQF$_{inv}$ values at 150 and 200 mAs in 16-MDCT.)

Mean values of CTIQF$_{inv}$ at 5/4 mm ST and various mAs with increasing kVp
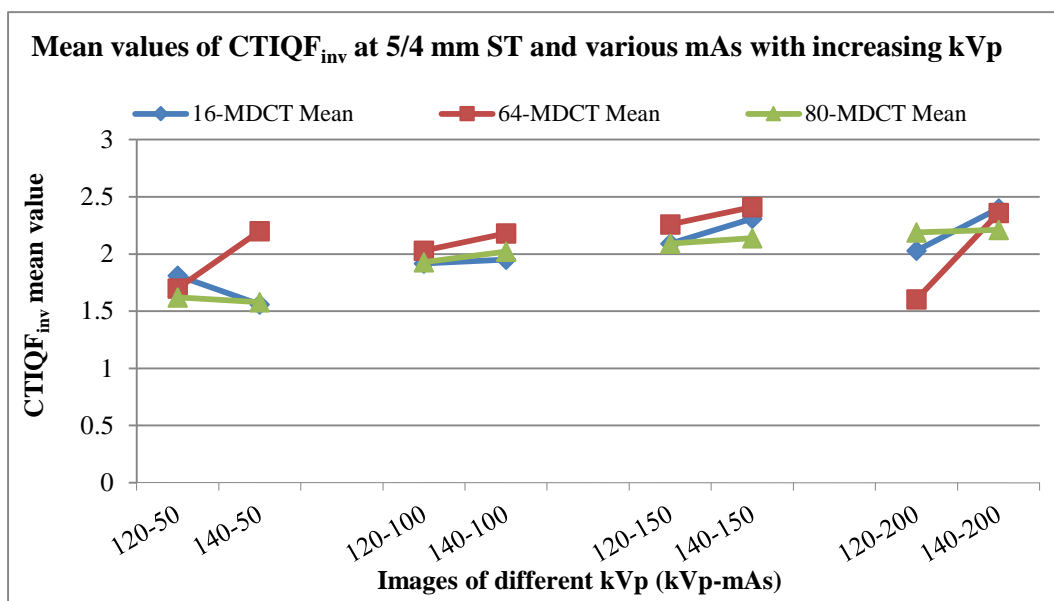
Figure 7.12   The higher kVp is, the higher the CTIQF$_{inv}$ values, with 5 mm slice thickness images for all CT scanners. (Note the change in CTIQF$_{inv}$ values 50 mAs in 16-MDCT and 80-MDCT.)

Table 7.6   The differences (*p* values, Student t-tests) between the images of same mAs and slice thicknesses with changing kVp in each CT scanners

(J) Image code (kVp-mAs-slice thickness)	(I) Image code (kVp-mAs-slice thickness)	Sig. (*p* values, Student t-tests)		
		16-MDCT	64-MDCT	80-MDCT
120-50-1.25/1	140-50-1.25/1	< 0.001	< 0.001	< 0.001
120-50-2.5/2	140-50-2.5/2	< 0.001	< 0.001	< 0.001
120-50-5/4	140-50-5/4	< 0.001	< 0.001	0.614
120-100-1.25/1	140-100-1.25/1	< 0.001	0.320	< 0.001
120-100-2.5/2	140-100-2.5/2	0.034	0.667	< 0.001
120-100-5/4	140-100-5/4	0.946	0.104	< 0.001
120-150-1.25/1	140-150-1.25/1	< 0.001	1.000	0.499
120-150-2.5/2	140-150-2.5/2	0.004	< 0.001	0.021
120-150-5/4	140-150-5/4	< 0.001	0.233	0.430
120-200-1.25/1	140-200-1.25/1	< 0.001	< 0.001	< 0.001
120-200-2.5/2	140-200-2.5/2	< 0.001	< 0.001	< 0.001
120-200-5/4	140-200-5/4	< 0.001	< 0.001	0.017

Effects of mAs on CTIQF$_{inv}$ values

The use of higher mAs levels generally resulted in better CTIQF$_{inv}$ values, particularly at thicker slice thicknesses in all CT scanners (Figures 7.13 to 7.18). In some cases, particularly at thinner slice thicknesses and when the mAs increased from 100 to 150, there were declines in CTIQF$_{inv}$ values when the mAs increased. There were mostly significant improvements in CTIQF$_{inv}$ values when the mAs increased from 50 to 100, 150 or 200 (Table 7.7).
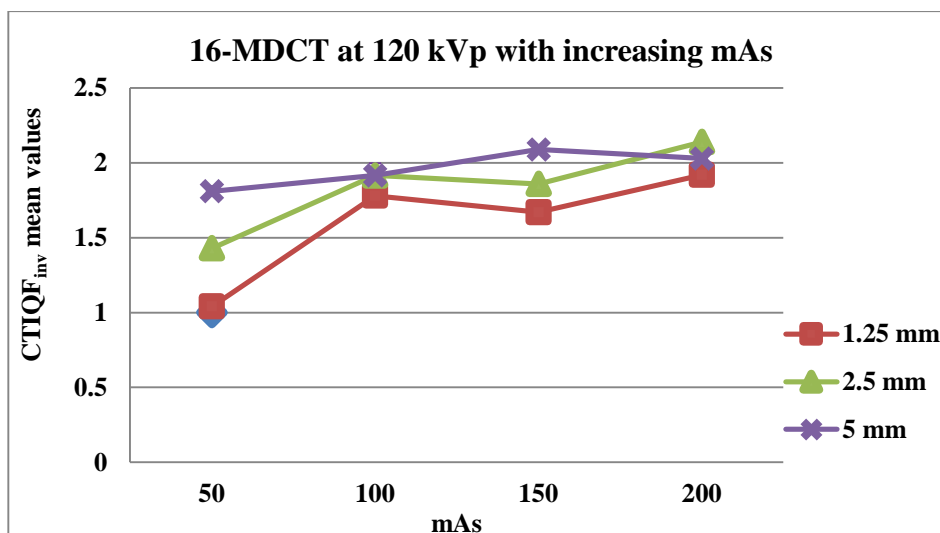
Figure 7.13 Higher mAs resulted in higher CTIQF$_{inv}$ values at 120 kVp with different slice thickness images for the 16-MDCT scanner. (Note the change in CT CTIQF$_{inv}$ values when the mAs increased from 100 to 150 mAs at 1.25 and 2.5 mm slice thickness images and when the mAs increased from 150 to 200 mAs at 5 mm slice thickness images.)
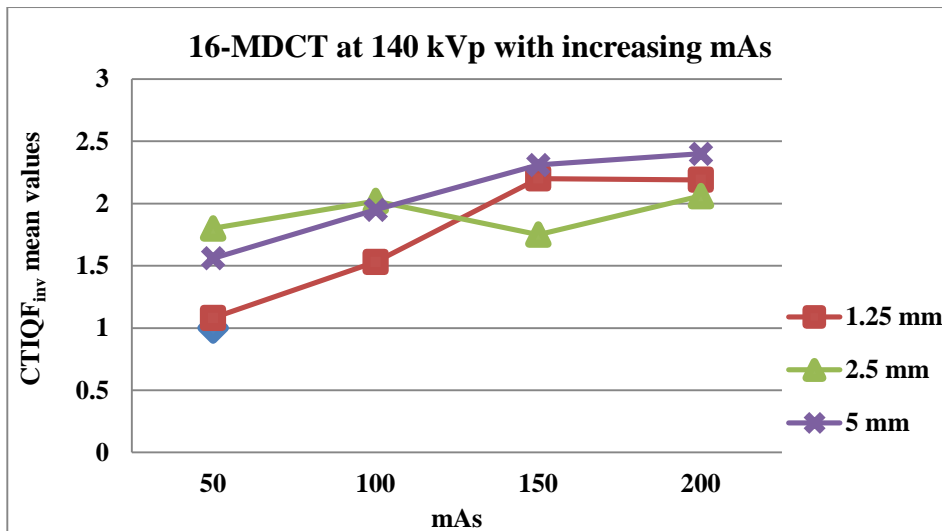
Figure 7.14 Higher mAs resulted in higher CTIQF$_{inv}$ values at 140 kVp with different slice thickness images for the 16-MDCT scanner. (Note the change in CTIQF$_{inv}$ values when the mAs increased from 100 to 150 mAs at 2.5 mm slice thickness images.)
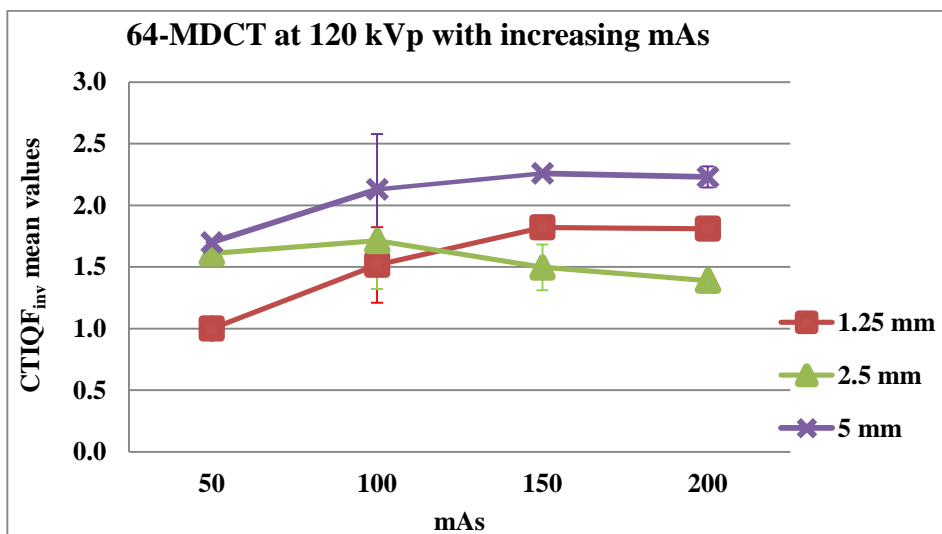
Figure 7.15   Higher mAs resulted in higher CTIQF$_{inv}$ values at 120 kVp with different slice thickness images for the 64-MDCT scanner. (Note the change in CTIQF$_{inv}$ values when mAs increased from 100 to 150 and to 200 mAs at 2.5 mm slice thickness images and when mAs increased from 150 to 200 mAs at 5 mm slice thickness images.)

256
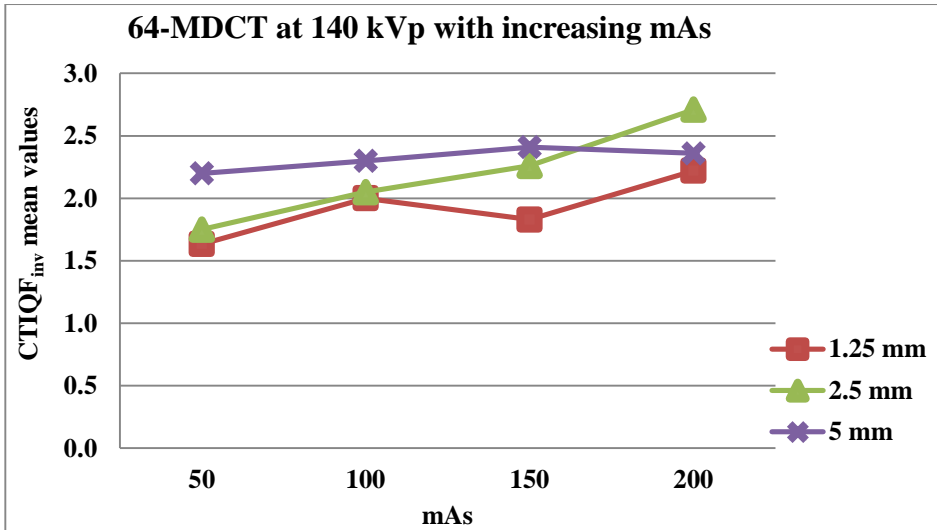
Figure 7.16 Higher mAs resulted in higher CTIQF$_{inv}$ values at 140 kVp with different slice thickness images for the 64-MDCT scanner. (Note the change in CTIQF$_{inv}$ values when mAs increased from 100 to 150 mAs at 1.25 mm slice thickness images.)
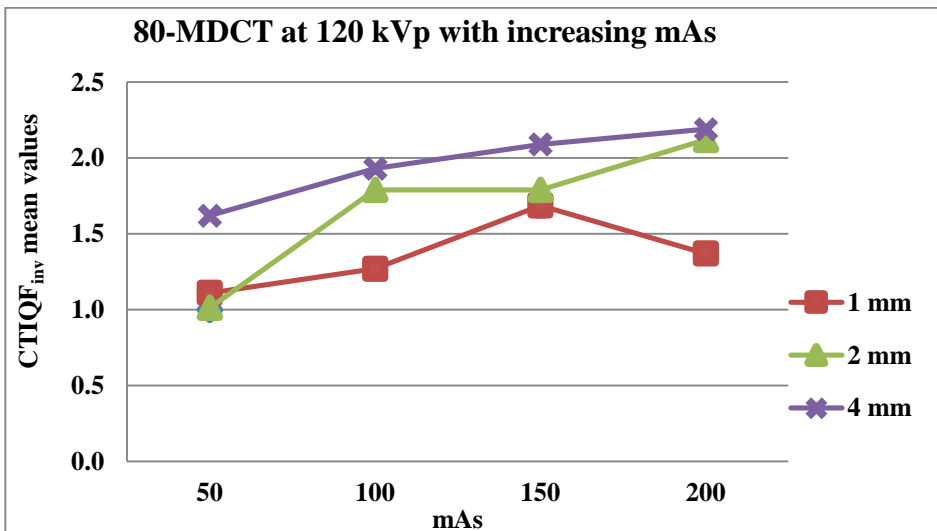
Figure 7.17 Higher mAs resulted in higher CTIQF$_{inv}$ values at 120 kVp with different slice thickness images for the 80-MDCT scanner. Note the change in CTIQF$_{inv}$ values when mAs increased from 100 to 150 mAs at 2 mm slice thickness images and when mAs increased from 150 to 200 mAs at 1 mm slice thickness images.)
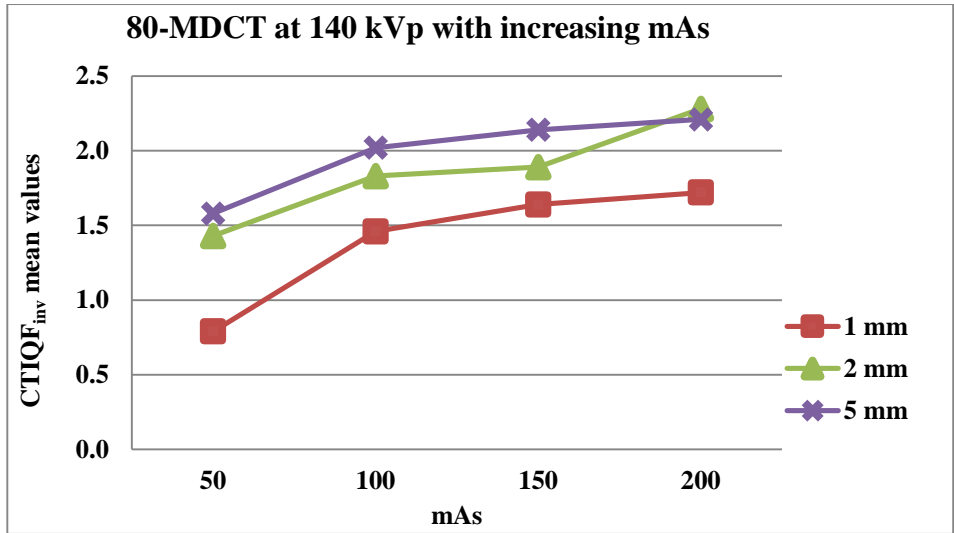
Figure 7.18 Higher mAs resulted in higher CTIQF$_{inv}$ values at 140 kVp with different slice thickness images for the 80-MDCT scanner.

Table 7.7   The differences (*p* values, Student t-tests) between the images of same kVp and mAs with changing mAs in each CT scanner

Image code kVp-mAs-ST	Image code kVp-mAs-ST	Sig. (*p* values, Student t-tests)		
		16-MDCT	64-MDCT	80-MDCT
120-50-1.25/1	120-100-1.25/1	< 0.001	0.014	< 0.001
	120-150-1.25/1	< 0.001	0.001	< 0.001
	120-200-1.25/1	< 0.001	0.001	< 0.001
120-100-1.25/1	120-150-1.25/1	< 0.001	0.149	< 0.001
	120-200-1.25/1	< 0.001	0.167	0.008
120-150-1.25/1	120-200-1.25/1	< 0.001	1.000	< 0.001
120-50-2.5/2	120-100-2.5/2	< 0.001	0.934	< 0.001
	120-150-2.5/2	< 0.001	0.916	< 0.001
	120-200-2.5/2	< 0.001	0.620	< 0.001
120-100-2.5/2	120-150-2.5/2	0.292	0.631	1.000
	120-200-2.5/2	< 0.001	0.329	< 0.001
120-150-2.5/2	120-200-2.5/2	< 0.001	0.929	< 0.001
120-50-5/4	120-100-5/4	0.011	0.353	< 0.001
	120-150-5/4	< 0.001	0.067	< 0.001
	120-200-5/4	< 0.001	0.952	< 0.001
120-100-5/4	120-150-5/4	< 0.001	0.626	< 0.001
	120-200-5/4	0.004	< 0.001	< 0.001
120-150-5/4	120-200-5/4	0.271	0.032	< 0.001
140-50-1.25/1	140-100-1.25/1	< 0.0011	< 0.001	< 0.001
	140-150-1.25/1	< 0.001	< 0.001	< 0.001
	140-200-1.25/1	< 0.001	< 0.001	< 0.001
140-100-1.25/1	140-150-1.25/1	< 0.001	< 0.001	< 0.001
	140-200-1.25/1	< 0.001	< 0.001	< 0.001
140-150-1.25/1	140-200-1.25/1	0.366	< 0.001	0.043
140-50-2.5/2	140-100-2.5/2	0.003	< 0.001	< 0.001
	140-150-2.5/2	0.235	< 0.001	< 0.001
	140-200-2.5/2	< 0.001	< 0.001	< 0.001
140-100-2.5/2	140-150-2.5/2	< 0.001	< 0.001	0.178
	140-200-2.5/2	0.679	< 0.001	< 0.001
140-150-2.5/2	140-200-2.5/2	< 0.001	< 0.001	< 0.001
140-50-5/4	140-100-5/4	< 0.001	0.144	< 0.001
	140-150-5/4	< 0.001	< 0.001	< 0.001
	140-200-5/4	< 0.001	< 0.001	< 0.001
140-100-5/4	140-150-5/4	< 0.001	< 0.001	< 0.001
	140-200-5/4	0.001	< 0.001	< 0.001
140-150-5/4	140-200-5/4	0.031	0.001	< 0.001

Effects of slice thickness on CTIQF$_{inv}$ values

The use of thicker slices generally resulted in better CTIQF$_{inv}$ in all CT scanners (Figures 7.19 to 7.20). In some cases there were declines in CTIQF$_{inv}$ values when slice thickness increased, although there were mostly significant improvements in CTIQF$_{inv}$ values when slice thickness increased from 1.25/1 to 2.5/2 or 5/4 mm (Table 7.8). Despite this, there were some exceptions, as there were insignificant differences in CTIQF$_{inv}$ values between different slice thickness images (Table 7.8).
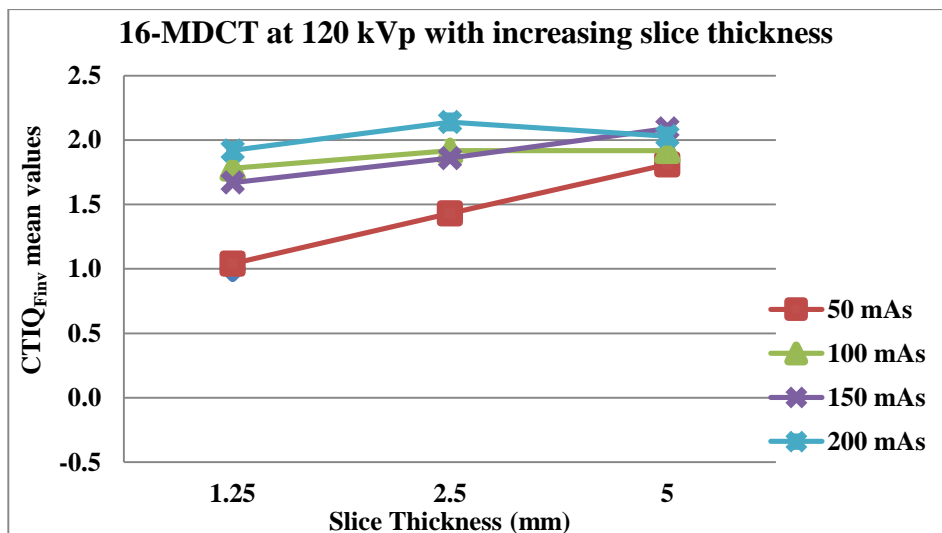
Figure 7.19   Thicker slice images resulted in higher CTIQF$_{inv}$ values at 120 kVp with different mAs levels for the 16-MDCT scanner. (Note the change in CTIQF$_{inv}$ values when the slice thickness increased from 2.5 to 5 mm at 100 and 200 mAs.)
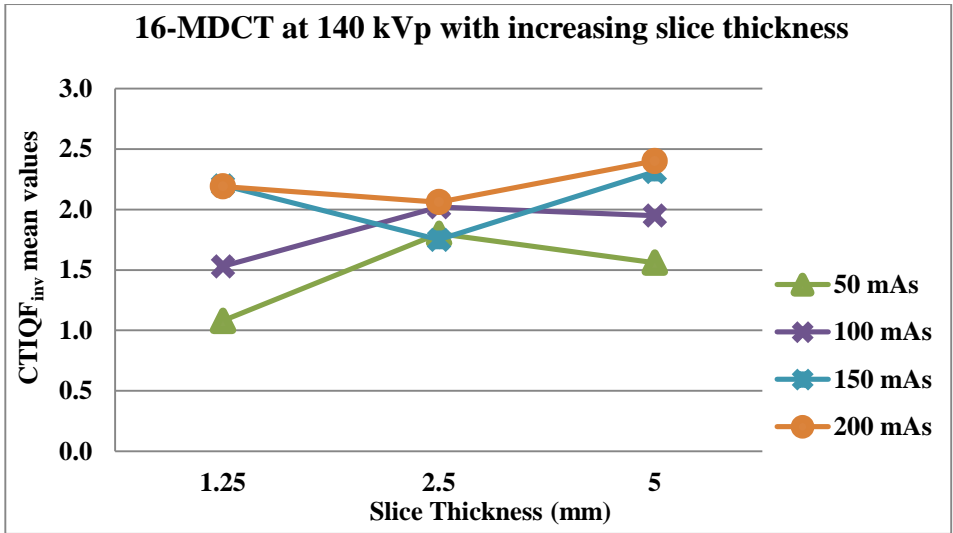
Figure 7.20   Thicker slice images mostly resulted in higher CTIQF$_{inv}$ values at 140 kVp with different mAs levels for the 16-MDCT scanner. (Note the changes in CTIQF$_{inv}$ values when the slice thickness increased from 1.25 to 2.5 mm at 150 and 200 mAs and when the slice thickness increased from 2.5 to 5 mm at 50 and 100 mAs.)
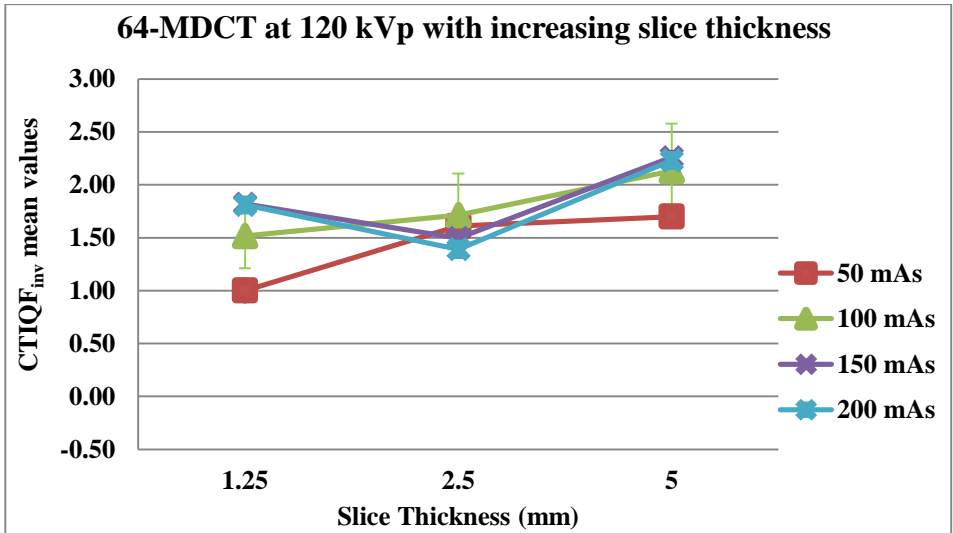
Figure 7.21 Thicker slice images resulted in higher CTIQF$_{inv}$ values at 120 kVp with different mAs levels for the 64-MDCT scanner. (Note the changes in CTIQF$_{inv}$ values when the slice thickness increased from 1.25 to 2.5 mm at 150 and 200 mAs.)

261
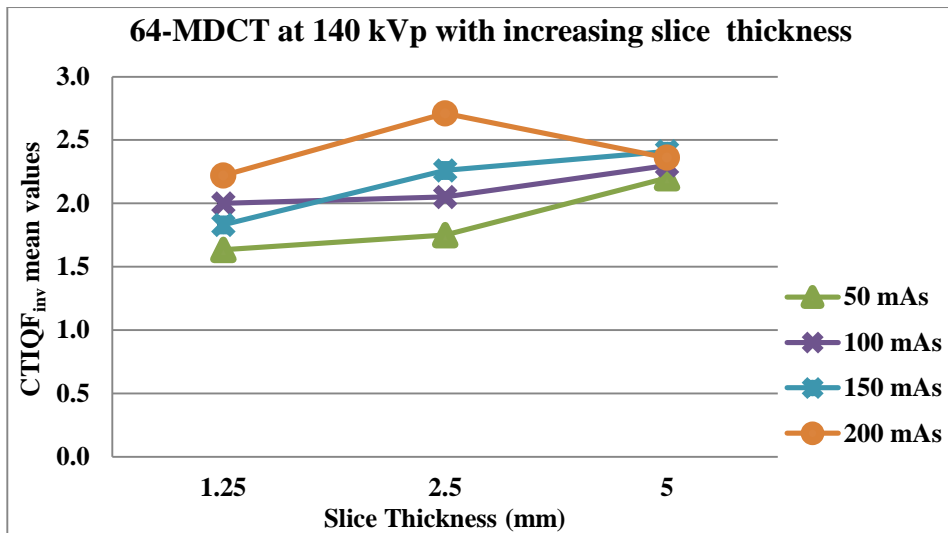
Figure 7.22 Thicker slice images mostly resulted in higher CTIQF$_{inv}$ values at 140 kVp with different mAs levels for the 64-MDCT scanner. (Note the change in CTIQF$_{inv}$ values when the slice thickness increased from 2.5 to 5 mm at 200 mAs.)
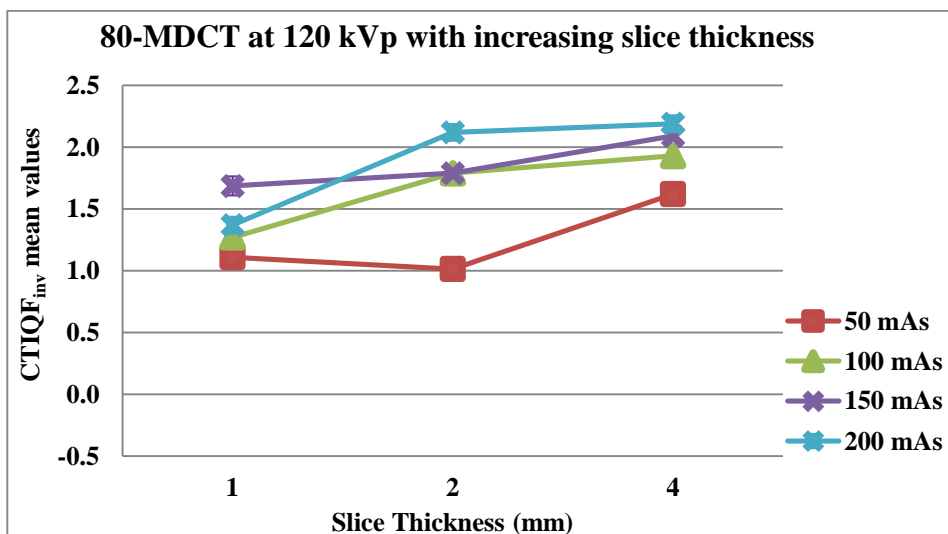
Figure 7.23   Thicker slice images resulted in higher CTIQF$_{inv}$ values at 120 kVp with different mAs levels for the 80-MDCT scanner. (Note the change in CTIQF$_{inv}$ values when the slice thickness increased from 1 to 2 mm at 50 mAs.)
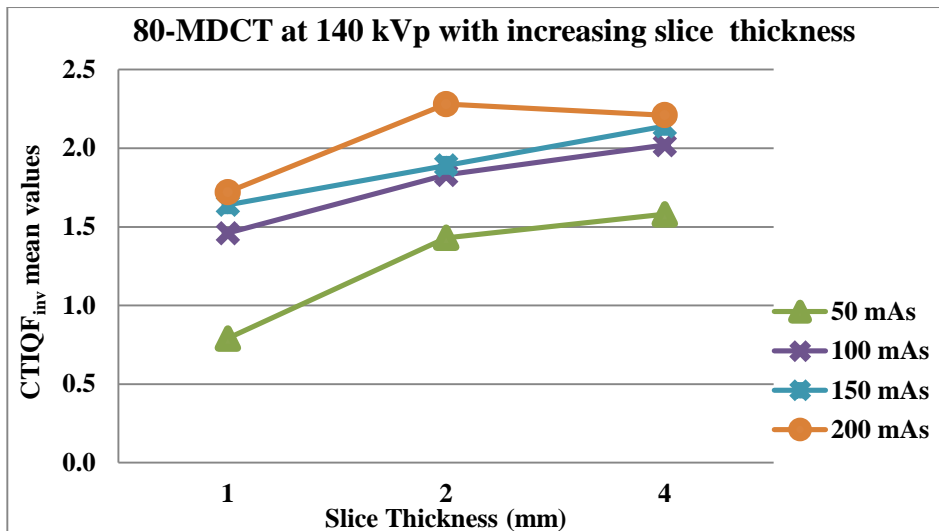
Figure 7.24   Thicker slice images resulted in higher CTIQF$_{inv}$ values at 140 kVp with different mAs levels for the 16-MDCT scanner. (Note the change in CTIQF$_{inv}$ values when the slice thickness increased from 2 to 4 mm.)

Table 7.8   The differences (p values, Student t-tests) between the images of same kVp and mAs with changing slice thicknesses in each CT scanners

(I) Image code	(J) Image code	Sig. (p values, Student t-tests)		
		16-MDCT	64-MDCT	80-MDCT
120-50-1.25/1	120-50-2.5/2	< 0.001	< 0.001	0.021
120-50-1.25/1	120-50-5/4	< 0.001	< 0.001	< 0.001
120-50-2.5/2	120-50-5/4	< 0.001	< 0.001	< 0.001
120-100-1.25/1	120-100-2.5/2	0.034	0.944	< 0.001
120-100-1.25/1	120-100-5/4	0.034	0.028	< 0.001
120-100-2.5/2	120-100-5/4	0.993	0.195	< 0.001
120-150-1.25/1	120-150-2.5/2	< 0.001	0.002	0.017
120-150-1.25/1	120-150-5/4	< 0.001	< 0.001	< 0.001
120-150-2.5/2	120-150-5/4	< 0.001	0.223	< 0.001
120-200-1.25/1	120-200-2.5/2	< 0.001	< 0.001	< 0.001
120-200-1.25/1	120-200-5/4	< 0.001	< 0.001	< 0.001
120-200-2.5/2	120-200-5/4	< 0.001	< 0.001	< 0.001
140-50-1.25/1	140-50-2.5/2	< 0.001	< 0.001	< 0.001
140-50-1.25/1	140-50-5/4	< 0.001	< 0.001	< 0.001
140-50-2.5/2	140-50-5/4	< 0.001	< 0.001	0.001
140-100-1.25/1	140-100-2.5/2	< 0.001	1.000	< 0.001
140-100-1.25/1	140-100-5/4	< 0.001	0.961	< 0.001
140-100-2.5/2	140-100-5/4	< 0.001	0.990	< 0.001
140-150-1.25/1	140-150-2.5/2	< 0.001	< 0.001	< 0.001
140-150-1.25/1	140-150-5/4	< 0.001	< 0.001	< 0.001
140-150-2.5/2	140-150-5/4	< 0.001	< 0.001	< 0.001
140-200-1.25/1	140-200-2.5/2	< 0.001	< 0.001	< 0.001
140-200-1.25/1	140-200-5/4	< 0.001	0.004	< 0.001
140-200-2.5/2	140-200-5/4	< 0.001	< 0.001	< 0.001

Comparison of CTIQF$_{inv}$ values between scanners

Based on measurements of CTIQF$_{inv}$ values, 64-MDCT generally showed superior performance than other CT scanners, particularly at 140 kVp (Figures 7.25 to 7.32). There were mostly significant differences among CT scanners (Table 7.9), although there were some exceptions. For example, at 120 kVp and 100 mAs, with different slice thicknesses, there were insignificant differences among the scanners (Table 7.9).
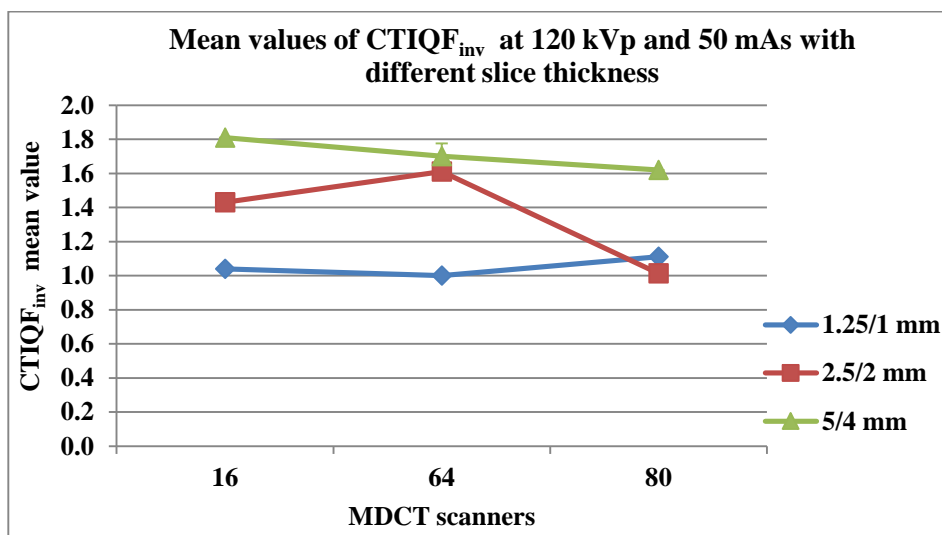
Figure 7.25 Average CTIQF$_{inv}$ values at 120 kVp and 50 mAs for each CT scanner show the superiority of 64-MDCT over other scanners at 2.5/2 mm slice thickness and the superiority of 16-MDCT over other scanners at 5/4 mm slice thickness.
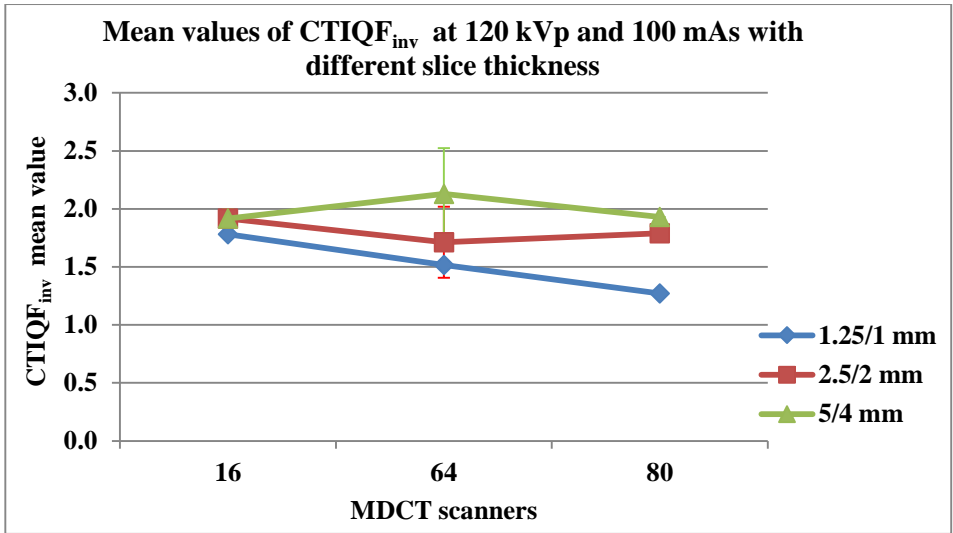
Figure 7.26   Average CTIQF_inv values at 120 kVp and 100 mAs for each CT scanner show the superiority of 16-MDCT over other scanners at 1.25/1 and 2.5 mm slice thicknesses and the superiority of 64-MDCT over 80-MDCT at 1.25/1 mm. (Note the differences among the scanners at 5/4 mm slice thickness.)
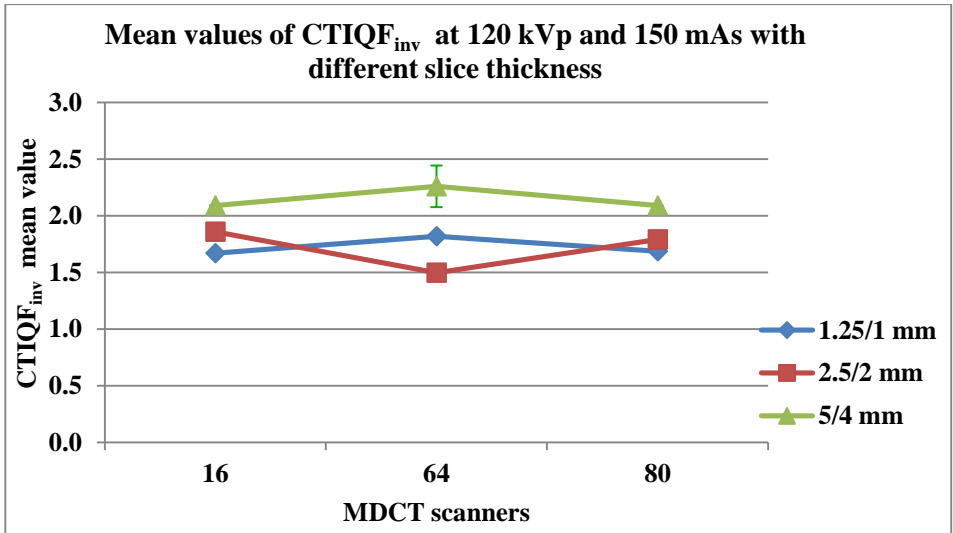
Figure 7.27   Average CTIQF_inv values at 120 kVp and 150 mAs for each CT scanner show the slight superiority of 64-MDCT over other scanners. (Note the supeiority of 16-MDCT and 80-MDCT over 64-MDCT at 2.5 mm slice thickness. The average CTIQF_inv values show that 16-MDCT and 80-MDCT are generally comparable.)
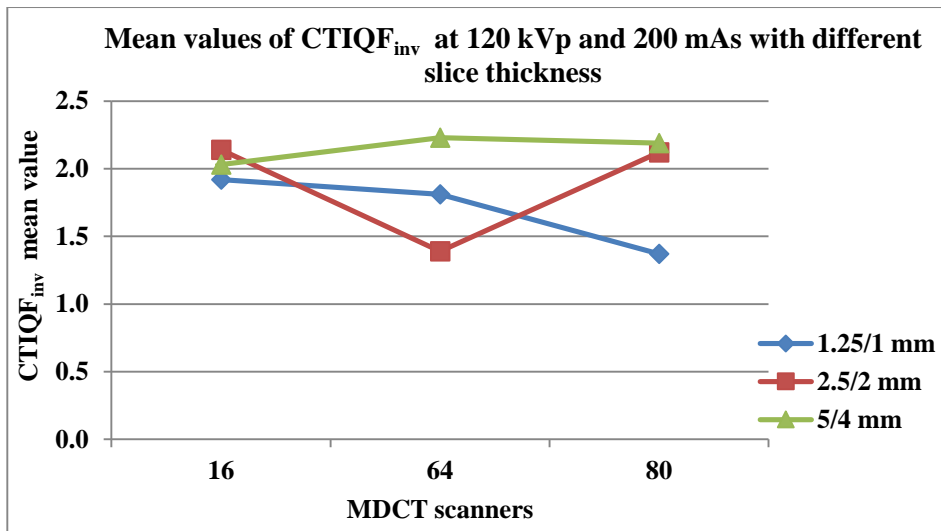
Figure 7.28   Average CTIQF$_{inv}$ values at 120 kVp and 200 mAs for each CT scanner show the superiority of 16-MDCT over 64-MDCT and the superiority of 80-MDCT over 64-MDCT. (Note the supeiority of 16-MDCT over 80-MDCT at 1.25/1 mm slice thickness and the superiority of 64-MDCT over 80-MDCT at 5/4 mm slice thickness.)
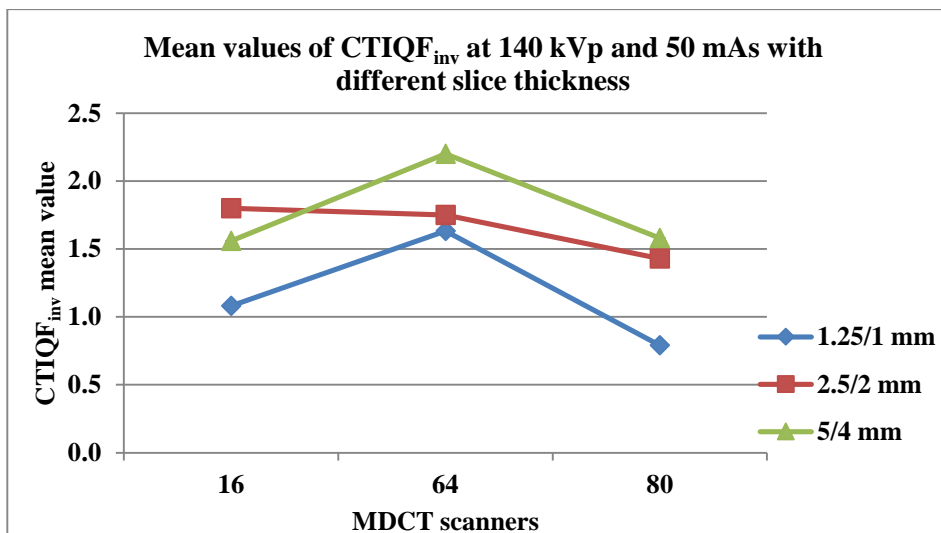
Figure 7.29   Average CTIQF$_{inv}$ values at 140 kVp and 50 mAs for each CT scanner show the superiority of 64-MDCT over other scanners and the superiority of 16-MDCT over 80-MDCT. (Note the supeiority of 16-MDCT over 64-MDCT at 2.5 mm slice thickness.)
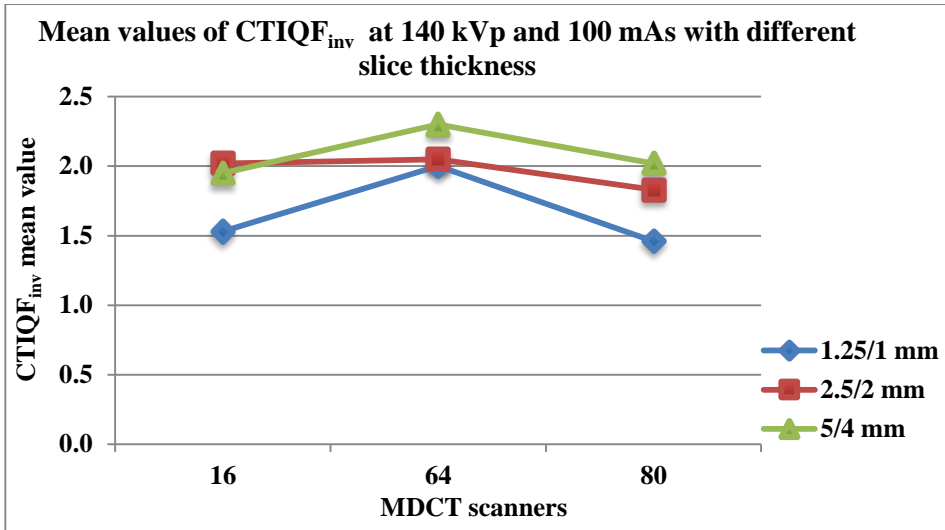
Figure 7.30   Average CTIQF$_{inv}$ values at 140 kVp and 100 mAs for each CT scanner show the superiority of 64-MDCT over other scanners and the superiority of 16-MDCT over 80-MDCT. (Note the differences between 16-MDCT and 64-MDCT at 2.5 mm slice thickness.)
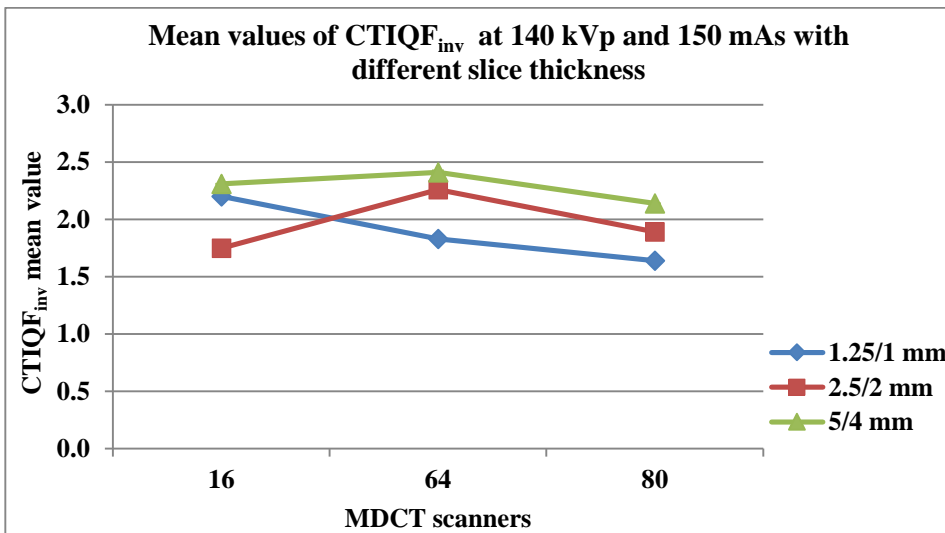
Figure 7.31   Average CTIQF$_{inv}$ values at 140 kVp and 150 mAs for each CT scanner show the superiority of 64-MDCT over other scanners and the superiority of 16-MDCT over 80-MDCT. (Note the supeiority of 16-MDCT over 64-MDCT at 1.25 mm slice thickness and the supeiority of 80-MDCT over 16-MDCT at 1.25 mm slice thickness.)
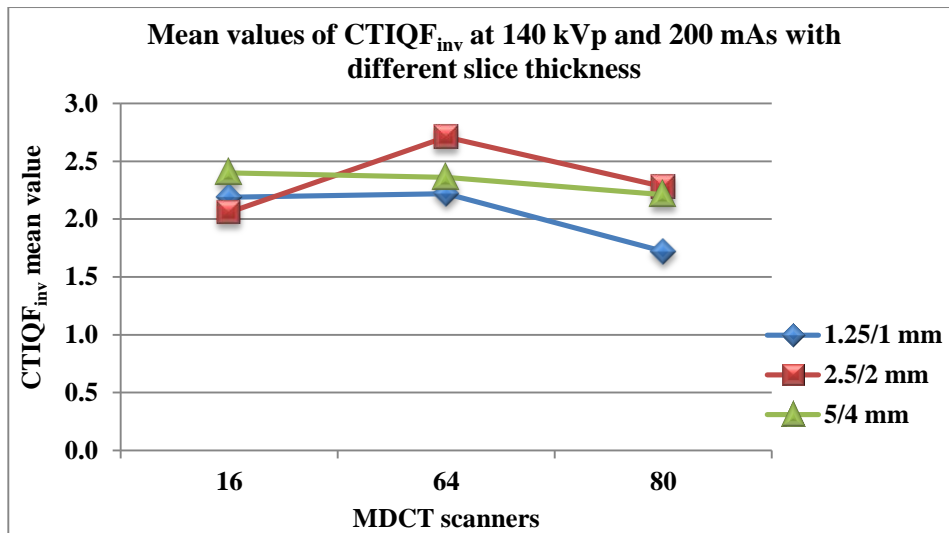
Figure 7.32 Average CTIQF$_{inv}$ values at 140 kVp and 200 mAs for each CT scanner show the superiority of 64-MDCT over other scanners and the superiority of 16-MDCT over 80-MDCT. (Note the differences between 16-MDCT and 64-MDCT at 1.25 and 5 mm slice thicknesses.)

Table 7.9   The differences (*p* values, Student t-tests) between the images of same factors and slice thicknesses from different CT scanners.

kVp	mAs	ST	Sig. (*p* values, Student t-tests)		
			16-MDCT x 64-MDCT	16-MDCT x 80-MDCT	64-MDCT x 80-MDCT
120	50	1.25/1	0.636	0.076	0.002
120	50	2.5/2	< 0.001	< 0.001	< 0.001
120	50	5/4	< 0.001	< 0.001	< 0.001
120	100	1.25/1	0.876	0.197	0.909
120	100	2.5/2	0.967	0.998	1.000
120	100	5/4	0.838	1.000	0.949
120	150	1.25/1	0.222	1.000	0.320
120	150	2.5/2	< 0.001	0.924	0.001
120	150	5/4	0.105	1.000	0.094
120	200	1.25/1	0.004	< 0.001	< 0.001
120	200	2.5/2	< 0.001	0.993	< 0.001
120	200	5/4	< 0.001	< 0.001	< 0.001
140	50	1.25/1	< 0.001	< 0.001	< 0.001
140	50	2.5/2	0.001	< 0.001	< 0.001
140	50	5/4	< 0.001	0.398	< 0.001
140	100	1.25/1	< 0.001	< 0.001	< 0.001
140	100	2.5/2	< 0.001	< 0.001	< 0.001
140	100	5/4	< 0.001	< 0.001	< 0.001
140	150	1.25/1	< 0.001	< 0.001	< 0.001
140	150	2.5/2	< 0.001	< 0.001	< 0.001
140	150	5/4	< 0.001	< 0.001	< 0.001
140	200	1.25/1	< 0.001	< 0.001	< 0.001
140	200	2.5/2	< 0.001	< 0.001	< 0.001
140	200	5/4	< 0.001	< 0.001	< 0.001

7.4.4 Discussion

The results of the new LCD evaluation method software scoring are as expected in the outer object locations, however the software scoring results are not as expected in the central region (Tables 7.4 and 7.5). The software did not calculate the $CTIQF_{inv}$ values for centre object locations in a consistent manner, nor were the $CTIQF_{inv}$ values consistent with the expected results from theory. There are several possible reasons for this. The automatic adjustment, which is required for the alignment and the orientation of the phantom in the software, may not yet be optimised. As such, manual adjustments were made and these may not be fully accurate. Additionally, the automated software may not yet be optimised to maximise the $CTIQF_{inv}$ values. The current design of the CDCT phantom may also not yet be optimised.

The average $CTIQF_{inv}$ values of the outer and centre location levels, in addition to the total location levels, were not calculated and recorded. The results from the outer object location of each image were only used in the validation study of the automated approach of the new methodology of LCD detectability performance. Consequently, the effects of object location levels on LCD detectability could not be evaluated.

As expected, higher kVp and/or mAs generally resulted in better $CTIQF_{inv}$ values from all CT scanners. There were mostly significant improvements in $CTIQF_{inv}$ values when the kVp increased from 120 to 140. Increasing the kVp setting, when all other factors remain constant, increases the number of photons that reach the detectors. As a result, the noise is reduced (Alsleem & Davidson 2013; Seibert 2004) and the $CTIQF_{inv}$ values increase. It was also expected that, when mAs increased, the x-ray photon numbers would also increase, as radiation dose increases linearly with mAs. Increasing mAs increases the amount of the produced photons—or radiation dose—and that reaches the detectors

(Bushberg et al. 2012.; Funama et al. 2005; Toth 2012) and consequently $CTIQF_{inv}$ values improve.

It was also shown that, with thicker slice thicknesses, $CTIQF_{inv}$ values generally increased. Thicker slices increase photon numbers reaching the detectors and hence reduce the noise and improve image quality (von Falck, Galanski & Shin 2010). The study results generally showed significant changes in $CTIQF_{inv}$ values when kVp, mAs and/or slice thickness were changed. These results are supported by the results of Chapter 5. However, there were some exceptions to the general assessment of the results for the new evaluation methodology of automated LCD detectability performance.

When the new methodology was used to compare different CT scanners, the results showed that these scanners have different LCD detectability performance, which were also influenced differently by changing protocol parameters. 64-MDCT had better results consistency, with changing protocol parameters, than other scanners.

7.4.5 Conclusion

The resultant image quality, in terms of $CTIQF_{inv}$ values, generally changed in an expected manner as the protocol parameters of kVp, mAs and slice thickness changed. The new evaluation methodology of automated LCD detectability performance is generally a feasible method to evaluate image quality and to measure the influences of protocol parameters on CT image quality in terms of $CTIQF_{inv}$ values. Comparing the LCD detectability performance between different scanners is also possible with the automated approach of the new methodology. It has the ability to directly and objectively evaluate and compare the image quality between different scanners, processing technology and protocol

parameters. The new automated software and the CDCT phantom need to be optimised to enable the software correctly calculate $CTIQF_{inv}$ values for centre object locations to evaluate the object location levels on LCD detectability performance.

7.5 Section 4 of Phase 4: Comparing the results from software and radiographers

7.5.1 Introduction

In the previous two sections, Section 2 and 3 of Phase 4, the new methodology of LCD detectability performance as a tool of CT image quality evaluation and optimisation was evaluated, based on radiographers' assessment and software scoring. The effects of exposure factors on image quality in terms of $CTIQF_{inv}$ values were assessed. In this section, Section 4 of Phase 4, the assessment results of radiographers and scoring results of software are compared. The aim of this section is to examine the validity and reliability of the objective approach of the new methodology of LCD detectability performance as a method of CT image evaluation and optimisation.

7.5.2 Materials and methodology

The results of Section 2 of Phase 4 were used in the current study (Section 4 of Phase 4). The same CT images of CDCT phantom used in the study of Section 2 of Phase 4 were loaded into the new software. The three notch markers of each image were manually localised to adjust the correct orientation of the image in the software. The images were then scored by software to calculate the values of $CTIQF_{inv}$ for each image. The $CTIQF_{inv}$

271

values were recorded for the centre and external rings, which are provided in Table 7.4 and 7.5. Each image was scored three times by the software. The scoring results from radiographers and software for these images were compared.

Statistical analysis

The statistical test of Pearson correlation coefficients was used to examine the direction and the strength of the linear relationship between the mean scoring results of software and the radiographers. Pearson correlation coefficients can range from -1 to +1, +1 indicates a perfect positive correlation, -1 indicates a perfect negative correlation and 0 indicates no relationship between the two variables (Pallant 2013). The correlation between detectability performance results—of radiographers compared with software analyser scoring—was performed for all images that scored by both radiographers and software. Student t-tests, at an Alpha value of 0.05, was undertaken to determine if significant differences existed between the mean scoring results of software and the average assessment results of radiographers (Pallant 2013).

7.5.3 Results

There exists a positive correlation ($r = 0.86$) between radiographers and the software analyser in terms of detectability performance evaluation (Figure 7.33). $CTIQF_{inv}$ values from radiographer assessments and software scoring results were influenced in a similar way when changing exposure factors and slice thicknesses (Table 7.10). Figures 7.1 to 7.3 show the changes in $CTIQF_{inv}$ values when kVp, mAs or slice thickness increased, based

on the assessment results of the radiographers. Figures 7.34 to 7.36 show the changes in $CTIQF_{inv}$ values when kVp, mAs or slice thickness increased based on software scoring. Based on the results of radiographers and software, there was significant increase ($p < 0.001$) in $CTIQF_{inv}$ values with increasing the kVp, mAs and slice thickness. However, the results showed significant differences between the assessment results from radiographers and those from software scoring ($p = < 0.001$). While the mean of $CTIQF_{inv}$ values of the images that were scored by radiographers was 2.634, the mean was only 2.123 for the images that were scored by software.
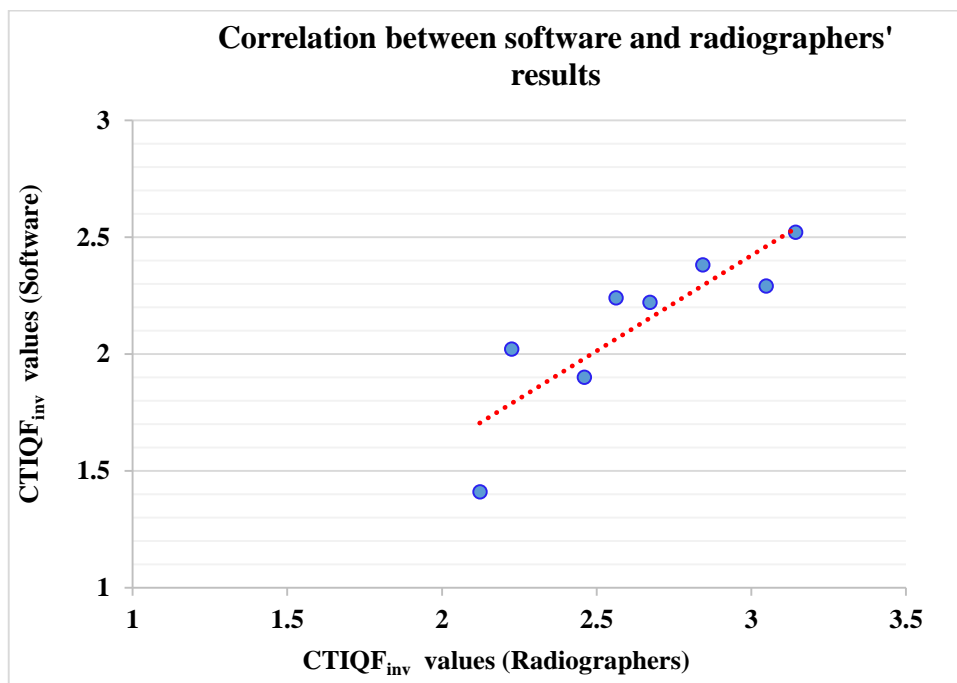
Figure 7.33 The assessment results of radiographers have good positive
correlation coeffecient with the scoring results of software (r = 860).

Table 7.10 CTIQF$_{inv}$ mean values of eight images obtained from 64-MDCT and based on radiographers' assessments compared with the software scoring results of CTIQF$_{inv}$ mean values of the same eight images

kVp	mAs	Slice thickness (mm)	Radiographers								Software	
			Total		Centre		Outer (Rings)		Centre		Outer (Rings)	
			Mean	SD	Mean	SD	Mean	SD	Mean	SD	Mean	SD
120	100	1.25	2.1225	0.29	2.17	0.3	2.075	0.28	1.16	< 0.001	1.41	< 0.001
120	100	5	2.6725	0.3	2.62	0.3	2.725	0.3	1.13	< 0.001	2.22	< 0.001
120	200	1.25	2.4600	0.26	2.49	0.3	2.43	0.25	0.65	< 0.001	1.90	< 0.001
120	200	5	3.0475	0.29	2.96	0.3	3.135	0.26	0.97	< 0.001	2.29	< 0.001
140	100	1.25	2.2250	0.29	2.28	0.3	2.17	0.27	0.68	< 0.001	2.02	< 0.001
140	100	5	2.8425	0.29	2.74	0.3	2.945	0.26	0.64	< 0.001	2.38	< 0.001
140	200	1.25	2.5625	0.31	2.46	0.3	2.665	0.28	0.61	< 0.001	2.24	< 0.001
140	200	5	3.1425	0.34	2.94	0.3	3.345	0.26	1.02	< 0.001	2.52	< 0.001
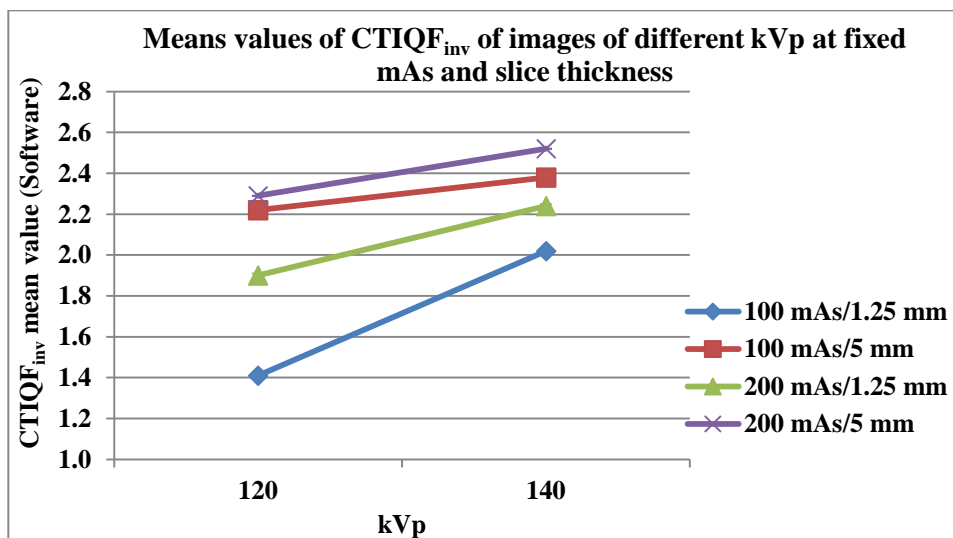
Figure 7.34 Higher kVp resulted in higher CTIQF$_{inv}$ values with different mAs levels and slice thicknesses.
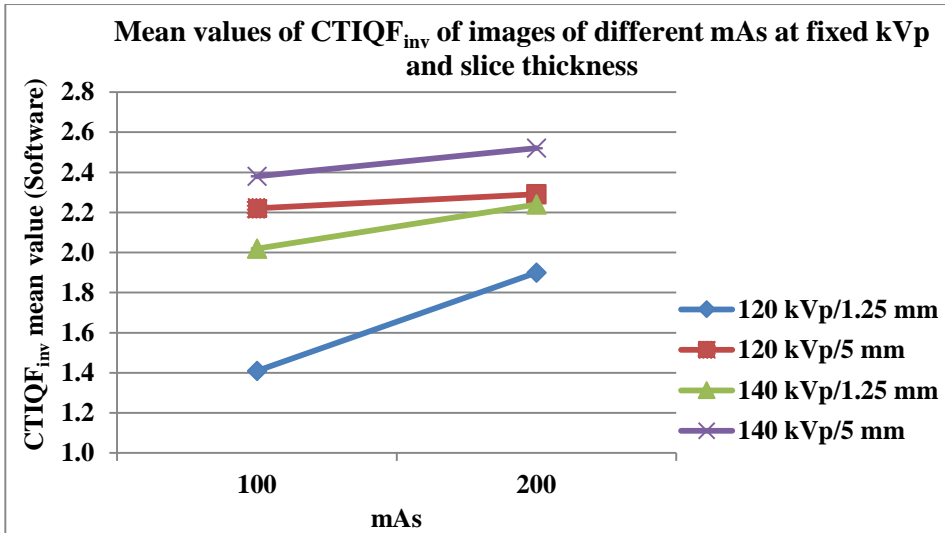
*Figure 7.35 Higher mAs resulted in higher CTIQF$_{inv}$ values at different kVp
selections with different slice thickness. There were also significant changes
between the images when the mAs increased.*
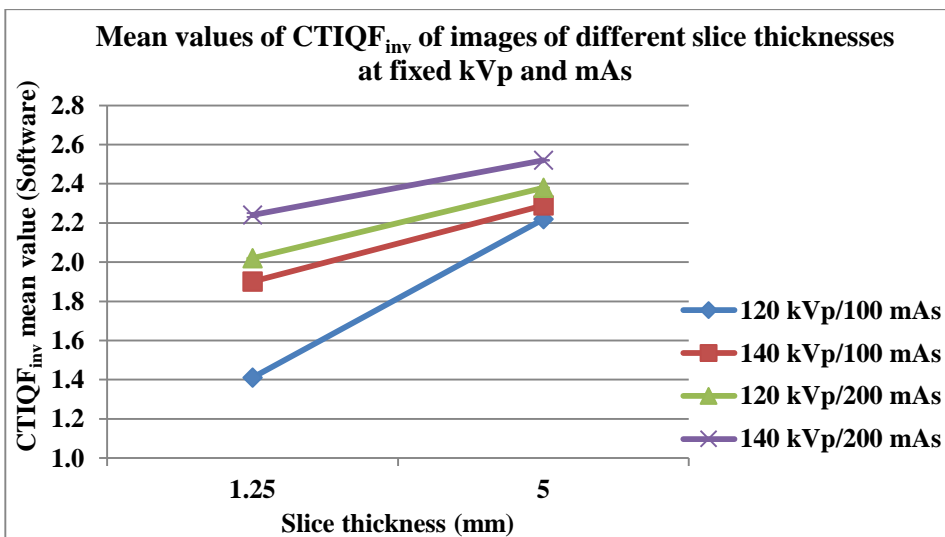
*Figure 7.36 Thicker slice thicknesses resulted in higher CTIQF$_{inv}$ values at
different kVp selections and mAs levels. There were also significant changes
when the mAs increased.*

7.5.4   Discussion

As discussed previously in Section 2 of Phase 4, the radiographers' results of CTIQF$_{inv}$

values were as expected for inner and outer regions of images. When the software was used

to determine the outer area $CTIQF_{inv}$ values, the results were also as expected. This was not the case for inner region, as shown in Section 3 of Phase 4. Hence, the software results of outer location $CTIQF_{inv}$ values were only used in the comparison study with the results of radiographers. Even though there were significant differences ($p < 0.001$) in $CTIQF_{inv}$ values between the results of radiographers and software scoring, there was a positive correlation coefficient ($r = 0.860$) between them. The average results of the radiographers and software also agreed that higher kVp, mAs or thicker slice thickness resulted in significant increase in $CTIQF_{inv}$ values. These results generally prove the validity of the objective approach and the reliability of the subjective approach, with respect to the new methodology of LCD detectability performance to evaluate and optimise CT image quality.

The subjective results based on radiographer assessments were generally higher than the objective results of software for the outer object locations of images. In addition, the software results for the centre areas of images were not as expected, when compared to the results of radiographers for the same areas of images. In comparison with software, and as discussed in Section 2 of Phase 4, comparing between the different location levels (in terms of $CTIQF_{inv}$) was possible and the results were as expected, most of the time. There may be several reasons for the differences between the software and radiographer results. For example, the lower radiation received in the centre location area increases the amount of noise in that area, which may cause the radiographers to inaccurately report variations in the background as an object, hence the overall higher $CTIQF_{inv}$ results. In other words, they may have guessed as to the existence of some artefacts or noise. The automated software may also not yet be optimised, as it wasn't able to correctly calculate the $CTIQF_{inv}$ values for centre regions of phantom images. The automated alignment of the phantom image in the software may also not yet be optimised to maximise the $CTIQF_{inv}$ values. Finally, the

current design of the phantom may not yet be optimised, as the software could not correctly measure the $CTIQF_{inv}$ values of centre areas of phantom images.

7.5.5 Limitations

The new CT methodology of LCD detectability performance has limitations as the design of the CDCT phantom and the automated software alignment is not yet optimised. As discussed in Section 3 of Phase 1, when the evaluation method of LCD detectability performance was used for digital radiography, the assessment results of observers were typically lower than the software scoring results in terms of $CTIQF_{inv}$ values. The software is generally more sensitive to contrast changes than human observers, but this was not the case using the CDCT phantom, nor with comparing radiographers against software scoring. In digital radiography, the observers score the image by selecting randomly placed small holes with the designated grid, as discussed in Chapter 2. This requires observers to specify which quadrant of the grid the hole is located in. The current design of the CDCT phantom does not have this. In this evaluation work of the phantom, the improved results by the radiographers over the software could be due to 'guessing' where the next smallest object is located. A reliance on the software in future work could overcome this problem.

7.6 Conclusion

The subjective results based on the assessment of radiographers, and the objective results based on software scoring, generally show the validity and the reliability of the new methodology of LCD detectability performance to evaluate and optimise CT image quality.

Both results show consistency with prior knowledge of image quality in relation to change of mAs, kVp and slice thickness settings. However, this new methodology was limited by the design of CDCT phantom and/or software, as the $CTIQF_{inv}$ values of the centre region of phantom images were not as expected when calculated by the current software version. The current limitations of the new automated methodology of LCD detectability performance for CT could be overcome in future work by optimising the phantom design and/or software. The study was also hindered by limitations of the new phantom that have been mentioned previously.

Chapter 8   Conclusion

The evaluation of digital radiographic image quality though the use of low contrast-detail (LCD) detectability methods has been shown by this work and others to be an appropriate tool. Digital radiography includes computed radiography (CR) and direct digital radiography (DR). DR is of two main types: indirect conversion DR (IDR) and direct conversion DR (DDR). While this evaluation method based on LCD detectability performance is well established in digital radiography, there is no similar methodology for computed tomography (CT). The central aim of this project was to translate the methodology of LCD detectability performance in digital radiography to CT.

The effects of mAs and kVp on image quality of different digital radiography systems were evaluated by using the method of LCD detectability performance as a measure of image quality. These studies used the assessment of radiographers and software scoring to determine image quality results. The next phase of the project evaluated CT image quality using contrast-to-noise ratio (CNR) as a measure of quality. The commonly available phantom, Catphan® 600 (Phantom Laboratory, Cambridge, NY), was used to evaluate the influences of CT protocol parameters on image quality. This method was assessed as not appropriate to measure LCD detectability performance in CT. In the third phase, a new method was proposed to evaluate LCD detectability performance of CT based on the findings of previous studies. A new contrast-detail CT (CDCT) phantom was designed and manufactured and dedicated software was developed. This newly developed CDCT phantom and software method was validated as a tool for measuring the LCD detectability performance of CT images and optimising CT image quality. Radiographers' assessment and software scoring results (of the effects of changing CT protocol parameters on the LCD detectability) were used to examine the validity and the reliability of this new method.

279

8.1 Key findings

In digital radiography, the first phase was designed to evaluate the effects of radiographic factors, kVp and mAs, on LCD detectability performance of CR, IDR and DDR. The inverse image quality figure (IQF_{inv}) was calculated and used as a measure of LCD detectability performance. Based on software results, it was shown that there was a direct and linear relationship between mAs and LCD detectability performance. Higher mAs resulted in better detectability performance in all digital imaging systems. In contrast, changing the kVp did not significantly improve LCD detectability performance, particularly in DDR and at higher mAs settings in IDR.

The results of the first phase experiments indicated that mAs is the dominant factor of LCD detectability performance in digital radiography. Caution is needed when considering the approach of increasing mAs to improve LCD detectability in a digital radiograph, as increasing mAs also increases the risk from higher radiation doses to patients. The use of kVp to change the image contrast is well known in film/screen radiographic systems, however when using digital radiographic systems kVp does not change image contrast. Image contrast can instead be changed independently using digital image processing methods. The effects of kVp and mAs on LCD detectability performance differ from one digital radiography system to another. IDR and DDR had better LCD detectability performance than CR. IDR had better detectability performance than DDR only at higher mAs and higher kVp settings. The selection of an imaging system can also be based on the type of examinations it will be used for. DDR is recommended to examine small organs and mammography, as the DDR system shows better detectability performance with lower exposure factors than IDR.

The first phase of this project also set out to evaluate radiographer performance in observing LCD in digital radiography systems. The average scoring results of radiographers led to similar results of software scoring in terms of the effects of mAs and kVp on LCD detectability performance. Radiographers' results agreed with the software results in that IDR had better detectability performance than other systems. However, the results also showed that there were significant differences between the average results of radiographers and software. In addition, the results showed that the ability of radiographers to detect LCD in an image is lower compared with software scoring results. These results support the premise that the reliability of radiographers' results is deteriorated by the subjectivity of human observation and inter-radiographer differences. Thus, evaluation procedures based on radiographers will require many radiographers to reduce human subjectivity and increase result reliability. Based on the experience gained from this study when using human observers, the researcher concludes that such a subjective approach can be time consuming and cumbersome.

The findings of the first phase indicated that the evaluation approach of LCD detectability performance based on the assessment of human observers is not ideal for routine image quality evaluation and optimisation. As discussed above, the main limitations of the subjective approach are overcome in the automated approach. Indeed, the automated approach of the LCD detectability performance method (using the software) has the potential to provide an understanding with respect to the effects of exposure factors on image quality and radiation dose. An implication of this is that automated LCD detectability performance is an effective tool to evaluate and optimise image quality of radiography.

The second phase of this study was undertaken to evaluate the effects of kVp, mAs, slice thicknesses, reconstruction algorithms, object contrast levels and object sizes in CT. It

evaluated image quality based on the statistical measurements of CNR. The method chosen was CNR measurements using a Catphan® 600 phantom, the commonly available CT LCD phantom. This phase of the study was also conducted to examine the feasibility of this method, based on CNR measurements, to evaluate LCD detectability performance of CT images for different CT scanners.

The results of the second phase showed that the objective method of LCD evaluation, based on CNR measurements and Catphan® 600 phantom, was able to evaluate the effects of kVp, mAs, slice thicknesses, reconstruction algorithms and object contrast levels on image quality. One of the most significant findings to emerge from this study is that the effects of object size could not be evaluated by this method, as CNR has been shown to be insensitive to change of object sizes. The smallest object that was examined (5 mm diameter) and objects below this size cannot be evaluated for LCD changes using these phantoms or methods. Furthermore, this method is also limited by the commercially available LCD phantoms. The current CT LCD phantoms cannot be used to evaluate objects of the same contrast levels and size at different location levels. These findings indicate that these methods of LCD evaluation, based on CNR measurements, are not appropriate tools to measure CT LCD detectability performance. Given these findings, it was suggested that a new evaluation approach, based on a new designed phantom, should be developed to assess CT LCD detectability performance.

The central purpose of the project was to develop a new method, similar to that used in digital radiography, to evaluate LCD detectability performance of CT images. In the third phase of the project a new CDCT phantom was designed and manufactured to be used in the proposed method. The new phantom was scanned at a variety of CT settings. The results showed that the design of the phantom was suitable for its intended purpose. Dedicated

software was also developed and used to eliminate the potential subjectivity of the new method. The CT inverse image quality figure (CTIQF$_{inv}$) was devised as a new measure of LCD detectability performance. The methods to calculate the CTIQF$_{inv}$ were developed. The CTIQF$_{inv}$ has been shown to be an objective measure of LCD in CT.

The last study phase of the project—using the newly designed phantom and developed software—was undertaken to validate this new method of LCD detectability performance of CT images. The results from radiographers and software showed a consistent relationship with prior knowledge of image quality in relation to change of mAs, kVp and slice thickness settings. The most important finding to emerge from this study is that this new method is a valid and reliable method to evaluate the effects of changes in protocol parameters on the quality of CT images in terms of LCD detectability performance. The results showed that this new method is an effective tool to evaluate the effects of exposure factors and other protocol parameters on CT image quality in terms of LCD detectability performance. In addition, the new method can be used to compare different scanners of different technology and from different manufacturers. However, the CTIQF$_{inv}$ values of the centre regions of phantom images, based on software scoring results, were not as expected. This suggests that the new automated evaluation method of LCD detectability performance was limited by the design of CDCT and/or the current software version.

8.2 Limitations

The project has several limitations that need to be acknowledged. The first phase was limited by the fact that only one manufacturer was used to test each type of digital radiography systems. In addition, the digital radiographic phase only examined one object

thickness, being 10 cm of Perspex. The study did not measure radiation dose and did not consider the beam filtration, which are essential to determine the dose delivered by each system. Different combinations of mAs and kVp deliver different radiation dose. The study was also limited by the numbers of radiographers, as this number was relatively small and each image was only scored by six radiographers. In addition, the phase was limited by the fact that the demographic data of the radiographers—including age, qualifications, speciality and years of experience—were not considered in this study. Such information could provide a deeper understanding of radiographers' detectability performance.

The limitations of the second phase of this study included the fact that only CNR measurements were used as a measure, and that only one scanner system from one manufacturer was evaluated. The study was also limited by that fact that 5 mm was the smallest size of phantom object that the researcher was able to measure.

The new evaluation method of LCD detectability performance of CT images was limited by the design of the CDCT phantom and/or the automated software. Even though the results of the software were as expected for outer regions of CDCT phantom images, the results of the centre areas were not. This suggests that the design of the CDCT phantom and/or software may be not yet optimised. One additional weakness of the CDCT phantom was that incorrect material was used for one object.

8.3   Further work

Further research is needed to fully evaluate the effects of exposure factors on image quality in terms of LCD detectability performance of different digital radiography systems for different manufacturers. Further work is also needed to evaluate the influence of different

attenuation thicknesses on image quality optimisation of digital radiography. Radiation dose and filters should also be considered in future work to obtain deeper understanding of image quality optimisation of digital radiography. It is also recommended that the radiographers undergo further clinical practice or training in image viewing to improve their LCD detectability performance, as they bear the responsibility of determining what appropriate image quality is.

Future changes to the CDCT phantom design—and/or software of the new evaluation method of LCD detectability performance—should be made to overcome their current limitations. It is also recommended to evaluate the LCD detectability performance ability of the new CDCT phantom against images from a wider range of CT protocol parameters, including kVp, mAs, slice thickness, kernel filters and reconstruction algorithm. Further investigations are needed to include a measure of the radiation dose to obtain a deeper understanding of the quality optimisation of CT images. A further study could also assess and compare different CT scanners of different technology, systems and manufacturers.

8.4   Conclusion

The overall findings of this project support the need for the newly-devised method of evaluating LCD detectability in CT. However, due to its current limitations, this new method of LCD detectability is still not ready to be implemented in clinical situations. Further work is strongly recommended to overcome these limitations. Once the new LCD phantom and software are optimised, a strong recommendation is to implement this newly developed evaluation method as a tool to evaluate and optimise image quality of CT. This evaluation method of LCD detectability performance can also play an essential role in

providing a deep understanding of the effects of protocol parameters on CT image quality optimisation. With this method, LCD detectability performance of CT scanners and images could be standardised across different scanners, systems and manufacturers. The performance of different systems and technology of CT scanners could then be directly and simply evaluated and compared.

References

Abe, H, MacMahon, H, Engelmann, R, Li, Q, Shiraishi, J, Katsuragawa, S, Aoyama, M, Ishida, T, Ashizawa, K & Metz, C 2003, 'Computer-aided Diagnosis in Chest Radiography: Results of Large-Scale Observer Tests at the 1996–2001 RSNA Scientific Assemblies', *Radiographics*, vol. 23, no. 1, pp. 255-65.

Achenbach, S 2006, 'Computed tomography coronary angiography', *J Am Coll Cardiol*, vol. 48, no. 10, pp. 1919-28.

Achenbach, S, Anders, K & Kalender, W 2008, 'Dual-source cardiac computed tomography: image quality and dose considerations', *Eur Radiol*, vol. 18, no. 6, pp. 1188-98.

Aichinger, H, Dierker, J, Joite-Barfuß, S & Sabel, M 2012, 'Image quality and dose', in *Radiation exposure and image quality in x-ray diagnostic radiology*, 2nd edn, Springer, Erlangen, pp. 85-101.

Alsleem, H & Davidson, R 2012, 'Quality parameters and assessment methods of digital radiography images', *The Radiographer*, vol. 59, no. 2, pp. 46-55.

---- 2013, 'Factors affecting contrast-detail performance in computed tomography: a review', *JMIRS*, vol. 44, no. 2, pp. 62-70.

American Association of Physicists in Medicine 2006, *Report of AAPM Task Group 10, Report 93. Acceptance testing and quality control of photostimulable storage phosphor imaging systems*, College Park, MD: American Association of Physicists in Medicine. Available from http://aapm.org/pubs/reports/RPT_93.pdf.

ASTM International *Standard test method for measurement of computed tomography (CT) system performance.* http://www.astm.org/Standards/E1695.htm, viewed 10\3\2011.

Aufrichtig, R & Xue, P 2000, 'Dose efficiency and low-contrast detectability of an amorphous silicon x-ray detector for digital radiography', *Phys Med Biol*, vol. 45, no. 9, pp. 2653-69.

Australian Institute of Radiography 2007, *Guidelines for professional conduct for radiographers, radiation therapists and sonographers*, viewed 07\11\2013 <http://www.air.asn.au/airethics.php>.

Bacher, K, Smeets, P, De Hauwere, A, Voet, T, Duyck, P, Verstraete, K & Thierens, H 2006, 'Image quality performance of liquid crystal display systems: influence of display resolution, magnification and window settings on contrast-detail detection', *Eur J Radiol*, vol. 58, no. 3, pp. 471-9.

Bacher, K, Smeets, P, Vereecken, L, De Hauwere, A, Duyck, P, De Man, R, Verstraete, K & Thierens, H 2006, 'Image quality and radiation dose on digital chest imaging:

comparison of amorphous silicon and amorphous selenium flat-panel systems', *Am J Roentgenol*, vol. 187, no. 3, pp. 630-7.

Baker, M, Dong, F, Primak, A, Obuchowski, N, Einstein, D, Gandhi, N, Herts, B, Purysko, A, Remer, E & Vachani, N 2012, 'Contrast-to-Noise Ratio and Low-Contrast Object Resolution on Full-and Low-Dose MDCT: SAFIRE Versus Filtered Back Projection in a Low-Contrast Object Phantom and in the Liver', *Am J Roentgenol*, vol. 199, no. 1, pp. 8-18.

Bardo, E & Brown, P 2008, 'Cardiac multidetector computed tomography: basic physics of image acquisition and clinical applications', *Curr Cardiol Rev*, vol. 4, no. 3, pp. 231-43.

Barnes, J 1992, 'Characteristics and control of contrast in CT', *Radiographics*, vol. 12, no. 4, pp. 825-37.

Barreto, M, Schoenhagen, P, Nair, A, Amatangelo, S, Milite, M, Obuchowski, N, Lieber, M & Halliburton, S 2008, 'Potential of dual-energy computed tomography to characterize atherosclerotic plaque: ex vivo assessment of human coronary arteries in comparison to histology', *J Cardiovasc Comput Tomogr*, vol. 2, no. 4, pp. 234-42.

Barrett, F & Keat, N 2004, 'Artifacts in CT: Recognition and avoidance', *Radiographics*, vol. 24, no. 6, pp. 1679-91.

Bath, M 2010, 'Evaluating imaging systems: Practical applications', *Radiat Prot Dosimetry*, vol. 139, no. 1-3 pp. 26-36.

Bath, M & Mansson, L 2007, 'Visual grading characteristics (VGC) analysis: a non-parametric rank-invariant statistical method for image quality evaluation', *Br J Radiol*, vol. 80, no. 951, pp. 169-76.

Beister, M, Kolditz, D & Kalender, W 2012, 'Iterative reconstruction methods in X-ray CT', *Phys Med biol*, vol. 28, no. 2, pp. 94-108.

Berlin, L 1996, 'Malpractice issues in radiology. Perceptual errors', *Am J Roentgenol*, vol. 167, no. 3, pp. 587-90.

Berlin, L & Berlin, J 1995, 'Malpractice and radiologists in Cook County, IL: trends in 20 years of litigation', *Am J Roentgenol*, vol. 165, no. 4, pp. 781-8.

Berrington de Gonzalez, A, Mahesh, M, Kim, K, Bhargavan, M, Lewis, R, Mettler, F & Land, C 2009, 'Projected cancer risks from computed tomographic scans performed in the United States in 2007', *Archives of Internal Medicine*, vol. 169, no. 22, pp. 2071-7.

Bissonnette, P, Moseley, J & Jaffray, A 2008, 'A quality assurance program for image quality of cone-beam CT guidance in radiation therapy', *Med Phys*, vol. 35, no. 5, pp. 1807-15.

Borasi, G, Nitrosi, A, Ferrari, P & Tassoni, D 2003, 'On site evaluation of three flat panel detectors for digital radiography', *Med Phys*, vol. 30, no. 7, pp. 1719-31.

Bourne, R 2010, *Fundamentals of digital imaging in medicine*, 1st edn, Springer, Verlag.

Brenner, D & Hricak, H 2010, 'Radiation exposure from medical imaging: time to regulate?', *Jama*, vol. 304, no. 2, pp. 208-9.

Brooks, R & Di Chiro, G 1976, 'Statistical limitations in x-ray reconstructive tomography', *Med Phys*, vol. 3, no. 4, pp. 237-40.

Burgess, A 1999, 'The Rose model, revisited', *JOSA A*, vol. 16, no. 3, pp. 633-46.

Bushberg, J, Seibert, J, Leidholdt, E & Boone, J 2012, *The essential physics of medical imaging*, 3rd edn, Lippincott Williams & Wilkins, Philadelphia

Bushong, S 2013, *Radiologic Science for Technologists: Physics, Biology, and Protection*, 10th edn, Elsevier Mosby.

Carlton, R & Adler, K 2012, *Principles of radiographic imaging: an art and a science*, 5th edn, Delmar, Cengage Learning.

Chao, E, Toth, T, Bromberg, N, Williams, E, Fox, S & Carleton, D 2000, 'A statistical method of defining low contrast detectability', *Radiology*, vol. 217, no. Suppl S, pp. 162-.

Chotas, G, Dobbins, T & Ravin, E 1999, 'Principles of digital radiography with large-area, electronically readable detectors: a review of the basics', *Radiology*, vol. 210, no. 3, pp. 595-9.

Cierniak, R 2011, *X-Ray computed tomography in biomedical engineering*, Springer Poland.

Cowen, A, Davies, A & Kengyelics, S 2007, 'Advances in computed radiography systems and their physical imaging characteristics', *Clin Radiol*, vol. 62, no. 12, pp. 1132-41.

Cowen, A, Kengyelics, S & Davies, A 2008, 'Solid-state, flat-panel, digital radiography detectors and their physical imaging characteristics', *Clin Radiol*, vol. 63, no. 5, pp. 487-98.

Davidson, R 2007, 'Radiographic contrast-enhancement masks in digital radiography [PhD Thesis].Thesis location: http://hdl.handle.net/2123/1932.', The University of Sydney.

Davidson, R & Sim, J 2008, 'Computed radiography and dosimetry: some practical tips for dose optimization procedures', *JMIRS*, vol. 39, no. 3, pp. 109-14.

De Crop, A, Bacher, K, Van Hoof, T, Smeets, P, Smet, B, Vergauwen, M, Kiendys, U, Duyck, P, Verstraete, K, D'Herde, K & Thierens, H 2012, 'Correlation of Contrast-

Detail Analysis and Clinical Image Quality Assessment in Chest Radiography with a Human Cadaver Study', *Radiology*, vol. 262, no. 1, pp. 298-304.

De Hauwere, A, Bacher, K, Smeets, P, Verstraete, K & Thierens, H 2005, 'Analysis of image quality in digital chest imaging', *Radiat Prot Dosimetry*, vol. 117, no. 1-3, pp. 174-7.

Drose, W, Reese, D & Hornof, W 2008, 'Digital radiography artifacts', *Vet Radiol Ultrasound*, vol. 49, no. 4, pp. 321-32.

Eckstein, M, Abbey, C & Bochud, F 2000, 'A practical guide to model observers for visual detection in synthetic and natural noisy images', *Handbook of medical imaging*, vol. 1, pp. 593-628.

Engel-Hills, P 2006, 'Radiation protection in medical imaging', *Radiography*, vol. 12, no. 2, pp. 153-60.

Ertl-Wagner, B, Hoffmann, R, Bruning, R, Herrmann, K, Snyder, B, Blume, J & Reiser, M 2004, 'Multi–Detector Row CT Angiography of the Brain at Various Kilovoltage Settings1', *Radiology*, vol. 231, no. 2, pp. 528-35.

EXXIM Computing Corporation *Cone-Beam CT*, viewed 8/02/2012 <http://www.exxim-cc.com/cone-beam_ct.html>.

Fauber, T 2013, *Radiographic imaging & exposure*, 4th edn, Elsevier.

Faulkner, K & Moores, B 1984, 'Noise and contrast detection in computed tomography images', *Phys Med Biol*, vol. 29, no. 4, pp. 329-39.

Fishman, E 2007, 'Hot topics in CT', *Appl Radiol*, vol. 36, no. 11, pp. 4-9.

Flohr, G, McCollough, H, Bruder, H, Petersilka, M, Gruber, K, Süss, C, Grasruck, M, Stierstorfer, K, Krauss, B & Raupach, R 2006, 'First performance evaluation of a dual-source CT (DSCT) system', *Eur Radiol*, vol. 16, no. 2, pp. 256-68.

Flohr, T, Stierstorfer, K, Ulzheimer, S, Bruder, H, Primak, A & McCollough, C 2005, 'Image reconstruction and image quality evaluation for a 64-slice CT scanner with z-flying focal spot', *Med Phys*, vol. 32, no. 8, pp. 2536-47.

Funama, Y, Awai, K, Nakayama, Y, Kakei, K, Nagasue, N, Shimamura, M, Sato, N, Sultana, S, Morishita, S & Yamashita, Y 2005, 'Radiation Dose Reduction without Degradation of Low-Contrast Detectability at Abdominal Multisection CT with a Low–Tube Voltage Technique: Phantom Study1', *Radiology*, vol. 237, no. 3, pp. 905-10.

Geijer, H, Norrman, E & Persliden, J 2009, 'Optimizing the tube potential for lumbar spine radiography with a flat-panel digital detector', *Br J Radiol*, vol. 82, no. 973, pp. 62-8.

Gibson, D & Davidson, R 2012, 'Exposure creep in computed radiography: A longitudinal study', *Acad Radiol*, vol. 19, no. 4, pp. 458-62.

Giger, M, Chan, H & Boone, J 2008, 'Anniversary paper: History and status of CAD and quantitative image analysis: The role of medical physics and AAPM', *Med Phys*, vol. 35, no. 12, pp. 5799-820.

Giovanni, B, Ehsan, S, Marco, B, Andrea, N & Davide, T 2006, 'Contrast-detail analysis of three flat panel detectors for digital radiography', *Med Phys*, vol. 33, no. 6, pp. 1707-19.

Godoy, M, Heller, S, Naidich, D, Assadourian, B, Leidecker, C, Schmidt, B & Vlahos, I 2010, 'Dual-energy MDCT: Comparison of pulmonary artery enhancement on dedicated CT pulmonary angiography, routine and low contrast volume studies', *Eur J Radiol*, vol. 79, no. 2, pp. E11-E7.

Goldman, L 2007, 'Principles of CT: radiation dose and image quality', *J Nucl Med Technol*, vol. 35, no. 4, pp. 213-25.

Gomi, T, Koshida, K, Miyati, T, Miyagawa, J & Hirano, H 2006, 'An Experimental Comparison of Flat-Panel Detector Performance for Direct and Indirect Systems (Initial Experiences and Physical Evaluation)', *J Digit Imaging*, vol. 19, no. 4, pp. 362-70.

Goodenough, D & Weaver, K 'Factors related to low contrast resolution in CT scanners', *Computerized Radiology*, vol. 8, no. 5, pp. 297-308.

Green, D & Swets, J 1988, *Signal detection theory and psychophysics*, Reprint edn, Peninsula Publishing.

Gupta, A 2013, *Diagnostic Radiology: Recent Advances and Applied Physics in Imaging*, 2nd edn, JP Medical Ltd.

Gupta, R, Cheung, A, Bartling, S, Lisauskas, J, Grasruck, M, Leidecker, C, Schmidt, B, Flohr, T & Brady, T 2008, 'Flat-Panel Volume CT: Fundamental Principles, Technology, and Applications', *Radiographics*, vol. 28, no. 7, pp. 2009-22.

Haider, M, Amitai, M, Rappaport, D, O'Malley, M, Hanbidge, A, Redston, M, Lockwood, G & Gallinger, S 2002, 'Multi–Detector Row Helical CT in Preoperative Assessment of Small ($\leq$ 1.5 cm) Liver Metastases: Is Thinner Collimation Better? 1', *Radiology*, vol. 225, no. 1, pp. 137-42.

Hamer, O, VÖLK, M, Zorger, N, Feuerbach, S & Strotzer, M 2003, 'Amorphous silicon, flat-panel, x-ray detector versus storage phosphor-based computed radiography: contrast-detail phantom study at different tube voltages and detector entrance doses', *Invest Radiol*, vol. 38, no. 4, pp. 212-20.

Hanson, K 1977, 'Detectability in the presence of computed tomographic reconstruction noise', paper presented to Application of Optical Instrumentation in Medicine VI.

Hasegawa, B 1991, *The physics of medical x-ray imaging: (or the photon and me, how I saw the light)*, 2 edn, Medical Physics Publishing Corporation United States.

Hasegawa, B, Cacak, R, Mulvaney, J & Hendee, W 1982, 'Problems with contrast-detail curves for CT performance evaluation', *Am J Roentgenol*, vol. 138, no. 1, pp. 135-8.

Hasegawa, M, Sone, S, Takashima, S, Li, F, Yang, Z, Maruyama, Y & Watanabe, T 2000, 'Growth rate of small lung cancers detected on mass CT screening', *Br J Radiol*, vol. 73, no. 876, pp. 1252-9.

Hayton, A, Wallace, A, Edmonds, K & Tingey, D 2010, *Application of the European DOSE DATAMED methodology and reference doses for the estimate of Australian MDCT effective dose (mSv). In Proceedings of the Third European IRPA Congress 2010*, ARPANSA, Helsinki.

Hendee, W & Ritenour, E 2002, *Medical imaging physics*, 4th edn, Am J Roentgenol, John Wiley & Sons, Inc., New York.

Hernandez-Giron, I, Geleijns, J, Calzado, A & Veldkamp, W 2011, 'Automated assessment of low contrast sensitivity for CT systems using a model observer', *Med Phys*, vol. 38, no. S1, pp. S25-S35.

Heyer, C, Mohr, P, Lemburg, S, Peters, S & Nicolas, V 2007, 'Image Quality and Radiation Exposure at Pulmonary CT Angiography with 100-or 120-kVp Protocol: Prospective Randomized Study1', *Radiology*, vol. 245, no. 2, pp. 577-83.

Hill, R, Kuncic, Z & Baldock, C 2010, 'The water equivalence of solid phantoms for low energy photon beams', *Med Phys*, vol. 37, no. 8, pp. 4355-63.

Honey, I & Mackenzie, A 2009, 'Artifacts found during quality assurance testing of computed radiography and digital radiography detectors', *J Digit Imaging*, vol. 22, no. 4, pp. 383-92.

Hsiao, E, Rybicki, F & Steigner, M 2010, 'CT coronary angiography: 256-slice and 320-detector row scanners', *Curr Cardiol Rep*, vol. 12, no. 1, pp. 68-75.

Hsieh, J 2009, *Computed tomography: Principles, design, artifacts, and recent advances*, 2nd edn, SPIE, Bellingham.

Hsieh, J & Toth, T 2008, ' Low-Contrast Detectability for X-Ray Computed Tomography', *Med Phys*, vol. 35, no. 6, pp. 2645-.

Hu, H 1999, 'Multi-slice helical CT: scan and reconstruction', *Med Phys*, vol. 26, no. 1, pp. 5-18.

Huda, W, Lieberman, K, Chang, J & Roskopf, M 2004, 'Patient size and x-ray technique factors in head computed tomography examinations. II. Image quality', *Med Phys*, vol. 31, no. 3, pp. 595-601.

Huda, W, Scalzetti, E & Levin, G 2000, 'Technique Factors and Image Quality as Functions of Patient Weight at Abdominal CT', *Radiology*, vol. 217, no. 2, pp. 430-5.

Hurlock, G, Higashino, H & Mochizuki, T 2009, 'History of cardiac computed tomography: single to 320-detector row multislice computed tomography', *Int J Cardiovasc Imaging*, vol. 25, no. Suppl 1, pp. 31-42.

Imai, K, Ikeda, M, Enchi, Y & Niimi, T 2009, 'Statistical characteristics of streak artifacts on CT images: Relationship between streak artifacts and mA s values', *Med Phys*, vol. 36, no. 2, pp. 492-9.

International Commission on Radiation Units and Measurements (ICRU) 1989, *Tissue substitutes in radiation dosimetry and measurement*, 44, Bethesda (MD).

International Commission on Radiological Protection 2007, *Managing patient dose in multi-detector computed tomography (MDCT). ICRP Publication 102*, vol. 37, Annals of the ICRP, Elsevier, Amsterdam.

Judy, F, Balter, S, Bassano, D, McCullough, C, Payne, T & Rothenberg, L 1977, *Phantoms for performance evaluation and quality assurance of CT scanners*, 1888340045, AAPM, Chicago.

Kalender, W & Khadivi, K 2011, *Computed tomography: fundamentals, system technology, image quality, applications*, 3rd edn, Med phys, Publicis Publishing Erlangen.

Kalra, M 2008, *MDCT: from protocols to practice*, revised edn, Springer Verlag.

Kanal, K, Chung, J, Wang, J, Bhargava, P, Kohr, J, Shuman, W & Stewart, B 2011, 'Image Noise and Liver Lesion Detection With MDCT: A Phantom Study', *Am J Roentgenol*, vol. 197, no. 2, pp. 437-41.

Kasap, S, Frey, J, Belev, G, Tousignant, O, Mani, H, Greenspan, J, Laperriere, L, Bubon, O, Reznik, A & DeCrescenzo, G 2011, 'Amorphous and Polycrystalline Photoconductors for Direct Conversion Flat Panel X-Ray Image Sensors', *Sensors*, vol. 11, no. 5, pp. 5112-57.

Kato, Y, Nair, S, Sano, H, Sanjaykumar, M, Katada, K, Hayakawa, M & Kanno, T 2002, 'Multi-slice 3D-CTA–an improvement over single slice helical CTA for cerebral aneurysms', *Acta Neurochir*, vol. 144, no. 7, pp. 715-22.

Keat, N & Edyvean, S 2003, *Low contrast detail detectability measurements on multi-slice CT scanners*, RSNA, Chicago.

Khan, A, Khosa, F, Nasir, K, Yassin, A & Clouse, M 2011, 'Comparison of radiation dose and image quality: 320-MDCT versus 64-MDCT coronary angiography', *Am J Roentgenol*, vol. 197, no. 1, pp. 163-8.

Kitajima, K, Maeda, T, Ohno, Y, Yoshikawa, T, Konishi, M, Kanda, T, Onishi, Y, Matsumoto, K, Koyama, H & Takenaka, D 2011, 'Capability of abdominal 320-

detector row CT for small vasculature assessment compared with that of 64-detector row CT', *Eur J Radiol*, vol. 80, no. 2, pp. 219-23.

Korner, M, Weber, C, Wirth, S, Pfeifer, K, Reiser, M & Treitl, M 2007, 'Advances in digital radiography: Physical principles and system overview', *Radiographics*, vol. 27, no. 3, pp. 675-86.

Krupinski, E & Berbaum, K 2009, 'The medical image perception society update on key issues for image perception research', *Radiology*, vol. 253, no. 1, pp. 230-3.

Krupinski, E, Williams, B, Andriole, K, Strauss, J, Applegate, K, Wyatt, M, Bjork, S & Seibert, A 2007, 'Digital radiography image quality: Image processing and display', *J Am Coll Radiol*, vol. 4, no. 6, pp. 389-400.

Lanca, L & Silva, A 2009a, 'Digital radiography detectors - a technical overview: Part 2', *Radiography*, vol. 15, no. 2, pp. 134-8.

---- 2009b, 'Digital radiography detectors – A technical overview: Part 1', *Radiography*, vol. 15, no. 1, pp. 58-62.

Launders, J, Cowen, A, Bury, R & Hawkridge, P 2001, 'Towards image quality, beam energy and effective dose optimisation in digital thoracic radiography', *Eur Radiol*, vol. 11, no. 5, pp. 870-5.

Ledenius, K, Gustavsson, M, Johansson, S, Stalhammar, F, Wiklund, L & Thilander-Klang, A 2009, 'Effect of tube current on diagnostic image quality in paediatric cerebral multidetector CT images', *Br J Radiol*, vol. 82, no. 976, pp. 313-20.

Leng, S, Yu, L, Zhang, Y, Carter, R, Toledano, A & McCollough, C 2013, 'Correlation between model observer and human observer performance in CT imaging when lesion location is uncertain', *Med Phys*, vol. 40, no. 8, p. 081908.

Levison, M & Restle, F 1968, 'Invalid results from the method of constant stimuli', *Perception & Psychophysics*, vol. 4, no. 2, pp. 121-2.

Lin, C-H, Lin, C-Y, Cheng, Y-J & Chan, Y-K 2012, 'An Automatic Evaluation System for Contrast-Detail Phantom Images in Digital Radiography', *Int J Imaging Syst Technol*, vol. 22, no. 4, pp. 15-26.

Lu, Z, Nickoloff, E, So, J & Dutta, A 2003, 'Comparison of computed radiography and film/screen combination using a contrast-detail phantom', *J Appl Clin Med Phys*, vol. 4, no. 1, pp. 91-8.

Ludewig, E, Richter, A & Frame, M 2010, 'Diagnostic imaging-evaluating image quality using visual grading characteristic (VGC) analysis', *Vet Res Commun*, vol. 34, no. 5, pp. 473-9.

MacMahon, H, Austin, J, Gamsu, G, Herold, C, Jett, J, Naidich, D, Patz, E & Swensen, S 2005, 'Guidelines for management of small pulmonary nodules detected on CT

scans: a statement from the Fleischner Society', *Radiology*, vol. 237, no. 2, pp. 395-400.

Mahesh, M 2009, *MDCT Physics: The basics-technology, image quality and radiation dose*, 1st edn, Lippincott Williams & Wilkins, Philadelphia.

Mansson, L 2000, 'Methods for the evaluation of image quality: a review', *Radiat Prot Dosimetry*, vol. 90, no. 1-2, pp. 89-99.

Marin, D, Nelson, R, Barnhart, H, Schindera, S, Ho, L, Jaffe, T, Yoshizumi, T, Youngblood, R & Samei, E 2010, 'Detection of Pancreatic Tumors, Image Quality, and Radiation Dose during the Pancreatic Parenchymal Phase: Effect of a Low-Tube-Voltage, High-Tube-Current CT Technique-Preliminary Results', *Radiology*, vol. 256, no. 2, pp. 450-9.

Marin, D, Nelson, R, Rubin, G & Schindera, S 2011, 'Body CT: Technical Advances for Improving Safety', *Am J Roentgenol*, vol. 197, no. 1, pp. 33-41.

Martinsen, A, Saether, H, Olsen, D, Wolff, P & Skaane, P 2010, 'Improved image quality of low-dose thoracic CT examinations with a new postprocessing software*', *J of Appl Clin Med Phys*, vol. 11, no. 3.

McEntee, M, Frawley, H & Brennan, P 2007, 'A comparison of low contrast performance for amorphous silicon/caesium iodide direct radiography with a computed radiography: A contrast detail phantom study', *Radiography*, vol. 13, no. 2, pp. 89-94.

Miller, J, Rochitte, C, Dewey, M, Niinuma, H, Arbab-Zadeh, A, Gottlieb, I, Paul, N, Clouse, M, Shapiro, E, Hoe, J, Bush, D, Lardo, A, Roos, A, Cox, C, Texter, J, Vaver, A, Lima, J & Brinker, J 2010, 'Quantitative and Diagnostic Accuracy of 64-mdcta for segmental coronary artery stenosis detection: results from the core-64 multicenter international study', *JACC*, vol. 55, no. 10A, pp. E757-E9.

Miracle, A & Mukherji, S 2009, 'Conebeam CT of the head and neck, part 1: physical principles', *Am J Neuroradiol*, vol. 30, no. 6, pp. 1088-95.

Morgan, C & Miller, M 1983, *Basic principles of computed tomography*, University Park Press, Baltimore.

Neitzel, U 2005, 'Status and prospects of digital detector technology for CR and DR', *Radiat Prot Dosimetry*, vol. 114, no. 1-3, pp. 32-8.

Niimi, T, Imai, K, Maeda, H & Ikeda, M 2007, 'Information loss in visual assessments of medical images', *Eur J Radiol*, vol. 61, no. 2, pp. 362-6.

Obuchowski, N 2003, 'Receiver operating characteristic curves and their use in radiology', *Radiology*, vol. 229, no. 1, pp. 3-8.

Olaf, D & Wolfgang, S 2009, 'Optimization of Exposure Factors and Image Quality for Computed Radiography', in *World Congress on Medical Physics and Biomedical Engineering*, Springer vol. 25/2, pp. 251-4.

Orzel, J & Berlin, L 2003, 'Correction of interpretive errors', *Am J Roentgenol*, vol. 180, no. 5, pp. 1477-.

Ozgun, A, Rollven, E, Blomqvist, L, Bremmer, S, Odh, R & Fransson, A 2005, 'Polyp detection with MDCT: A phantom-based evaluation of the impact of dose and spatial resolution', *Am J Roentgenol*, vol. 184, no. 4, pp. 1181-88.

Pallant, J 2013, *SPSS Survival Manual: A step by step guide to data analysis using IBM SPSS*, Maidenhead: McGraw-Hill.

Park, H, Jung, S, Lee, Y, Cho, W, Do, K, Kim, S & Kim, K 2009, 'The relationship between subjective and objective parameters in CT phantom image evaluation', *Korean J Radiol*, vol. 10, no. 5, pp. 490-5.

Park, S, Clarkson, E, Kupinski, M & Barrett, H 2005, 'Efficiency of the human observer detecting random signals in random backgrounds', *J Opt Soc Am A Opt Image Sci Vis*, vol. 22, no. 1, pp. 3-16.

Pascoal, A, Lawinski, C, Honey, I & Blake, P 2005, 'Evaluation of a software package for automated quality assessment of contrast detail images—comparison with subjective visual assessment', *Phys Med Biol*, vol. 50, no. 23, pp. 5743-57.

Paul, N, Blobel, J, Kashani, H, Rice, M & Ursani, A 2010, 'Quantification of arterial plaque and lumen density with MDCT', *Med Phys*, vol. 37, no. 8, pp. 4227-37.

Peldschus, K, Herzog, P, Wood, S, Cheema, J, Costello, P & Schoepf, U 2005a, 'Computer-Aided Diagnosis as a Second Reader*', *Chest*, vol. 128, no. 3, p. 1517.

Peldschus, K, Herzog, P, Wood, S, Cheema, J, Costello, P & Schoepf, U 2005b, 'Computer-aided diagnosis as a second reader: spectrum of findings in CT studies of the chest interpreted as normal', *Chest*, vol. 128, no. 3, pp. 1517-23.

Rahn, J, Lemmi, F, Lu, J, Mei, P, Apte, R, Street, R, Lujan, R, Weisfield, R & Heanue, J 1999, 'High resolution X-ray imaging using amorphous silicon flat-panel arrays', *Nuclear Science*, vol. 46, no. 3, pp. 457-61.

Ramaseshan, R, Kohli, K, Cao, F & Heaton, R 2008, 'Dosimetric evaluation of Plastic Water Diagnostic Therapy', *J Appl Clin Med Phys*, vol. 9, no. 2, pp. 98-111.

Ranger, N, Samei, E, Dobbins, J & Ravin, C 2007, 'Assessment of Detective Quantum Efficiency: Intercomparison of a Recently Introduced International Standard with Prior Methods', *Radiology*, vol. 243, no. 3, pp. 785-95.

Reiner, B, Siegel, E, Siddiqui, K & Musk, A 2006, 'Quality assurance: The missing link', *Radiology*, vol. 238, no. 1, pp. 13-5.

Reiser, I, Lu, Z & Nishikawa, R 2012, 'Contrast-To-Noise Ratio Is Not an Appropriate Measure of CT Image Quality When Comparing Different Iterative Reconstruction Algorithms', <http://www.aapm.org/meetings/2012AM/PRAbs.asp?mid=68&aid=19367>.

Romans, L 2011, *Computed Tomography for Technologists: A comprehensive Text*, 1st edn, Lippincott Williams & Wilkins, Philadelphia.

Rubin, G 2003, '3-D imaging with MDCT', *Eur J Radiol*, vol. 45, no. S1, pp. S37-S41.

Rubin, G & Rofsky, N 2012, *CT and MR angiography: comprehensive vascular assessment*, Lippincott Williams & Wilkins, Philadelphia.

Samei, E 2003a, 'Performance of digital radiographic detectors: quantification and assessment methods', *Advances in digital radiography: RSNA*, pp. 37-47.

Samei, E 2003b, 'Performance of digital radiography detectors: factors affecting sharpness and noise', *Advances in digital radiography: RSNA*, pp. 49–61.

Samei, E & Flynn, M 2003, 'An experimental comparison of detector performance for direct and indirect digital radiography systems', *Med Phys*, vol. 30, no. 4, pp. 608-22.

Samei, E, Ranger, N & Delong, D 2008, 'A comparative contrast-detail study of five medical displays', *Med Phys*, vol. 35, no. 4, pp. 1358-64.

Samei, E, Ranger, N, Dobbins, J & Chen, Y 2006, 'Intercomparison of methods for image quality characterization. I. Modulation transfer function', *Med Phys*, vol. 33, no. 5, pp. 1454-65.

Samei, E, Ranger, N, MacKenzie, A, Honey, I, Dobbins, J & Ravin, C 2008, 'Detector or System? Extending the Concept of Detective Quantum Efficiency to Characterize the Performance of Digital Radiographic Imaging Systems', *Radiology*, vol. 249, no. 3, pp. 926-37.

---- 2009, 'Effective DQE (eDQE) and speed of digital radiographic systems: An experimental methodology', *Med Phys*, vol. 36, no. 8, pp. 3806–17.

Samei, E, Seibert, A, Andriole, K, Badano, A, Crawford, J, Reiner, B, Flynn, M & Chang, P 2004, 'AAPM/RSNA tutorial on equipment selection: PACS equipment overview', *Radiographics*, vol. 24, no. 1, pp. 313-34.

Schaefer-Prokop, C, De Boo, D, Uffmann, M & Prokop, M 2009, 'DR and CR: Recent advances in technology', *Eur J Radiol*, vol. 72, no. 2, pp. 194-201.

Schaefer-Prokop, C, Neitzel, U, Venema, H, Uffmann, M & Prokop, M 2008, 'Digital chest radiography: An update on modern technology, dose containment and control of image quality', *Eur Radiol*, vol. 18, no. 9, pp. 1818-30.

Schindera, S, Hareter, L, Raible, S, Torrente, J, Rusch, O, Rosskopf, A, Marin, D, Vock, P & Szucs-Farkas, Z 2012, 'Effect of Tumor Size and Tumor-to-Liver Contrast of Hypovascular Liver Tumors on the Diagnostic Performance of Hepatic CT Imaging', *Invest Radiol*, vol. 47, no. 3, pp. 197-201.

Schindera, S, Nelson, R, Mukundan, S, Paulson, E, Jaffe, T, Miller, C, DeLong, D, Kawaji, K, Yoshizumi, T & Samei, E 2008, 'Hypervascular Liver Tumors: Low Tube Voltage, High Tube Current Multi–Detector Row CT for Enhanced Detection— Phantom Study', *Radiology*, vol. 246, no. 1, pp. 125-32.

Seeram, E 2009, *Computed tomography: physical principles, clinical applications and quality assurance*, 3rd edn, Saunders/Elsevier.

Seibert, J 2004, 'Tradeoffs between image quality and dose', *Pediatr Radiol*, vol. 34, no. 3, pp. 183-95.

---- 2009, 'Digital radiography: The bottom line comparison of CR and DR technology', *Appl Radiol*, vol. 38, no. 5, pp. 21-8.

Shet, N, Chen, J & Siegel, E 2011, 'Continuing challenges in defining image quality', *Pediatr Radiol*, vol. 41, no. 5, pp. 582-7.

Shetty, C, Barthur, A, Kambadakone, A, Narayanan, N & Kv, R 2011, 'Computed Radiography Image Artifacts Revisited', *Am J Roentgenol*, vol. 196, no. 1, pp. W37-W47.

Singh, S & Kalra, M 2012, 'Scan Parameters and CT Radiation Dose', in D Tack, MK Kalra & PA Gevenois (eds), *Radiation Dose from Multidetector CT*, 2nd edn, Springer, Berlin Heidelberg, pp. 119-29.

Smith-Bindman, R 2010, 'Is computed tomography safe', *N Engl J Med*, vol. 363, no. 1, pp. 1-4.

Smith-Bindman, R, Miglioretti, D, Johnson, E, Lee, C, Feigelson, H, Flynn, M, Greenlee, R, Kruger, R, Hornbrook, M & Roblin, D 2012, 'Use of diagnostic imaging studies and associated radiation exposure for patients enrolled in large integrated health care systems, 1996-2010', *Jama*, vol. 307, no. 22, pp. 2400-9.

Smith, S 1997, *The Scientist and Engineer's Guide to Digital Signal Processing*, California Technical Publishing.

Spahn, M 2005, 'Flat detectors and their clinical applications', *Eur Radiol*, vol. 15, no. 9, pp. 1934-47.

Sprawls, P 1992, 'AAPM tutorial. CT image detail and noise', *Radiographics*, vol. 12, no. 5, pp. 1041-6.

---- 1995, *Physical principles of medical imaging*, 2nd edn, Medical Physics Publishing Corporation, Gaithersburg.

Strang, J & Dogra, V 2006, *Body CT secrets*, 1st edn, Secrets series, Mosby Elsevier, Philadelphia.

Suess, C, Kalender, W & Coman, J 1999, 'New low-contrast resolution phantoms for computed tomography', *Med Phys*, vol. 26, no. 2, pp. 296-302.

Sun, J, Zhang, Z, Lu, B, Yu, W, Yang, Y, Zhou, Y, Wang, Y & Fan, Z 2008, 'Identification and Quantification of Coronary Atherosclerotic Plaques: A Comparison of 64-MDCT and Intravascular Ultrasound', *Am J Roentgenol*, vol. 190, no. 3, pp. 748-54.

Sundaram, P, Beaulieu, C, Paik, D, Schraedley-Desmond, P & Napel, S 2003, 'CT colonography: Does improved z resolution help computer-aided polyp detection?', *Med Phys*, vol. 30, no. 10, pp. 2663-74.

Swets, J, Green, D, Getty, D & Swets, J 1978, 'Signal detection and identification at successive stages of observation', *Percept Psychophys*, vol. 23, no. 4, pp. 275-89.

Taguchi, K & Anno, H 2000, 'High temporal resolution for multislice helical computed tomography', *Med Phys*, vol. 27, no. 5, pp. 861-72.

Tapiovaara, M 2008, 'Review of relationships between physical measurements and user evaluation of image quality', *Radiat prot dosimetry*, vol. 129, no. 1-3, pp. 244-8.

Tapiovaara, M & Sandborg, M 2004, 'How should low-contrast detail detectability be measured in fluoroscopy?', *Med Phys*, vol. 31, no. 9, pp. 2564-76.

The International Society of Radiographers and Radiological Technologists 2004, *Guidelines for the education of entry-level professional practice in medical radiation sciences*, viewed 15/07/2013 <http://www.isrrt.org/isrrt/Education_Standards.asp>.

Theocharopoulos, N, Damilakis, J, Perisinakis, K & Gourtsoyiannis, N 2007, 'Energy imparted-based estimates of the effect of z overscanning on adult and pediatric patient effective doses from multi-slice computed tomography', *Med Phys*, vol. 34, no. 4, pp. 1139-52.

Thijssen, M, Thijssen, H, Merx, J, Lindeijer, J & Bijkerk, K 1989, 'A definition of image quality: The image quality figure', *BIR report*, vol. 20, pp. 29-34.

Thijssen, M, Thijssen, H, Merx, J & Woensel, M 1988, 'Quality analysis of DSA equipment', *Neuroradiology*, vol. 30, no. 6, pp. 561-8.

Thilander-Klang, A, Ledenius, K, Hansson, J, Sund, P & Båth, M 2010, 'Evaluation of subjective assessment of the low-contrast visibility in constancy control of computed tomography', *Radiat prot dosimetry*, vol. 139, no. 1-3, pp. 449-54.

Toth, T 2012, 'Image Quality in CT: Challenges and Perspectives', in D Tack, MK Kalra & PA Gevenois (eds), *Radiation Dose from Multidetector CT*, 2 edn, Springer Berlin Heidelberg, pp. 81-100.

Tsai, D, Lee, Y & Matsuyama, E 2008, 'Information entropy measure for evaluation of image quality', *J Digit Imaging*, vol. 21, no. 3, pp. 338-47.

Uchida, S & Tsai, D 1978, 'Evaluation of radiographic images by entropy: Application to development process', *Jpn J Appl Phys*, vol. 17, pp. 2029-34.

Uffmann, M, Neitzel, U, Prokop, M, Kabalan, N, Weber, M, Herold, C & Schaefer-Prokop, C 2005, 'Flat-Panel–Detector Chest Radiography: Effect of Tube Voltage on Image Quality', *Radiology*, vol. 235, no. 2, pp. 642-50.

Uffmann, M & Schaefer-Prokop, C 2009, 'Digital radiography: The balance between image quality and required radiation dose', *Eur J Radiol*, vol. 72, no. 2, pp. 202-8.

Uffmann, M, Schaefer-Prokop, C, Neitzel, U, Weber, M, Herold, J & Prokop, M 2004, 'Skeletal applications for flat-panel versus storage-phosphor radiography: Effect of exposure on detection of low-contrast details', *Radiology*, vol. 231, no. 2, pp. 506-14.

van der Molen, A & Geleijns, J 2007, 'Overranging in Multisection CT: Quantification and Relative Contribution to Dose—Comparison of Four 16-Section CT Scanners', *Radiology*, vol. 242, no. 1, pp. 208-16.

van der Wall, E, de Graaf, F, van Velzen, J, Jukema, J, Bax, J & Schuijf, J 2012, '320-row CT: does beat-to-beat motion of the coronary arteries affect image quality?', *Int J Cardiovasc Imaging*, vol. 28, no. 1, pp. 147-51.

Van Uitert, R, Summers, R, White, J, Deshpande, K, Choi, J & Pickhardt, P 2008, 'Temporal and Multiinstitutional Quality Assessment of CT Colonography', *Am J Roentgenol*, vol. 191, no. 5, pp. 1503-8.

Veldkamp, W, Kroft, L & Geleijns, J 2009, 'Dose and perceived image quality in chest radiography', *Eur J Radiol*, vol. 72, no. 2, pp. 209-17.

Verdun, F, Denys, A, Valley, J, Schnyder, P & Meuli, R 2002, 'Detection of Low-Contrast Objects: Experimental Comparison of Single–and Multi–Detector Row CT with a Phantom', *Radiology*, vol. 223, no. 2, pp. 426-31.

von Falck, C, Galanski, M & Shin, H 2010, 'Informatics in Radiology: Sliding-Thin-Slab Averaging for Improved Depiction of Low-Contrast Lesions with Radiation Dose Savings at Thin-Section CT', *Radiographics*, vol. 30, no. 2, pp. 317-26.

Warren-Forward, H, Arthur, L, Hobson, L, Skinner, R, Watts, A, Clapham, K, Lou, D & Cook, A 2007, 'An assessment of exposure indices in computed radiography for the posterior-anterior chest and the lateral lumbar spine', *Br J Radiol*, vol. 80, no. 949, pp. 26-31.

Warren, R 1984, 'Detectability of low-contrast features in computed tomography', *Phys Med Biol*, vol. 29, no. 1, pp. 1-13.

Weatherburn, G, Ridout, D, Strickland, N, Robins, P, Glastonbury, C, Curati, W, Harvey, C & Shadbolt, C 2003, 'A comparison of conventional film, CR hard copy and PACS soft copy images of the chest: Analyses of ROC curves and inter-observer agreement', *Eur J Radiol*, vol. 47, no. 3, pp. 206-14.

Wedegartner, U, Lorenzen, M, Nagel, H, Koops, A, Weber, C, Nolte-Ernsting, C, Schoder, V & Adam, G 2004, 'Image quality of thin- and thick-slice MSCT reconstructions in low-contrast objects (liver lesions) with equal doses', *Rofo*, vol. 176, no. 11, pp. 1676-82.

Williams, B, Krupinski, A, Strauss, J, Breeden, K, Rzeszotarski, S, Applegate, K, Wyatt, M, Bjork, S & Seibert, A 2007, 'Digital radiography image quality: Image acquisition', *J Am Coll Radiol*, vol. 4, no. 6, pp. 371-88.

Willis, C, Thompson, S & Shepard, S 2004, 'Artifacts and misadventures in digital radiography', *Appl Radiol*, vol. 33, no. 1, pp. 11-21.

Winklehner, A, Karlo, C, Puippe, G, Schmidt, B, Flohr, T, Goetti, R, Pfammatter, T, Frauenfelder, T & Alkadhi, H 2011, 'Raw data-based iterative reconstruction in body CTA: evaluation of radiation dose saving potential', *Eur Radiol*, vol. 21, no. 12, pp. 2521-6.

Wormanns, D, Diederich, S, Lentschig, M, Winter, F & Heindel, W 2000, 'Spiral CT of pulmonary nodules: interobserver variation in assessment of lesion size', *Eur Radiol*, vol. 10, no. 5, pp. 710-3.

Wunderlich, A & Noo, F 2008, 'Image covariance and lesion detectability in direct fan-beam x-ray computed tomography', *Phys Med Biol*, vol. 53, no. 10, pp. 2471-93.

Xia, Q 2007, *Dedicated computed tomography of the breast: Image processing and its impact on breast mass detectability*, ProQuest.

Yamaguchi, M, Fujita, H, Bessho, Y, Inoue, T, Asai, Y & Murase, K 2010, 'Investigation of optimal display size for detecting ground-glass opacity on high resolution computed tomography using a new digital contrast-detail phantom', *Eur J Radiol*, vol. 80, no. 3, pp. 845-50.

Yoo, S, Kim, Y, Hammoud, R, Elder, E, Pawlicki, T, Guan, H, Fox, T, Luxton, G, Yin, F & Munro, P 2006, 'A quality assurance program for the on-board imager', *Med Phys*, vol. 33, no. 11, pp. 4431-47.

Yu, L, Liu, X, Leng, S, Kofler, J, Ramirez-Giraldo, J, Qu, M, Christner, J, Fletcher, J & McCollough, C 2009, 'Radiation dose reduction in computed tomography: Techniques and future perspective', *Imaging Med*, vol. 1, no. 1, pp. 65-84.

Zarb, F, Rainford, L & McEntee, M 2010, 'Image quality assessment tools for optimization of CT images', *Radiography*, vol. 16, no. 2, pp. 147-53.

Zhang, C, Zhang, Z, Yan, Z, Xu, L, Yu, W & Wang, R 2011, '320-row CT coronary angiography: effect of 100-kV tube voltages on image quality, contrast volume, and radiation dose', *Int J Cardiovasc Imaging*, vol. 27, no. 7, pp. 1059-68.

Appendices

Appendix 1   Publication arising from this work

Appendix 1a   Alsleem, H & Davidson, R 2012, 'Quality parameters and assessment methods of digital radiography images', *The Radiographer*, vol. 59, no. 2, pp. 46-55

Appendix 1b   Alsleem, H & Davidson, R 2013, 'Factors affecting contrast-detail performance in computed tomography: a review', *JMIRS*, vol. 44, no. 2, pp. 62-70

 Appendix 1c   Alsleem, H & Davidson, R 2013, Effects of radiographic techniques (kVp and mAs) on the low contrast-detail detectability performance of different digital radiography systems. *Radiologic Technology* (accepted for publication, 2013)

Appendix 1a   Publication arising from this work (1)

Quality parameters and assessment methods of digital radiography images

Abstract This article reviews the parameters that characterise the image quality of digital radiography and the available evaluation methods that are used to measure these parameters. The article also discusses the factors that affect each parameter of image quality. Digital imaging systems are the most commonly utilised technology in the field of radiology. Screen-film radiography systems are almost replaced by digital radiography. The data acquisition and image processing principles of digital radiography differ from that of conventional radiography. The required exposure factors for each digital radiography system are not the same. Therefore, the image quality should be optimised while lower radiation dose is maintained according to the properties of the specific imaging system. Distinguishing image quality parameters and understanding the factors that control each image quality parameter are essential to optimise and maintain image quality and to reduce radiation dose to the patient. The degree of factors effects on the images of different digital radiography types and systems are not exactly same. There are different methods and approaches that are used to evaluate the quality of medical images and to assess the performance of imaging systems and each has its own rewards and limits. Therefore, these methods should be utilised and employed according to their aptitudes to improve imaging process.

Keywords: digital radiography, evaluation methods, image quality parameters.

H Alsleem[1]
MSc, BSc

R Davidson[2]
PhD, MAppSc(MI), BBus, FIR

[1]Discipline of Medical Radiation
RMIT University,
Bundoora,
Victoria 3083,
Australia.

[2]Discipline of Medical Radiation
Science,
School of Dentistry and Health
Sciences,
Faculty of Science,
Charles Sturt University,
Wagga Wagga 2678,
Australia.

Correspondence to
haney.alsleem@rmit.edu.au

Figure 1: The parameters of image quality and the influence factors of each parameter.

Introduction

Digital images have vital advantages in health services. Image quality has been improved and patient radiation dose reduced by the introduction of digital imaging systems including computed radiography (CR) and digital radiography (DR). In addition, digital imaging modalities have revolutionised communication between radiographers, radiologists, and physicians.[1,2]

However, CR and DR also have some limitations such as higher initial cost, particularly for DR. In addition, consistent feedback that is required to obtain optimal acquisition may not be available for technologists. Potential increase in radiation dose, due to wide dynamic range of digital systems, is also

a potential drawback of CR and DR. Patients may be overexposed with more radiation than is required for a diagnostically sufficient image. Diagnostic information may be suppressed as a result of suboptimum image processing.[2,3] Therefore, it is essential to regularly investigate image quality to ensure correct and accurate image interpretation.

No clinical detector can perfectly absorb all the incident x-ray photons. Some x-ray photons pass straight through the x-ray detector. Others that are absorbed may be re-emitted and exit the detector. As a result, there is loss in primary information. Additionally, noise arises from the amorphous array and readout electronics of the detector. These factors degrade image quality.[4] Reliable diagnosis requires regular maintenance of the technology employed and alongside regular clinical evaluation of image quality.[5] The criteria of optimum image quality should be determined and recognised.[5]

The purpose of this review is to provide an overview of the parameters and their factors that influence image quality and to recognise the different evaluation methods and their corresponding approaches that are used to assess image quality and system performance.

Image quality parameters

There are several parameters that characterise the quality of digital images. Resolution, noise, and artefacts are the main parameters of image quality.[6] Some studies include blur factors which relate so far to the spatial resolution.[7,8] Figure 1 summarises these parameters and their influences.

Resolution describes the ability of medical imaging process to discriminate adjacent structures in organ tissues being examined. Signal from detected photon should be recorded with sufficient resolution in space, intensity and possibly time to produce a digital image that enables a medical interpretation of tissue structure and function. Therefore resolution is of three main categories, spatial resolution (space), contrast resolution (intensity) and temporal resolution (time).[10] However, temporal resolution is more related to the digital radiography application of fluoroscopy, therefore it will be not discussed in this paper.

Spatial resolution and/or blur

Spatial resolution refers to the ability of imaging system to detect and discriminate small objects that are close together.[2] The size of pixels and the spacing between them (the pitch) define the maximum spatial resolution. The smaller pixel sizes the higher the spatial resolution. However, this is not always true because the spatial resolution is influenced by other causes such as blur factors.[9,10] Image processing alters image spatial resolution however the image noise is excessively increased.[9] Zooming or targeting and scanned field of view functions influence spatial resolution.[2]

Measurement methods including the point-spread function (PSF), line spread function (LSF) and the modular transfer function (MTF), are used to quantify and evaluate spatial resolution.[11]

Spatial resolution is affected by four blur factors, namely subject blur, geometric blur, motion blur, and receptor blur.[13] Image blur refers to the element of blurring to boundaries in the object (patient). Sharp image describes the well-defined boundaries of the object (patient).[12]

Subject blur is caused by object shape or/and structure composition. This factor is also called object blur.[12]

Geometric blur results from the geometry of the image-construction procedures. The main influences of this factor are focal spot size of the x-ray tube, the distance between the x-ray source and patient and between the patient and image receptor. Border-blur increases with the increasing of focal spot size and with increases in the distance between patient and image receptor. Unequal magnification of different organ structures cause distortion in the radiographic images, which is called image distortion. For example, tissues close to the image receptor are magnified less than those further away.[8] When the distance between the patient and image receptor increases, blur factor decreases.[12]

Motion blur is the most problematic blur factor. When motion occurs, the boundaries of patient structures will move from their actual position during image processing. Consequently, the boundaries are blurred in the image. This motion originates from anatomic region being imaged and it can be either voluntary action of the patient or involuntary physiologic process. Voluntary motion can mostly be controlled by applying short examinations, instructing the patient to remain still during the examination and in certain situation using physical restraints and anaesthetics. However, such techniques are sometimes ineffective. Involuntary motion such as heart beats and bowel peristalsis cannot be stopped or minimised its influences on the images by using examinations of very short duration.[12]

Receptor blur refers to the blur results from the image receptor. Image receptor gathers data produced during the imaging process and presents it as a visual image. Spatial resolution basically depends on physical detector characteristics. For example, the intrinsic spatial resolution of amorphous selenium utilised in direct conversion DR system is higher than that of structured caesium iodide utilised in indirect conversion systems. The detectors of structured caesium iodide has much higher intrinsic spatial resolution than that of unstructured scintillators.[11] The thickness and material composition of the detector will determine its blur features. The factor of the blur increases with increasing thickness of receptor. The thickness also influences the sensitivity of the receptor which increases with increasing thickness.[8]

Receptor blur is also caused by scattering or photoelectric interactions within the image receptor when the photon energy dissipates. A part or all energy of the photon deposited somewhere in the detector other than the original point of entry causing the blur. The scattering and movement of the laser beam, that is used to stimulate storage plate in the CR system, are sources of blur.[12] Scattering of the laser light beam during storage plate readout is the primary source of special resolution loss in CR.[2] The thicker the phosphor plates, the greater the scattering depth and blur. Dual reader systems reduce scattering problems. The introduction of structured phosphor allowed the use of thicker plates and provided improved detection efficiency without much loss of spatial resolution.[2]

In indirect conversion DR (IDR), the source of spatial resolution loss is the spread of light photons during the x-ray-to-light conversion process which results in blur. Utilising structure phosphor increases detection efficiency and minimises the scattering light. However, direct conversion DR (DDR) does not suffer from this effect; because of the limitation of the spread of the electrons within the photoconductor material as they are directed towards the thin-film transistor(TFT) array.[2]

Width of the detector, matrix size, pixel size, detectors pitch (spacing between detectors) are factors of spatial resolution loss in CR and DR systems.[2] Locations of different x-ray absorptions within an element may be undistinguishable because all x-rays within an exposure contributes to a single quantity (the summed charge read from that element). So that, when the imaged structures of a patient are smaller than the size of a

single element of the detector, they are smeared out and their contrast is reduced unless they are inherently high contrast objects. For example, when microcalcification is smaller than an element, it may be recognised as a calcification since its attenuation properties are so different from the other tissue in the element.[2]

Contrast resolution

Contrast resolution refers to the ability of an imaging system to discriminate objects with small density differences and/or differentiate small attenuation variety on the image.[2] Contrast resolution explains how well the image discriminates subtle structures in organs being examined.[8] Contrast resolution can be inherited by recording the information of interest with sufficient intensity resolution to discriminate the contrast details of interest.[9] While the first step of digitisation, sampling in space, affects the spatial resolution, the second step, quantisation in signal intensity, influences the contrast resolution or the gray-scale bit depth.[13]

Contrast resolution is sometimes called tissue resolution.[2] If there are two small objects with large difference in densities, the area between them is considered as high frequency or high contrast region. Conversely, low contrast region refers to the area between two small objects with small difference in densities.[6]

Contrast resolution is affected by tube collimation, number of photons, noise, scatter radiation, beam filtration, detector properties and algorithmic reconstruction used.[6] Image contrast depends on subject contrast, detector contrast and displayed contrast.[8]

Subject contrast

The anatomical and physiological characteristics of the region being imaged are considered to be the intrinsic factors of image contrast, which are called intrinsic, subject, object, or patient contrast. Low intrinsic contrast tissues such as breast tissues have very subtle differences in composition. In radiography, the physical properties of atomic number, physical density differences among different tissues and patient thickness influence intrinsic or subject contrast.[8]

Imaging methods and techniques are the second major factor which control image contrast. Selecting careful exposure techniques for specific tissues and for certain purposes greatly enhances image contrast to obtain the desired information. For example, low kVp and small amounts of beam filtration are preferable in mammography to discriminate subtle differences among tissues. In chest radiography, however, high kVp and large amounts of beam filtration are used to demonstrate the wide range of varying tissues densities (lung, bone tissues). This technique helps in detecting lesions of increased physical density in the under the ribs.[8]

Introducing enhancement material or medium into the body improves image contrast by altering subject contrast. Contrast media changes photon attenuation properties from those of the surrounding tissues and therefore provide signal differences.[8]

Detector (receptor) contrast

A detector's characteristics play an important role in producing contrast in the final image. Detector contrast is determined principally by how the detector detects and converts the energy into the output signal. The dynamic range of the detector influences the contrast resolution of image.[8] The dynamic range of CR and DR, which is the ratio of the maximum to minimum input x-ray intensities incident on the detector surface, ranges from 1,000:1 to 10,000:1 compared with the dynamic range of film screen radiography which ranges from 10:1 to 100:1.[2]

Displayed contrast

The attributes of image displaying that is utilised to produce and demonstrate the final image influence the contrast of diagnostic images. For example, displaying images on a video screen gives one the flexibility to alter and adjust image contrast, unlike film based images. Viewing diagnostic images digitally demonstrates the data of images in a wide range of grayscale images. It also allows use of a wide range of exposures for display image. Consequently, image contrast is enhanced and radiation dose is reduced by utilising digital system.[8] Therefore displaying process and devices of digital imaging systems (particularly for primary display or diagnostic interpretation) should be in compliance with the current Digital Imaging and Communications in Medicine (DICOM) standard of the American College of Radiology (ACR) and the National Electrical Manufacturers Association (particularly on grayscale displays).[13]

There are two categories for displaying digital images, small matrix (for CT, digital fluorography, and digital angiography) and large matrix size (CR and DR and digital mammography). A monitor of 5 megapixel (MP) typically 2048 x 2560 pixels, is sufficient for viewing digital images particularly CR and DR images. It is important to utilise zooming and roaming display functions to achieve a correspondence between the display pixel matrix and the detector element matrix in order to avoid resolution limitations of the monitor for partially displayed images. Moreover, display luminance influences image quality and therefore appropriate luminance should be uniform over the entire display and at a level of at least 200 cd/m2, especially for CR and DR. Bit depth resolution, which controls luminance quantification of soft copy display, is recommended to be large to prevent the loss of contrast details or the appearance of contour artefacts. Viewing environment and conditions also affect image display quality such room lighting and other display monitors light reflection.[13]

Noise

Noise is produced by the statistical fluctuation of value from pixel to pixel. Noise is recognised by a grainy appearance of the image. It is also characterised by a salt and pepper pattern on the image.[6] Noise is un-useful information.[14] The noise level is explained by the standard deviation, a measure of how spread out the pixel's values are. The lower the standard deviation, the higher the accuracy of the average pixel value.

Noise images relates to the number of x-ray photons that are logged in each pixel (for DDR) or in each small area of the image (for CR and IDR).[12,15]

Goldman[6] categorised the noise sources into three types, namely quantum noise, electronic or detector noise and computational or quantisation noise.

Quantum noise

Quantum noise appears when too few photons, after being attenuated by organs, are received. The lower the number of attenuated photons at the detector the higher the image noise.[12] The main factors of quantum noise are anatomical structure size, decreasing pixel size, and scatter radiation. The disturbing anatomic background variability is often called anatomical noise.[15]
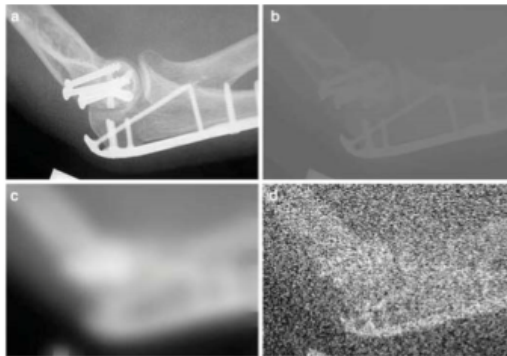
Figure 2: Optimum image quality has adequate resolution and contrast, and a low noise level, as demonstrated in image (a). Image (b) has high spatial resolution and low noise, but it has almost zero contrast. Image (c) has low noise and high contrast, but very poor spatial resolution. In image (d) has high spatial resolution but very high noise level which destroyed the image contrast.[9]

Detector noise

Noise originates from internal sources mainly image receptors which contain what is called electronic noise.[2] Detector or receptor noise is produced because of non-uniform response to a uniform x-ray beam.[14] This type of noise has fixed correlation to locations on the receptor, therefore it is called fixed pattern noise. Fixed pattern noise can be largely eliminated in digital imaging systems through post processing stages. Additionally, defects in the receptor's elements which may occur during the manufacturing process form unrelated structure in the image.[2] Structured noise originates from different causes which creates unwanted signals or features on the image. Variations in pixel-to-pixel sensitivity and linearity, dead pixels and detector-response non-uniformities are the main causes of structure noise, particularly in DR.[12]

Conversion noise occurs because of the fluctuations of the generated energy per detected photons. Conversion noise which is also called instrumentation noise can be reduced by utilising higher-intensity scanning laser in CR detectors and brighter phosphor screens in indirect flat-panel detectors to collect and generate more secondary energy carriers and hence improve QDE. In addition, lowering the number of conversion stages of process can also reduce conversion noise.[12]

Quantisation noise

Quantisation noise is another source of noise which occurs during the digitisation process, translating analogue output voltage of detectors to discrete pixel values (grayscale values). The range of these values is determined by bits, binary on-off channels. Detectors of 10 to 14 bits (1024 to 16,384 digital values) are recommended to minimise quantisation noise in CR and DR systems.[2]

Noise is also produced by scatter radiation which reduces subject contrast and decrease signal to noise ratio (SNR) and consequently degrades image quality. Using grid in CR and DR reduces scatter radiation and consequently reduces noise effect. However, the signal (incomplete transmission of the primary radiation by the grid) is also reduced.[2]

Artefacts

Features that occur on the image and mask or mimic clinical features are called artefacts.[16] Digital image artefacts are caused by image acquisition or object artefacts, hardware or image receptor artefacts, and software artefacts.[17-19]

Image acquisition/object artefacts

Radiographers usually perform image acquisition by using image receptor. Therefore, image acquisition artefacts are due to operator errors. These artefacts include inappropriate exposure factors, un-collimated images, improper grid usage, scatter radiation, delayed scanning, twin artefacts, exposed image receptors and handling carelessness.[18]

Incorrect patient position, patient motion, improper x-ray beam collimation, and double exposure cause object artefacts.[20] Inappropriate histogram selection can cause object artefacts. Errors of histogram analyses are associated with improper collimation of exposure field, leading to very noisy, very dark or very white images.[17] Metal objects also cause artefacts.[20]

Hardware/receptor artefacts

Digital image receptor artefacts can be caused by rough handling, dust, malfunction of pixels, faulty construction, and scratches and cracks on image detectors.[18] Artefacts that results from faulty pixels cannot be treated and therefore the image receptor may need to be replaced. Malfunction of rollers in digitiser of CR image plates causes defective scanning resulting in artefacts.[18]

Partial erasure of a previous image cause artefacts called ghost image, particularly on image plates of CR. Ghost artefacts can also be caused by environmental radiation.[17]

Software artefacts

Dead pixels in image receptors cause artefacts during the image processing stage and are called software artefacts. A few dead pixels may not interfere with diagnosis however many of these faults must be corrected. Radiation variation of x-ray beam over the image produce irregular configuration which again interfere with diagnosis. This can be corrected by equalising the response of each pixel to a uniform x-ray beam by utilising software pre-processing manipulation, namely flat fielding. Image compression is employed to facilitate transmitting and archiving of images. However, lossy compression techniques may cause redundancy of data and hence create software artefacts.[17] Artefacts may occur through inappropriate use of software filters of grid suppression, low pass spatial frequency filter, and blur masking.[19] Image transmission (communication) errors or failures cause artefacts.[18] Incorrect flat field corrections and a failing amplifier are other sources of artefacts.[19]

The above discussed parameters are judged objectively (statically measurement) or/and subjectively (human observation) to determine image quality level.[15] In order to improve the quality of image, image quality parameters are manipulated because they are not independent. There are trade-offs in manipulating these parameters individually.[9,15] Figure 2 demonstrates the dependent relationship between image quality parameters.[10] Therefore image quality should be optimised for each specific purpose and specific region. For example, when spatial resolution is increased to get better image quality for bone tissue, the noise of image is also enhanced or hence increased visually.[6]
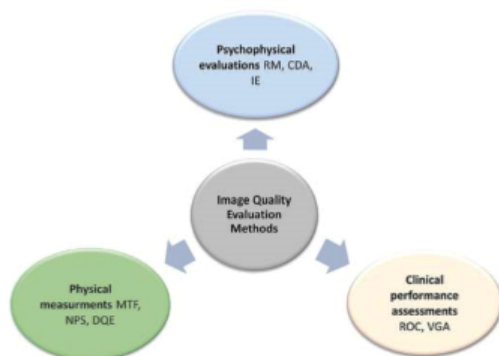
Figure 3: The types of evaluation methods of image quality.

Figure 4: Evaluation tools used to assess image quality and imaging system performance.

However, there is a fundamental principle, radiation dose minimisation, which should be considered beside these parameters. Therefore, image quality is the balancing between image quality parameters and radiation dose.[21,22]

Optimum image quality relies on the balancing of the image quality and patient dose and depends on the region being studied and case being examined. To optimise image quality, image quality parameters mentioned previously should be manipulated and altered according to the purpose of examination with respect to the patient dose. Moreover, eliminating or limiting the effects of image degradation factors are also essential in optimising image quality.[21,22]

Image quality and radiation dose

Optimal image quality is achieved at the lowest possible patient radiation dose. The high flexibility of CR and DR increases the opportunity of image quality optimising and radiation dose lowering.[23] The minimum level of image quality and radiation dose should be determined based on diagnostic purpose.[3] It is essential to recognise the parameters that affect radiation dose and their influences on image quality. Exposure factors including mA, time and kVp are the most important factors that control the radiation dose to the patient. The other factors that also affect radiation dose are patient size and detector properties.[23]

Reducing mAs decreases radiation dose and consequently decreases SNR as the noise is associated with lower radiation dose. Lower radiation dose deteriorates contrast resolution of the image. High noise level images increase the risk of diagnostic details loss.[24]

Lowering the kVp is essential to increase x-ray attenuation and consequently the contrast resolution of structures is improved. Lower voltage increases DQE of the detectors of digital system. As a result, image quality can be improved.[25] In CR and DR, Lower kVp techniques are more likely to improve SNR and hence the contrast resolution of image. However, low kVp techniques may increase radiation dose and image blur as a result of time increasing.[3] Uffmann, *et al.*[26] in their study found that selecting 90 kVp demonstrates the anatomic structure superior than that of 120 and 150 kVp without increasing the radiation dose to the patients. Changing tube voltage from 102 to 133 kV did not significantly improve contrast resolution of CR and DR.[27] However, higher kVp should be used for thicker body organs to optimise the contrast resolution of the image.[28]
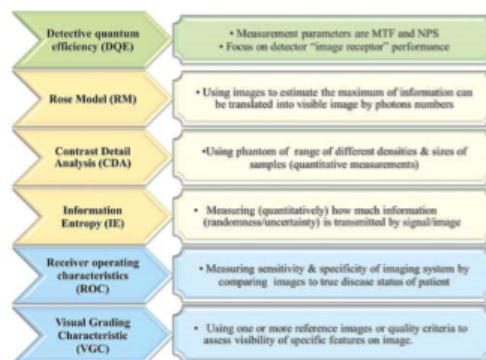
In addition, selecting higher kVp may cause blooming or pixel saturation. The problem of blooming occurs when the saturation of the detectors is exceeded by illumination. The charge leaks to other pixels when the overfilled pixels lose their ability to accommodate additional charge. As a result the image quality is degraded.[29]

Different detector systems have different detection efficiency and radiation dose reduction ability and hence different image quality. For example, the detector of IDR can provide better image contrast resolution than that of CR.[28] Thicker detectors have better detection efficiency and hence higher ability of dose reduction.[30] Spatial resolution of the image can be improved with small detector elements however high radiation dose is required.[23]

Therefore, good understanding of the influences of radiation dose factors on image quality is essential to obtain optimal image quality while maintaining lower radiation dose.

Evaluation methods of image quality and imaging system performance

The utility of radiologic images and the accuracy of image interpretation depend on two main factors; the quality of images and the ability of the interpreter. Good image quality is a major factor that allows physicians to interpret the image most accurately, correctly and timely.[31]

Certain attributes are required for image quality evaluation tools and techniques to be used as quality control constancy examination. These tools should directly describe diagnostic performance, sensitively detect changes in the imaging system and not be expensive or too labour-intensive.[15]

Several methods are used to measure the quality parameters of DR images and the performance of imaging systems. These methods are either physical, psychological or clinical (observers/diagnostic) performance (Figure 3). Physical methods include modulation transfer factor (MTF), noise, SNR, and detection quantum efficiency (DQE). Psychophysical evaluation methods include rose model (RM), contrast-detail analysis (CDA) and subjective assessment of physical parameters. Clinical performance measurement methods include receiver-operating characteristics (ROC) and visual grading characteristic (VGC).[32,33] Figure 4 summarises the different evaluation methods of image quality and imaging system performance.

Detective quantum efficiency

The evaluation method of detective quantum efficiency (DQE) focuses on detector "image receptor" performance to assess image quality of certain imaging systems. Assessing detector performance method is based on purely quantitative analyses by measuring objective parameters related to detector performance. Such methods are considered indirect methods of image quality evaluation. DQE has been commonly used as a tool for image quality assessment and medical imaging system performance in general.[34] DQE is based on linear-systems analysis (LSA) which is used to assess the ability of the system to transfer a signal and to characterise the noise associated with the system. The main measurement parameters of DQE methods are the modulation transfer function (MTF) of the system and the noise power spectrum (NPS). The MTF describes a system with the ability to reproduce and preserve the information of spatial frequency contained in the incident x-ray signal. The NPS describes the frequency content of the noise in the spatial frequencies of the system image.[7,35]

There are several ways to calculate MTF which alter DQE approach and quantities. In fact, MTF was used separately before as a tool of image quality assessment. However, the sharpness of the final image is not described by DQE.[35] DQE quantifies signal-to-noise ratio to the number of incident x-ray photons and characterises image quality.[36] The main limitation of this method is that it ignores significant factors that affect image quality such as scatter radiation and image processing. Additionally, time consuming is considerable limitation of this method which makes it impractical in hospital basis environment.[34]

Recently, DQE has been modified and improved to another method of image quality evaluation called effective detective quantum efficiency (eDQE).[37] Some limitations of DQE are removed in eDQE. For example, factors that influence image quality such as scattering, magnification and image processing are now considered in eDQE.[37,38] However, observers who are the second element in reliable radiology diagnosis are totally ignored in these methods. Moreover, they are difficult to implement as regular evaluation tools of image quality assessment due to the fact that they are time consuming and complex to some extent.[34]

In general, the main limitations of the DQE method and its relative approaches have two drawbacks. Firstly, they do not provide description of all components in the imaging process. They give limited information about the characteristics of the produced image. Factors such as dose level and display characteristics which influence final appearance of the image are not considered in these methods and relative approaches. Secondly, they do not consider the anatomical background which limits the observer performance in detecting pathology. Anatomical background is considered as a factor of hindering detection of pathology.[35] The ability of observers to detect details is reduced by anatomical details, even though the mechanism of this effect is not clear and is not really understood.[15] Therefore, the reliability and validity of recent approach of DQE and relative approaches are high in providing accurate measurement of the ability of information transfer. However, their validity is low in assessing the entire imaging system.[35]

The Rose model

The method of RM, SNR based method, is another tool used to evaluate image quality of digital radiographic images. Rose, in 1953, used images to estimate the maximum amount of information that can be translated into visible image by numbers of photons. Quantum efficiency (absolute scale) is used in this method to evaluate the performance of

imaging systems by utilising a simple model of signals detect ability which is assessed by human observation. Later, Rose's quantum signal detection model is based on SNR. It gives a description of visibility of an object in an image.[39] Phantom of a number of disc-like objects of different size (0.3–8.0 mm diameters) and diverse contrast, represented by sample depth (0.3–8.0 mm), is utilised as well. SNR is calculated to measure image quality in this method based on linking the mathematically calculated SNR to the results of detection examinations. SNR describes noise and resolution characteristics of image and human visual system.[40]

There are some problems with this method which influence its validity and reliability in evaluating image quality. First, the size of the objects are not considered in SNR measurements in this method. Second, the noise description used in SNR is overly simplistic for observers who are sensitive to the noise characteristics. Third, to offer the same imaging conditions, a larger number of photons for the image are used with smaller pixels. Meanwhile, the observers are mostly not interested in single pixel values and are not affected by the pixel-to-pixel variations. Fourth, observers are not often affected by pure noise from the anatomical background. Hence, the validity of using SNR methods is very low to measure image quality. Therefore, it is not recommended that using SNR methods to compare different imaging systems or various image processing procedures.[35]

Information entropy

Tsai, *et al.*[7] suggested a new evaluation method of image quality, IE, which is a quantitative measure of the information transmitted by the image. The concept of information entropy describes how much information (randomness/uncertainty) is provided by the signal or image. It is a simple and straightforward method based on single parameter, transmitted information.[41] Step wedge phantoms of varying thicknesses are used in this method. Images of phantoms are detected, for example, by storage phosphoric plate for CR. Several images are taken with a variety of exposure times. Because of the variety of thickness of step wedge phantom, the images demonstrate a gradual scale of grey level with diverse values. The more information conveyed the better the image quality.[41]

The authors found that IE is a useful method for the evaluation of physical image quality in medical imaging system. The results of their study demonstrated that there was a correlation between the transmitted information and both image noise and image blurring.[41]

The main advantage of this method over DQE is that the final image is considered in the evaluation procedure. Other advantages of this method which include simplicity of computation and experimentation and the combined assessment of image noise and spatial resolution. However, its validity still low as human observers are not used in this method. In addition, the simplicity of the used phantom reduces the reliability of this method. Step wedge phantom is limited by several different thicknesses without considering sample sizes. Tsai, *et al.*[7] state some limitations of IE evaluation methods. Unlike MTF and NPS, information entropy measures do not provide frequency information. In addition, this method does not separately demonstrate the effects of different noise sources such as the electronic noise and structural noise.

Information loss theory is a newly evolved method of image quality based on entropy theory. Contrast detail phantoms are also used in this method.[42] In fact, utilising CDA allows to consider the whole parameters of image quality.[15] This method proves more sensitive in evaluating the contrast-detail image quality than using the average values of detectability,

and it allows to measure observers' differences in unit of bits. This method is based on measuring the Total Information Loss (TIL).[42] Niimi, et al.[42] concluded that TIL can be used as a tool of performance assessment of different medical imaging modalities

Contrast–detail analysis

A commonly and widely used tool to evaluate image quality is contrast detail analysis (CDA). This method provides quantitative evaluations of low contrast and small detail measurement of medical images.[30,35]

CDA originated from the theory of signal detection which implies that low contrast-detail detectability is related to internal signal-to-noise ratio of the observer.[30,63] The main assumption of this theory is that noise from different sources interferes with sensory stimuli to the observer.[44] The ability of imaging system to visualise small objects which are of very low contrast describes low contrast-detail detectability of the system.[44]

Low contrast-detail detectability can be assessed by measuring the ability of observers to detect the smallest objects which have varying contrast differences with the background. CDA is an approach to describing the image quality in terms of detail (drilled holes of varying diameter) and contrast (varying depth).[45] Low contrast-detail detectability implies that the detectability of details increases with increasing the size of objects and/or contrast between the objects and the background. For example, when the objects' size increases while keeping the contrast differences the same, the detectability will increase. The detectability will also increase when the contrast differences between the objects and the background increases while maintaining object size.[46] In other words, the large objects can have lower contrast than smaller objects for the same detectability performance[46,67]

Human observation is mostly involved in the process of evaluation to visually measure contrast-detail on the image. Therefore, this method is considered a subjective evaluation.[34]

Observers are asked to score what they can detect on the phantom image on the first three rows and to score and locate (in which corner the object is) what they detect on the rest rows in order to limit false positive score. By plotting the smallest visible diameter (Cj) against the smallest visible depth (Di), for all rows i, a contrast-detail curve is obtained. The next equation is used to calculate inversed image quality figure inverse (IQFinv). The greater value of the IQ_{Finv}, the better is the low contrast detectability.[27]

$$IQF_{inv} = \frac{100}{\sum_{j=1}^{15} C_j * D_{th,j}}$$

Where C_jth, is threshold contrast
$D_{j,th}$, is threshold detail[27]

CDA method provides quantitative evaluations of low contrast and small detail measurement of medical images. Therefore, it is considered straightforward and direct method of image quality assessment.[30,35] Moreover, low CDA studies consider the whole processes of imaging systems such as detector design, x-ray parameters, image acquisition and processing, image post processing, and image displaying. Therefore, CDA is selected to provide insightful understanding of CR and DR systems.[68]

A recent study by De Crop, et al.[49] investigated the correlation of low contrast-detail performance measurement and clinical image quality assessment in chest radiography. The findings of this study suggested that there is significant correlation between physical (low

contrast-detail measurements) and clinical evaluation methods. The researchers concluded that the CDA method is relevant for image quality optimisation.[49] While this method was based on a phantom, it does not require volunteer patients. Therefore, the evaluation method of CDA can be used to compare and contrast the image quality of different systems.[30]

In fact, the reliability and the detectability of such methods are affected by the variation of human perceptions and decisions. Furthermore, visual assessment of image quality by the human observer is time-consuming and arduous and may lead to wrong results in many situations.[34]

Pascoal, et al.[34] in their study suggested an objective CDA method to assess image quality by utilising automated scoring by employing a software package (CDRAD analyser). It is suggested that this avoids the subjectivity of commonly used method, CDA, because it is based on measurements of image data such as signal-to-noise ratio.[16] Even though the method of employed CDRAD analyser proves more sensitive to detect smaller low-contrast variations; human observation is able to detect smaller details.[34] CDAs are useful for quality control, standardisation purposes and for indicating typical or acceptable performance of medical imaging systems.[15]

However, using CDA is still criticised because they are based on homogeneous patient simulating phantoms and they do not represent the real situation. Noise from anatomical background which effects detesting ability is simply not considered in such evaluation methods. The detectability of objects are often much more limited by anatomical background structure than by noise from an imaging system.[15]

Receiver–operating characteristics analysis

The evaluation method of ROC is another tool used to evaluate imaging performance of imaging systems. ROC is a task-based method and it involves human observers. It measures the sensitivity and specificity to evaluate the accuracy of diagnostic imaging systems. The sensitivity and the specificity measurements describe the abilities of imaging system to assist interpreters to correctly diagnose the disease when the patient actually has the disease and to correctly exclude the disease when the patient truly does not have the disease.[51] The sensitivity measures the probability that a patient who actually has the disease is determined as having a disease by image interpreters. On the other hand, the specificity measures the probability that the patient who truly does not have the disease is determined as not having the disease by image interpreters.[35]

In ROC, the results of imaging system are compared to the true disease status of the patient to evaluate the accuracy of that imaging system.[50] There are several types and approaches of ROC analysis methods such as ROC curve, multiple-reader multiple-case, and free-response ROC analysis. ROC and ROC-related methods are considered as the gold standard for image quality evaluation, particularly when evaluating the accuracy of imaging system or comparing different imaging modalities in terms of detectability of specific pathology.[35]

However, applying the ROC method and related types requires a large number of cases and therefore such methods may be cumbersome. Observers, even experienced radiologists, may behave differently in an experimental environment compared with that in a clinical environment. Hence, the reliability of ROC and related methods are relatively low.[35]

Visual grading characteristic

The common clinical based evaluation method of image quality is visual garding characteristic (VGC). The theory of this method, which

310

is based on the ability to detect and perceive pathology, correlates well with precise anatomical demonstration. There are two ways to perform VGC, namely relative grading and absolute grading approaches. In the relative grading approach, one or several reference images are used by observers to evaluate the quality of images. The observers compare the display quality of the image being assessed with the matching landmark of the reference image. The observers categorise their decisions to a scale of 3, 5, or 7 points. For example, a 5 points scale is +2 = much better, +1 = slightly better, 0 = equal, -1 = slightly worse and -2 much worse.[51]

In the absolute grading approach, the observers state their decisions on the visibility of specific features in the assessed image without using a reference image to evaluate the image quality. Typical grading scale of this approach ranges from 4 to 7 points to categorise an observer's decisions. This feature is also called quality criteria.[52] For example, five point grading scale analysis of absolute approach includes excellent image quality (no limitations for clinical use), good image quality (minimal limitations for clinical use), sufficient image quality (moderate limitations for clinical use but no considerable loss of information), restricted image quality (relevant limitations for clinical use, clear loss of information), and finally poor image quality (image must be repeated because of information loss).[51]

Quality criteria for each radiologic examination are used to evaluate image quality of specific examination. These criteria, developed by professional radiologists, technologists and physicists, describe physical and anatomical characteristics of image appearance and dose level. For example, chest examination criteria are used to evaluate chest images by letting experienced radiologists and technologist to determine the level of fulfilling these criteria in that image.[35] This method has several advantages which make it preferable, but again it still has some limitations.[51]

Several factors make this method useful. First, almost all process components of imaging system which control image quality are considered in the evaluation procedures of VGC. These components include image processing, recording, post processing, and reading by expert radiologist. Therefore, the practical validity of this method is considered high. Second, VGC is based on the visualisation of clinically relevant available standards to evaluate image quality. The conducting process of VGC is similar to that of daily clinical situation. Third, this evaluation method has easier procedures and makes for less work than some other methods such as ROC. Furthermore, the required time that the observers are required to read the images is reasonable and therefore there is no real barrier with this regard to have participants.[51] This method can also be used to compare the performance of different imaging modalities in terms of image quality and dose level.[35]

The limitations of these methods include false positive fractions of limited or no clinical relevance. Furthermore, fulfilled criteria that are judged by the observer may correspond to an unacceptable image.[52] Additionally, there are difficulties in analysing the uncertain data from VGC. Hence, the underlying reasons of the uncertainty cannot be identified whether these reasons are related to poor image quality, observer influences or other factors.[51] In addition, VGC suffers from the subjectivity of observers which minimises its reliability.[35]

According to the above discussion, evaluation methods related to pure statistical measurement such as DQE has a low validity when used to measure the clinical performance of an imaging system unless complete imaging procedures, including image processing, display and the response of the observer, are considered.[35] However, DQE is the most
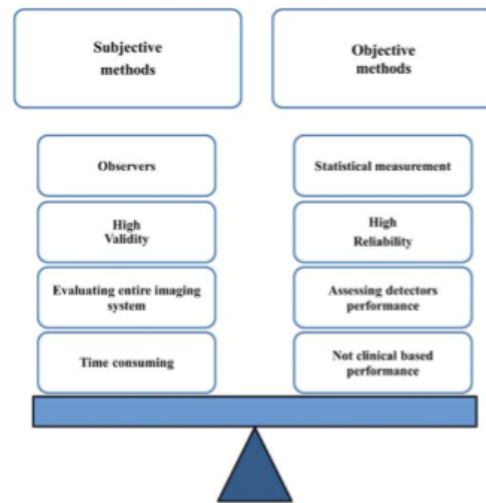

Figure 5: Subjective versus objective evaluation methods of imaging system.

effective evaluation method for objectively assessing the performance of the detectors of imaging systems.[4] Even though, the reliability and validity of DQE is high in providing accurate measurement of the ability of information transfer, its validity is low in assessing an entire imaging system.[35]

On the other hand, methods that involve human observers such as ROC and VGC are valid for evaluating an entire imaging system. Even though, ROC and VGC methods are also considered as gold standard for evaluating the accuracy of imaging system or/and comparing different imaging modalities, their reliability is limited because they suffer from the subjectivity of observers (Figure 5).[35,50,51]

Tapiovaara[15] investigated the relationship between the results of different procedures of image quality evaluation including physical quantities measurements, phantom experiment evaluations and clinical performance assessment. It was found that this relationship is not clear and not fully understood.[15] Until recently, there has been no image quality method to resolve the gap among methods of physical measurements, CDA, and human observers, despite continuous studies and heavy efforts.[35]

Conclusion
The relationship between the quality parameters of digital radiographic images including resolution (spatial resolution and contrast resolution), noise, and artefacts is complicated, meaning that there is a trade-off between them, improving one parameter may deteriorate another. Hence, optimising these parameters is not a simple task. Optimising image quality parameters in regard to radiation dose make it a more complicated task. Additionally, the effect levels of these parameters on image quality of different digital radiography systems and units are not exactly the same even though they share the principles of image quality parameters. The only way to optimise image quality parameters while maintaining low

radiation dose is to deeply understand the effects of these parameters on each other, the influence factors and their impact on the radiation dose for each different digital radiographic systems. Each of the available evaluation methods has its own advantages and limitations. Therefore each evaluation method should be utilised and employed according to its aptitudes to improve image quality and imaging process.

References

1 Körner M, Weber CH, Wirth S, Pfeifer KJ, Reiser MF, Treitl M. Advances in digital radiography: physical principles and system pverview. *Radiographics* 2007; 27 (3): 675–86.

2 Williams MB, Krupinski EA, Strauss KJ, Breeden Iii WK, Rzeszotarski MS, Applegate K, et al. Digital radiography image quality: image acquisition. *J Am Coll Radiol* 2007; 4 (6): 371–88.

3 Schaefer-Prokop C, Neitzel U, Venema H, Uffmann M, Prokop M. Digital chest radiography: an update on modern technology, dose containment and control of image quality. *Eur Radiol* 2008; 18 (9): 1818–30.

4 Cowen A, Kengyelics S, Davies A. Solid-state, flat-panel, digital radiography detectors and their physical imaging characteristics. *Clin Radiol* 2008; 63 (5): 487–98.

5 Uffmann M, Schaefer-Prokop C. Digital radiography: The balance between image quality and required radiation dose. *Eur J Radiol* 2009; 72 (2): 202–08.

6 Goldman LW. Principles of CT: radiation dose and image quality. *J Nucl Med Technol* 2007; 35 (4): 213–25.

7 Tsai D, Lee Y, Matsuyama E. Information entropy measure for evaluation of image quality. *J Digit Imaging* 2008; 21 (3): 338–47.

8 Hendee WR, Ritenour ER. Influences on image quality. Medical imaging physics. (4th edition). John Wiley & Sons, Inc.; 2003. p. 265–80.

9 Bourne R. Fundamentals of digital imaging in medicine. (1st edition). Springer; 2010.

10 Chotas HG, Dobbins JT, Ravin CE. Principles of digital radiography with large-area, electronically readable detectors: a review of the basics. *Radiology* 1999; 210 (3): 595–99.

11 Samei E, Ranger NT, Dobbins JT III, Chen Y. Intercomparison of methods for image quality characterization. I. Modulation transfer function. *Med Phys* 2006; 33 (5): 1454–65.

12 Samei E. Performance of digital radiography detectors: factors affecting sharpness and noise. In: Advances in Digital Radiography. Oak Brook: Radiological Society of North America2003.

13 Krupinski EA, Williams MB, Andriole K, Strauss KJ, Applegate K, Wyatt M, et al. Digital radiography image quality: Image processing and display. *J Am Coll Radiol* 2007; 4 (6): 389–400.

14 Sprawls P. Physical principles of medical imaging. (2nd edition). Medical Physics Pub Corp; 1995.

15 Tapiovaara M. Relationships between physical measurements and user evaluation of image quality in medical radiology – a review. Vantaa: Radiation and Nuclear Safety Authority 2006.

16 Willis CE, Thompson SK, Shepard SJ. Artifacts and misadventures in digital radiography. *Appl Radiol* 2004; 33 (1): 11–21.

17 Bushong S. Radiologic science for technologists: physics, biology, and protection. (9th edition). Mosby; 2001.

18 Shetty CM, Barthur A, Kambadakone A, Narayanan N, Kv R. Computed radiography image artifacts revisited. *AJR* 2011; 196 (1): W37–47.

19 Honey ID, Mackenzie A. Artifacts found during quality assurance testing of computed radiography and digital radiography detectors. *J Digit Imaging* 2009; 22 (4): 383–92.

20 Jiménez DA, Drose WM, Reese DJ, Hornof WJ. Digital radiography artifacts. *Vet Radiol Ultrasound* 2008; 49 (4): 321–32.

21 Seeram E. Computed tomography: Physical principles, clinical applications and quality assurance. (3rd edition). Saunders; 2009.

22 Kalender W, Khadivi K. Computed tomography: fundamentals, system technology, image quality, applications. (3rd edition). John Wiley & Sons; 2011.

23 Seibert JA. Tradeoffs between image quality and dose. *Pediatr Radiol* 2004; 34 (2): 183–84.

24 Aichinger H, Dierker J, Joite-Barfuß S, Säbel M. Image quality and dose radiation exposure and image quality in x-ray diagnostic radiology. (2nd edition). Erlangen: Springer; 2012. pp 85–101.

25 Launders J, Cowen A, Bury R, Hawkridge P. Towards image quality, beam energy and effective dose optimisation in digital thoracic radiography. *Eur Radiol* 2001; 11 (5): 870–75.

26 Uffmann M, Neitzel U, Prokop M, Kabalan N, Weber M, Herold CJ, et al. Flat-panel–detector chest radiography: effect of tube voltage on image quality. *Radiology* 2005; 235 (2): 642–50.

27 De Hauwere A, Bacher K, Smeets P, Verstraete K, Thierens H. Analysis of image quality in digital chest imaging. *Radiat Prot Dosimetry* 2005; 117 (1-3): 174–77.

28 Dössel O, Schlegel WC. Optimization of exposure factors and image quality for computed radiography. World congress on medical physics and biomedical engineering: Springer 2009. pp 251–4.

29 Rahn J, Lemmi F, Lu J, Mei P, Apte R, Street R, et al. High resolution x-ray imaging using amorphous silicon flat-panel arrays. Nuclear Science. *IEEE Transactions on.* 1999; 46 (3): 457–61.

30 Uffmann M, Schaefer-Prokop C, Neitzel U, Weber M, Herold CJ, Prokop M. Skeletal Applications for flat-panel versus storage-phosphor radiography: effect of exposure on detection of low-contrast details. *Radiology* 2004; 231 (2): 506–14.

31 Krupinski EA, Berbaum KS. The Medical Image Perception Society update on key issues for image perception research. *Radiology* 2009; 253 (1): 230–33.

32 Mansson L. Methods for the evaluation of image quality: a review. *Radiat Prot Dosimetry* 2000; 90 (1): 89–99.

33 Zarb F, Rainford L, McEntee MF. Image quality assessment tools for optimization of CT images. *Radiography* 2010; 16 (2): 147–53.

34 Pascoal A, Lawinski C, Honey I, Blake P. Evaluation of a software package for automated quality assessment of contrast detail images – comparison with subjective visual assessment. *Phys Med Biol* 2005; 50 (23): 5743–57.

35 Bath M. Evaluating imaging systems: practical applications. *Radiat Prot Dosimetry* 2010; 139 (1-3): 26–36.

36 Ranger N, Samei E, Dobbins J, Ravin C. Assessment of detective quantum efficiency: intercomparison of a recently introduced international standard with prior methods. *Radiology* 2007; 243 (3): 785–95.

37 Samei E, Ranger N, MacKenzie A, Honey I, Dobbins J III, Ravin C. Effective DQE (eDQE) and speed of digital radiographic systems: An experimental methodology. *Med Phys* 2009; 36 (8): 3806–17.

38 Samei E, Ranger N, MacKenzie A, Honey I, Dobbins J, Ravin C. Detector or system? Extending the concept of detective quantum efficiency to characterize the performance of digital radiographic imaging systems 1. *Radiology* 2008; 249 (3): 926–37.

39 Burgess A. The Rose model, revisited. *JOSA A* 1999; 16 (3): 633–46.

40 Giovanni B, Ehsan S, Marco B, Andrea N, Davide T. Contrast-detail analysis of three flat panel detectors for digital radiography. *Med Phys* 2006; 33 (6): 1707–19.

41 Uchida S, Tsai D. Evaluation of radiographic images by entropy: Application to development process. *Jpn J Appl Phys* 1978; 17: 2029–34.

42 Niimi T, Imai K, Maeda H, Ikeda M. Information loss in visual assessments of medical images. *Eur J Radiol* 2007; 61 (2): 362–66

43 Swets JA, Green DM, Getty DJ, Swets JB. Signal detection and identification at successive stages of observation. *Percept Psychophys* 1978; 23 (4): 275–89.

44 Chao E, Toth T, Bromberg N, Williams E, Fox S, Carleton D. A statistical method of defining low contrast detectability. *Medicine* [serial on the Internet]. 2000: Available from: http://www.mendeley.com/research/statistical-method-defining-low-contrast-detectability/.

45 Lu Z, Nickoloff E, So J, Dutta A. Comparison of computed radiography and film/screen combination using a contrast-detail phantom. *J Appl Clin Med Phys* 2003; 4 (1): 91–98.

312

46 Davidson R. Radiographic contrast-enhancement masks in digital radiography [PhD Thesis]. Sydeny: The University of Sydney; 2007. Thesis location: http://hdl.handle.net/2123/1932.

47 Faulkner K, Moores B. Noise and contrast detection in computed tomography images. *Phys Med Biol* 1984; 29 (4): 329–39.

48 Aufrichtig R, Xue P. Dose efficiency and low-contrast detectability of an amorphous silicon x-ray detector for digital radiography. *Phys Med Biol* 2000; 45 (9): 2653–69.

49 De Crop A, Bacher K, Van Hoof T, Smeets P, Smet B, Vergauwen M, *et al.* Correlation of contrast-detail analysis and clinical image quality assessment in chest radiography with a human cadaver Study. *Radiology* 2012; 262 (1): 298–304.

50 Obuchowski N. Receiver operating characteristic curves and their use in radiology. *Radiology* 2003; 229 (1): 3–8.

51 Ludewig E, Richter A, Frame M. Diagnostic imaging – evaluating image quality using visual grading characteristic (VGC) analysis. *Vet Res Commun* 2010; 34 (5): 473–79.

52 Bath M, Mansson LG. Visual grading characteristics (VGC) analysis: a non-parametric rank-invariant statistical method for image quality evaluation. *Br J Radiol* 2007; 80 (951): 169–76.

53 Green D, Swets. JA. Signal detection theory and psychophysics: Krieger Pub. Co.; 1974.

Appendix 1b   Publication arising from this work (2)

JOURNAL OF MEDICAL IMAGING
AND RADIATION SCIENCES

JOURNAL DE L'IMAGERIE MÉDICALE
ET DES SCIENCES DE LA RADIATION

Factors Affecting Contrast-Detail Performance in Computed Tomography: A Review

Haney Alsleem, BSc, MSc[a]* and Robert Davidson, PhD, MAppSc(MI), BBus, FIR[b]

[a] RMIT University, Bundoora, Victoria 3083, Australia
[b] School of Dentistry and Health Sciences, Faculty of Science, Charles Sturt University, Wagga Wagga 2678, Australia

ABSTRACT

This article reports on recent research findings into the factors that influence the detectability performance of different systems of computed tomography (CT) scanners. These systems include multidetector CT (MDCT) of different slice numbers, dual-source CT (DSCT), and cone-beam CT (CBCT). The introduction of more slices for MDCT, DSCT, and the new technology of CBCT increases the need to optimize the image quality and to examine the potential reduction of radiation doses to the patient. Low-contrast detail detectability is a method that has proven to be an appropriate evaluation method for this purpose. However, it is essential to recognize factors that affect detectability performance and understand how these factors influence image quality and radiation dose. It is argued that deep understanding of the influences of these factors is the key to image quality optimization in terms of contrast-detail detectability and radiation dose reduction. The purpose of this article is, therefore, to specify these factors and to explain their influence on detectability performance and hence on CT image quality. Further low-contrast detail studies are required to optimize imaging performance of different CT systems and scanners.

RÉSUMÉ

Cet article porte sur les résultats de recherches récentes sur les facteurs qui influencent le rendement de détection des scanners de différents systèmes de tomodensitométrie (TDM). Ces systèmes comprennent les systèmes de TDM à détecteurs multiples avec des nombre de tranches différents, la TDM à double source et la TDM à faisceaux coniques. L'introduction d'un plus grand nombre de tranches pour la TDM à détecteurs multiples, la TDM à double source et la TDM à faisceaux coniques augmentent la nécessité d'optimiser la qualité de l'image et d'examiner la possibilité de diminuer la dose de radiation pour le patient. La détectabilité des détails à faible contraste est une méthode d'évaluation qui s'est avérée appropriée à cette fin. Cependant, il est essentiel de reconnaître les facteurs qui influent sur le rendement de détectabilité et de comprendre comment ces facteurs influencent la qualité de l'image et le dosage de radiation. On croit qu'une compréhension approfondie de l'influence de ces facteurs serait la clé de l'optimisation de la qualité de l'image en termes de détectabilité des détails à faible contraste et de réduction de la dose de radiation. Le but de cet article est donc de déterminer ces facteurs et d'expliquer leur influence sur le rendement de détectabilité, et donc sur la qualité des images de TDM. Il faudra d'autres études sur les détails à faible contraste pour optimiser le rendement d'imagerie de différents systèmes et scanners de TDM.

Keywords: Low-contrast detail detectability; image quality; MDCT; CBCT

Mots-clés: Détectabilité des détails à faible contraste; qualité de l'image; TDM à détecteurs multiples; TDM à faisceaux coniques

Introduction

Computed tomography (CT) imaging technology is rapidly changing the conditions of image quality optimization and radiation dose reduction. Each CT system has its own specific image quality [1]. The introduction of multidetector CT (MDCT), using an increasing number of slices, dual-source

CT (DSCT), and cone-beam CT (CBCT) has enormously increased the range of examinations, which has in turn increased the number of CT examinations [2, 3]. To further add to this technological complexity, different technical applications and software are utilized in systems from different manufacturers, and various models of CT scanners utilize different algorithmic software [1].

Several studies have shown that there is still misdiagnosis or loss of information in CT images, as some pathologic lesions and details are not detected by interpreters [4–6].

* Corresponding author: Haney Alsleem, BSc, MSc, RMIT University, Discipline of Medical Radiation, Bundoora, Victoria 3083, Australia.
E-mail address: haniims@hotmail.com (H. Alsleem).

315

Although contrast and temporal resolutions have been significantly improved by the current advanced technology of MDCT, the spatial resolution or in-plane spatial resolution has not improved. Therefore, there are still some limitations in the rate of detection and accurate assessment [7–9]. Furthermore, the highest radiation dose from medical imaging modalities is received from CT scans [10]. Thus, dose reduction has become a very important goal in CT applications [11]. However, there are tradeoffs between image quality and dose; the higher the dose contributing to the image, the lower image noise, and hence, the better visualization of low-contrast structures. Detection of low-contrast details and lesions is primarily limited by noise, which can be reduced by increasing radiation dose [12, 13]. Consequently, there is an imperative need for image quality optimization and radiation dose reduction for CT images.

Several methods are used to evaluate imaging performance and image quality. Detection quantum efficiency, receiver-operating characteristics, visual grading characteristics, and low-contrast detail (LCD) detectability are all commonly used methods [14, 15]. However, several authors state that LCD is the most appropriate method to optimize image quality and to examine the potential of radiation dose reduction [16, 17].

Since the common task of diagnostic CT scan images is the visual detection of lesions, detectability performance is an important measure of image quality [18]. The theory behind LCD implies that the detectability of details increases with the increasing size of objects or contrast between objects and their background [14, 19]. LCD is usually measured by using low-contrast detail phantoms that contain cylindrical objects of a range of different sizes and low-contrast levels [20, 21]. LCD phantom images are assessed subjectively by interpreter observation or objectively by measuring the contrast-to-noise ratio (CNR) [22]. LCD can also be used to compare and contrast the performance of different imaging systems [23]. LCD studies are also useful to examine image optimization and to assess the potential of dose reduction of imaging systems [17, 24]. However, recognizing and understanding the factors that influence the detectability performance of different CT scan systems are fundamental concerns in effectively implementing this method.

The purpose of this review is to determine the factors influencing LCD performance of different CT systems and to explain their influences on image quality optimization.

Factors Affecting Low-Contrast Detail Performance in CT

Detectability performance of CT imaging systems is influenced by CT system specification, milliampere-second, peak kilovoltage, slice thickness, pitch, and beam collimation, as well as image processing and visualization. These factors should be adjusted to optimize image quality in terms of LCD performance by lowering image noise and maintaining lower radiation dose to the patient (Figure 1).
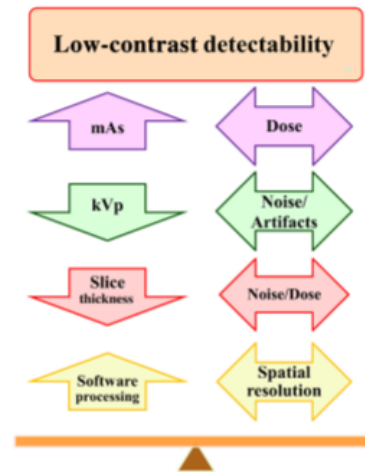

Figure 1. The detectability performance can be optimized by balancing between the adjusted protocols parameters (milliampere-second [mAs], peak kilovolt [kVp], slice thickness/pitch, and software processing) and tolerated noise and artifacts while maintaining low radiation dose.

Scanner Systems

Each CT system and model has its own performance ability according to its properties and specifications (Figure 2). The design criteria employed in CT systems fundamentally characterize the type of noise, which in turn affects the detectability performance of the produced images [25]. Image blur is largely determined by scanner specifications. The size of the sampling aperture is regulated by the focal spot size and the detector size; the size of the voxels is considered a blurring source [26]. Each system has limited gantry rotation time and area coverage, which influence image quality and lesion detectability [11, 27]. Accordingly, the influences of imaging factors on image quality vary across different systems, models, and manufacturers.

The following discussion will show that the detectability performance of different CT systems and scanners is not the same. Although the latest MDCT and other newer technologies are suggested to have better image quality, they still have limitations that may affect the LCD.

Spiral CT (Single-Slice CT)

The introduction of spiral or helical CT in 1989 increased the advantages and the applications of CT systems [9]. Spiral CT involves continuous patient translation and continuous radiation exposure during the rotation of x-ray tube and data acquisition (Figure 2A). Therefore, a volume dataset is obtained in a relatively short period of time compared to single-slice CT [9]. However, in single-slice spiral CT, coronary artery imaging could only be possible by gating or under
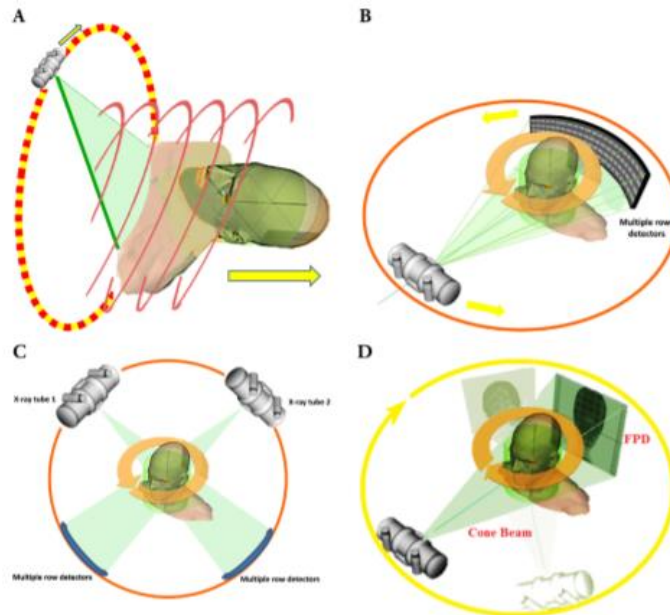
Figure 2. **A**, Spiral computed tomography (CT) single slice, helical CT scanner with single row detector (modified from Exxim Computing Corp). [39]. **B**, Multi-detector CT, CT scanner with multiple row detectors (modified from Exxim Computing Corp). [39]. **C**, Dual-source CT, CT scanner with two x-ray tubes (modified from Exxim Computing Corp). [39]. **D**, Cone-beam CT, CT scanner with flat panel detector (FPD) (modified from Exxim Computing Corp) [39].

ideal imaging conditions with slow heart rates, and even then they can have biphasic motion artifacts [28].

Multidetector CT

MDCT is a spiral CT scanner with more than one row of detectors; there may be 4, 16, 64, 256, or 320 detector rows that are able to generate many slices simultaneously and complete multiple scans in seconds or in a subsecond period (Figure 2B). Recent MDCT can also provide isotropic resolution and reconstruct cross-sectional images in arbitrary planes [28, 29].

It is accepted that MDCT improves and enhances the image quality of CT studies. MDCT systems are better than single-slice CT because they have faster scanners and smaller detector element size, cover a larger area, and use enhanced reconstruction algorithms. Sensitivity and specificity of MDCT to detect pathologies, particularly cardiovascular diseases, are much higher than that of single-slice CT [28]. The entire chest of a patient can be scanned by multislice CT with 1-mm slices and within one breathhold. Spatial resolution becomes much higher with MDCT [28, 29]. Hence, the accuracy of diagnostic applications is improved.

The development of more row detectors CT has reduced examination time and has improved image quality. Gantry rotation time is significantly reduced by using faster MDCT

scanners, and thinner slices are obtained by utilizing thinner detector rows. Shorter gantry rotation time improves temporal resolution, which is essential to reduce the effects of motion artifacts. Thinner slices improve spatial resolution, which minimizes the effects of partial volume average and calcium artifacts [28]. Stair-step artifacts (Figure 3) are almost eliminated with more detector rows scanners, particularly with 64 or more detector rows MDCT. Stair-step artifacts occur around the edges of structures in the volume or
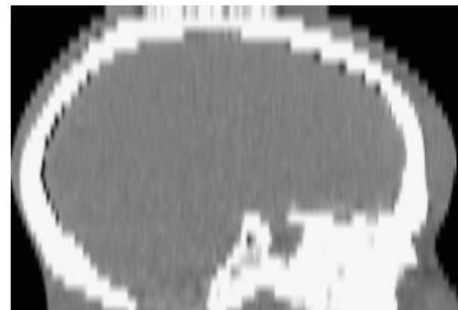

Figure 3. Sagittal reformatted computed tomography image obtained with 5-mm collimation and a 5-mm reconstruction interval shows stair-step artifacts [30].

317

multiplanar reformatted images, in particular when wide collimations and nonoverlapping scanning are used [30].

The 256–detector row MDCT is able to cover 128 mm of anatomy with 0.5 mm slices. In addition, the number of channels in the radial axis has been increased in this scanner. It is able to generate fine, isotropic resolution of structures. Cardiac imaging is especially difficult because of heart beating motion and tiny coronary arteries structures. The 256 MDCT scanner provides higher image quality and has higher potential of radiation dose reduction than that of previous scanners. It ensures more accurate and quicker diagnoses [28]. The possibility of fusing the images with CT angiography examinations allows morphologic and functional assessment [31].

The most recent development of MDCT includes an increased number of detector rows, up to 320. The gantry rotation time (350 milliseconds) is shorter than many 256 MDCT scanners; a 320 MDCT system achieves complete coverage of the heart within a single rotation without table movement, as this system can cover 160 mm of anatomy [28, 32]. Volumetric imaging of the entire heart is completed within one cardiac cycle [31]. This system enables assessment of smaller coronary vessels up to 1.5 mm and detection of small volume plaque [8]. The results of the study conducted by Khan et al [33] suggest that with the same image quality of 64 MDCT, 320 MDCT has the capability to significantly reduce radiation doses delivered to patients. The wider area coverage and faster gantry rotation offered by 320 MDCT improves the temporal resolution and avoids exposure-intensive overscanning [34]. The higher temporal resolution offers a potential to significant dose reduction and reduces the motion effects of heart structures on the image [34].

However, multiplanar and three-dimensional reformation approaches generate artifacts. Zebra artifacts appear as faint stripes, with an increased degree of noise (Figure 4) [30]. Interpolation methods, which were developed with the introduction spiral scanning, also contribute to additional artifacts on images [35]. Because of the continuous tube and table motion, the projections processed in a spiral motion around the patient and did not lie in a single plane. Hence,
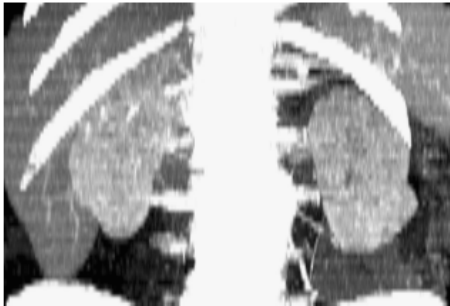

Figure 4. Computed tomography image obtained with helical shows zebra artifacts [30].

interpolation reconstruction algorithms methods are used to generate projections in a single plane [11]. The effects of interpolation artifacts increases as pitch and the number of detector rows increase. Interpolation artifacts also cause inaccuracies in CT number assessment, which leads to misdiagnosis [35].

Furthermore, one of the main disadvantages of the MDCT system is the use of wider beam collimation, which leads to image deterioration compared to sequential type scanners [35]. Wider collimation is required for more detector rows, and the x-ray beam, in turn, becomes cone shaped. The new image reconstruction technology using cone-beam algorithms creates negative effects on image quality called *cone-beam artifacts*. The greater the divergence of cone beams is, the larger the artifact effects [35]. Cone-beam artifacts occur because the data collected from each detector during gantry rotation do not correspond to the ideal flat plane but actually to volume contained between two cones. The artifacts caused by cone beam are similar to those caused by partial volume around off-axis structures. Cone-beam artifacts are less pronounced for the inner detector rows than for the outer rows [30].

In-plane spatial resolution is not improved by the current advanced technology of MDCT. Current reconstruction methods are focused on cross-plane spatial resolution, and the focus has not been on spatial resolution with the two-dimensional image plane [8, 9].

Dual-Source CT

DSCT utilizes two x-ray tubes that are arranged in a single gantry at a 90-degree offset. Although the two tubes and detectors are operated simultaneously, a quarter rotation of the gantry is sufficient to collect the data necessary for one image. So that a gantry rotation time of 330 milliseconds provides an effective scan time of 83 milliseconds in the centre of rotation, the exposure time can be reduced by a factor of two (Figure 2C) [36]. As a result, temporal resolution can be increased by the same factor [28, 36, 37]. However, DSCT has similar difficulties of recent MDCT because of the intrinsic limitations of CT image reconstruction matrix and spatial resolution [38].

Flat-Panel Volume or CBCT

The most recent development in CT technology is CBCT. In CBCT (Figure 2D), flat-panel detectors instead of the multidetector rows in MDCT are utilized [39]. CBCT is promising for diagnostic and interventional clinical purposes because of the capability for high-spatial resolution volumetric imaging and dynamic CT scanning [40].

The wide coverage (z-axis) flat-panel detector allows for imaging of entire organs, such as an entire heart or brain, in one axial scan. Moreover, flat-panel detectors mostly consist of ≤200 μm detector element size. CBCT detector with a 150-μm element size can provide ultrahigh spatial resolution up to 150×150 μm. Therefore, CBCT is superior in its spatial resolution compared with MDCT, which provides

spatial resolution only up to approximately 400 μm in plane and approximately 500 μm in the z-axis direction. The two-dimensional flat panel detectors allow for imaging at any arbitrary angle. In comparison with MDCT, CBCT allows for thinner sections using similar radiation doses as MDCT [40]. However, the two processes are different in the sense that MDCT has superior contrast resolution compared with CBCT. In addition, MDCT also allows for a faster scanning time compared with CBCT, which has a slow caesium iodide scintillator that is utilized in the flat-panel detector. Their use limits the projection acquisition time to 100 frames per second, compared with 900 to 1,200 projections during a single 0.5-second rotation for MDCT [40].

Tube Current, Tube Current-Time Product, and Radiation Dose

Image quality improvement requires reducing noise and increasing signal-to-noise ratio (SNR); however, this typically implies additional radiation to the patient. Doubling the signal, the radiation dose, is required to increase SNR by a factor of 1.4. The clinical situation determines the acceptable radiation dose, although the high-dose protocol is not recommended (Figure 5) [41]. Decreasing the milliampere-second reduces radiation dose, but at the same time, it increases image noise and reduces the contrast-to-noise ratio (CNR). The visibility of structures is negatively influenced by the reduction of x-ray quanta amount [42, 43]. Furthermore, spatial resolution properties can also be affected by the radiation dose, and there is a tradeoff between them [44]. However, the acceptable level of tradeoff in image quality should be determined according to the diagnostic purpose and clinical task being performed [13].

LCD is improved by increasing the milliampere-second to reduce the noise. However, milliampere-second should be adjusted to minimize radiation dose while maintaining optimum LCD.

Tube Potential

Subject contrast is increased with reducing kilovoltage. Low kilovoltage increases photoelectric interactions, which improve the attenuation level, leading to image contrast enhancement and improved detail visualization [13, 45]. However, subject contrast must not be confused with visualized or displayed contrast, which can be altered on the monitor.

Godoy et al [46] suggest that, although the measured image noise was higher in the low-kilovolt images, the subjective quality of the image was higher for 80 kVp than for 140 kVp images. This result highlights the fact that SNR and CNR determine the image quality more than image noise. Further, Funama et al [43] found that low kilovolts can improve CNR, and their result suggests using 90 kVp rather than selecting 120 kVp. The noise with low-kilovoltage images did not cause a reduction in image quality due to the higher SNR and higher attenuations (Figure 6) [46–48].

Radiation dose to the patient is not linear with kilovoltage, but reducing the kilovoltage does reduce the amount of radiation when other exposure factors are fixed [13]. Funama et al [43] suggest that the radiation dose can be reduced by 29% without affecting the CNR by selecting 90 kVp instead of 120 kVp [43]. A study conducted by Zhang et al [49] suggested that selecting 100 kVp compared with 120 kVp in 320 MDCT can reduce the radiation dose to patients without degrading image quality.

A multireader study conducted by Ertl-Wagner et al [45] examined the impact of various kilovoltages, specifically 80, 120, and 140 kVp, while all other exposure factors were fixed on image quality of vessel delineation with cranial MDCT. Their study showed that the higher voltages were superior in terms of having the greatest effects for vessels close to bone and subsegmental arteries.

Lower kilovoltage techniques reduce the total energy flux if other exposure factors are not adjusted, which increases the image noise, leading to reduction in image quality and diagnostic accuracy of CT [13, 45, 46, 50]. Artifacts, such as beam hardening, may also be increased with low-energy beams, such as 80 kVp [13]. Huda et al [50] suggest that image noise from low kilovoltage can be suppressed by utilizing a new adaptive filter.
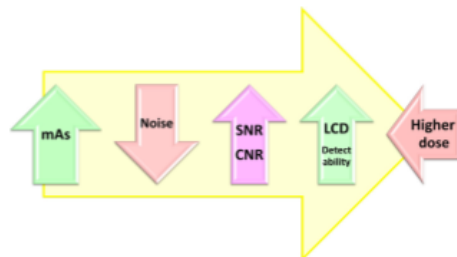

Figure 5. The relationship between milliampere-second [mAs], noise, signal-to-noise ratio (SNR) and contrast-to-noise ratio (CNR) and the low-contrast detail (LCD) detectability is illustrated. Increasing milliampere-second reduces the noise and increases SNR and CNR and as a result LCD is improved. However, increasing milliampere-second increases the radiation dose to the patient.
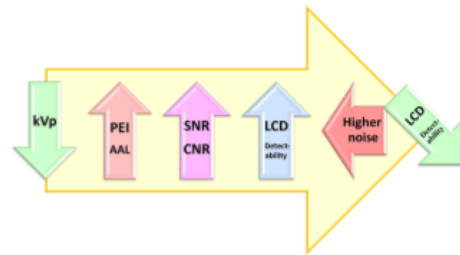
Figure 6. The relationship between peak kilovoltage (kVp), signal-to-noise ratio (SNR), contrast-to-noise ratio (CNR), noise, and the low-contrast detail (LCD) detectability is illustrated. Appropriately lowering kilovoltage increases photoelectric interaction (PEI) and the attenuation level (AAL), which leads to an increase in SNR and CNR, and hence LCD performance is improved. However, the noise level increases with excessively lowering kilovoltage or if the other exposure factors are not adjusted.

319

In addition, although the selection of low kilovoltage minimizes radiation to patients, kilovoltage should be selected depending on the patient's cross-section diameter and should be adjusted according to the task. For example, while 80 kVp should be used in small children, 140 kVp should be used in obese patients [9].

According to the above discussion, the interdependence of image quality and radiation dose on kilovoltage is very complex. The kilovoltage should be optimized to be low enough to increase contrast resolution in order to improve LCD, but high enough to reduce the noise and minimize radiation. Patient size and examination purpose should also be considered in kilovoltage selection to optimize LCD performance.

Pitch, Beam Collimation, and Slice Width

Thinner submillimetre slice thicknesses are routinely acquired when using MDCT and provide high-resolution isotropic image datasets. Therefore, through-plane, partial-volume averaging effects are minimized and image postprocessing, such as three-dimensional reconstruction, multiplanar reformatting software-assisted lesion detection, and quantification, is optimized [9, 51]. However, when thinner slices are used, noise will be increased. This is important because low-contrast detectability is degraded by noise [41]. Thus, exposure factors should be increased to reduce image noise. To do so, the radiation dose to patient will also be increased (Figure 7) [13, 41].

Radiation dose from slice thickness selection is also influenced by overranging and overbeaming. *Overranging* is when additional gantry rotations are automatically performed by the scanner to acquire enough data for image construction, where the rotation number increases with increasing collimation, when increasing section thickness in the primary reconstruction, and when increasing pitch [52, 53].

Overbeaming occurs when the actual profile beam collimation, which is determined by changing the active detectors number or their length in MDCT, widens larger than the nominal beam widths to keep uniform distribution of
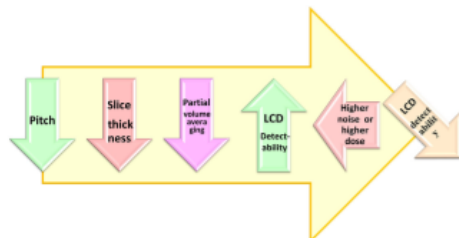
radiation across the detector bank [53]. Overbeaming is explained as the resultant penumbra effect, which depends on the type of MDCT scanner. Overbeaming increases the radiation dose, but it may be reduced by selecting thicker slices or by utilizing more channels. For example, overbeaming effects are diminished much more with 16 MDCT scanners compared with 4 MDCT [53]. Therefore, there is a tradeoff between the advantages of nearly isotropic voxels, which influence spatial resolution, and the disadvantages of image noise and radiation dose when determining the choice of section thickness [41].

Noise from thin slice thickness can be reduced to improve low-contrast lesion detectability by increasing radiation doses to increase SNR, using soft reconstruction kernels, applying various data filters, adjusting window and level settings, and utilizing sliding-thin-slab averaging. Using a sliding-thin-slab averaging algorithm with thin-section scanning during image reconstruction can reduce the effects of through-plane, partial-volume averaging and improve the detectability of low-contrast objects by the retrospective generation of thicker sections [41].

Thus, selecting slice thickness, according to the diagnostic purposes, is fundamental to acquiring higher LCD while maintaining desired spatial resolution and lower radiation dose.

Image Reconstruction, Processing, and Visualization

CT images are available in digital form, which can then be processed, manipulated, and modified directly by computer algorithms. Density values, histograms, and other tissue parameters can be determined at any time in digital CT images. Different orientation views, such as coronal, sagittal, and oblique planes, can be reformed from the original axial images. Two-dimensional images can be reconstructed to three-dimensional displays. Virtual endoscopic views, interactive manipulation of image volumes, and four-dimensional animated studies are also possible applications in CT imaging. Automatic determination of specific tissues is now possible with advanced image processing approaches [9].

The recent implementation of iterative reconstruction techniques that are being used instead of filtered back-projection is a promising strategy for decreasing noise and artifacts on CT images. Iterative reconstruction algorithms are statistical reconstruction methods that require higher computational capabilities compared to analytical methods such as filtered back-projection. Iterative reconstruction methods consist of three main steps. First, the artificial raw data are created, then the artificial and measured raw data are compared, and then an updated image is computed, which is then back-projected to the current volumetric image. These steps are repeated iteratively and form the iterative reconstruction loop. When the loop is terminated, the final volumetric image is produced [54].

Iterative reconstruction techniques demonstrate impressive improvements in noise reduction and image quality in comparison with filtered back-projection [54–56]. Iterative

Figure 7. The relationship between pitch, slice thickness, noise, and low-contrast detail (LCD) detectability is illustrated. Selecting lower pitch allows producing thinner image slices. Thinner image slices reduce the problem of partial volume averaging and hence the LCD is improved. However, thinner slices selection increase image noise, which in turn deteriorates LCD, if the radiation dose is not increased.

320

reconstruction algorithms have the potential to reduce the radiation dose as they reduce image noise and various artifacts. In addition, iterative methods avoid introducing new artifacts because of approximations, as more intuitive and natural ways of image reconstruction are represented by these methods. They also improve image quality, as they are more suited for dealing with missing data or irregular sampling. Iterative methods provide higher flexibility in the scan geometry, as many various trajectories are possible since no explicit expression of an inverse transform is needed [54].

Different iterative techniques are implemented in clinical CT. GE Healthcare started with adaptive statistical iterative reconstruction in 2008, followed by GE's Veo technology, a more complex model-based iterative reconstruction method, in 2009. Siemens implemented image reconstruction in image space in 2009, and recently introduced is the sinogram-affirmed iterative reconstruction, a technique that works in both raw data and image space. Philips announced their iterative reconstruction, iDose, in 2009 [54, 56]. Iterative reconstruction techniques are performed either from the image data alone, such as iterative reconstruction in image space, Siemens Healthcare, from both the projection and image data such as adaptive statistical iterative reconstruction, sinogram-affirmed iterative reconstruction, and iDose, or from projection data alone. These techniques may be used either to reduce the amount of image noise in order to improve image quality in large patients or to reduce radiation doses in small or intermediate-sized patients while maintaining diagnostically adequate noise [56].

The detectability of low-contrast detail can be improved by selecting appropriate soft reconstruction kernels while maintaining low radiation doses to the patient [57, 58]. Consequently, diagnostic accuracy is improved [58]. Using the wrong filters for the reconstruction algorithm degrades image quality and reduces diagnostic reliability [59]. Unfortunately, there is no general recommendation that can be made for the optimum settings of reconstruction algorithms because their properties are not standardized and vary greatly between vendors and scanner types [58]. Generally, there is a tradeoff between selection of a specific reconstruction algorithm and the desired spatial resolution and the tolerated image noise [12].

The window level and window width can be adjusted to display a CT image with appropriate contrast. Although the window level determines the centre CT number value displayed by the range of grey scale, the window width determines that range of CT numbers. The window level and window width settings dictate how the actual measurements of tissue attenuation are converted into a grey-scale image. They are adjusted according to the tissue properties and diagnostic purposes. For example, to precisely visualize soft tissues, narrow width can be selected, and to accurately demonstrate the bone width, wide window widths can be used [60].

The factors of soft image display, such as monitor brightness, display function, resolution, room illumination, and image size, also affect the detectability of lesions [61]. High display contrast is required to visualize low-contrast features. That can be achieved by increasing the contrast of the monitor and by reducing window width as far as possible without loss of diagnostic information of medical image [62].

The commonly available display devices are liquid-crystal display monitors (LCDM) and cathode-ray tube (CRT) monitors. LCDM are increasingly used in medical imaging departments for their inherent advantages [63]. The dynamic range provided by LCDM is larger than that provided by CRT monitors. Higher small-spot contrast ratio is provided by LCDM more so than CRT monitors. However, when LCDM are visualized from different angulated views, the contrast resolution is extremely decreased. This is considered the main limitation of LCDM [63]. Low-contrast detail detectability can be improved using high-resolution LCDM and by utilizing the interactive adjustment of brightness and contrast of digital images [64].

From the above discussion, utilizing correct image reconstruction algorithms and image processing applications improves the performance of LCD while maintaining the desired spatial and contrast resolution and the tolerated noise. Display monitors and visualizing conditions are also essential to acquire higher detectability performance.

Conclusion

The effects of low-contrast detail performance of different CT scanner systems have been discussed in this article. The impact level of the factors of contrast detail detectability on image quality is complex and does not exactly match from one type of scanner to another or from one unit to another. These factors are the ultimate key to optimizing image quality in terms of detail detectability, while utilizing lower doses.

Although the performance detectability within CT is inherent to the system type and unit specification and cannot be controlled by radiographers, radiographers play an essential role to improve system performance and image quality by effectively controlling and adjusting exposure factors. It is recommended that radiographers have a greater understanding of the various CT scanners systems in order to improve the image quality while lowering radiation dose to the patient. Further studies of contrast-detail performance are required to further enhance the understanding of the influences of the exposure factors on image quality and radiation dose.

References

[1] Ledenius, K., Gustavsson, M., Johansson, S., Stalhammar, F., Wiklund, I. I.-M., & Thilander-Klang, A. (2009). Effect of tube current on diagnostic image quality in paediatric cerebral multidetector CT images. *Br J Radiol* 82, 313–320.

[2] Fishman, E. (2007). Hot topics in CT. *Appl Radiol* 36, 4–9.

321

[3] Kato, Y., Nair, S., & Sano, H., et al. (2002). Multi-slice 3D-CTA–an improvement over single slice helical CTA for cerebral aneurysms. *Acta Neurochir* 144, 715–722.

[4] Peldschus, K., Herzog, P., Wood, S., Cheema, J., Costello, P., & Schoepf, U. (2005). Computer-aided diagnosis as a second reader. *Chest* 128, 1517.

[5] Imai, K., Ikeda, M., Enchi, Y., & Niimi, T. (2009). Statistical characteristics of streak artifacts on CT images: relationship between streak artifacts and mA s values. *Med Phys* 36, 492–499.

[6] Miller, J. M., Rochitte, C. E., & Dewey, M., et al. (2010). Quantitative and diagnostic accuracy of 64-MDCTA for segmental coronary artery stenosis detection: results from the core-64 multicenter international study. *JACC* 55, E757–E759.

[7] Sun, J., Zhang, Z., & Lu, B., et al. (2008). Identification and quantification of coronary atherosclerotic plaques: a comparison of 64-MDCT and intravascular ultrasound. *AJR Am J Roentgenol* 190, 748–754.

[8] Paul, N., Blobel, J., Kashani, H., Rice, M., & Ursani, A. (2010). Quantification of arterial plaque and lumen density with MDCT. *Med Phys* 37, 4227–4237.

[9] Kalender, W., & Khadivi, K. (2011). Computed tomography: fundamentals, system technology, image quality, applications, (3rd ed.). Erlangen: Publicis.

[10] Hayton A., Wallace A., Edmonds K., & Tingey D. (2010). Application of the European DOSE DATAMED methodology and reference doses for the estimate of Australian MDCT effective dose (mSv). In *Proceedings of the Third European IRPA Congress 2010*. Helsinki: ARPANSA.

[11] Mahesh, M. (2009). MDCT physics: the basics–technology, image quality and radiation dose. Philadelphia: Lippincott Williams & Wilkins.

[12] Goldman, L. W. (2007). Principles of CT: radiation dose and image quality. *J Nucl Med Technol* 35, 213–225.

[13] Seibert, J. A. (2004). Tradeoffs between image quality and dose. *Pediatr Radiol* 34, 183–195.

[14] Bath, M. (2010). Evaluating imaging systems: practical applications. *Radiat Prot Dosimetry* 139, 26–36.

[15] Cowen, A., Kengyelics, S., & Davies, A. (2008). Solid-state, flat-panel, digital radiography detectors and their physical imaging characteristics. *Clin Radiol* 63, 487–498.

[16] Baker, M. E., Dong, F., & Primak, A., et al. (2012). Contrast-to-noise ratio and low-contrast object resolution on full-and low-dose MDCT: SAFIRE versus filtered back projection in a low-contrast object phantom and in the liver. *AJR Am J Roentgenol* 199, 8–18.

[17] Alsleem, H., & Davidson, R. (2012). Quality parameters and assessment methods of digital radiography images. *Radiographer* 59, 46–55.

[18] Wunderlich, A., & Noo, F. (2008). Image covariance and lesion detectability in direct fan-beam x-ray computed tomography. *Phys Med Biol* 53, 2471–2493.

[19] Davidson, R. (2007). Radiographic contrast-enhancement masks in digital radiography. Thesis, University of Sydney. Available at: http://hdl.handle.net/2123/1932. Accessed December 20, 2012.

[20] Suess, C., Kalender, W. A., & Coman, J. M. (1999). New low-contrast resolution phantoms for computed tomography. *Med Phys* 26, 296–302.

[21] Zarb, F., Rainford, L., & McEntee, M. F. (2010). Image quality assessment tools for optimization of CT images. *Radiography* 16, 147–153.

[22] Verdun, F. R., Denys, A., Valley, J. F., Schnyder, P., & Meuli, R. A. (2002). Detection of low-contrast objects: experimental comparison of single–and multi–detector row CT with a phantom. *Radiology* 223, 426–431.

[23] Hernandez-Giron, I., Geleijns, J., Calzado, A., & Veldkamp, W. (2011). Automated assessment of low contrast sensitivity for CT systems using a model observer. *Med Phys* 38, S25.

[24] Hamer, O. W., Völk, M., Zorger, N., Feuerbach, S., & Strotzer, M. (2003). Amorphous silicon, flat-panel, x-ray detector versus storage phosphor-based computed radiography: contrast-detail phantom study at different tube voltages and detector entrance doses. *Invest Radiol* 38, 212–220.

[25] Faulkner, K., & Moores, B. (1984). Noise and contrast detection in computed tomography images. *Phys Med Biol* 29, 329–339.

[26] Hsieh, J. (2009). Computed tomography: principles, design, artifacts, and recent advances, (2nd ed.). Hoboken, NJ: SPIE.

[27] Seeram, E. (2009). Computed tomography: physical principles, clinical applications and quality assurance, (3rd ed). New York: Saunders/Elsevier.

[28] Hurlock, G. S., Higashino, H., & Mochizuki, T. (2009). History of cardiac computed tomography: single to 320-detector row multislice computed tomography. *Int J Cardiovasc Imaging* 25(Suppl 1), 31–42.

[29] Bardo, E., & Brown, P. (2008). Cardiac multidetector computed tomography: basic physics of image acquisition and clinical applications. *Curr Cardiol Rev* 4, 231–243.

[30] Barrett, F., & Keat, N. (2004). Artifacts in CT: recognition and avoidance. *Radiographics* 24, 1679–1691.

[31] Hsiao, E. M., Rybicki, F. J., & Steigner, M. (2010). CT coronary angiography: 256-slice and 320-detector row scanners. *Curr Cardiol Rep* 12, 68–75.

[32] Kitajima, K., Maeda, T., & Ohno, Y., et al. (2011). Capability of abdominal 320-detector row CT for small vasculature assessment compared with that of 64-detector row CT. *Eur J Radiol* 80, 219–223.

[33] Khan, A., Khosa, F., Nasir, K., Yassin, A., & Clouse, M. E. (2011). Comparison of radiation dose and image quality: 320-MDCT versus 64-MDCT coronary angiography. *AJR Am J Roentgenol* 197, 163–168.

[34] van der Wall, E., de Graaf, F., van Velzen, J., Jukema, J., Bax, J., & Schuijf, J. (2012). 320-Row CT: does beat-to-beat motion of the coronary arteries affect image quality? *Int J Cardiovasc Imaging* 28, 147–151.

[35] Romans, L. E. (2010). Computed tomography for technologists: a comprehensive text. Philadelphia: Lippincott Williams & Wilkins.

[36] Achenbach, S., Anders, K., & Kalender, W. A. (2008). Dual-source cardiac computed tomography: image quality and dose considerations. *Eur Radiol* 18, 1188–1198.

[37] Flohr, G., McCollough, H., & Bruder, H., et al. (2006). First performance evaluation of a dual-source CT (DSCT) system. *Eur Radiol* 16, 256–268.

[38] Barreto, M., Schoenhagen, P., & Nair, A., et al. (2008). Potential of dual-energy computed tomography to characterize atherosclerotic plaque: ex vivo assessment of human coronary arteries in comparison to histology. *J Cardiovasc Comput Tomogr* 2, 234–242.

[39] EXXIM Computing Corporation. Cone-beam CT. Available at: http://www.exxim-cc.com/cone-beam_ct.html. Accessed December 20, 2012.

[40] Gupta, R., Cheung, A. C., & Bartling, S. H., et al. (2008). Flat-panel volume CT: fundamental principles, technology, and applications. *Radiographics* 28, 2009–2022.

[41] von Falck, C., Galanski, M., & Shin, H. (2010). Informatics in radiology: sliding-thin-slab averaging for improved depiction of low-contrast lesions with radiation dose savings at thin-section CT. *Radiographics* 30, 317–326.

[42] Toth, T. L. (2012). Image quality in CT: challenges and perspectives. In: D. Tack, M. K. Kalra, & P. A. Gevenois (Eds.), *Radiation dose from multidetector CT*, (2nd ed.). (pp. 81–100) Berlin Heidelberg: Springer.

[43] Funama, Y., Awai, K., & Nakayama, Y., et al. (2005). Radiation dose reduction without degradation of low-contrast detectability at abdominal multisection CT with a low–tube voltage technique: phantom study. *Radiology* 237, 905–910.

[44] Özgün, A., Rollvén, E., Blomqvist, L., Bremmer, S., Odh, R., & Fransson, A. (2005). Polyp detection with MDCT: a phantom-based evaluation of the impact of dose and spatial resolution. *AJR Am J Roentgenol* 184, 1181–1188.

[45] Ertl-Wagner, B. B., Hoffmann, R.-T., & Bruning, R., et al. (2004). Multi–detector row CT angiography of the brain at various kilovoltage settings. *Radiology* 231, 528–535.

[46] Godoy, M. C. B., Heller, S. L., & Naidich, D. P., et al. (2010). Dual-energy MDCT: comparison of pulmonary artery enhancement on dedicated CT pulmonary angiography, routine and low contrast volume studies. *Eur J Radiol* 79, E11–E17.

322

[47] Schindera, S. T., Nelson, R. C., & Mukundan, S., et al. (2008). Hypervascular liver tumors: low tube voltage, high tube current multi–detector row CT for enhanced detection—phantom study. *Radiology* 246, 125–132.

[48] Marin, D., Nelson, R. C., & Barnhart, H., et al. (2010). Detection of pancreatic tumors, image quality, and radiation dose during the pancreatic parenchymal phase: effect of a low-tube-voltage, high-tube-current CT technique—preliminary results. *Radiology* 256, 450–459.

[49] Zhang, C., Zhang, Z., Yan, Z., Xu, L., Yu, W., & Wang, R. (2011). 320-row CT coronary angiography: effect of 100-kV tube voltages on image quality, contrast volume, and radiation dose. *Int J Cardiovasc Imaging* 27, 1059–1068.

[50] Huda, W., Scalzetti, E. M., & Levin, G. (2000). Technique factors and image quality as functions of patient weight at abdominal CT. *Radiology* 217, 430–435.

[51] Rubin, G. D. (2003). 3-D imaging with MDCT. *Eur J Radiol* 45(S1), S37–S41.

[52] van der Molen, A. J., & Geleijns, J. (2007). Overranging in multisection CT: quantification and relative contribution to dose—comparison of four 16-section CT scanners. *Radiology* 242, 208–216.

[53] Theocharopoulos, N., Damilakis, J., Perisinakis, K., & Gourtsoyiannis, N. (2007). Energy imparted-based estimates of the effect of z overscanning on adult and pediatric patient effective doses from multi-slice computed tomography. *Med Phys* 34, 1139–1152.

[54] Beister, M., Kolditz, D., & Kalender, W. A. (2012). Iterative reconstruction methods in x-ray CT. *Phys Med* 28, 94–108.

[55] Winklehner, A., Karlo, C., & Puippe, G., et al. (2011). Raw data-based iterative reconstruction in body CTA: evaluation of radiation dose saving potential. *Eur Radiol* 21, 1–6.

[56] Marin, D., Nelson, R. C., Rubin, G. D., & Schindera, S. T. (2011). Body CT: technical advances for improving safety. *AJR Am J Roentgenol* 197, 33–41.

[57] Yoo, S., Kim, Y., & Hammoud, R., et al. (2006). A quality assurance program for the on-board imager. *Med Phys* 33, 4431–4447.

[58] Bissonnette, P., Moseley, J., & Jaffray, A. (2008). A quality assurance program for image quality of cone-beam CT guidance in radiation therapy. *Med Phys* 35, 1807–1815.

[59] Flohr, T., Stierstorfer, K., Ulzheimer, S., Bruder, H., Primak, A., & McCollough, C. (2005). Image reconstruction and image quality evaluation for a 64-slice CT scanner with z-flying focal spot. *Med Phys* 32, 2536–2547.

[60] Barnes, J. (1992). Characteristics and control of contrast in CT. *Radiographics* 12, 825–837.

[61] Yamaguchi, M., Fujita, H., Bessho, Y., Inoue, T., Asai, Y., & Murase, K. (2010). Investigation of optimal display size for detecting ground-glass opacity on high resolution computed tomography using a new digital contrast-detail phantom. *Eur J Radiol* 80, 845–850.

[62] Warren, R. (1984). Detectability of low-contrast features in computed tomography. *Phys Med Biol* 29, 1–13.

[63] Samei, E., Ranger, N. T., & Delong, D. M. (2008). A comparative contrast-detail study of five medical displays. *Med Phys* 35, 1358–1364.

[64] Bacher, K., Smeets, P., & De Hauwere, A., et al. (2006). Image quality performance of liquid crystal display systems: influence of display resolution, magnification and window settings on contrast-detail detection. *Eur J Radiol* 58, 471–479.

323

Appendix 1c   Publication arising from this work (3)

Effects of Radiographic Techniques (kVp and mAs) on the Contrast-Detail Detectability Performance of Different Digital Radiography Systems

Haney Alsleem
BSc, MSc
Discipline of Medical radiation
RMIT University
Bundoora, Victoria 3083, Australia
Tel. +61 3 9925 7075
Fax: +61 3 9925 7063
E-mail: haney.alsleem@rmit.edu.au
http://www.rmit.edu.au/medicalsciences
Affiliation: Dammam University

Paul U
MappSc (Med Phys)
Principal Medical Physicist
Tel: 9496 5589
Fax: 9496 5746
Mob: 0407 811 000
Email: paul.u@austin.org.au

Kam Shan Mong
Medical Physicist
Tel: 9496 2066
Mob: 0401 663 541
Email: lisa.mong@austin.org.au

Professor Robert Davidson
PhD, MAppSc(MI), BBus, FIR
Professor of Medical Imaging and Head, Discipline of Medical Radiation Science
School of Dentistry and Health Sciences, Faculty of Science
Charles Sturt University, Wagga Wagga 2678, Australia
Tel: +61 2 6933 2667
Fax: +61 2 6933 2835
Email: rdavidson@csu.edu.au
http://www.csu.edu.au/faculty/science/dentistry-health/

Affiliation   (the sponsor of Haney to study PhD in RMIT)
University of Dammam
Ministry of Higher Education
Kingdom of Saudi Arabia
Phone: 0096638571304
Fax: 0096638587105
E-Mail: info@ud.edu.sa, pr@ud.edu.sa
www.ud.edu.sa

1

Effects of Radiographic Techniques (kVp and mAs) on the Contrast-Detail Detectability Performance of Different Digital Radiography Systems

Abstract

PURPOSE: To evaluate the effects of x-ray exposure factors of tube voltage (kVp) and tube current-time (mAs) on the contrast-detail detectability performance of different planar digital radiography systems. This paper will also compare the detectability performance between computed radiography (CR), indirect digital radiography (IDR) and direct digital radiography (DDR) in terms of their low-contrast detail detectability.

MATERIALS AND METHODS: A contrast-detail phantom was inserted within 10 cm thickness of Perspex. The images were obtained with different kVp and mAs setting from CR, IDR and DDR systems. CDRAD analyzer software was used to score the images and to calculate inverse image quality figure (IQFinv).

RESULTS: The higher mAs levels in each kVp selection result in higher IQFinv in CR, IDR and DDR. In IDR, IQFinv values significantly increase with increasing kVp in only 1 and 2 mAs. There were insignificant differences in IQFinv values when altering kVp in each mAs level in DDR. The IDR system generally shows a better detectability performance than CR and DDR. However DDR shows a better detectability performance than IDR at lower kVp and mAs and CR at lower kVp.

CONCLUSION: Increasing mAs in all digital imaging systems generally improves detectability performance. However changing the kVp setting shows no significant change to the IQFinv and hence no change to detectability of objects in a digital radiograph. The selection of an imaging system should now be considered based on the typical radiographic examinations. Further studies are recommended to examine different manufacturers of systems and various Perspex thicknesses.

Key words

Contrast-detail detectability; IQFinv; CR; IDR and DDR

2

Introduction

Planar digital radiography imaging systems currently used in clinical settings are either computed radiography (CR) or digital radiography (DR). These systems have replaced conventional film/screen radiography due to their performance capabilities.[1]

Computed radiography systems consist of storage phosphor plates enclosed in cassettes. The exposed plates are read by a laser digitizer to construct the radiographic image.[2] Solid-state flat panel detectors (FPD) are used in DR to create a radiographic image.[3] Currently there are two principal designs of FPD systems available, indirect-conversion DR (IDR), which is based on an x-ray scintillator, and direct-conversion DR (DDR), which is based on an x-ray photoconductor.[4-6] Planar radiographic image quality has been improved and patient radiation dose has been reduced by the introduction of these systems.[7,8] However, they still have some drawbacks.

The use of CR, IDR and DDR has the potential to increase patient radiation dose due to their wide dynamic range.[9] Patients may be overexposed with more radiation than is required for a diagnostically sufficient image.[2,8] Radiographic images should be regularly evaluated to ensure adequate diagnostic image quality and that low doses are delivered to patients.[10] Even though the detectability performance of digital radiography is inherent to the system type and unit specification and cannot be controlled by radiographers, they can play an essential role in improving system performance and image quality by effectively controlling and adjusting exposure factors.[11] However many radiographers still operate in a "film like" world.[12] For example, they operate using film/screen factors on digital equipment, while required exposure factors and image quality optimisation technique of digital radiography

3

326

image and radiography film are not similar.[13]

The low contrast-detail evaluation method is the choice for image optimization.[13] This method is based on the use of phantoms and it does not require volunteer patients. The method is also helpful to predict the influence of lower exposure factors on image quality and diagnostic efficacy in order to determine exposure parameters that provide optimum image quality while maintaining lower radiation doses. Low contrast-detail measurements can determine the trade-offs among perceived image quality, diagnosis efficacy, and exposure dose.[14] The low contrast-detail analysis method provides quantitative evaluations of low contrast and small detail measurement of clinical images. Therefore, it is considered a straightforward and direct method of image quality assessment.[15,16] The subjectivity of low contrast-detail analysis is avoided by utilizing automated scoring employing a software package. This software utilizes a mathematical model of the human visual system based on measurements of signal-to-noise ratio (SNR).[14,17]

This study aimed to acquire a deeper understanding of exposure effects of the kVp and the mAs on the image quality optimization of various CR, IDR and DDR systems in terms of detectability performance of low contrast detail. The detectability performance was also compared between CR, IDR and DDR.

Materials and Methods

Phantom Model (CDRAD phantom)

The CDRAD type 2.0 phantom (Artinis Medical Systems, Zetten, http://www.artinis.com) was used as the contrast-detail object and has a size of 26.5 x 26.5 x 1 cm. The phantom consists of a square Plexiglas plate containing drilled holes of varying depths (0.3–8.0 mm) and diameters (0.3– 8.0 mm). The phantom has 225 areas with varying drilled hole sizes and

4

depths to provide varying contrast-detail within the resultant image as illustrated in Figure 1a and 1b.

The CDRAD phantom was inserted between 10 cm thickness of Perspex sheets, 5 cm thickness above and 5 cm underneath the phantom. This thickness of Perspex, which is a transparent plastic (polymethyl methacrylate), was used to simulate attenuation of anatomical region of 10 cm soft tissue and to provide homogeneous scatter source thickness. This layout of Perspex and the phantom is shown in Figure 2 and is similar to approaches used in other similar projects.[16,18]
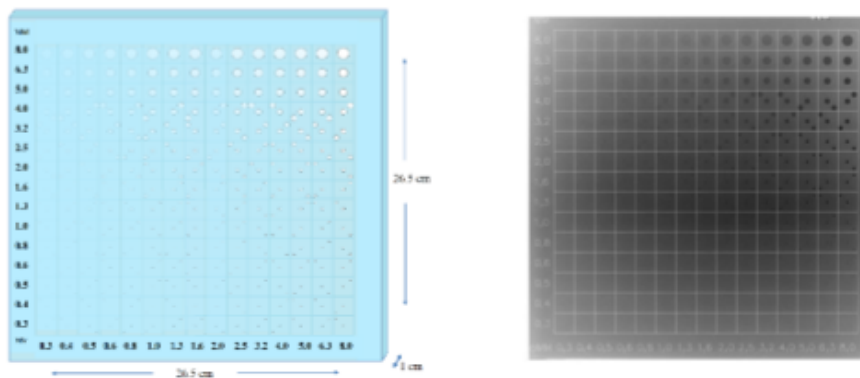
Figure 1   Schematic diagram of CDRAD phantom (a), A radiograph of CDRAD phantom (b)

http://www.artinis.com.
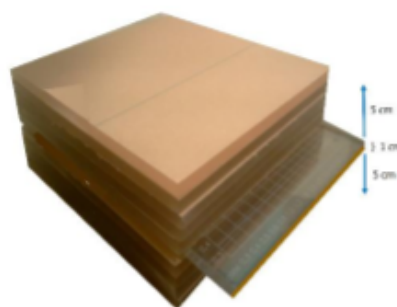
Figure 2   10 cm thickness of Perspex plates, the phantom is inserted in the middle of the plates.

5

Detector Types

Radiographs of the CDRAD phantom were obtained from CR and both direct and indirect DR conversion types. The specifications of these systems are provided in Table 1. Quality assurance tests of x-ray units' performance including half value layer (HVL), linearity and reciprocity, and accuracy and reproducibility were undertaken and all units passed all tests.

Table 1   Specifications of digital radiographic systems.

System type	CR	IDR	DDR
Product name	AGFA/CR 75.0 /IP CDMD 4.1	Carestream DRX-1C	Shimadzu RADspeed Safire
Tube	Trex TM65	Varian A-192	Shimadzu
Focal spot	Large (1.2mm)	Large (1.2 mm)	Large (1.2mm)
Detector material	The phosphor (BaFBrx I1-x)	CsI scintillator	Amorphous selenium 1000 μm
Pixel size	150 μm/pixel (6 pixels/mm)	139 μm	150 μm
Detector size/type	350 x 430 mm IP code 38	350 x 430 mm FPD	432 x 432 mm FPD
Anti-scatter Grid	Bucky table 8:1 103/inch	Bucky table 8:1 115/inch	Bucky table 10:1 100/inch
Resolution	Standard: 3.4lp/mm High: 5.0 lp/mm	3.6 lp/mm	3.3lp/mm
DQE DQE(1lp/mm) DQE(2lp/mm)	20% to 30% 18% 9%	60% to 80% 50% 35%	40% 55% 40%
QA tests	Pass	Pass	Pass

Image Acquisition

The CDRAD phantom and 10 cm Perspex sheets were imaged at various values of tube voltage (80, 90, 100, and 110 kVp) and dose levels (1, 2, 4 and 8 mAs). The 8 mAs setting was only used with 80 kVp. The size of the collimation area was fixed to the phantom size. The source to image distance (SID) was maintained at a fixed distance of 100 cm as most radiography examinations are performed at this distance. The table bucky grid was used for all images. The large focal spot was selected for all images. Three images at each exposure

6

329

setting from each system, CR, IDR and DDR, were acquired of CDRAD phantom. The soft copy images were saved on CD-ROMs as image files in DICOM format.

Image scoring

Image scoring can be undertaken by observers or via the use of dedicated software. For this project only software analysis was undertaken. The CDRAD Analyzer, version 2.1.9 (Artinis Medical Systems, Zetten), is an automated software assessment tool designed to provide an analysis of image quality. The CDRAD analyzer software was developed for quantitative analysis of images produced with the CDRAD test object. The software measures the detectability of the phantom holes in the DICOM images and calculates the inverse image quality figure (IQFinv) values using equation (1).[18,19]

$$IQFinv = \frac{100}{\sum_{i=1}^{15} Ci \cdot Di, th}$$

(1)

where Ci refers to hole depth-column i and Di correspond to the minimum diameter (threshold diameter) detected for hole-column i.[18,19]

All image sets, consisting of three images with identical exposure factors, were evaluated by the CDRAD analyzer software. At each of the 255 matrix locations, the software determines if a difference between the object and background exists. Welch Satterthwhaite test (Student t-Test with Welch correction) is applied in order to determine whether a certain contrast-detail combination was detected or not.[18] An a-priori-difference of means (APD) is also applied to allow a valid comparison of automated scores obtained from images stored with different bit-depth.[18]

This project only evaluated the changes in IQFinv that resulted from a change in the radiographic factors of kVp and mAs. Whilst it is understood that radiation dose also changes

7

330

with change of kVp and mAs,[2,6,8] it was felt that clinicians better understand changes in radiographic factors and hence would then be able to relate these changes to image quality. As such, no dose measurements were recorded.

Statistical Analysis

Analysis of IQFinv values was undertaken to determine if significant differences existed between kVp groups exposed at the same mAs and between mAs groups at the same kVp. Student t-Tests, at an Alpha of 0.05, were used to determine significance. A two-way between-groups analysis of variance the Tukey HSD test were also conducted to evaluate the effects of exposure factors on IQFinv values and to compare between radiography systems.

Results

The average IQFinv value for each of the three exposures in each exposure group for CR, IDR and DDR were calculated and are shown in Table 2. Table 2 also shows the variance of the IQFinv of the 3 images and the differences between images using, p values from Student t-Test.

As the mAs was increased at each kVp setting for each planar radiography recording system, the relationship between the mAs values and the IQFinv values was evaluated. Even though the radiation dose measurement is out of this study scope, mAs (with respect to other dose factors) can be used as indicator of radiation dose as the dose increases linearly with increases of mAs.[13]

8

Table 2 IQFinv values of the images, these values are the average of 3 identical exposures. The differences between images (*p* values, Student t-Test). Ref; refers to the reference image that other images of same kVp group were compared with.

kVp	mAs	CR images			IDR images			DDR images		
		Mean	StDev	*p* (S t-Test) one-tail	Mean	StDev	*p* (S t-Test) one-tail	Mean	StDev	*p* (S t-Test) one-tail
80	1	3.033	0.45	Ref	3.987	0.20	Ref	4.903	0.45	Ref
80	2	4.073	0.31	0.006	4.717	0.26	0.001	4.980	0.23	0.034
80	4	4.327	0.29	0.003	5.317	0.13	0.0001	4.987	0.23	0.008
80	8	4.427	0.36	0.0001	5.333	0.22	0.0001	5.263	0.12	0.007
90	1	4.673	0.35	Ref	5.457	0.19	Ref	5.723	0.33	Ref
90	2	4.963	0.11	0.027	5.853	0.18	0.001	6.003	0.31	0.006
90	4	5.087	0.15	0.002	6.533	0.32	0.001	6.010	0.33	0.002
100	1	5.393	0.49	Ref	6.813	0.38	Ref	6.127	0.16	Ref
100	2	5.427	0.55	0.082	6.883	0.39	0.005	6.360	0.24	0.004
100	4	5.847	0.45	0.004	7.117	0.33	0.001	6.660	0.22	0.0001
110	1	5.920	0.44	Ref	7.523	0.49	Ref	6.667	0.46	Ref
110	2	6.210	0.27	0.017	7.523	0.16	0.02	6.710	0.08	0.054
110	4	6.623	1.04	0.046	7.630	0.06	0.009	7.140	0.26	0.01

Discussion

When calculating the mean IQFinv values for each image, there was minimal variance between individual images of the same kVp and mAs setting for each planar radiography recording system. The variance is shown in Table 2 as the standard deviation which shows high consistency of the x-ray units and recording systems used.

9

Changes to IQFinv when using different mAs settings.

It was expected that the increased photon count from the higher mAs would result in increased signal to noise ratio (SNR) and thus increased detectability. High noise level images increase the risk of diagnostic detail loss.[10] Therefore, higher radiation dose improve the detectability performance.

When comparing mean IQFinv values resulting from changes in the mAs when a fixed kVp was used, there were significant differences in mean IQFinv ($p < 0.05$) when increasing the mAs and seeing a resultant increase in the IQFinv values (Table 2). Figure 3 shows an example of typical results as mAs is increased, the IQFinv values increase in the 80 kVp setting. There were several exceptions to these results when no significant increase to IQFinv occurred as a result of an increase of mAs. These were:

when using CR, at 100kVp with 1 and 2 mAs increase ($p = 0.082$)

when using DDR, at 110kVp with 1 and 2 mAs increase ($p = 0.054$)
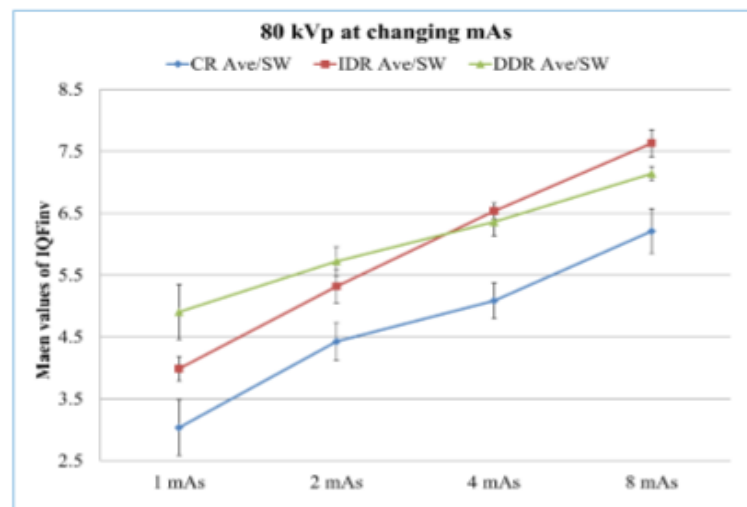
Figure 3 Average IQFinv values at 80 kVp for each system. Increases in mAs show increased detectability.

10

Changes to IQFinv when using different kVp settings

Increasing the kVp has two effects on the x-ray beam, these being increasing the average photon energy of the beam and increasing the number of photons in the beam.[20] There were significant differences in mean IQFinv ($p < 0.05$) when comparing mean IQFinv values resulting from changes in the kVp with a fixed mAs in CR. When IDR and DDR were used, the expected effect on an increase in the IQFinv values was not always seen. Figures 4 and 5 show examples of when increasing kVp did not have consistent results.
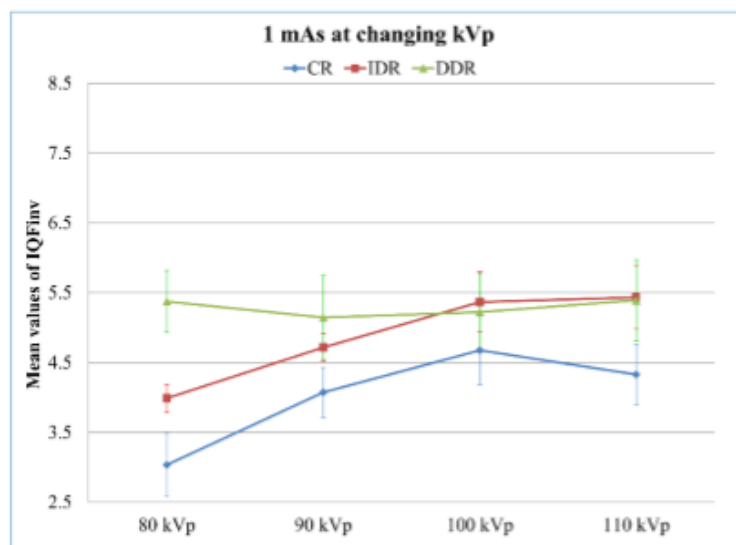
Figure 4 Average IQFinv values at 1 mAs for each system. Note the change in IQFinv values for IDR at 100 and 110 kVp and DDR for 90 and 100 kVp.

11
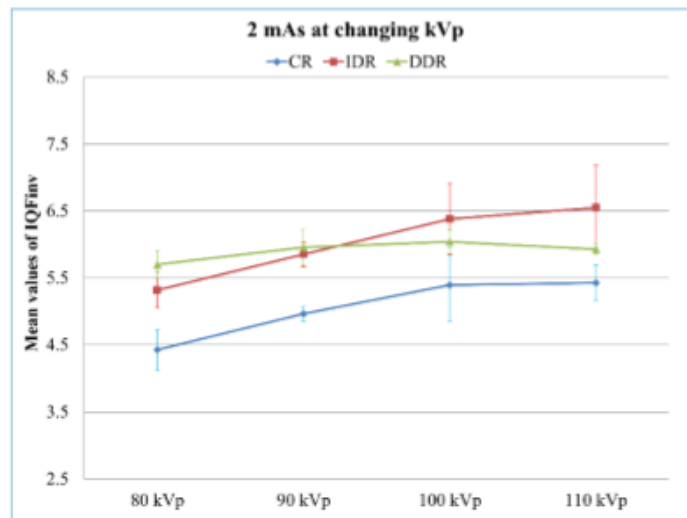
Figure 5 Average IQFinv values at 2 mAs for each system. Note the change in IQFinv values using DDR for 90, 100 and 110 kVp.

When between subject effects were analyzed using two way ANOVA test, there was no significant difference ($p = 0.781$) when mAs was kept constant and kVp was varied for all radiographic systems. There was also no significant difference ($p = 0.770$) when mAs was kept constant and kVp was varied in each radiographic system. Tukey HSD post-hoc test was conducted and when evaluating all radiographic systems, there was no significant differences 80 and 90 kVp ($p = 0.889$) and between 100 and 110 kVp ($p = 0.909$).

Lowering the kVp increases x-ray attenuation and consequently the subject contrast is improved.[21-23] Whilst this is well understood, the ability to visualize this contrast change in the image was not seen. When using digital recording systems, changing the kVp setting has no significant effect on detectability of objects. An example of this is seen in Figure 6 with DDR. At the various mAs setting, when changing the kVp the IQFinv essentially did not change.

12
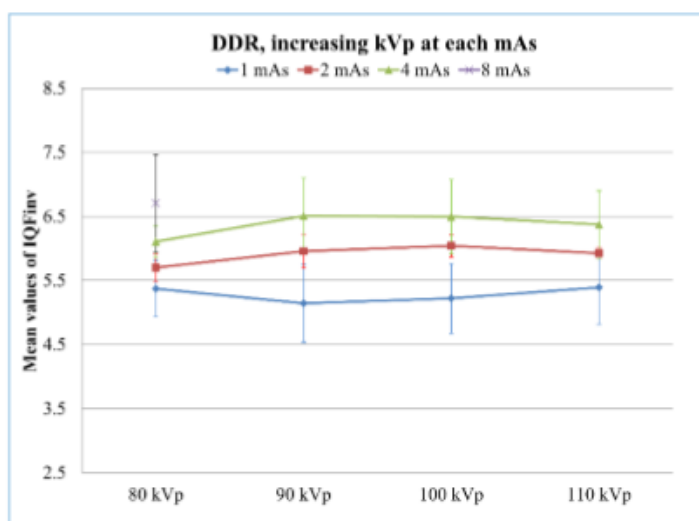
Figure 6   Average IQFinv values for DDR at various kVp and mAs settings.

Changes to IQFinv when using different radiographic imaging systems

There were significant differences ($p < 0.05$) between IQFinv values at the various kVp setting between each type of radiographic system. The different design principle of CR, IDR and DDR detectors are attributed as the reason behind the differences.

DDR has higher IQFinv than IDR at low exposure kVp settings mainly at 80 or 90 kVp at 1 mAs. DDR detectors are potentially less susceptible to conversion noise compared to IDR detectors as they require no light-to-charge conversion.[24] DDR has better performance than IDR at the higher spatial frequencies as DDR systems show less blurring of the image signal.[6]

IDR has higher IQFinv values than CR in all the cases and DDR in most cases, Figures 4 and 5 show examples of this. This reflects the stronger detective quantum efficiency (DQE)

13

336

of IDR (0.6-0.8) compared with that of DDR (0.4) and CR (0.2-0.3).[25,26] CsI:Tl, which is used in IDR systems for fluorescence, is an excellent x-ray photon absorber due to its high atomic number (Z= 53).[27] The use of needle-like structures of CsI reduces light spreading in the scintillators similarly to regular CR systems. Consequently, a thicker layer of CsI can be utilized to maximize the detection efficiency.[28]

One of the contributing factors to these results is the absorption efficiency of each system at various photon energies. Materials used in IDR have low energy k-edges and generally greater absorption efficiency at all energies compared with materials use in CR and DDR. The weaker DQE of DDR versus IDR detectors reflects the lower x-ray absorption efficiency of a-Se compared with CsI:Tl.[25,29]

Conclusion

Increasing mAs in all digital imaging systems generally improves detectability performance. There is a direct relationship between mAs and the number of x-ray photons produced and hence dose, so caution is needed when considering this approach to improving detectability of objects in a digital radiograph.

Changing the kVp setting shows no significant change to the IQFinv and hence no change to detectability of objects in a digital radiograph. This shows that change of average photon energy of the x-ray beam and resultant change in subject contrast is not being seen in the digital radiograph. An increase in kVp, without a change in mAs, is known to increase the number of x-ray photons produced. This increase number of photons also had no significant effect on object detectability. The use of kVp to change radiographic or image contrast when the recording system was film / screen was well known, this is now not the case when using digital radiographic systems.

14

Both IDR and DDR show better detectability performance than CR. IDR has better detectability performance than DDR only at higher mAs setting and at higher kVp settings (100 and 110 kVp). The differences between them are significant only at high exposure factors (100 or 110 kVp and 2 or 4 mAs). DDR show better detectability performance with lower exposure factors than IDR. The selection of an imaging system should now also be considered based on the typical radiographic examinations. IDR has better detectability performance when using high kVp while DDR has better noise handling capability at lower radiographic factors.

The limitation of this study is that only one manufacturer of each type of radiographic system was tested. Furthermore, only one thickness being 10 cm of Perspex was examined. Radiation dose was not measured and/or beam filtration was not considered which are essential to determine the dose delivered by each systems.

Further research is needed to fully evaluate the effects on changes of diagnostic ability when changing the kVp, mAs and using different digital recording systems.

15

References

1. Weatherburn GC, Ridout D, Strickland NH, et al. A comparison of conventional film, CR hard copy and PACS soft copy images of the chest: analyses of ROC curves and inter-observer agreement. *Eur J Radiol.* 2003;47(3):206-214.
2. Schaefer-Prokop C, Neitzel U, Venema H, Uffmann M, Prokop M. Digital chest radiography: an update on modern technology, dose containment and control of image quality. *Eur Radiol.* 2008;18(9):1818-1830.
3. Lanca L, Silva A. Digital radiography detectors - A technical overview: Part 2. *Radiography.* 2009;15(2):134-138.
4. Seibert JA. Digital radiography: The bottom line comparison of CR and DR technology. *Applied Radiology.* 2009;38(5):21-28.
5. Schaefer-Prokop C, De Boo DW, Uffmann M, Prokop M. DR and CR: Recent advances in technology. *Eur J Radiol.* 2009;72(2):194-201.
6. Veldkamp W, Kroft L, Geleijns J. Dose and perceived image quality in chest radiography. *Eur J Radiol.* 2009;72(2):209-217.
7. Korner M, Weber CH, Wirth S, Pfeifer KJ, Reiser MF, Treitl M. Advances in Digital Radiography: Physical Principles and System Overview. *Radiographics.* 2007;27(3):675-686.
8. Williams B, Krupinski A, Strauss J, et al. Digital Radiography Image Quality: Image Acquisition. *J Am Coll Radiol.* 2007;4(6):371-388.
9. Gibson D, Davidson R. Exposure Creep in Computed Radiography: A Longitudinal Study. *Acad Radiol.* 2012;19(4):458-462.
10. Uffmann M, Schaefer-Prokop C. Digital radiography: The balance between image quality and required radiation dose. *Eur J Radiol.* 2009;72(2):202-208.
11. Davidson R, Sim J. Computed radiography: some practical tips for dose optimization. *JMIRS.* 2008;39(3):109-114.
12. Reiner BI, Siegel EL, Siddiqui KM, Musk AE. Quality Assurance: The Missing Link1. *Radiology.* 2006;238(1):13-15.
13. Alsleem H, Davidson R. Quality parameters and assessment methods of digital radiography images. *The Radiographer.* 2012;59(2):46-55.
14. Shet N, Chen J, Siegel EL. Continuing challenges in defining image quality. *Pediatr Radiol.* 2011;41(5):582-587.
15. Bath M. Evaluating imaging systems: practical applications. *Radiat Prot Dosimetry.* 2010;139(1-3):26-36.
16. Uffmann M, Schaefer-Prokop C, Neitzel U, Weber M, Herold J, Prokop M. Skeletal Applications for Flat-Panel versus Storage-Phosphor Radiography: Effect of Exposure on Detection of Low-Contrast Details. *Radiology.* 2004;231(2):506-514.
17. Tapiovaara M. *Relationships between physical measurements and user evaluation of image quality in medical radiology-a review.* Vantaa/Finland: Radiation and Nuclear Safety Authority; 2006.
18. Pascoal A, Lawinski C, Honey I, Blake P. Evaluation of a software package for automated quality assessment of contrast detail images—comparison with subjective visual assessment. *Phys Med Biol.* 2005;50(23):5743-5757.
19. Thijssen M, Thijssen H, Merx J, Lindeijer J, Bijkerk K. A definition of image quality: the image quality figure. *BIR report.* 1989;20:29-34.
20. Carlton R, Adler K. *Principles of radiographic imaging: an art and a science.* 5 ed: Delmar, Cengage Learning; 2012.
21. Spahn M. Flat detectors and their clinical applications. *Eur Radiol.* 2005;15(9):1934-1947.

22. Geijer H, Norrman E, Persliden J. Optimizing the tube potential for lumbar spine radiography with a flat-panel digital detector. *Br J Radiol.* January 1, 2009 2009;82(973):62-68.

23. Launders J, Cowen A, Bury R, Hawkridge P. Towards image quality, beam energy and effective dose optimisation in digital thoracic radiography. *Eur Radiol.* 2001;11(5):870-875.

24. Samei E. Performance of digital radiography detectors: factors affecting sharpness and noise. In: Advances in digital radiography. *RSNA* 2003:49–61.

25. Neitzel U. Status and prospects of digital detector technology for CR and DR. *Radiat Prot Dosimetry.* 17 May 2005 2005;114(1-3):32-38.

26. Gomi T, Koshida K, Miyati T, Miyagawa J, Hirano H. An Experimental Comparison of Flat-Panel Detector Performance for Direct and Indirect Systems (Initial Experiences and Physical Evaluation). *J Digit Imaging.* 2006;19(4):362-370.

27. Achenbach S. Computed tomography coronary angiography. *J Am Coll Cardiol.* 2006;48(10):1919-1928.

28. Abe H, MacMahon H, Engelmann R, et al. Computer-aided Diagnosis in Chest Radiography: Results of Large-Scale Observer Tests at the 1996–2001 RSNA Scientific Assemblies1. *Radiographics.* 2003;23(1):255.

29. American Association of Physicists in Medicine. *Report of AAPM Task Group 10, Report 93. Acceptance testing and quality control of photostimulable storage phosphor imaging systems.* College Park, MD: American Association of Physicists in Medicine. Available from http://aapm.org/pubs/reports/RPT_93.pdf.2006.

17

340

Appendix 2　Quality assurance for x-ray units

A-　QA Austin equipment (CR, AGFA) 9 11 2011

Machine Details:			Date: 9/11/2011		
Room ID:	Manufacturer:		Model:	Type of Generator:	
Room # 5	Trex TM65		TM65	Rad/fluoro	
Tube Details:			Generator:		
Focal Spot:	Large	Added filtration:	Rating:	kVp:	
Stated:			kW	min.	max.
Measured:		mm Al			

HVL:							
Settings:					Pass/Fail Criteria		
kVp	81		mA	200	Min HVL	2.5	mm Al
time:	100		FFD	60 cm			
Al Thick.	0	1	2	3	4	HVL	3.1778 mm Al
dose 1	0.55	0.45	0.37	0.32	0.27	P/F	Pass
dose 2	0.54	0.44	0.37	0.32	0.27		
dose 3	0.55	0.45	0.37	0.32	0.27		
Average	0.54667	0.44667	0.37	0.32	0.27		
ln dose	-0.6039	-0.8059	-0.9943	-1.1394	-1.3093		
slope	-5.712100411		intercept	-3.544025967			

Linearity and Reciprocity:									
Settings:					Pass/Fail Criteria				
kVp	70	time:	100	FFD	60 cm	0.05			
						Reciprocity Variance		Linearity Variance	
mA	Dose (D) Inputs				Average	D/mAs	RV	P/F LV	P/F
160	1.259 1.256 1.259	1.257	1.259		1.258	7.9E-05	0.00119	Pass 0.032	Pass
125	0.96 0.96 0.96	0.96	0.96		0.96	7.7E-05	0.00	Pass	
100	0.754 0.756 0.752	0.758	0.754		0.7548	7.5E-05	0.00397	Pass	
80	0.591 0.588 0.59	0.59	0.591		0.59	7.4E-05	0.00254	Pass	
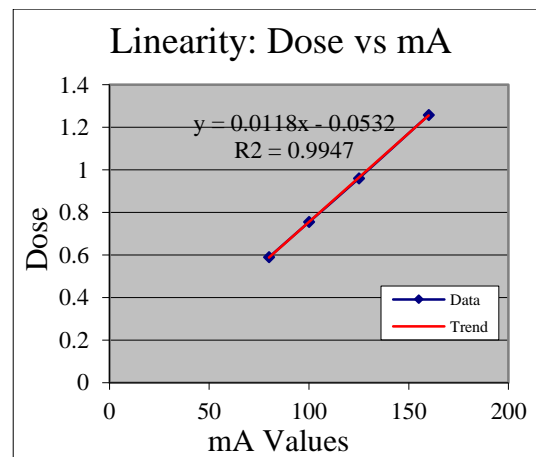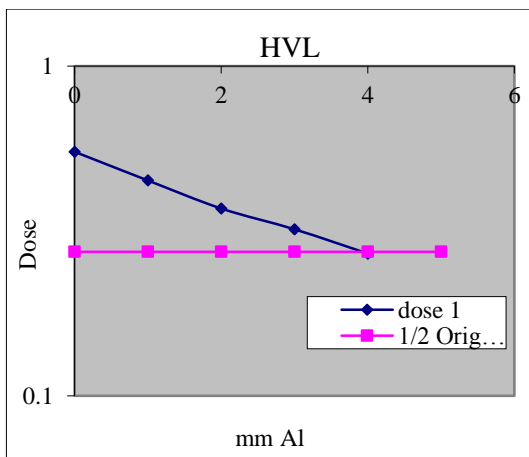
HVL

Linearity: Dose vs mA

$y = 0.0118x - 0.0532$
$R2 = 0.9947$

Accuracy and Reproducibility:												
Settings:		Measured:						Accuracy			Reproducibility	
								Pass/Fail Criteria:	kVp	time		
									0.08	0.06	0.05	
								Average	% Error	P/F	CV	P/F
kVp	81	kVp	80.6	80.4	80.4	80.5	80.5	80.48	0.6%	Pass	0.00104	Pass
kVp	90	kVp	90.3	90.4	90.2	90.3	90.3	90.3	0.33%	Pass	0.00078	Pass
kVp	100	kVp	101.4	101.4	101.3	101.4	101.4	101.38	1.38%	Pass	0.00044	Pass
kVp	110	kVp	111.8	111.9	111.7	111.8	111.8	111.8	1.64%	Pass	0.00063	Pass
time	1000	time	983.6	975.3	975.6	982.6	983.6	980.14	1.99%	Pass	0.00439	Pass
time	500	time	484.2	483.4	484.2	485.2	484	484.2	3.16%	Pass	0.00134	Pass
time	250	time	238.7	238.6	238.7	238.8	238.5	238.66	4.54%	Pass	0.00048	Pass
time	125	time	118.2	118.4	118.2	118.5	118.2	118.3	5.36%	Pass	0.0012	Pass
time	100	time	94.4	94	94.1	94.3	94.4	94.24	5.76%	Pass	0.00193	Pass
time	63	time	59.6	59.7	59.6	59.7	59.5	59.62	5.37%	Pass	0.0014	Pass
mA	160	dose	1.259	1.256	1.259	1.257	1.259	1.258			0.00112	Pass
mA	100	dose	0.96	0.96	0.96	0.96	0.96	0.96			0	Pass
mA	50	dose	0.754	0.756	0.752	0.758	0.754	0.7548			0.00302	Pass
mA	20	dose	0.591	0.588	0.59	0.59	0.591	0.59			0.00208	Pass

Accuracy: time

$y = 0.9833x - 4.7882$
$R^2 = 1$

time Data
time Trend

Accuracy: kVp

$y = 1.0827x - 7.139$
$R^2 = 0.9998$

kVp Data
kVp Trend
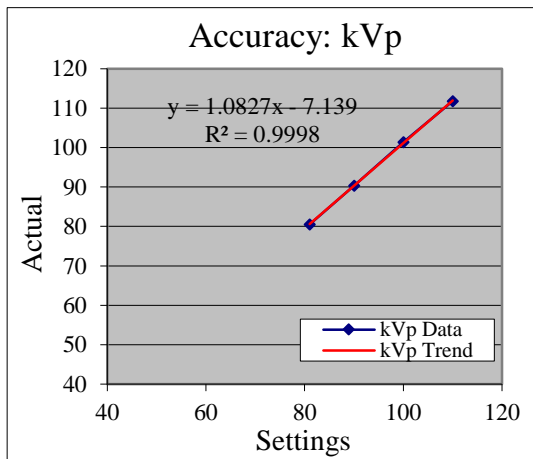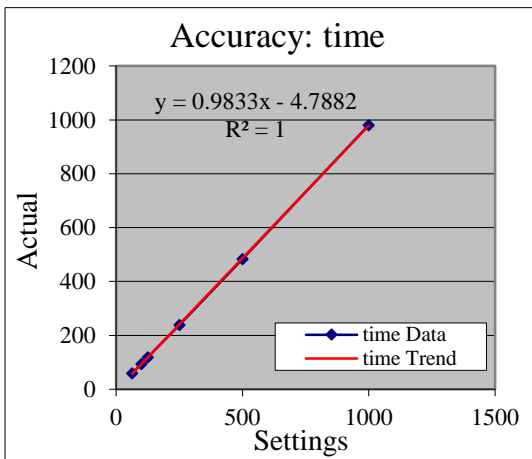
B- QA ARPANSA equipment (IDR) 9 11 2011

Machine Details:			Date: 9/11/2011		
Room ID:	Manufacturer:	Model:		Type of Generator:	
Room # 133	Toshiba	Tube name VARIAN A-192		Rad/fluoro	
Tube Details:			Generator:		
Focal Spot:	Large	Added filtration:	Rating:	kVp:	
Stated:	large		kW	min.	max.
Measured:		mm Al			

HVL:								
Settings:					Pass/Fail Criteria			
kVp	80		mA	200	Min HVL	2.5	mm Al	
time:	25		FFD	60 cm				
Al Thick.	0	1	2	3	4	HVL	3.1778	mm Al
dose 1	0.62	0.48	0.39	0.32	0.27	P/F	Pass	
dose 2	0.62	0.48	0.39	0.32	0.27			
dose 3	0.63	0.48	0.39	0.32	0.27			
Average	0.6233	0.48	0.39	0.32	0.27			
ln dose	-0.473	-0.734	-0.942	-1.139	-1.309			
slope	-4.78		intercept	-2.395				

Linearity and Reciprocity:											
Settings:						Pass/Fail Criteria					
kVp	70	time:	100	FFD	60 cm	0.05					
						Reciprocity Variance			Linearity Variance		
mA	Dose (D) Inputs					Average	D/mAs	RV	P/F	LV	P/F
160	1.573	1.613	1.577	1.576	1.579	1.5836	1E-04	0.0126	Pass	0.0056	Pass
100	0.987	0.987	0.989	0.992	0.989	0.9888	1E-04	0.00	Pass		
50	0.487	0.495	0.488	0.49	0.49	0.49	1E-04	0.0082	Pass		
20	0.197	0.2	0.197	0.2	0.197	0.1982	1E-04	0.0076	Pass		

HVL chart — Dose vs mm Al; series "dose 1" and "1/2 Orig Dose"

Linearity: Dose vs mA
$y = 0.0118x - 0.0532$
$R^2 = 0.9947$

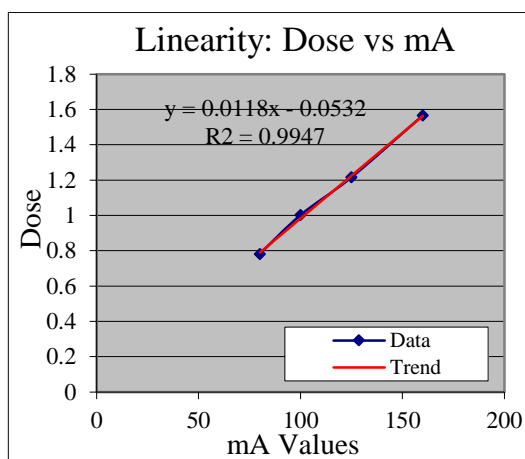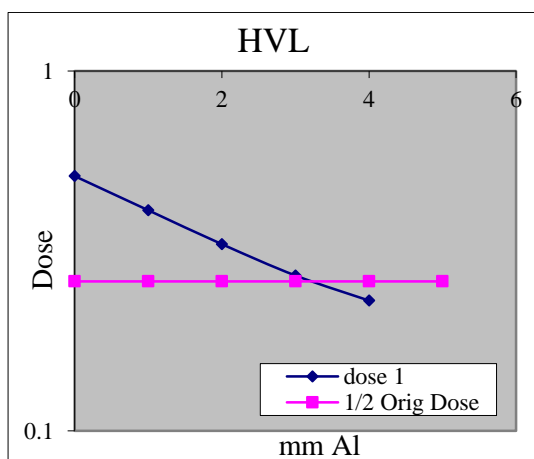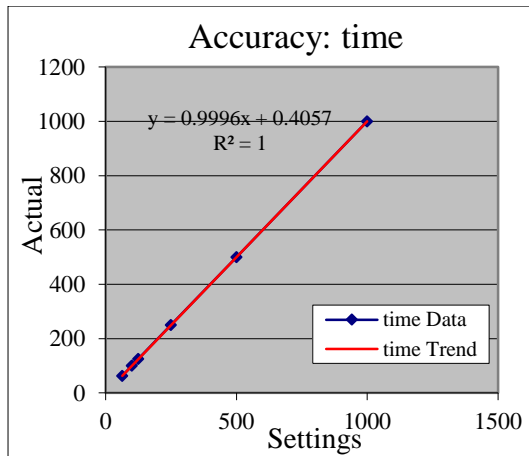| Accuracy and Reproducibility:													
Settings:		Measured:						Accuracy				Reproducibility	
								Pass/Fail Criteria:	kVp 0.08	time 0.06		0.05	
								Average	% Error	P/F		CV	P/F
kVp	81	kVp	79.2	79.1	78.7	78.9	78.6	78.9	2.6%	Pass		0.0032	Pass
kVp	90	kVp	89.4	89.4	89.5	89.4	89.4	89.42	0.64%	Pass		0.0005	Pass
kVp	100	kVp	100.7	100.7	100.6	100.6	100.6	100.64	0.64%	Pass		0.0005	Pass
kVp	110	kVp	110.8	110.8	110.8	110.7	110.7	110.76	0.69%	Pass		0.0005	Pass
time	1000	time	999.4	999.5	999.4	999.5	999.5	999.46	0.05%	Pass		5E-05	Pass
time	500	time	499.7	499.6	499.7	499.6	499.6	499.64	0.07%	Pass		< 0.001	Pass
time	250	time	249.5	249.5	249.5	249.4	249.4	249.46	0.22%	Pass		0.0002	Pass
time	125	time	124.8	124.8	124.8	124.6	124.7	124.74	0.21%	Pass		0.0007	Pass
time	100	time	99.9	99.9	99.9	99.9	99.9	99.9	0.10%	Pass		0	Pass
time	63	time	62.9	62.9	62.9	62.9	62.9	62.9	0.16%	Pass		0	Pass
mA	160	dose	1.573	1.613	1.577	1.576	1.579	1.5836				0.0105	Pass
mA	100	dose	0.987	0.987	0.989	0.992	0.989	0.9888				0.0021	Pass
mA	50	dose	0.487	0.495	0.488	0.49	0.49	0.49				0.0063	Pass
mA	20	dose	0.197	0.2	0.197	0.2	0.197	0.1982				0.0083	Pass

Accuracy: kVp

$y = 1.1003x - 9.8743$
$R^2 = 0.999$

(Actual vs Settings; legend: kVp Data, kVp Trend)

Accuracy: time

$y = 0.9996x - 0.1816$
$R^2 = 1$

(Actual vs Settings; legend: ti..)

344
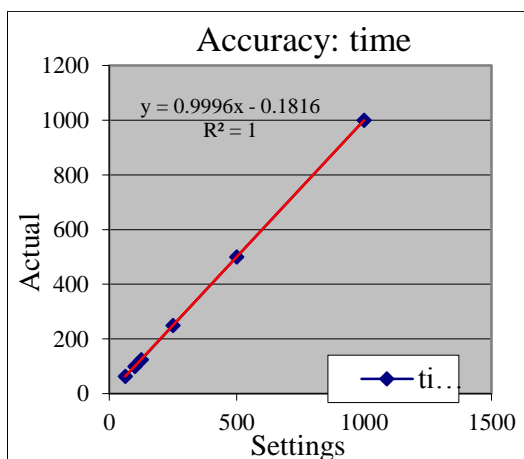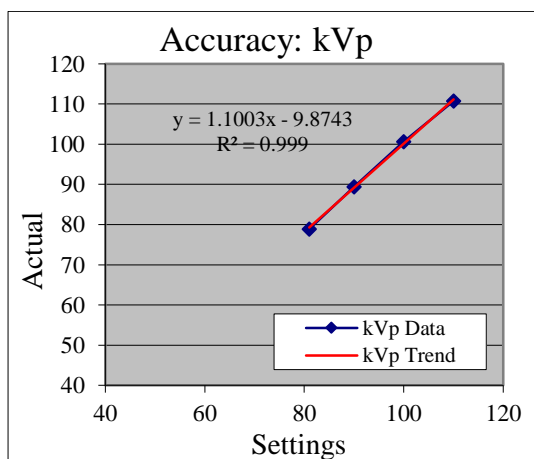
C- QA Box Hill equipment (DDR)

Machine Details:			Date: 9/11/2011			
Room ID:	Manufacturer:		Model:		Type of Generator:	
Room # 2	Shimadzu		RADspeed Safire		Rad/fluoro	
Tube Details:				Generator:		
Focal Spot:	Large		Added filtration:	Rating:		kVp:
Stated:	large			kW	min.	max.
Measured:			mm Al			

HVL:								
Settings:						Pass/Fail Criteria		
kVp	80		mA	50		Min HVL	2.5	mm Al
time:	100		FFD	60 cm				
Al Thick.	0	1	2	3	4	HVL	3.1331 mm Al	
dose 1	0.51	0.41	0.33	0.27	0.23	P/F	Pass	
dose 2	0.54	0.4	0.32	0.26	0.22			
dose 3	0.51	0.39	0.32	0.26	0.22			
Average	0.52	0.4	0.32333	0.26333	0.22333			
ln dose	-0.6539	-0.9163	-1.1291	-1.3343	-1.4991			
slope	-4.710945512		intercept	-3.2129				

Linearity and Reciprocity:											
Settings:						Pass/Fail Criteria					
kVp	70	time:	100	FFD	60 cm	0.05					
								Reciprocity Variance		Linearity Variance	
mA	Dose (D) Inputs					Average	D/mAs	RV	P/F	LV	P/F
160	1.539	1.586	1.56	1.578	1.565	1.5656		0.01501	Pass	0.0056	Pass
125	1.24	1.176	1.23	1.212	1.22	1.2156		0.03	Pass		
100	1.005	1.015	1.018	1	0.97	1.0016		0.02396	Pass		
80	0.788	0.774	0.784	0.789	0.771	0.7812		0.01152	Pass		

Accuracy and Reproducibility:										
Settings:	Measured:					Accuracy			Reproducibility	
						Pass/Fail Criteria:	kVp 0.08	time 0.06	0.05	
						Average	% Error	P/F	CV	P/F
kVp 81	kVp 77.4	77.5	77.2	77.3	77.7	77.42	3.2%	Pass	0.00248455	Pass
kVp 90	kVp 84.8	84.8	84.8	84.8	84.7	84.78	5.80%	Pass	0.000527499	Pass
kVp 100	kVp 97.3	97.2	97.2	97.1	97.2	97.2	2.80%	Pass	0.000727476	Pass
kVp 110	kVp 108.4	108.6	108.5	108.4	108.4	108.46	1.40%	Pass	0.000824661	Pass
time 1000	time 1000	1000	1000	1000	1000	1000	0.00%	Pass	0	Pass
time 500	time 500.3	500.2	500.3	500.3	500.3	500.28	0.06%	Pass	8.9E-05	Pass
time 250	time 250.3	250.5	250.4	250.4	250.3	250.38	0.15%	Pass	0.00033	Pass
time 125	time 125.3	125.3	125.4	125.3	125.3	125.32	0.26%	Pass	0.00036	Pass
time 100	time 100.3	100.3	100.3	100.3	100.3	100.3	0.30%	Pass	0	Pass
time 63	time 63.4	63.4	63.4	63.4	63.4	63.4	0.63%	Pass	0	Pass
mA 160	dose 1.539	1.586	1.56	1.578	1.565	1.5656			0.01156	Pass
mA 100	dose 1.24	1.176	1.23	1.212	1.22	1.2156			0.02016	Pass
mA 50	dose 1.005	1.015	1.018	1	0.97	1.0016			0.01908	Pass
mA 20	dose 0.788	0.774	0.784	0.789	0.771	0.7812			0.01053	Pass

Accuracy: kVp

$y = 1.0554x - 8.298$
$R^2 = 0.9898$

Accuracy: time

$y = 0.9996x + 0.4057$
$R^2 = 1$
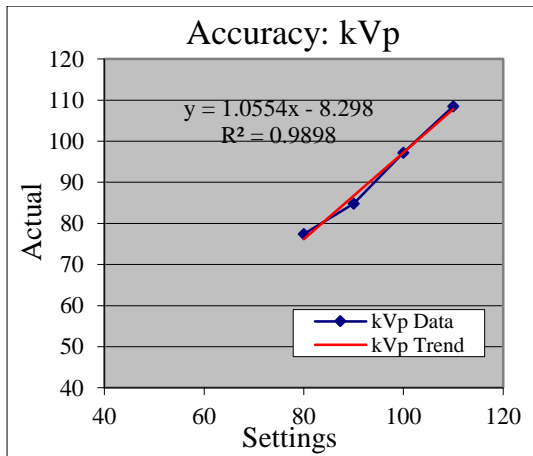
Appendix 3 Ethics Approval Letter (Radiography)

RMIT
UNIVERSITY

31st March 2011

RMIT University

Science Engineering
and Health

College Human Ethics
Advisory Network
(CHEAN)

Plenty Road
Bundoora VIC 3083

PO Box 71
Bundoora VIC 3083
Australia

Tel. +61 3 9925 7096
Fax +61 3 9925 6506
● www.rmit.edu.au

Haney Alsleem
44 Bickley Avenue
Thomastown VIC   3074

Dear Haney

ABSEHAPP 11 – 11 ALSLEEM Innovative method for CT and digital radiology image quality assessment based on information loss

Thank you for submitting your amended application for review.

I am pleased to inform you that the CHEAN has approved your application for a period of **21 Months** to **December 2012** and your research may now proceed.

The CHEAN would like to remind you that:

All data should be stored on University Network systems. These systems provide high levels of manageable security and data integrity, can provide secure remote access, are backed up on a regular basis and can provide Disaster Recover processes should a large scale incident occur. The use of portable devices such as CDs and memory sticks is valid for archiving; data transport where necessary and for some works in progress. The authoritative copy of all current data should reside on appropriate network systems; and the Principal Investigator is responsible for the retention and storage of the original data pertaining to the project for a minimum period of five years.

Annual reports are due during December for all research projects that have been approved by the College Human Ethics Advisory Network (CHEAN).

The necessary form can be found at: http://www.rmit.edu.au/governance/committees/hrec

Yours faithfully,

Linda Jones
Acting Chair, Science Engineering & Health
College Human Ethics Advisory Network 'A'

Cc	CHEAN Member:	Amanda Kimpton School of Health Sciences
	Supervisor/s:	Moshi Geso School of Medical Science
	Other Investigator/s:	Paul U Austin and Repatriation Centre

347

Appendix 4   Instructions for Images

i. Images of Contrast-Detail Phantom (Dicom form) are sent to you on a CD. These images are obtained from 2 radiographic systems at various exposure conditions.

ii. These images are to be displayed on a three megapixel, diagnostic quality monochrome liquid crystal display monitor. The recommended monitor is Eizo Radioforce R-31 Specs, 3 MP color LCD monitor

iii. The room light must be maintained as reporting room environment.

iv. The operating conditions, including the phantom background level and the display contrast enhancement factor and zoom factor can be controlled to achieve the best possible observer performance.

v. Assessment of the images quality should be done individually by scoring the faintest discs in each row that you can detect in the corresponding location.

vi. Indicate the location of the second spot in each square in each row.

vii. The participants are advised to practice interpretation and scoring of the phantom images for about 10 min.

viii. No scoring time limitation is imposed

ix. Participants will not be provided with feedback about their scoring performance unless requested.

x. It is estimated that image scoring task would take about a half hour to be completed.

xi. It would be greatly appreciated if you could complete the scoring form before
   a.   / /2011.

xii. Return the completed sheets by mailing them to Medical Radiations Department (Building 201, Level 8, Bundoora campus west, Plenty Road, Bundoora, Victoria 3083), you do not have to return the CD.

Appendix 5　Scoring form of CDRAD radiographic image

Radiographer no:_____   Date:　/　/ 2011
Monitor (specification):
Displayer software:

Image code: _____															
	0.3	0.4	0.5	0.6	0.8	1.0	1.3	1.6	2.0	2.5	3.2	4.0	5.0	6.3	8.0	
8.0																8.0
6.3																6.3
5.0																5.0
4.0																4.0
3.2																3.2
2.5																2.5
2.0																2.0
1.6																1.6
1.3																1.3
1.0																1.0
0.8																0.8
0.6																0.6
0.5																0.5
0.4																0.4
0.3																0.3
	0.3	0.4	0.5	0.6	0.8	1.0	1.3	1.6	2.0	2.5	3.2	4.0	5.0	6.3	8.0	

Appendix 6   Reviewing procedures (CDRAD Manual)

4.1. Correction scheme
In the correction scheme, there are three possibilities for each observation:
-T: the eccentric hole was indicated at the true position
-F: the eccentric hole was indicated at a false position
-N: the eccentric hole was not indicated at all

The two main rules within the correction scheme are:
1. A True needs 2 or more correctly indicated nearest neighbours to remain a True.
2. A False or Not indicated hole will be considered as True when it has 3 or 4 correctly indicated nearest neighbours.

Exceptions on the two main rules are:
1. A True which has only 2 nearest neighbours (at the edges of the phantom) needs only 1 correctly indicated nearest neighbour to remain True.
2. A False or Not indicated hole which has only 2 nearest neighbours will be regarded True if both nearest neighbours are correctly indicated.

4.2. Correction examples
Six examples of the correction scheme are discussed below.

T	T	T	T
N	T*	T	T
N	F*	T	T
N	N	N	T

Example 1: The common situation. T* remains T because of its 2 correctly indicated nearest neighbours. F* remains F because it has only 2 correctly indicated nearest neighbours.

T	T	T	T
N	T*	F*	T
N	N	T*	T
N	N	N	T

Example 2: F* is considered T because it has more than 2 correctly indicated nearest neighbours. Both T*'s however have only 1 correctly identified nearest neighbour, and thus are considered to be F's.

T*	T	T	T
N	N	T	T
N	N	N	T
N	N	N	N

Example 3: T* remains T because it has 1 out of 2 correctly indicated nearest neighbours.

F*	T	T	T
T*	T	T	T
N	N	T	T
N	N	N	T

Example 4: F* will be considered as a T because of its 2 out of 2 correctly indicated nearest neighbours. T* will be considered as an F because it has only 1 correctly indicated nearest neighbour.

F*	T*	T	T
N	N	T	T
N	T*	N	T
N	N	N	N

Example 5: F* remains an F, because it has only 1 out of 2 correctly indicated nearest neighbours. Both T*'s are considered as F's because they have none respectively 1 correctly indicated nearest neighbour.

T*	F*	T	T
T	T	T	T
N	T	T	T
N	N	T	T

Example 6: T* remains T because it has 1 out of 2 correctly indicated nearest neighbours. F* will be considered as a T because of 3 correctly indicated nearest neighbours.

Appendix 7   MATLAB contrast-detail script

```
% MATLAB m file to measure ROI's in all CT images in a specified directory

% OUTPUT ROI measurement to an Excel file
% OUTPUT CT images with ROI's to a jpeg format file
clear all;

% set directories as needed
dirName='D:\Data\CSU\HDRStudents\Haney\ct_phantom\A 16 MDCT GE alfred';% is the directory of the CT images
dirName2='D:\Data\CSU\HDRStudents\Haney\ct_phantom';% is the directory where the XLS file will be stored
dirName3='D:\Data\CSU\HDRStudents\Haney\ct_phantom\figures';% the directory where jpegs will be saved
xlsName='GE Alfred.xls';

% directories of DICOM images
cd(strcat(dirName));
[fname,fpath]=uigetfile('*.*');
files=dir(fpath);
fileNames={files.name}';
[dirSize, dirSize2]=size(fileNames);

% Measurement ROI object details [X-cen, Y-cen, size] - 23 objects -
%  values taken from previous measurement from CT scan images
% Contract objects - First 16 objects (#1-6 1.0% contrast (blue),
%  #7-11 0.5% contrast (red) & #12-15 0.3% contrast (green).
%  Background #16-19 (yellow) & Noise in air #20-23 (cyan)
Obj=[261, 188, 10;
   283, 193, 6;
   301, 201, 5;
   312, 214, 4;
   320, 228, 4;
   324, 243, 3;
   193, 288, 10;
            187, 267, 6;
            187, 248, 5;
            192, 229, 4;
            201, 215, 4;
            314, 296, 10;
            299, 310, 6;
            283, 323, 5;
            265, 327, 4;
   256, 256, 20;
   230, 176, 15;
            338, 281, 15;
            206, 324, 15;
   100, 140, 40;
            420, 140, 40;
            100, 380, 40;
            420, 380, 40];

% Create Excel file for storing results of measurements
% and write column heading for each calculated value
cd(strcat(dirName2));
infolineXLS={'File Name','CD 1.0% 15mm - Mean', 'CD 1.0% 15mm - Std', 'CD 1.0% 15mm - NoPixels','CD 1.0% 9mm - Mean', 'CD 1.0% 9mm - Std',
'CD 1.0% 9mm - NoPixels','CD 1.0% 8mm - Mean', 'CD 1.0% 8mm - Std', 'CD 1.0% 8mm - NoPixels','CD 1.0% 7mm - Mean', 'CD 1.0% 7mm - Std',
'CD 1.0% 7mm - NoPixels',   'CD 1.0% 6mm - Mean', 'CD 1.0% 6mm - Std', 'CD 1.0% 6mm - NoPixels','CD 1.0% 5mm - Mean', 'CD 1.0% 5mm - Std',
'CD 1.0% 5mm - NoPixels','CD 0.5% 15mm - Mean', 'CD 0.5% 15mm - Std', 'CD 0.5% 15mm - NoPixels','CD 0.5% 9mm - Mean', 'CD 0.5% 9mm - Std',
'CD 0.5% 9mm - NoPixels',   'CD 0.5% 8mm - Mean', 'CD 0.5% 8mm - Std', 'CD 0.5% 8mm - NoPixels','CD 0.5% 7mm - Mean', 'CD 0.5% 7mm - Std',
'CD 0.5% 7mm - NoPixels','CD 0.5% 6mm - Mean', 'CD 0.5% 6mm - Std', 'CD 0.5% 6mm - NoPixels','CD 0.3% 15mm - Mean', 'CD 0.3% 15mm - Std',
'CD 0.3% 15mm - NoPixels','CD 0.3% 9mm - Mean', 'CD 0.3% 9mm - Std', 'CD 0.3% 9mm - NoPixels','CD 0.3% 8mm - Mean', 'CD 0.3% 8mm - Std',
'CD 0.3% 8mm - NoPixels','CD 0.3% 7mm - Mean', 'CD 0.3% 7mm - Std', 'CD 0.3% 7mm - NoPixels',' ', 'BG - Mean', 'BG - Std', 'BG - NoPixels', ' ',
'Noise - Mean', 'Noise - Std', 'Noise - NoPixels',};
xlswrite(xlsName, infolineXLS,'Image Data');

% Select all images in directory and undertake ROI measurement;
% populate Excel file with ROI data & create jpeg's of images with ROI's

for i=3:dirSize% start value of 3 excludes non-file names in the directory
   ImageName=fileNames(i,1);
   cd(strcat(dirName));
   Image=dicomread(char(ImageName));% read DICOM file to "Image"
   Image=Image-1024;% convert image values to HU values
   h=figure; imshow(Image,'DisplayRange',[30,70]);title(char(ImageName));

  % Write filename on Excel row
  loc_XLS=strcat('A',int2str(i));
  cd(strcat(dirName2));
  xlswrite(xlsName,ImageName ,'Image Data', loc_XLS);

  % draw circle on image
  [rr cc] = meshgrid(1:512);% NB - match CT scan of size 512 x 512
  for m=1:23
    C = sqrt((rr-Obj(m,1)).^2+(cc-Obj(m,2)).^2)<=Obj(m,3);
```

```matlab
    structBoundaries = bwboundaries(C);
    xy=structBoundaries{1};% Get n by 2 array of x,y coordinates.
    x = xy(:, 2);% Columns.
    y = xy(:, 1);% Rows.
    hold on;% leave the image open
    if m>=1 && m<=6
        plot(x, y, 'Color','blue','LineWidth', 2);
    elseif m>=7 && m<=11
        plot(x, y, 'Color','red','LineWidth', 2);
    elseif m>=12 && m<=15
        plot(x, y, 'Color','green','LineWidth', 2);
    elseif m>=16 && m<=19
        plot(x, y, 'Color','yellow','LineWidth', 2);
    else
        plot(x, y, 'Color','cyan','LineWidth', 2);
    end

    % Select only the values within the circle
    blackMaskedImage = Image;
    blackMaskedImage(~C) = 0;

% Calculate the mean, standard deviation and no of pixels
% for values within each the circles
% only for the contrast objects
 if m>=1 && m<=15
    meanObj = mean(blackMaskedImage(C));
    stdObj = std2(blackMaskedImage(C));
    numberOfPixels = sum(C(:));
    objData=[meanObj, stdObj, numberOfPixels];
    cd(strcat(dirName2));

    % Write the mean, std and no pixels to the Excel file
    if m==1
        loc_XLS=strcat('B',int2str(i));
        xlswrite(xlsName,objData ,'Image Data', loc_XLS);
    elseif m==2
        loc_XLS=strcat('E',int2str(i));
        xlswrite(xlsName,objData ,'Image Data', loc_XLS);
    elseif m==3
        loc_XLS=strcat('H',int2str(i));
        xlswrite(xlsName,objData ,'Image Data', loc_XLS);
    elseif m==4
        loc_XLS=strcat('K',int2str(i));
        xlswrite(xlsName,objData ,'Image Data', loc_XLS);
    elseif m==5
        loc_XLS=strcat('N',int2str(i));
        xlswrite(xlsName,objData ,'Image Data', loc_XLS);
    elseif m==6
        loc_XLS=strcat('Q',int2str(i));
        xlswrite(xlsName,objData ,'Image Data', loc_XLS);
    elseif m==7
        loc_XLS=strcat('T',int2str(i));
        xlswrite(xlsName,objData ,'Image Data', loc_XLS);
    elseif m==8
        loc_XLS=strcat('W',int2str(i));
        xlswrite(xlsName,objData ,'Image Data', loc_XLS);
    elseif m==9
        loc_XLS=strcat('Z',int2str(i));
        xlswrite(xlsName,objData ,'Image Data', loc_XLS);
    elseif m==10
        loc_XLS=strcat('AC',int2str(i));
        xlswrite(xlsName,objData ,'Image Data', loc_XLS);
elseif m==11
        loc_XLS=strcat('AF',int2str(i));
        xlswrite(xlsName,objData ,'Image Data', loc_XLS);
    elseif m==12
        loc_XLS=strcat('AI',int2str(i));
        xlswrite(xlsName,objData ,'Image Data', loc_XLS);
    elseif m==13
        loc_XLS=strcat('AL',int2str(i));
        xlswrite(xlsName,objData ,'Image Data', loc_XLS);
    elseif m==14
        loc_XLS=strcat('AO',int2str(i));
        xlswrite(xlsName,objData ,'Image Data', loc_XLS);
    elseif m==15
        loc_XLS=strcat('AR',int2str(i));
        xlswrite(xlsName,objData ,'Image Data', loc_XLS);
    end
 end

% Calculate the mean, standard deviation and no of pixels
% for values within each the circles
% for the background and noise objects
 if m==16
    ObjBG1 = blackMaskedImage(C);
```

```matlab
            numberOfPixelsBG1 = sum(C(:));
        elseif m==17
            ObjBG2 = blackMaskedImage(C);
            numberOfPixelsBG2 = sum(C(:));
        elseif m==18
            ObjBG3 = blackMaskedImage(C);
            numberOfPixelsBG3 = sum(C(:));
        elseif m==19
            ObjBG4 = blackMaskedImage(C);
            numberOfPixelsBG4 = sum(C(:));
        end

        if m==20
            ObjN1 = blackMaskedImage(C);
            numberOfPixelsN1 = sum(C(:));
        elseif m==21
            ObjN2 = blackMaskedImage(C);
            numberOfPixelsN2 = sum(C(:));
        elseif m==22
            ObjN3 = blackMaskedImage(C);
            numberOfPixelsN3 = sum(C(:));
        elseif m==23
            ObjN4 = blackMaskedImage(C);
            numberOfPixelsN4 = sum(C(:));
        end
    end

% Combine the background values to calcuate 1 value of mean,
% std and total no of pixels. Write this to Excel
 meanObjBG = mean(double([ObjBG1; ObjBG2; ObjBG3; ObjBG4]));
 stdObjBG = std(double([ObjBG1; ObjBG2; ObjBG3; ObjBG4]));
 numberOfPixelsBG = numberOfPixelsBG1 + numberOfPixelsBG2 + numberOfPixelsBG3 +numberOfPixelsBG4;
 objDataBG=[meanObjBG, stdObjBG, numberOfPixelsBG];
 loc_XLS=strcat('AV',int2str(i));
 cd(strcat(dirName2));
 xlswrite(xlsName,objDataBG ,'Image Data', loc_XLS);

% Combine the noise values to calcuate 1 value of mean,
% std and total no of pixels. Write this to Excel
 meanObjN = mean(double([ObjN1; ObjN2; ObjN3; ObjN4]));
 stdObjN = std(double([ObjN1; ObjN2; ObjN3; ObjN4]));
 numberOfPixelsN = numberOfPixelsN1 + numberOfPixelsN2 + numberOfPixelsN3 +numberOfPixelsN4;
 objDataN=[meanObjN, stdObjN, numberOfPixelsN];
 loc_XLS=strcat('AZ',int2str(i));
 cd(strcat(dirName2));
 xlswrite(xlsName,objDataN ,'Image Data', loc_XLS);

% Save figure with circles to an image in jpeg format
 cd(strcat(dirName3));
 jpgName=strcat(ImageName, '.jpg');
 saveas(h,char(jpgName),'jpg')

 close (h);
end
```

Appendix 8   Ethics Approval Letter (CT)

RMIT
UNIVERSITY

RMIT University

Science Engineering
and Health

College Human Ethics
Advisory Network
(CHEAN)

Plenty Road
Bundoora VIC 3083

PO Box 71
Bundoora VIC 3083
Australia

Tel. +61 3 9925 7096
Fax +61 3 9925 6506
• www.rmit.edu.au

22nd April 2013

Haney Alsleem
44 Bickley Avenue
Thomastown VIC   3074

Dear Haney

ABSEHAPP 11 – 11 ALSLEEM Evaluation of factors that affect contrast-detail in digital x-ray and computed tomography

Thank you for requesting an amendment to your Human Research Ethics project titled: *Evaluation of factors that affect contrast-detail in digital x-ray and computed tomograph* which was originally approved by Science Engineering and Health CHEAN in March 2011.

I am pleased to inform you that the CHEAN has **approved** your amendment request subject to you providing them with copies of permission to advertise and recruit participants from the Box Hill Hospital, Wagga Wagga Base Hospital, Clear Radiology and the Saudi Government Hospital

Please Note: you must provide the CHEAN with copies of approvals to advertise prior to placing any advertising material. The CHEAN will accept these approvals electronically or hard copy.

The committee would like to remind you that:

All data should be stored on University Network systems. These systems provide high levels of manageable security and data integrity, can provide secure remote access, are backed up on a regular basis and can provide Disaster Recover processes should a large scale incident occur. The use of portable devices such as CDs and memory sticks is valid for archiving; data transport where necessary and for some works in progress; The authoritative copy of all current data should reside on appropriate network systems; and the Principal Investigator is responsible for the retention and storage of the original data pertaining to the project for a minimum period of five years.

Annual reports are due during December for all research projects that have been approved by the Human Research Ethics Sub-Committee.

The necessary form can be found at: http://www.rmit.edu.au/governance/committees/hrec

Yours faithfully,

Linda Jones
Chair, Science Engineering & Health
College Human Ethics Advisory Network

Cc   Supervisors/s: Robert Davidson School of Medical Sciences RMIT University
                       Moshi Geso School of Medical Sciences RMIT University

Appendix 9   Instructions for Images Scoring

i.   Images of Contrast-Detail Phantom (Dicom form) are sent to you on a CD. These images are obtained from CT scanner at various protocol parameters.

ii.   These images are to be displayed on a threemegapixel, diagnostic quality monochrome liquid crystal display monitor. The recommended monitor is Eizo Radioforce R-31 Specs, 3 MP color LCD monitor. Other LCD monitors of 5 MP can be also used.

iii.   The room light must be maintained as reporting room environment.

iv.   The operating conditions, including the phantom background level and the display contrast enhancement factor and zoom factor can be controlled to achieve the best possible observer performance.

v.   Assessment of the images quality should be done individually by indicating the discs that you can detect in each corresponding square location.

vi.   The participants are advised to practice interpretation and scoring of the phantom images for about 25 min.

vii.   No scoring time limitation is imposed

viii.   Participants will not be provided with feedback about their scoring performance unless requested.

ix.   It is estimated that image scoring task would take about a half hour to be completed.

x.   It would be greatly appreciated if you could complete the scoring form before
   a.   / /2013.

xi.   Return the completed sheets by mailing them to Medical Radiations Department (Building 201, Level 8, Bundoora campus west, Plenty Road, Bundoora, Victoria 3083), you do not have to return the CD.

Appendix 10   Scoring form of CDCT phantom image

Scoring form of CDCT phantom image
Date: /   / 2013

Radiographer no.		Hospital beds no.	
Gender & age:		Monitor specification	
Specialty:			
Recent qualification			
Years of experience:		Displayer software:	

Image code:_____